



SIPA1 as a modulator of HGF/MET induced tumour metastasis via the regulation of tight junction based cell to cell barrier

By

Chang Liu

Cardiff China Medical Research Collaborative (CCMRC)

School of Medicine, Cardiff University

Cardiff

April 2020

Thesis submitted to Cardiff University for the degree of

Doctor of Philosophy

Declaration

This work has not been submitted in substance for any other degree or award at this or any other university or place of learning, nor is being submitted concurrently in candidature for any degree or other award.

Signed Chang Liu (candidate) Date 01/04/2020

STATEMENT 1

This thesis is being submitted in partial fulfilment of the requirements for the degree of Ph.D.

Signed Chang Liu (candidate) Date 01/04/2020

STATEMENT 2

This thesis is the result of my own independent work/investigation, except where otherwise stated. Other sources are acknowledged by explicit references. The views expressed are my own.

Signed Chang Liu (candidate) Date 01/04/2020

STATEMENT 3

I hereby give consent for my thesis, if accepted, to be available for online in the University's Open Access repository and for inter-library loan, and for the title and summary to be made available to outside organisations.

Signed Chang Liu (candidate) Date 01/04/2020

STATEMENT 4: PREVIOUSLY APPROVED BAR ON ACCESS

I hereby give consent for my thesis, if accepted, to be available for photocopying and for inter-library loans after expiry of a bar on access previously approved by the Academic Standards & Quality Committee.

Signed Chang Liu (candidate) Date 01/04/2020

Acknowledgements

Firstly, I would like to thank my patient and gorgeous supervisors, Miss Rachel Hargest and Dr Tracey Martin, for your great support and guidance throughout my three-year study, your sincerely help made me become a better researcher. I would like to thank Professor Wen G. Jiang, and without you I couldn't have the chance to study at Cardiff University and complete my project.

Secondly, I am very grateful for all the current CCMRC members for their kindly help: Dr Lin Ye for your parental care and discussion on my career life; Dr Andrew Sanders for your delicate help at all times; Dr Yuxin Cui for your help on the my analysis of the online database; Fiona for v help on the IHC staining and all the efforts you did to make the lab working really enjoyable. And I also want to send my appreciation to the past CCMRC members: Juliet for the help in my application and enrolment; Dr Jun Cai for your discussion about science; Dr Moon Xie, my research role model; Dr Cathy Cai, the most delightful work partner. And I also would like to thank all the members in CCMRC who have been very nice, friendly and helpful all the time.

Finally, I would like to express my heartfelt thanks to the most important people in my life, my parents, for your support and encouragement both in my academic career and my life. Thanks for my lifetime love, Dr Molly Xu, I can't hold on for the three years without you on my back, I love you so much, my darling. And I would like to thank all my friends who helped and supported me.

Publications

- **C Liu**, W G. Jiang, R Hargest, T A. Martin. 2019. SIPA1 is a modulator of HGF induced tumour metastasis via the regulation of tight junctions in lung adenocarcinoma cells. *Annals of Oncology*. Volume 30, Issue Supplement_5, mdz238.079.
- **C Liu**, W G. Jiang, R Hargest, T A. Martin. 2019. SIPA1 in cancer and cancer metastasis. *Molecular and Clinical Oncology*. Accepted.
- Z Sun, S Cai, **C Liu**, Y Cui, J Ji, W G. Jiang and L Ye. 2020. Increased expression of Gremlin1 promotes proliferation and epithelial mesenchymal transition in gastric cancer cells and correlates with poor prognosis of patients with gastric cancer. *Cancer Genomics & Proteomics*. 17: 49-60.
- Z Sun, **C Liu**, W G. Jiang and L Ye. 2020. Deregulated bone morphogenetic proteins and their receptors are associated with disease progression of gastric cancer. *Computational and Structural Biotechnology Journal*. 18, 177-188
- J Liu, Z Zhao, Z Sun, **C Liu**, X Cheng, F Ruge, Y Yang, Wen G. Jiang and L Ye. 2020. Increased expression of Psoriasin is correlated with poor prognosis of bladder transitional cell carcinoma by promoting invasion and proliferation. *Oncology reports*. 43: 562-570.
- Z Sun, S Cai, C Zabkiewicz, **C Liu**, L Ye. 2020. Bone morphogenetic proteins mediate crosstalk between cancer cells and the tumour microenvironment at primary tumours and metastases (Review). *International Journal of Oncology*. 56(6):1335-1351. doi: 10.3892/ijo.2020.5030.

Conference Attendance

Oral presentation

- Travelling Surgical Society of Great Britain and Ireland Annual Meeting, Cardiff, UK. In Sep. 2018.
- Division of Cancer and Genetics PGR Day, University Hospital of Wales (UHW), Cardiff, UK. In Oct. 2018.
- Surgical innovation - Royal Society of Medicine (RSM), King's College London, London, UK. In Sep. 2019.

Poster presentation

- European Society for Medical Oncology (ESMO) Congress 2019, Barcelona, Spain. In Sep. 2019.

Abbreviations

AF6	Afadin
AIS	Adenocarcinoma in situ
AJs	Adherens junctions
Akt	Protein kinase B
ALK	Anaplastic lymphoma kinase
ANOVA	Analysis of Variance
APS	Ammonium Persulfate
AQP	Aquaporin
ASR	Age-standardized rate
ATCC	American Tissue Culture Collection
bp	base pair
BRAF	B-Raf proto-oncogene
Brd	Bromodomain protein
BSA	Bovine Serum Albumin
CaP	Prostate cancer
Cbl	Casitas B-lineage lymphoma
CCND	Cyclin D
CD	Cluster of Differentiation
cDNA	Complementary DNA
CDNA	Circulation DNA
CFC	Change from control
CIN85	Sh3 domain-containing kinase-binding protein 1
CLDN	Claudin
CSF-1	Colony-stimulating factor 1
CTCs	Circulating tumour cells
CTX	Cholera toxin
CXCL	C-X-C motif ligand
DAB	Diaminobenzidine

DAPI	4',6-diamidino-2-phenylindole
del	Deletion
DEPC	Diethylpyrocarbonate
DMEM	Dulbecco's modified Eagle's medium
DMSO	Dimethylsulphoxide
DNA	Deoxyribonucleic acid
DNMT	DNA methyltransferases
dNTPs	Deoxynucleotide triphosphates
E47	Transcription factor 3, TCF 3
ECIS	Electric Cell-Substrate Impedance Sensing
ECL	Enhanced chemiluminescence
ECM	Extracellular Matrix
EDTA	Ethylenediaminetetracetic acid
EGF	Epidermal Growth Factor
EGFR	Epidermal Growth Factor Receptor
eJM	Extracellular juxtamembrane
ELISA	Enzyme-Linked Immunosorbent Assay
EML4	Echinoderm microtubule-associated protein-like 4
EMT	Epithelial to Mesenchymal Transition
EP	Etoposide and platinums
ERK	Extracellular Regulated Kinases
ETS	Environmental tobacco smoke
EVOM	Epithelial Volt/Ohm Meter
FAK	Focal Adhesion Kinase
FBS	Foetal bovine serum
FITC	Fluorescein isothiocyanate
GAP	GTPase activation Proteins
GAPDH	Glyceraldehyde 3-phosphate dehydrogenase
GEF	Guanine Nucleotide Exchange Factor

GEO	Gene Expression Omnibus
GGA	Golgi Associated
Grb	Proliferation factor receptor bound protein
GRD	Gap related domain
GTP	Guanosine Triphosphate
HER2	Human epidermal growth factor receptor 2
HGF	Hepatocyte Growth Factor
HGFR	Hepatocyte growth factor receptor
HL	Hairpin loop
HRP	Horseradish peroxidase
IASLC	International Association for The Study of Lung Cancer
IF	Immunofluorescent
Ig	Immunoglobulin
IHC	Immunohistochemical
iJM	Intracellular juxtamembrane
ITGB1	Integrin beta 1
JAMs s	Junctional Adhesion Molecule
JNK	Jun amino-terminal kinase
kb	Kilo base pairs
KLF	Kruppel like factor
KRAS	KRAS proto-oncogene
LB	Liquid Broth
LCNEC	Large cell neuroendocrine carcinoma
LOX	Lysyl oxidase
LUSC	Lung squamous cell carcinoma
LUAD	Lung adenocarcinoma
LVSI	Lymph vascular space invasion
LZ	Leucine zipper
MAGI	Membrane-associated guanylate kinase

MAPK	Mitogen-activated Protein Kinase
MET	MET Proto-oncogene
MIA	Minimally invasive adenocarcinoma
MMP	Matrix metalloproteinase
mRNA	Message RNA
MTT	3-(4,5-dimethylthiazol-2-yl)-2,5-diphenyl tetrazolium bromide
NCCN	National Comprehensive Cancer Network
NGS	Next Generation Sequencing technology
NSCLC	Non-small cell lung cancer
nt	Nucleotide
ORF	Open reading frame
OS	Overall survival
OSCC	Oral squamous cell carcinoma
PBL	Peripheral blood lymphocytes
PBS	Phosphate Buffer Saline
PCP	Paracellular Permeability
PCR	Polymerase Chain Reaction
PD-1	Programmed death 1
PD-L1	Programmed death ligands 1
PD-L2	Programmed death ligands 2
PDZ	PSD 95 Dig and ZO1
PEST	Proline, glutamic acid, serine and threonine
PFS	Progression-free survival
Phe	Phenylalanine
PI3K	Phosphoinositide 3-Kinase
PM	Fine particular matter
PTP1 β	Protein tyrosine phosphatase 1-beta
qPCR	Quantitative Polymerase Chain Reaction

Ran	Ras related nuclear protein 1
Rap1	Ras proximate 1, Ras related protein 1
RET	RET proto-oncogene
RNA	Ribonucleic Acid
ROS1	ROS proto-oncogene 1
RPMI	Roswell Park Memorial Institute
rRNA	Ribosomal RNA
Rsr1	Ras related nuclear protein Rsr1
RT	Reverse Transcriptase
RTKs	Tyrosine kinase receptors
SCC	Squamous cell carcinoma
SCID	Severe combined immunodeficiency disease
SCLC	Small cell lung cancer
SD	Standard deviations
SDS	Sodium Dodecyl Sulphate
SDS-PAGs	Sodium dodecyl sulfate polyacrylamide gel electrophoresis
SEM	Standard Error of the Mean
Ser	Serine
SF	Scatter Factor
SFM	Serum Free Medium
Sh2	Src homology 2
Sh3	Src homology 3
SIPA1	Signal induced proliferation-associated protein 1
SIPAL1	Signal induced proliferation-associated protein 1 like1
SNPs	Single nucleotide polymorphisms
SOCS	suppressor of cytokine signalling
SPH	Serine protease homology
Src	Proto-oncogene tyrosine-protein kinase src
STAT3	Signal transducer and activator of transcription-3

TAMP	transmembrane adhesion membrane proteins
TBE	Tris-Boric-Acid
TCDD	2,3,7,8-tetrachlorodibenzo-para-dioxin
TEMED	Tetramethylethylenediamine
TER	Transepithelial resistance
TFs	Transcription factors
TGF- α	Transforming growth factor- α
TGF- β	Transforming growth factor- β
TJs	Tight Junctions
TKI	Tyrosine kinase inhibitors
TMB	Tumour mutational burden
TNM staging	Tumour, Lymph Node and Metastasis staging
TPA	Plasminogen Activator, PLAT
TRITC	Tetramethylrhodamine isothiocyanate
tRNA	Transfer RNA
TSN	Translin
TTF1	Transcription termination factor 1
Tween 20	Polyoxyethylene (20) sorbitan monolaurate
UTR	Untranstated region
VEGFs	Vascular endothelial growth factors
WB	Western Blotting
WHO	World Health Organisation
ZO	Zonula Occludin

Summary

Lung cancer is the leading cause of cancer-related death in the UK and worldwide. The development and metastasis of lung cancer is regarded as a complex process involving a number of mechanisms. Deep understanding of lung cancer metastasis is necessary to aid clinical diagnosis and management of the disease. SIPA1 (Signal Induced Proliferation Associated 1) is a mitogen induced GTPase activating protein (GAP). This protein may also hamper mitogen-induced cell cycle progression when abnormally or prematurely expressed. Some evidence suggests SIPA1 may be involved in the MET signalling pathway. There is also evidence showing that SIPA1 may be involved in the regulation of tight junctions, which are key components in the prevention of metastasis. The role of SIPA1 in lung cancer remains largely unknown. This study aimed to evaluate the importance of SIPA1 in the development of and progression lung cancer, showing the cellular function of SIPA1 and the molecular mechanism/s involved.

Expression of SIPA1 was found to be significantly higher in human lung cancer tissues compared to normal lung tissue. Lung cancer patients with higher SIPA1 levels had a poorer prognosis compared to patients with low SIPA1 level, especially in lung adenocarcinoma. *In vitro* cell models showed knockdown SIPA1 in A549 cells and SK MES1 cells decreased the aggressive behaviour in invasion and proliferation, and the SIPA1 knockdown cells demonstrated leaky cell to cell barriers. SIPA1 related gene expression correlation assays using our own lung cancer patient cohort and TCGA cohort demonstrated that SIPA1 had high correlation with cell signalling by receptor tyrosine kinases (RTKs), especially HGF/MET signalling pathways and TJ components. Kinexus™ protein kinase array analysis also revealed SIPA1 is involved in the regulation on the RTKs signalling and HGF/MET signalling. Co-culture of *in vitro* cell models with HGF showed that the regulation of HGF on cell barrier and invasion required the present of SIPA1. At the molecular level, knockdown of SIPA1 decreased tight junction based barrier function by downregulating MET. Knockdown of SIPA1 reduced the protein expression level of MET but not the transcript level, and

regulation was attained through silencing of Grb2, SCOS, and PKC μ , reducing the internalization and recycling of MET.

SIPA1 may act as a targeting molecule in cancer. Knockdown of SIPA1 reduced the growth and invasion potential of lung cancer cells *in vitro*. SIPA1 influences the tight junction proteins in cancer cell lines and further work may reveal the mechanism by which SIPA1 mediates the HGF influenced development and metastasis of tumours.

In conclusion, SIPA1 plays an essential role in tumorigenesis and metastasis of lung cancer. SIPA1 could be used as a biomarker for diagnosis and prediction of patients' prognosis. Moreover, the interaction of SIPA1 with MET showed SIPA1 can be a potential therapeutic target for patients with aberrant MET derived non-small cell lung cancer and drug resistance.

Contents

<i>Declaration</i>	<i>I</i>
<i>Acknowledgements</i>	<i>II</i>
<i>Publications</i>	<i>III</i>
<i>Conference Attendance</i>	<i>IV</i>
<i>Abbreviations</i>	<i>V</i>
<i>Summary</i>	<i>XI</i>
<i>Contents</i>	<i>XIII</i>
<i>List of Figures</i>	<i>XXII</i>
<i>List of Tables</i>	<i>XXX</i>
<i>Chapter-1 Introduction</i>	<i>1</i>
1.1 The lung and lung cancer	2
1.1.1 <i>The biology of the lung</i>	2
1.1.1.1 Lung Anatomy	2
1.1.2 <i>Lung histology</i>	5
1.1.2.1 Blood supply to the lungs	9
1.1.2.2 Development of lung	9
1.1.3 <i>Lung cancer</i>	10
1.1.3.1 Epidemiology of lung cancer	10
1.1.3.1.1 Incidence and mortality	10
1.1.3.1.2 Geographic Variation	13
1.1.3.2 Aetiology of lung cancer	17
1.1.3.2.1 Tobacco smoke	17

1.1.3.2.2 Ionising radiation.....	18
1.1.3.2.3 Air pollution.....	19
1.1.3.2.4 Occupational carcinogens	19
1.1.3.2.5 Family history.....	19
1.1.3.3 Classification of lung cancer.....	20
1.1.3.3.1 General classification	20
1.1.3.3.2 Histopathological classification	20
1.1.3.3.2.1 Lung adenocarcinoma (LUAD)	22
1.1.3.3.2.2 Squamous cell carcinoma (LUSC).....	24
1.1.3.3.2.3 Neuroendocrine tumours.....	24
1.1.3.3.2.4 Large cell carcinoma.....	25
1.1.3.3.2.5 Adenosquamous carcinoma	25
1.1.3.3.3 Molecular classification and biomarkers	26
1.1.3.4 Staging of lung cancer	29
1.1.3.5 Treatment of lung cancer.....	31
1.1.3.5.1 Surgery.....	31
1.1.3.5.2 Chemotherapy.....	32
1.1.3.5.3 Radiotherapy	32
1.1.3.5.4 Targeted therapy.....	33
1.1.3.5.5 Immunotherapy.....	35
1.2 Metastasis of cancer	35
1.2.1 <i>The invasion-metastasis cascade</i>	35
1.2.2 <i>Local invasion through extracellular matrix (ECM) and stromal cells.</i> ..	36
1.2.3 <i>Intravasation into the lumina of blood vessels.</i>	37
1.2.4 <i>Survival and transport within the circulatory system.</i>	38
1.2.5 <i>Extravasation and arrest at a distant site to form a secondary focus.</i> ..	38
1.2.6 <i>Formation of micrometastases.</i>	39
1.2.7 <i>Proliferation at secondary foci - metastatic colonization.</i>	39
1.3 SIPA1 and metastasis of cancer.....	40
1.3.1 <i>SIPA1 (Signal Induced Proliferation Associated 1)</i>	40
1.3.2 <i>Cloning and identifications of the gene of SIPA1</i>	40
1.3.3 <i>The structure and expression of SIPA1 protein</i>	41
1.3.4 <i>Germline polymorphisms in SIPA1</i>	43

1.3.5	<i>SIPA1 family and Rap1-GTPase activating proteins</i>	43
1.3.6	<i>SIPA1 interacting molecules (Figure 1.12)</i>	44
1.3.6.1	Nuclear SIPA1 and integrin β 1.....	44
1.3.6.2	Association of SIPA1 and AF6.....	44
1.3.6.3	SIPA1 colocalizes with AQP2 in renal collecting ducts	45
1.3.6.4	Brd4 interacts with SIPA1.....	45
1.3.7	<i>Multiple roles of SIPA1 in cancer and the mechanisms thereof</i>	46
1.3.7.1	Breast cancer.....	46
1.3.7.2	Prostate cancer	47
1.3.7.3	Oral squamous cell carcinoma	48
1.3.7.4	Colorectal cancer	48
1.3.7.5	Cervical cancer.....	49
1.3.7.6	Lung Cancer	49
1.3.7.7	Gastric cancer.....	50
1.3.7.8	Melanoma	50
1.3.8	<i>Summary of SIPA1 in cancer</i>	51
1.4	HGF/MET signalling pathway	51
1.4.1	<i>Hepatocyte growth factor</i>	51
1.4.2	<i>The HGF/MET pathway and receptor tyrosine kinase (RTK) families</i> ..	52
1.4.3	<i>The regulation of MET</i>	57
1.4.4	<i>Internalization and recycling of MET</i>	58
1.4.5	<i>HGF/MET activation in cancer.</i>	59
1.4.6	<i>HGF/MET in NSCLC</i>	61
1.5	Tight junctions	61
1.5.1	<i>The Tight Junction (TJ) structure and function</i>	61
1.5.2	<i>The structure of tight junctions</i>	62
1.5.3	<i>The tight junction proteins</i>	62
1.5.4	<i>The function of tight junctions</i>	63
1.5.5	<i>Tight junctions are barriers to cancer metastasis</i>	64

1.5.6	<i>Changes in TJs in lung cancer</i>	65
1.6	Hypothesis and aims of this study	66
Chapter-2 Materials and methods		68
2.1	General materials	69
2.1.1	<i>Cell lines</i>	69
2.1.2	<i>Collection of human cancer tissues</i>	69
2.1.3	<i>General compounds</i>	70
2.1.4	<i>General plastic consumables, hardware and software</i>	70
2.1.5	<i>Primers</i>	72
2.1.6	<i>Antibodies</i>	74
2.1.6.1	<i>Primary antibodies</i>	74
2.1.6.2	<i>Secondary antibodies</i>	75
2.1.7	<i>Preparation of Reagents, Buffers and Standard solutions</i>	76
2.1.7.1	<i>Solutions for molecular biology experiments</i>	76
2.1.7.2	<i>Solutions for use in cloning</i>	78
2.1.7.3	<i>Solutions for use in protein work</i>	78
2.2	Cell Culture	79
2.2.1	<i>Cell Culture, maintenance and Storage</i>	79
2.2.2	<i>Trypsinization and Counting of cell lines</i>	80
2.2.3	<i>Storage of cell lines in liquid nitrogen and cell resuscitation</i>	81
2.3	Methods for RNA detection	82
2.3.1	<i>RNA extraction</i>	82
2.3.2	<i>RNA Quantification</i>	83
2.3.3	<i>Reverse Transcription of RNA for production of cDNA</i>	83
2.3.4	<i>Polymerase chain reaction</i>	84
2.3.5	<i>Agarose gel electrophoresis and DNA visualization</i>	86
2.3.6	<i>Quantitative RT-PCR (QPCR)</i>	87
2.4	Methods for protein detection	91

2.4.1	<i>Protein extraction and preparation of cell lysates</i>	91
2.4.2	<i>Protein quantification and preparation of samples for SDS-PAGE</i>	91
2.4.3	<i>Sodium Dodecyl Sulphate Polyacrylamide Gel Electrophoresis (SDS-PAGE)</i>	92
2.4.4	<i>Western blotting: transferring proteins from gel to nitrocellulose membrane</i>	94
2.4.5	<i>Protein detection using specific Immuno-probing</i>	95
2.4.6	<i>Chemiluminescent protein detection</i>	96
2.4.7	<i>Immunohistochemical staining</i>	96
2.4.8	<i>Protein for Kinexus™ microarrays</i>	97
2.4.8.1	Sample preparation	97
2.4.8.2	Antibody microarrays	98
2.4.8.3	Key information derived from KAM1325.....	98
2.4.8.4	Antibody array analysis of SIPA1 interacting proteins	100
2.4.9	<i>Immunofluorescence staining</i>	100
2.5	Targeting SIPA1 gene expression	101
2.5.1	<i>Knock down of SIPA1 using Ribozyme Transgenes</i>	101
2.6	<i>In vitro</i> Function assay	105
2.6.1	<i>In vitro cell growth assay</i>	105
2.6.2	<i>In vitro thiazolyl blue tetrazolium bromide (MTT) cell growth assay</i> ...	106
2.6.3	<i>In vitro transwell cell invasion assay</i>	107
2.6.4	<i>In vitro cell adhesion assay</i>	108
2.6.5	<i>In vitro MTT cell adhesion assay</i>	109
2.6.6	<i>In vitro cell transwell migration assay</i>	110
2.6.7	<i>In vitro cell migration assay (wound healing assay)</i>	111
2.6.8	<i>Electric cell-substrate impedance sensing (ECIS)</i>	112
2.6.9	<i>Transepithelial Resistance (TER)</i>	115

Chapter-3 Expression of SIPA1 in lung cancer and its clinical relevance · 117

3.1	Introduction	118
3.2	Materials and methods	119
3.2.1	<i>Lung cancer tissues</i>	119
3.2.2	<i>Primers and antibody</i>	119
3.2.3	<i>RNA extraction, reverse transcription, PCR and QPCR</i>	120
3.2.4	<i>Immunohistochemistry (IHC) for lung tissue microarray</i>	120
3.2.5	<i>Statistical analysis</i>	120
3.3	Result	121
3.3.1	<i>Transcript level of SIPA1 in lung cancer</i>	121
3.3.2	<i>Protein level of SIPA1 in lung cancer</i>	126
3.3.3	<i>SIPA1 transcript and protein expression and histological type of lung cancer</i>	132
3.3.4	<i>SIPA1 in relation to the pathological tumour staging and clinical features of lung cancer</i>	140
3.3.5	<i>Correlation between SIPA1 expression and clinical outcome of the patients in the Peking cohorts</i>	145
3.4	Discussion	156

Chapter-4 Impact of SIPA1 expression on the cellular function behaviour of human lung cancer cells..... 159

4.1	Introduction	160
4.2	Material and methods	161
4.2.1	<i>Cell lines</i>	161
4.2.2	<i>Knockdown of SIPA1 by using ribozyme transgene</i>	161
4.2.3	<i>Primers and antibody</i>	162
4.2.4	<i>RNA extraction, RT-PCR, and QPCR</i>	162
4.2.5	<i>Protein extraction, SDS-PAGE, and western blot analysis</i>	163
4.2.6	<i>In vitro cell growth assay</i>	163

4.2.7	<i>In vitro cell invasion assay</i>	163
4.2.8	<i>Transepithelial Resistance (TER) and Paracellular Permeability (PCP) assay</i> 164	
4.2.9	<i>Electric Cell-Substrate Impedance Sensing (ECIS)</i>	164
4.2.10	<i>Statistical Analysis</i>	164
4.3	Result	165
4.3.1	<i>Knockdown of SIPA1 in lung cancer cell lines</i>	165
4.3.2	<i>Impact of SIPA1 on proliferation potential of lung cancer cells</i>	169
4.3.3	<i>Impact of SIPA1 on invasion potential of lung cancer cells</i>	169
4.3.4	<i>Impact of SIPA1 on tight junction of lung cancer cells</i>	171
4.4	Discussion	175
 <i>Chapter-5 SIPA1 and its intracellular signalling pathways in human lung cancer cells</i>		
		178
5.1	Introduction	179
5.2	Methods	181
5.2.1	<i>Protein extraction</i>	181
5.2.2	<i>Kinexus™ protein microarray in SIPA1 knockdown A549 cancer cells treat with/without HGF</i>	181
5.2.3	<i>TCGA database acquirement and statistical analysis</i>	181
5.3	Results	182
5.3.1	<i>Potential connection among SIPA1, HGF signalling pathway and tight junctions' components</i>	182
5.4	Discussion	238
 <i>Chapter-6 SIPA1 is a modulator of the regulation of HGF on cellular function behaviour of human lung cancer cells</i>		
		241
6.1	Introduction	242

6.2	Materials and methods	243
6.2.1	<i>RNA extraction, RT-PCR, and QPCR</i>	243
6.2.2	<i>Primers and antibody</i>	243
6.2.3	<i>Protein extraction, SDS-PAGE, and western blot analysis</i>	244
6.2.4	<i>In vitro cell growth assay</i>	244
6.2.5	<i>In vitro cell invasion assay</i>	244
6.2.6	<i>Electric Cell-Substrate Impedance Sensing (ECIS)</i>	245
6.2.7	<i>Immunofluorescence staining</i>	245
6.2.8	<i>Statistical Analysis</i>	245
6.3	Results	246
6.3.1	<i>The impact of HGF on the cellular behaviour of lung cancer cells</i>	246
6.3.2	<i>The impact of HGF on the barrier function of lung cancer cells</i>	248
6.3.3	<i>The interaction of SIPA1 and MET</i>	251
6.3.4	<i>Impact of SIPA1 on the expression of TJ components</i>	256
6.3.5	<i>The impact of SIPA1 on the morphology of the cells and TJs</i>	268
6.4	Discussion	271
	<i>Chapter-7 The key molecules regulated by the interaction of SIPA1 with HGF/MET signalling pathway in human lung cancer cells</i>	273
7.1	Introduction	274
7.2	Materials and methods	275
7.2.1	<i>Primary and secondary antibody</i>	275
7.2.2	<i>Protein extraction, SDS-PAGE, and western blot analysis</i>	275
7.2.3	<i>Statistical Analysis</i>	276
7.3	Results	276
7.4	Discussion	279
	<i>Chapter-8 General discussion</i>	280

8.1	The aims of the thesis.....	281
8.2	Influence of SIPA1 on the function of lung cancer cells.....	281
8.3	Influence of SIPA1 interaction with HGF/MET on the function of lung cancer cells.....	282
8.4	Intracellular interaction between SIPA1 and MET signalling pathway	282
8.5	Influence of SIPA1 on the regulation of MET receptor.....	283
8.6	Influence of SIPA1 interaction with HGF/MET on tight junction components	284
8.7	Clinical relevance of SIPA1	284
8.8	Final conclusion and perspectives.....	286
8.9	Future directions:.....	288
	<i>Chapter-9 Reference</i>	<i>289</i>
	<i>Chapter-10 Appendix.....</i>	<i>302</i>

List of Figures

Chapter-1 Introduction	1
Figure 1.1: Lung in situ: anterior view.	4
Figure 1.2: Lung: medial views. Atlas of Human Anatomy	5
Figure 1.3: Intrapulmonary airway: schema.	9
Figure 1.4: Pie Charts Present the Distribution of the number of Cases and Deaths for the 10 Most Common Cancers in 2018	12
Figure 1.5: Incidence and mortality of lung cancer	13
Figure 1.6: Geographic Variation of lung cancer in different countries.....	14
Figure 1.7: Geographic Variation of lung cancer in different continents	16
Figure 1.8: Countries with the most new-cases and deaths of lung cancer....	17
Figure 1.9: Alterations in targetable oncogenic pathways.....	28
Figure 1.10. The main steps in the formation of metastatic cascade	36
Figure 1.11. The structure of human SIPA1 gene and protein.	42
Figure 1.12: Schematic diagram of the SIPA1 interacting molecules.....	46
Figure 1.13: The schematic diagram of domain structures of HGF and MET- RTK	52
Figure 1.14: Introduction of the Human receptor tyrosine kinases (RTKs) Family Members.....	54
Figure 1.15: Schematic diagram of the major MET downstream signalling pathways and the regulation of cellular function.....	56
Figure 1.16: Schematic diagram of intracellular downstream signalling pathways activated by HGF/MET RTK	57
Figure 1.17: Simplified scheme of regulation of MET	58
Figure 1.18: Simplified scheme of the internalization and recycling of MET...	59
Figure 1.19: Schematic diagram of different molecular mechanisms activating MET in cancer	60
Chapter-2 Materials and methods	68

<i>Figure 2.1: Real time quantitative PCR using the fluorescent labelled Uniprimer. During the QPCR, primers containing the Z-sequence could recognise and bind to the specific 3' region in step 1. Then in step 2, the Z-sequence could be recognized by Uniprimer. Subsequently in the next cycle the Uniprimer was open to show the fluorescent signal for detection.</i>	<i>88</i>
<i>Figure 2.2: Diagram of standard curve generation.</i>	<i>90</i>
<i>Figure 2.3: Diagram of the electrophoresis equipment transferring proteins from gel to membrane.....</i>	<i>95</i>
<i>Figure 2.4: Antibody layout on a typical KAM1325 protein array, image supplied by Kinexus Inc. Using the protein microarray to compare the difference in these key signalling molecules between the control cells and SIPA1 knockdown cells. The different sites in the figure show different colours (red and green) because different antibodies are recognized and stained with different colour dyes, and black means the stain intensity is very low.</i>	<i>98</i>
<i>Figure 2.5: Olympus Fluorescence Microscope equipped with a Hamamatsu digital camera</i>	<i>101</i>
<i>Figure 2.6 A: Schematic diagram of the secondary structure of hammerhead ribozyme.....</i>	<i>102</i>
<i>Figure 2.6 B: Schematic diagram of the secondary structure of SIPA1 mRNA.</i>	<i>103</i>
<i>Figure 2.7: Schematic of the pEF6 plasmid.....</i>	<i>105</i>
<i>Figure 2.8: Schematic diagram of in vitro invasion assay</i>	<i>108</i>
<i>Figure 2.9: Schematic diagram of in vitro transwell migration assay.....</i>	<i>111</i>
<i>Figure 2.10: EVOS® FL2 Auto Imaging System with EVOS® Onstage Incubator</i>	<i>112</i>
<i>Figure 2.11: Electric cell-substrate impedance sensing (ECIS)</i>	<i>113</i>
<i>Figure 2.12: Diagram of current flow following cell attachment to the gold electrode.....</i>	<i>114</i>
<i>Figure 2.13: Schematic diagram of transepithelial resistance assay.....</i>	<i>116</i>
<i>Figure 2.14: EVOM² Epithelial Volt/Ohm Meter with chopstick electrode</i>	<i>116</i>

Chapter-3 Expression of SIPA1 in lung cancer and its clinical relevance · 117

Figure 3.1: Transcript level of SIPA1 between lung cancer and adjacent normal lung tissue. 124

Figure 3.2: Transcript level of SIPA1 between lung cancer and paired adjacent normal lung tissue. 125

Figure 3.3: Overall look of the IHC staining of SIPA1 on lung cancer TMA ... 127

Figure 3.4: Frequency analysis of the each IHC score in lung cancer tumour and normal tissue samples by chi-square test. 129

Figure 3.5: representative IHC SIPA1 staining images in the TMA. 130

Figure 3.6: Representative IHC SIPA1 staining images in the malignant tumour tissues. 131

Figure 3.7: Transcript level of SIPA1 in different histology of lung cancer. 133

Figure 3.8.1: Frequency analysis of the IHC scores in various histology of tumour samples and normal samples by chi-square test. 134

Figure 3.8.2: Frequency analysis of each IHC score in adenocarcinoma and SCC samples by chi-square test. 135

Figure 3.8.3: Frequency analysis of each IHC score in adenocarcinoma samples and other lung cancer samples by chi-square test. 136

Figure 3.8.4: Frequency analysis of each IHC score in SCC samples and other lung cancer samples by chi-square test. 137

Figure 3.8.5: Frequency analysis of each IHC score in adenocarcinoma samples and normal samples by chi-square test. 138

Figure 3.8.6: Frequency analysis of each IHC score in SCC samples and normal samples by chi-square test. 139

Figure 3.9: Transcript level of SIPA1 in different T stage lung cancer. 141

Figure 3.10: Transcript level of SIPA1 in different TNM stage lung cancer. ... 142

Figure 3.11: Transcript level of SIPA1 in different stage lung cancer. 143

Figure 3.12: Frequency analysis of the each IHC score various T stage samples by chi-square test. 144

<i>Figure 3.13: The Kaplan-Meier survival model of correlation between SIPA1 transcript levels and overall survival</i>	146
<i>Figure 3.14: The Kaplan-Meier survival model of correlation between SIPA1 transcript levels and post-progression survival (PPS)</i>	148
<i>Figure 3.15: The Kaplan-Meier survival model of correlation between SIPA1 transcript levels and prognosis</i>	149
<i>Figure 3.16: The Kaplan-Meier survival model of correlation between SIPA1 transcript levels and overall survival in various histology of lung cancer.</i>	151
<i>Figure 3.17: The Kaplan-Meier survival model of correlation between SIPA1 transcript levels and overall survival (OS) in lung adenocarcinoma patients.</i>	152
<i>Figure 3.18: The Kaplan-Meier survival model of correlation between SIPA1 transcript levels and progression-free survival (PFS) in lung adenocarcinoma patients</i>	153
<i>Figure 3.19: The Kaplan-Meier survival model of correlation between SIPA1 transcript levels and post-progression survival (PPS) in lung adenocarcinoma patients</i>	154
<i>Figure 3.20: The Kaplan-Meier survival model of correlation between SIPA1 transcript levels and overall survival (OS), progression-free survival (PFS) and post-progression survival (PPS) in lung squamous cell carcinoma patients</i> .	155
 <i>Chapter-4 Impact of SIPA1 expression on the cellular function behaviour of human lung cancer cells</i>	159
 <i>Figure 4.1: Verification of the knockdown of SIPA1 in SKMES1, CORL23 and A549 cell lines in mRNA level using PCR.</i>	166
<i>Figure 4.2: Verification of the knockdown of SIPA1 in SKMES1, CORL23 and A549 cell lines in mRNA level using QPCR.</i>	167
<i>Figure 4.3: Verification of the knockdown of SIPA1 in A549, SKMES1, and CORL23 cell lines in protein level using western blot.</i>	168
<i>Figure 4.4: Knockdown of SIPA1 decreased the growth of the A549 cells significantly.</i>	169

<i>Figure 4.5: Knockdown of SIPA1 decreased the invasion of the A549 and SKMES1 cells significantly</i>	170
<i>Figure 4.6.A: Knockdown of SIPA1 increased the cell-cell tight junction of the A549 cells significantly.</i>	171
<i>Figure 4.6.B: 3D figure showed knockdown of SIPA1 increased the cell-cell tight junction in different frequencies.</i>	172
<i>Figure 4.6.C: The effect of SIPA1 in enhancing tight junction is statistically significant.</i>	173
<i>Figure 4.7: The Effect of SIPA1 Knockdown on A549 cell line detected using Transepithelial Resistance (TER).</i>	174

Chapter-5 SIPA1 and its intracellular signalling pathways in human lung

***cancer cells*** 178

<i>Figure 5.1: Spearman's rank correlation coefficient between SIPA1, HGF related genes and tight junction component genes analysed from the lung cancer cohort (n=148).</i>	183
<i>Figure 5.2: Spearman's rank correlation coefficient between SIPA1 and HGF related genes analysed from TCGA LUAD database (n=576).</i>	184
<i>Figure 5.3: Spearman's rank correlation coefficient between SIPA1 and tight junction component genes analysed from TCGA LUAD database (n=576).</i> ..	186
<i>Figure 5.4: Overall images of a direct fluorescent-dye labelled KAM-1325 antibody microarray slide</i>	187
<i>Figure 5.5: Genome-wide overview of the signalling pathway which were downregulated by SIPA1 knockdown on A549 cells.</i>	193
<i>Figure 5.6: Genome-wide overview of the signalling pathway which were upregulated by SIPA1 knockdown on A549 cells.</i>	202
<i>Figure 5.7: Genome-wide overview of the signalling pathway which were downregulated by treatment with HGF on A549 pEF control cells</i>	209
<i>Figure 5.8: Genome-wide overview of the signalling pathway which were upregulated by treatment with HGF on A549 pEF control cells.</i>	216

<i>Figure 5.9: Genome-wide overview of the signalling pathway which were down regulated in SIPA1 knock down cells compared to pEF control cells after the treatment of HGF</i>	<i>222</i>
<i>Figure 5.10: Genome-wide overview of the signalling pathway which were up regulated in SIPA1 knock down cells compared to pEF control cells after the treatment of HGF.</i>	<i>234</i>
<i>Figure 5.11: Schematic diagram of signalling transduction process.</i>	<i>236</i>
<i>Figure 5.12: Schematic diagram of signalling by receptor tyrosine kinases. .</i>	<i>237</i>

Chapter-6 SIPA1 is a modulator of the regulation of HGF on cellular

function behaviour of human lung cancer cells *241*

<i>Figure 6.1: HGF increased the invasion potential of pEF-CT A549 cells, and knockdown of SIPA1 decreased invasion both in A549 pEF control and SIPA1 knockdown cells.</i>	<i>247</i>
<i>Figure 6.2 A: HGF decreases cell-cell tight junction function of A549 pEF-CT cells significantly, but did not decrease tight junction function of A549 SIPA1 knockdown cells.</i>	<i>249</i>
<i>Figure 6.2 B: HGF decreases cell-cell tight junction function of A549 pEF-CT cells significantly, but did not decrease tight junction function of A549 SIPA1 knockdown cells and this effect produced a similar result as that achieved when using the MET inhibitor.</i>	<i>250</i>
<i>Figure 6.3: The mRNA level of MET was not regulated by the knockdown of SIPA1 in A549 lung cancer cell lines examined using conventional PCR.</i>	<i>252</i>
<i>Figure 6.4 A: The mRNA level of MET was not regulated by the knockdown of SIPA1 in A549 lung cancer cell lines examined using QPCR.</i>	<i>253</i>
<i>Figure 6.4 B: The mRNA level of MET was not regulated by the knockdown of SIPA1 in SK MES1 lung cancer cell lines examined using QPCR.</i>	<i>253</i>
<i>Figure 6.5: The protein level of MET was down regulated by the knockdown of SIPA1 in A549 lung cancer cell lines examined using western blotting.</i>	<i>254</i>
<i>Figure 6.6: The protein level of MET was down regulated by the knockdown of</i>	

<i>SIPA1 in A549 and SKMES1 lung cancer cell lines examined using western blotting.</i>	<i>254</i>
<i>Figure 6.7: The phosphorylation level of MET was down regulated by the knockdown of SIPA1 in A549 lung cancer cell lines examined using western blotting.</i>	<i>255</i>
<i>Figure 6.8 A: The effect of SIPA1 knockdown on gene expression of Claudin family in A549 cells.</i>	<i>258</i>
<i>Figure 6.8 B: The effect of SIPA1 knockdown on gene expression of JAM family in A549 cells.</i>	<i>259</i>
<i>Figure 6.8 C: The effect of SIPA1 knockdown on gene expression of TJ proteins containing a PDZ domain in A549 cells.</i>	<i>260</i>
<i>Figure 6.8 D: The effect of SIPA1 knockdown on gene expression of TAMP proteins in A549 cells.</i>	<i>261</i>
<i>Figure 6.9 A: The effect of SIPA1 knockdown on gene expression of TJ proteins containing a PDZ domain in SK MES1 cells.</i>	<i>263</i>
<i>Figure 6.9 B: The effect of SIPA1 knockdown on gene expression of TAMP proteins in SK MES1 cells.</i>	<i>264</i>
<i>Figure 6.10: The effect of SIPA1 knockdown on expression TJ proteins in protein level in A549 cell line</i>	<i>266</i>
<i>Figure 6.11: The effect of SIPA1 knockdown on expression of AF6 and ZO1 in protein level in CORL23 cell line.</i>	<i>267</i>
<i>Figure 6.12: Immunofluorescence staining for ZO1 in A549 pEF-CT cells and SIPA1-KD cells.</i>	<i>269</i>
<i>Figure 6.13: Typical images displaying the immunofluorescence staining of ZO1 in the A549 pEF-CT cells and SIPA1-KD cells.</i>	<i>270</i>

Chapter-7 The key molecules regulated by the interaction of SIPA1 with HGF/MET signalling pathway in human lung cancer cells..... 273

<i>Figure 7.1: The protein level of PKCα is down regulated by the knockdown of SIPA1 in A549 and SKMES1 lung cancer cell lines examined using western</i>	
---	--

<i>blotting.</i>	<i>277</i>
<i>Figure 7.2: The protein level of Grb2 is down regulated by the knockdown of SIPA1 in A549 and SKMES1 lung cancer cell lines examined using western blotting.</i>	<i>277</i>
<i>Figure 7.3: The protein level of SOCS family in A549 and SKMES1 lung cancer cell lines examined using western blotting.</i>	<i>278</i>
<i>Chapter-8 General discussion</i>	<i>280</i>
<i>Figure 8.1: Diagram of the overview of the thesis outline. Schematic indicating the possible regulatory pathway for of SIPA1 in lung cancer cells and the control of tight junction function and assembly by HGF.</i>	<i>287</i>
<i>Chapter-9 Reference</i>	<i>289</i>
<i>Chapter-10 Appendix</i>	<i>302</i>

List of Tables

Chapter-1 Introduction	1
Table 1.1: WHO Classification of Tumours of the Lung, Pleura, Thymus and Heart. Fourth edition	22
Table 1.2: Major genetic changes and molecular biomarkers work as check points for diagnosis and molecular classification in SCLC and two major type of NSCLC	27
Table 1.3: Proposed T, N, and M descriptors for the eighth edition of TNM classification for lung cancer	30
Table 1.4: Proposed stage groupings for the eighth edition of the TNM classification for lung cancer	31
Table 1.5: Proteins involved in TJ structure, function and regulation.	63
Chapter-2 Materials and methods.....	68
Table 2.1: Details of lung cancer cell lines used in this study	69
Table 2.2: Chemicals and reagents.....	70
Table 2.3 Instruments, hardware and software	72
Table 2.4 Primers for conventional RT-PCR, QPCR and ribozyme synthesis ·	73
Table 2.5 Primary and secondary antibodies used in this study	75
Table 2.6: The system of RT-PCR.	84
Table 2.7: The reaction condition of RT-PCR	84
Table 2.8: The system of PCR.	85
Table 2.9: The reaction condition of PCR.	86
Table 2.10: The system of real time quantitative PCR.	88
Table 2.11: The reaction condition of real time quantitative PCR.	89
Table 2.12: Component of the 10% resolving gel	93
Table 2.13: Component of the stacking gel	93
Chapter-3 Expression of SIPA1 in lung cancer and its clinical relevance ·	117

<i>Table 3.1 A: Clinical and pathological demographics of the cohort and the level of expression of SIPA1 transcripts.</i>	<i>122</i>
<i>Table 3.1 B: Expression of SIPA1 transcripts in the clinical cohort of NSCLC lung cancers.</i>	<i>123</i>
<i>Table 3.2: Pathological information summary of lung cancer TMA</i>	<i>128</i>
<i>Chapter-4 Impact of SIPA1 expression on the cellular function behaviour of human lung cancer cells</i>	<i>159</i>
<i>Chapter-5 SIPA1 and its intracellular signalling pathways in human lung cancer cells</i>	<i>178</i>
<i>Table 5.1: Key markers whose phosphor-status were down regulated after SIPA1 knock down on A549 cells.</i>	<i>189</i>
<i>Table 5.2: Top signalling pathways which were downregulated by SIPA1 knockdown on A549 cells.</i>	<i>192</i>
<i>Table 5.3: Key markers whose phosphor-status were up regulated after SIPA1 knock down on A549 cells.</i>	<i>195</i>
<i>Table 5.4: Top signalling pathways which were up regulated by SIPA1 knockdown on A549 cells.</i>	<i>201</i>
<i>Table 5.5: Key markers whose phosphor-status were down regulated in A549 pEF control cells with treatment of HGF.</i>	<i>204</i>
<i>Table 5.6: Top signalling pathways which were downregulated by treatment with HGF on A549 pEF control cells.</i>	<i>208</i>
<i>Table 5.7: Key markers whose phosphor-status were upregulated in A549 pEF control cells with treatment of HGF.</i>	<i>211</i>
<i>Table 5.8: Top signalling pathways which were upregulated by treatment with HGF on A549 pEF control cells.</i>	<i>215</i>
<i>Table 5.9: Key markers whose phosphor-status were down regulated in SIPA1 knock down cells compared to pEF control cells with treatment of HGF.</i>	<i>218</i>
<i>Table 5.10: Top signalling pathways which were down regulated in SIPA1</i>	

<i>knock down cells compared to pEF control cells after the treatment of HGF.</i>	221
<i>Table 5.11: Key markers whose phosphor-status were up regulated in SIPA1 knock down cells compared to pEF control cells with treatment of HGF</i>	224
<i>Table 5.12: Top signalling pathways which were upregulated in SIPA1 knock down cells compared to pEF control cells after the treatment of HGF</i>	233
 <i>Chapter-6 SIPA1 is a modulator of the regulation of HGF on cellular function behaviour of human lung cancer cells</i>	 241
 <i>Chapter-7 The key molecules regulated by the interaction of SIPA1 with HGF/MET signalling pathway in human lung cancer cells.....</i>	 273
 <i>Chapter-8 General discussion</i>	 280
 <i>Chapter-9 Reference</i>	 289
 <i>Chapter-10 Appendix.....</i>	 302

Chapter-1 Introduction

1.1 The lung and lung cancer

1.1.1 The biology of the lung

1.1.1.1 Lung Anatomy

The lung is the most important organ in the respiratory system, located in the thoracic cavity, above the diaphragm, on both sides of the mediastinum, divided into the left lung and the right lung. The surface of the lungs covers the visceral pleura, and many polygonal structures called pulmonary lobules are seen through the pleura. Infection localised in these structures is called lobular pneumonia. The normal lungs in the living state are light red, soft, spongy, and elastic. Generally, the weight of an adult lung is about 1/50 of the weight of the person, the average male lung weighs 1000-1300 g, and the average female is 800-1000 g. Healthy adult males have an air capacity of approximately 5000-6500 ml in both lungs and females are smaller than males (Henry Gray, 2010).

The shape of the two lungs is different, the right lung is wider and shorter, and the left lung is narrower and longer. The lungs are conical, including an apex, a base, three surfaces, and three borders. The apex of the lung is the superior end of the lung, which is obtusely rounded and protrudes into the base of the neck through the thoracic inlet, reaching 2-3 cm above the medial third of the clavicle. The base of the lung is the inferior or diaphragmatic surface of the lung, which is attached to the diaphragm, and is indented by the diaphragm to form a half-moon depression. The costal surface is the lateral side of the lung adjacent to the lateral, anterior and posterior thoracic walls. The mediastinal surface of the lung is the medial surface, adjacent to the mediastinum and has an elliptical depression in the centre called the hilum or the first hilum of the lung. The hilum of the lung is the portal for access to the bronchi, blood vessels, nerves, and lymphatic vessels, which are wrapped by connective tissue. Together these structures are called the root of the lung. The structures in the two roots from the anterior to the posterior are the superior pulmonary vein, the pulmonary artery and the main bronchus. While the structures in

the roots of the left and right lungs are different from superior to inferior. The structures in the left lung root are the left pulmonary artery, the left main bronchus and the left inferior pulmonary vein from superior to inferior, and the structures in the right lung root are right superior lobar bronchus, right pulmonary artery and right inferior pulmonary vein from superior to inferior. The anterior border is the junction of the anterior edges of the costal surface and mediastinal surface, which is a sharp well-defined border. There is a cardiac notch in the inferior part of the left lung anterior border, and below the notch there is a protrusion called the lingua of the left lung. The posterior border is the junction of the posterior edges of the costal surface and the mediastinal surface, located in the lung groove on either side of the spine. The inferior border is the junction of costal surface and diaphragmatic surface, the position of which varies with breathing (Henry Gray, 2010, Frank H. Netter, 2018).

The lungs are divided into lobes by interlobular fissures. The interlobular fissure of the left lung is called the oblique fissure, which runs from posterior and superior to anterior and inferior of the hilum, and divides the left lung into a superior lobe and inferior lobe. In addition to an oblique fissure, the right lung has a horizontal fissure, which divides the right lung into the superior lobe, the middle lobe and the inferior lobe.

There are impressions or grooves formed by the impression of adjacent organs on the surface of the lung. Cardiac impressions are located anterior and inferior to both the left and right hilum. There is a groove for the oesophagus posteriorly and a groove for the azygos vein in the superior part of the right hilum. There are impressions for the thoracic aorta and arch of aortic in the posterior and superior part of the left hilum (Henry Gray, 2010, Frank H. Netter, 2018).

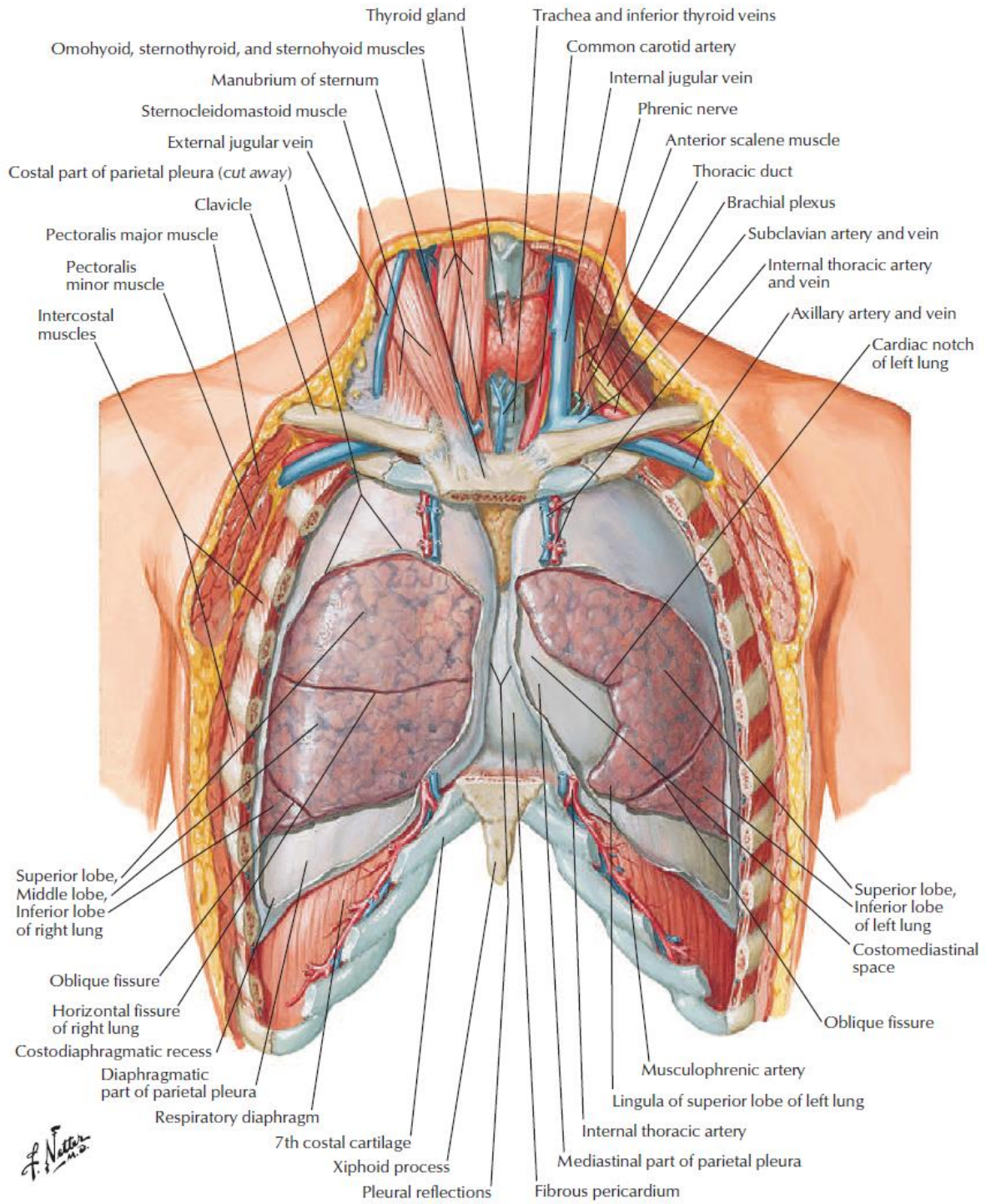


Figure 1.1: Lung in situ: anterior view. Atlas of Human Anatomy, Seventh Edition, 2018. Frank H. Netter, MD (Frank H. Netter, 2018).

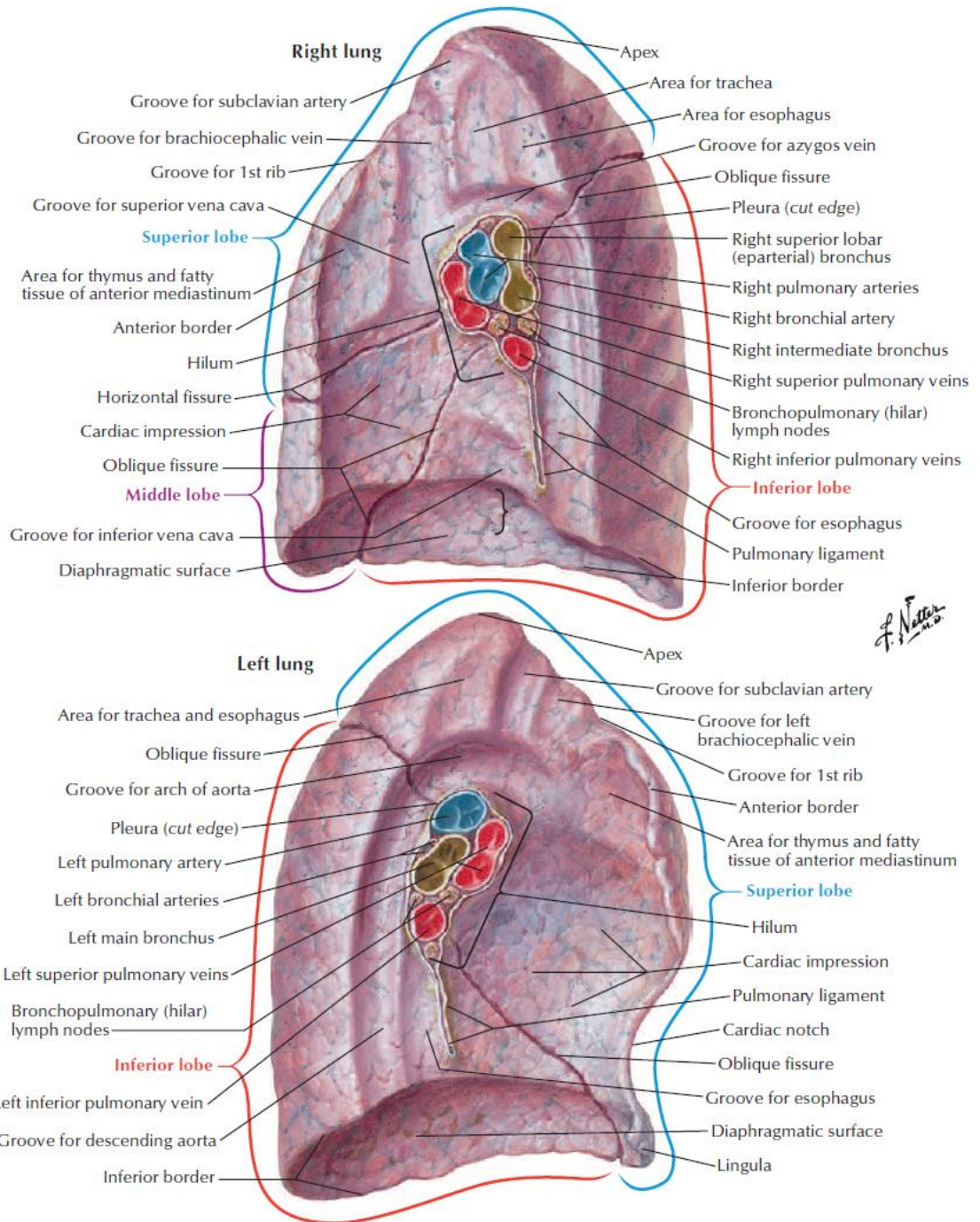


Figure 1.2: Lung: medial views. Atlas of Human Anatomy, Seventh Edition, 2018. Frank H. Netter, MD (Frank H. Netter, 2018).

1.1.2 Lung histology

The surface of the lung is covered with a smooth serosa (visceral pleura) and the connective tissue deep in the serosa penetrates into the lungs, dividing the lungs into

many pulmonary lobules. The lung tissue can be divided into two parts: pulmonary stroma and pulmonary parenchyma. The pulmonary stroma includes connective tissue and blood vessels, lymphatic vessels, and nerves. The pulmonary parenchyma comprises the branches of the intrapulmonary bronchus radiating out to a large number of alveoli peripherally. There are approximately 24 branches from the main bronchus (level 1) to the alveoli. The main bronchus enters the lung through the hilum, and the branches are divided successively into lobar bronchus, segmental bronchus, small bronchus, bronchioles, terminal bronchioles, respiratory bronchioles, alveolar ducts, alveolar sacs and alveoli. Because of the repeated divisions from the main bronchus peripherally, it is called the bronchial tree(Netter, 2014, Frank H. Netter, 2018).

From the lobar bronchus to the terminal bronchioles is the lung air conduction part. More distally is the lung respiratory part where alveolar cells appear in different degrees below the respiratory bronchioles(Netter, 2014, Frank H. Netter, 2018).

Each bronchiole, along with its branches and alveoli, constitutes a pulmonary lobule. The pulmonary lobules are conical, with the tip facing the hilum, the base facing the lung surface, and connective tissue separating adjacent pulmonary lobules. The contour of the base of the pulmonary lobules is visible on the surface of the lungs and is 1-2.5 cm in diameter. There are 50-80 pulmonary lobules in each lobe, they are the basic structural and functional units of the lung (Netter, 2014, Frank H. Netter, 2018, Ovalle William K., 2007).

A. Lung air conduction organisation

a. Lobar bronchus to small bronchus

The wall structure is similar to that of the main bronchus. The epithelium is a pseudostratified ciliated columnar epithelium, and the goblet cells, glands and cartilages are reduced. The smooth muscle fibres gradually increase more peripherally.

b. Bronchioles and terminal bronchioles

The epithelium gradually changes from pseudostratified ciliated columnar epithelium to single layer columnar epithelium. Goblet cells, glands and cartilages gradually disappear. Ringed smooth muscle is more pronounced, forming a complete circular smooth muscle layer. The ciliated cells in the terminal bronchioles are reduced. The cells are mainly cilia-free Clara cells, which have smooth surfaced endoplasmic reticulum and detoxification function.

B. Lung respiratory organisation

a. Respiratory bronchioles

A small number of alveoli appear on the wall of the tube, the epithelium are simple cuboidal epithelia which transition to simple squamous epithelia at the opening of the alveoli.

b. Alveolar ducts

The structure of the alveolar ducts' wall indistinct due to alveolus encroaching on the wall of the duct.

c. Alveolar sacs

Alveolar sacs are the common opening of several alveoli.

d. Pulmonary alveolus

The alveoli are semi-spherical small capsules with a diameter of about 200µm. They are open to the alveolar sac, alveolar duct or respiratory bronchioles. The alveoli are the part of the lung where gas is exchanged and constitute the main structure of the lung. The adult lung has 300-400 million alveoli, and the total surface area can reach 140m² while inhaling. The alveolar wall is very thin, and consists of a single layer of alveolar epithelium.

- Type I alveolar cells: are flat with a thickness of approximately 0.2µm, covering about 95% of the surface area of the alveoli. Type I alveolar cells are the site for gas exchange and have no proliferative capacity. If the type I alveolar cells is

damaged, then the type II alveolar cells will differentiate to supplement.

- Type II alveolar cells: are cubic or round and scattered between type I alveolar cells, covering 5% of the alveolar surface area. Type II alveolar cells are rich in mitochondria, lysosomes, rough surfaced endoplasmic reticulum and Golgi bodies. They have many secretory granules constituting the lamellar body and secrete the contents of the lamellar body via the mechanism of exocytosis to produce surfactant on the surface of the alveolar cells, which could reduce the surface tension of the alveoli.

e. Alveolar septum

The connective tissue between adjacent alveoli is called the alveolar septum, which contains fibroblasts, pulmonary macrophages, capillary lymphatic vessels and nerve fibres.

f. Pulmonary macrophage

Pulmonary macrophages are differentiated from monocytes in the blood and are widely distributed in the pulmonary stroma. Pulmonary macrophages have an active phagocytic function and play an important role in immune defence.

g. Alveolar pore

The alveolar pores are small holes for gas communication between the alveoli.

h. Blood-air barrier

The blood-air barrier is a structure through which the gas exchange between the alveoli and blood occurs with a thickness of 0.2-0.5µm, consisting of the surfactant layer, type I alveolar cell and its basement membrane, thin connective tissue, capillary basement membrane and continuous capillary endothelium (Ovalle William K., 2007).

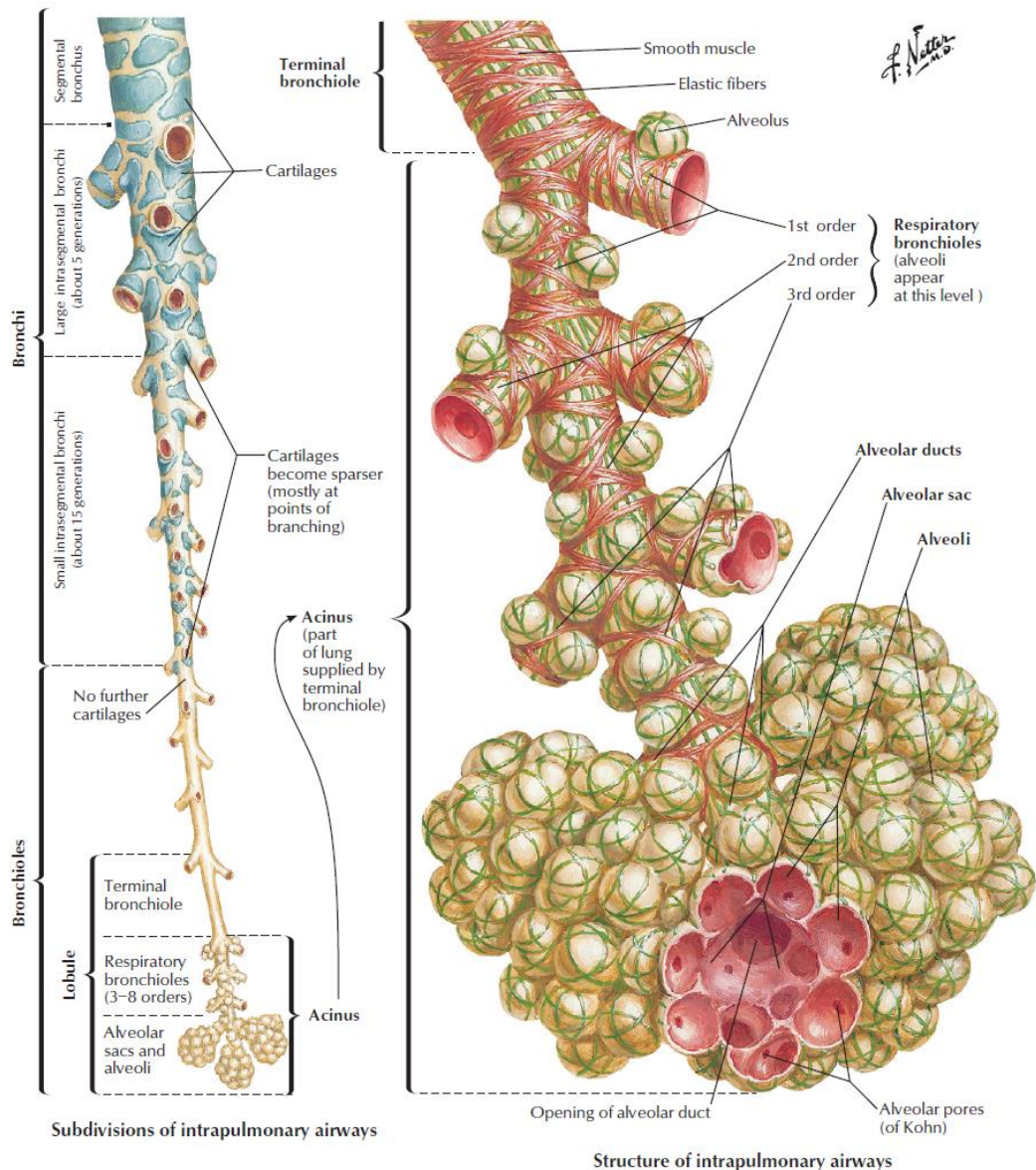


Figure 1.3: Intrapulmonary airway: schema. Atlas of Human Anatomy, Sixth Edition, 2014. Frank H. Netter, MD (Netter, 2014).

1.1.2.1 Blood supply to the lungs

The blood supply to the lungs comes from the pulmonary and bronchial arteries. The pulmonary arteries carry deoxygenated blood to the lungs whilst the bronchial arteries carry oxygenated blood to the lungs (Henry Gray, 2010).

1.1.2.2 Development of lung

At the fourth week of embryonic development lung buds appear. These are the primordial origins of the main bronchi and lungs. By the fifth week, the left and right lung buds are divided into two and three parts respectively, which would form the segmental bronchi of the left and right lungs. At the end of the second month, the lobar bronchi of the lungs form the segmental bronchus. At the end of the sixth month, terminal bronchus, respiratory bronchioles and a small number of alveoli appears. In the seventh month, the number of alveoli increases. A few weeks before birth, the lungs mature rapidly, the alveoli become larger, the alveolar wall becomes thinner, and alveolar surfactant is produced (Moore, 2011).

1.1.3 Lung cancer

1.1.3.1 Epidemiology of lung cancer

1.1.3.1.1 Incidence and mortality

Lung cancer is the leading cause of both cancer incidence and mortality worldwide. In 2018, it was estimated that there are 2,093,876 new cases of lung cancer. This accounts for 11.6% of all cancers. Estimated age-standardized rate (ASR) of incidence for lung cancer in 2018 was 22.5 per 100,000 person-years, ranking third place among all cancers. In males, both the estimated number of cases (1,368,524) and ASR of incidence (31.5 per 100,000 person-years) were the highest, and in females the estimated number of cases for lung cancer (725,352) and ASR of incidence (14.6 per 100,000 person-years) ranked third, after female breast cancer and colorectal (**Figure 1.4**) (Bray et al., 2018).

Regardless of the estimated number of deaths or ASR of mortality, lung cancer is the highest rate of cancer, both in the general population (1,761,007, 18.6 per 100,000 person-years) particularly in males (1,184,947, 27.1 per 100,000 person-years). In female patients, the mortality rate of lung cancer is only lower than that of breast cancer, with the estimated number of deaths of 57,606 and ASR of mortality of 11.2 per 100,000 person-years (**Figure 1.5**) (Bray et al., 2018).

In the UK, lung cancer is the 3rd most common cancer accounting for 13% in 2015. There were 46,700 newly diagnosed lung cancer patients every year from 2013 to 2015. Both in males and females in the UK, lung cancer is the 2nd most common cancer with the number of new cases of 24,500 in male and 21,900 in female in the year of 2015. Around 35,600 people died of lung cancer in the UK each year between 2014 and 2016; in 2016, 21% of cancer deaths were as a consequence of lung cancer. Lung cancer caused the most deaths in males (19,300) and females (16,300) in 2016 (Bray et al., 2018, Smittenaar et al., 2016).

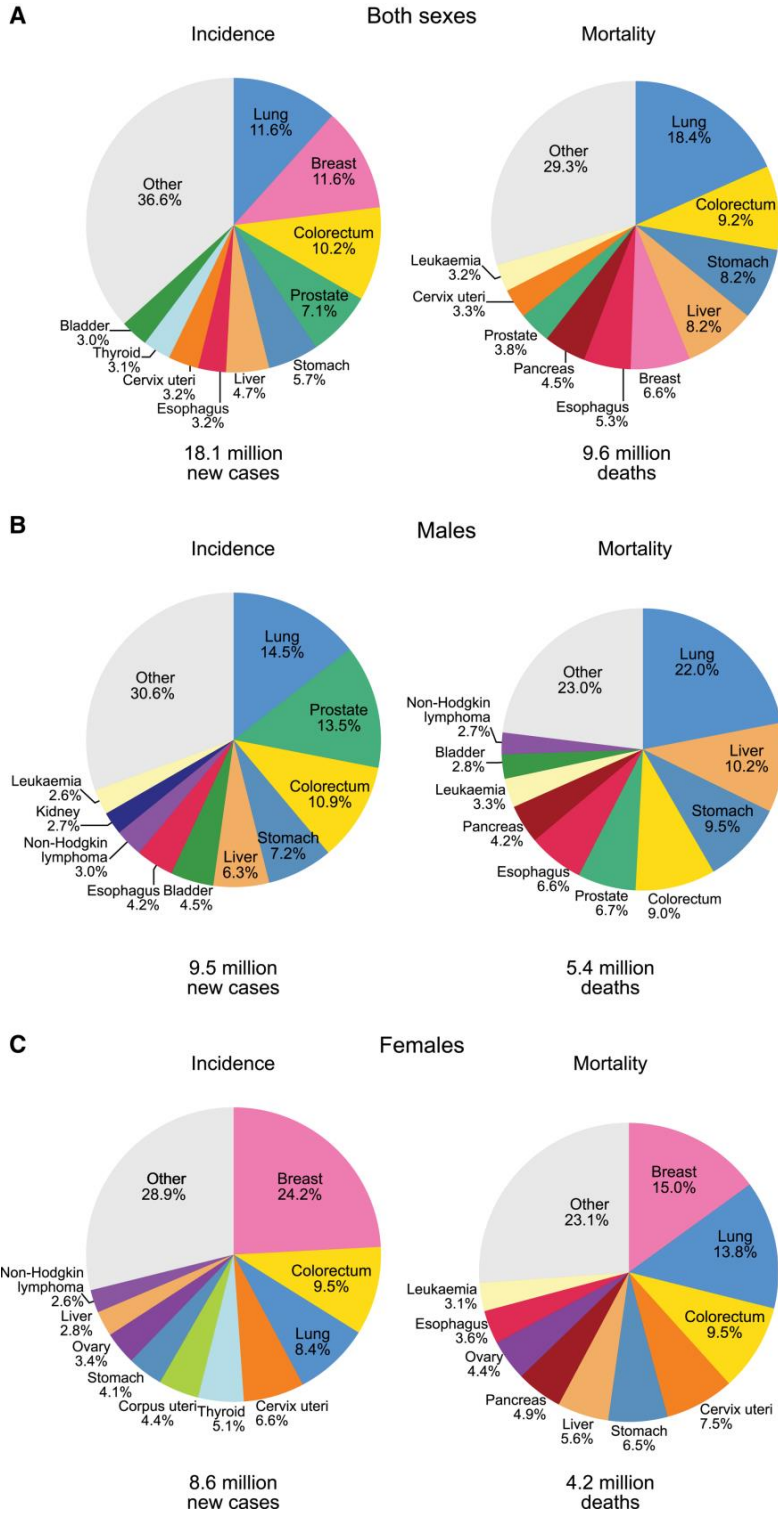


Figure 1.4: Pie Charts Present the Distribution of the number of Cases and Deaths for the 10 Most Common Cancers in 2018 for (A) Both Sexes, (B) Males, and (C) Females (Bray et al., 2018).

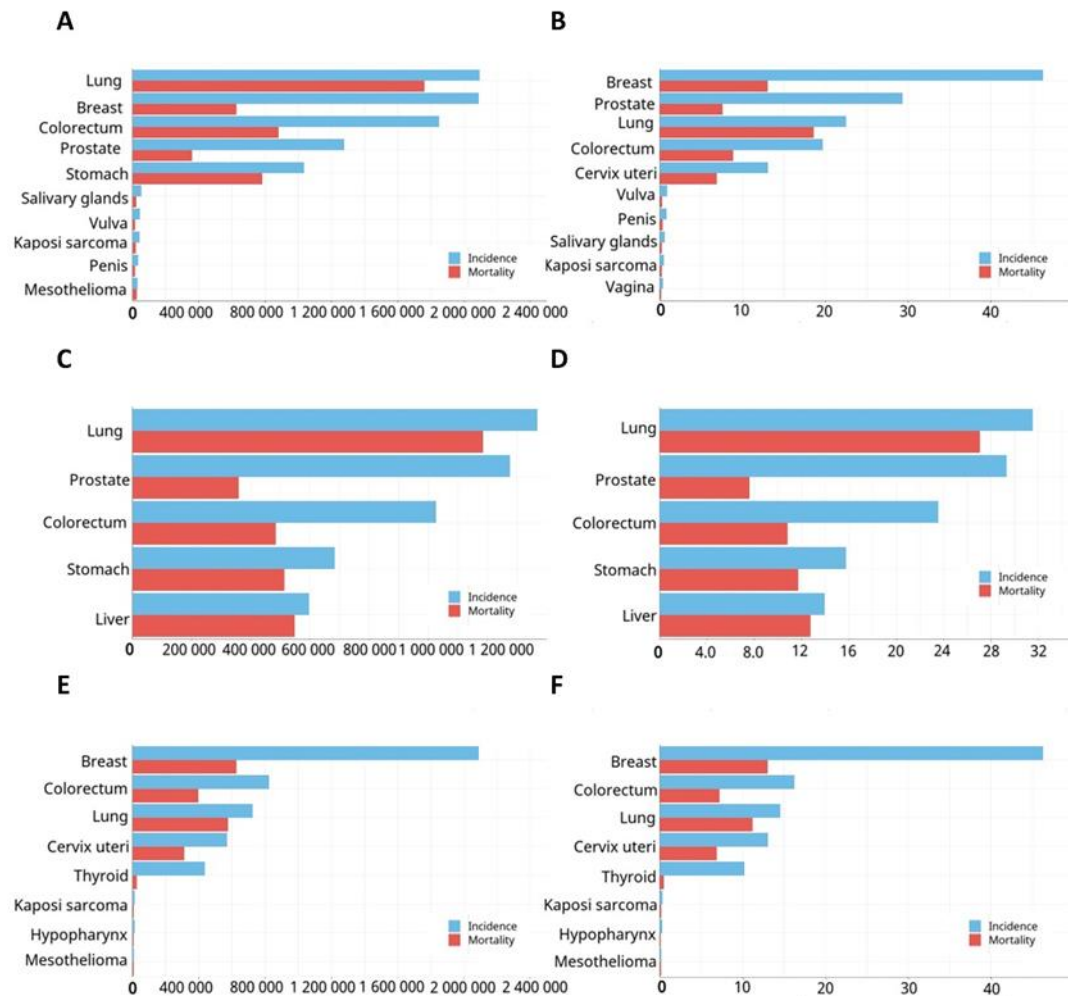


Figure 1.5: Incidence and mortality of lung cancer (Bray et al., 2018). (A) Estimated number of new cases and deaths in 2018 in both sexes. (B) Estimated ASR of new cases and deaths in 2018 in both sexes. (C) Estimated number of new cases and deaths in 2018 in male. (D) Estimated ASR of new cases and deaths in 2018 in male. (E) Estimated number of new cases and deaths in 2018 in female. (F) Estimated ASR of new cases and deaths in 2018 in the female.

1.1.3.1.2 Geographic Variation

Generally, incidence and mortality are higher in developed regions such as North America and Europe, whereas relatively low incidence and mortality are found in Oceania and Asia. The top 5 countries with the highest age standardized incidence and mortality rates are Hungary (56.7 per 100,000 for incidence rate and 44.4 per 100,000 for mortality rate, which is the highest in the world), Serbia, France New Caledonia, Greece and French Polynesia. Most of the countries with high incidence

and mortality rates are located in Europe and Oceania (**Figure 1.6**) (Bray et al., 2018).

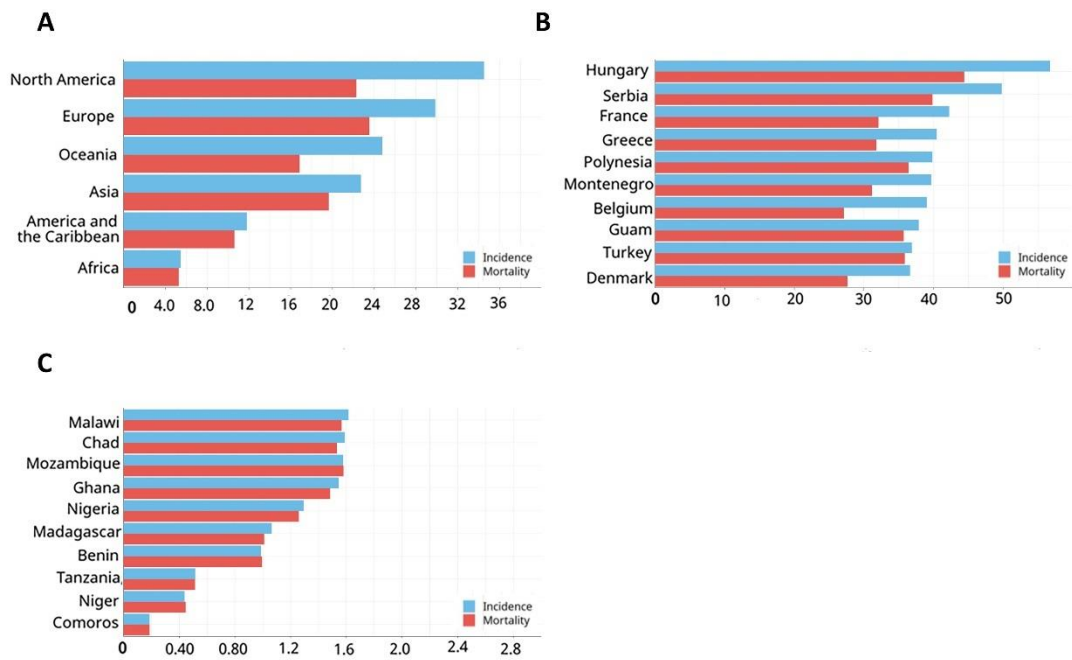


Figure 1.6: Geographic Variation of lung cancer in different countries (Bray et al., 2018). (A) Estimated ASR of new cases and deaths of lung cancer in 2018 in different continents. (B) Estimated top 10 ASR of new cases and deaths of lung cancer in 2018 in different countries. (C) Estimated bottom 10 ASR of new cases and deaths of lung cancer in 2018 in different countries.

Due to the large population base in Asian countries, especially in China, even though the incidence and mortality rates of lung cancer is not the highest in Asia compared to other continents, the number of new cases and deaths are the highest in the world. In 2018, the estimated number of new lung cancer cases in Asia was 1,225,029 and the number of deaths 1,068,862, accounting for 58.5% and 60.7% of the total number, exceedingly twice that of Europe (the number of new cases being 470,039 22.4%, deaths 387913 22%). The continents with the fewest number of new cases and deaths were Oceania and Africa; in Oceania there were only 16,937 reported new cases and 11,822 reported deaths (**Figure 1.7**) (Bray et al., 2018).

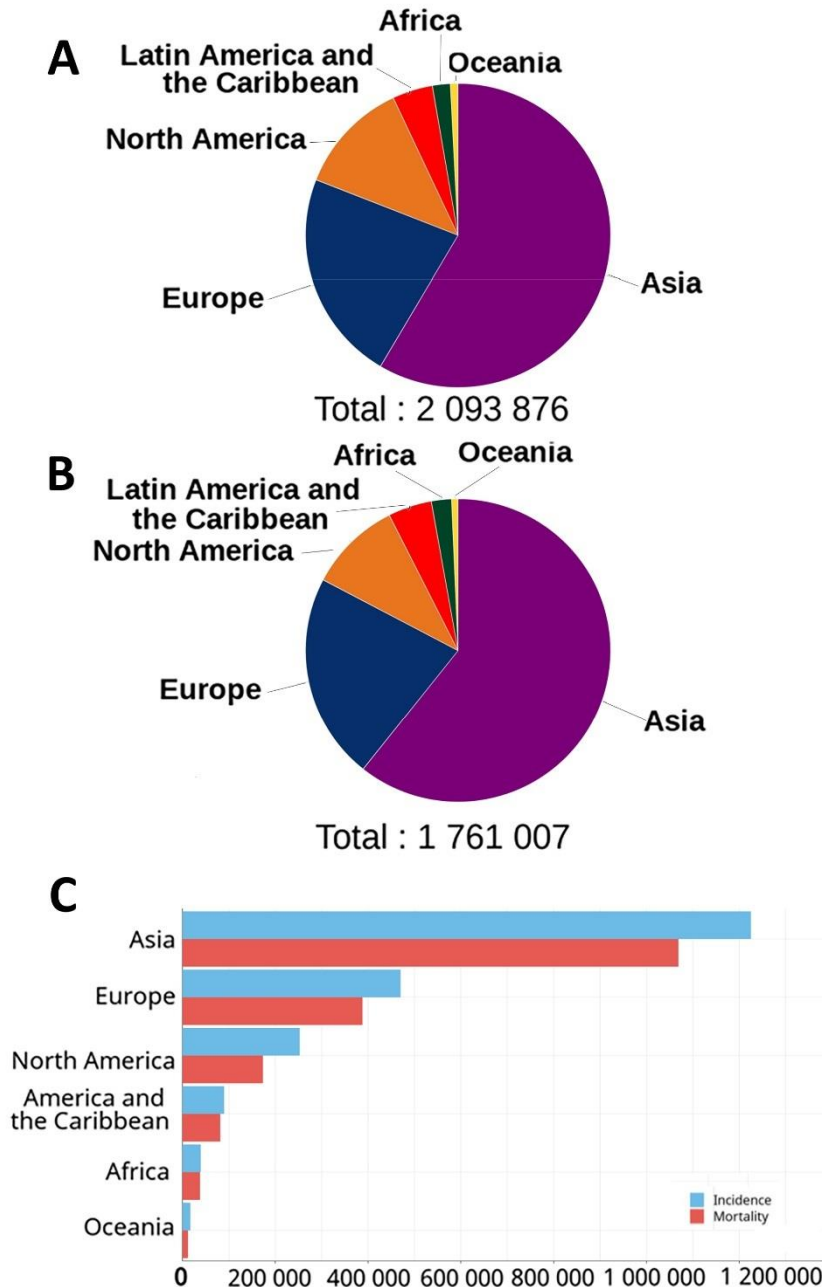


Figure 1.7: Geographic Variation of lung cancer in different continents (Bray et al., 2018). (A) Estimated numbers of new cases of lung cancer in 2018 in different continents. (B) Estimated numbers of deaths of lung cancer in 2018 in different continents. (C) Estimated number of new cases and deaths of lung cancer in 2018 in different continent.

There seems no doubt that China has the highest number of new cases of and deaths from lung cancer in the world. The number of new cases in China was 774,323 and the number of deaths 690,567, accounting for 37% and 39.2%, these ratios exceeding the proportion of China's population to the world's population. The USA, Japan and India are the second to fourth countries with the highest newest cases of

and deaths from lung cancer. In addition, the incidence of and mortality from lung cancer are relatively high in Germany, Russia, UK and France. Almost all of the countries with the greatest numbers of lung cancer are located in Asia and Europe, whilst the countries with lesser cases of lung cancer are in Africa, such as Comoros, Vanuatu and Sao Tome and Principe (**Figure 1.8**) (Bray et al., 2018).

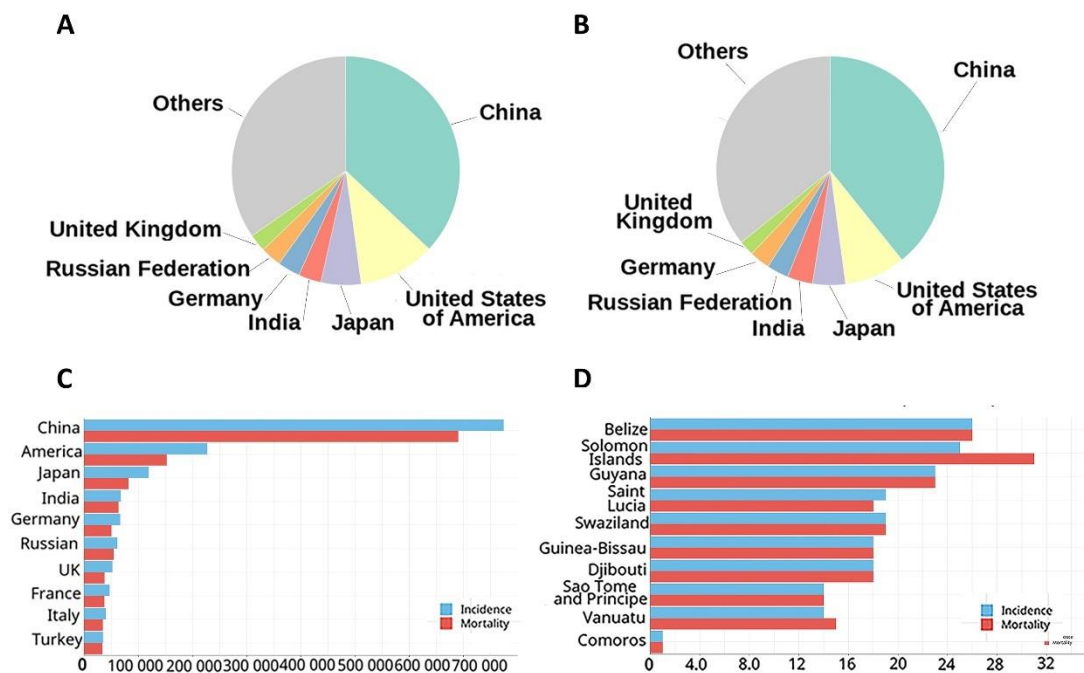


Figure 1.8: Countries with the most new-cases and deaths of lung cancer (Bray et al., 2018). (A) Estimated number of countries with the most new-cases of lung cancer in 2018. (B) Estimated number of countries with the most deaths of lung cancer in 2018. (C) Estimated number of countries with the most new-cases and deaths of lung cancer in 2018. (D) Estimated number of countries with the fewest new cases and deaths of lung cancer in 2018.

1.1.3.2 Aetiology of lung cancer

1.1.3.2.1 Tobacco smoke

Tobacco smoking is the most common cause of lung cancer. In the UK, 72% of lung cancer patients are associated with smoking, where 71% are caused by active smoking and 1% are caused by environmental tobacco smoke (Bray et al., 2018,

Brown et al., 2018). It is estimated that 86% of lung cancer deaths in the UK are caused by smoking (Bray et al., 2018). People who smoke more than 400-600 cigarettes a year have a significantly increased risk of lung cancer. Compared with people who never smoke, those who smoke more than 5500 cigarettes a year are 26 times more likely to develop lung cancer (Bray et al., 2018, Doll et al., 2005, Darby et al., 2005). Smoking is strongly associated with the risk of small cell lung cancer and squamous cell carcinoma (SCC) as compared with other types of lung cancer (Khuder, 2001, Pesch et al., 2012).

Smoking cessation has significant health benefits and can improve life expectancy compared to permanent smokers even for long-term smokers, older smokers and those people who quit smoking after lung cancer diagnosis, (Bray et al., 2018).

1% of lung cancer cases in the UK are caused by environmental tobacco smoke (ETS, also known as second-hand smoke). It is estimated that 15% of lung cancer cases in the UK are developed by those who have never smoked are related to ETS (Bray et al., 2018, Brown et al., 2018). Studies have shown that non-smokers who are exposed to ETS have a 31% higher risk of lung cancer than those who have not been exposed to ETS (Bray et al., 2018, Kim et al., 2014). The risk of lung cancer among non-smokers has doubled in people with the highest levels of exposure to ETS in the workplace compared to those who do not (Bray et al., 2018, Stayner et al., 2007).

The development of lung cancer requires decades of long-term smoking; the demographic effects of e-cigarettes may not show up until the middle of this century. Currently there is little evidence to determine whether the impact of e-cigarettes is less than that of combustible tobacco products in terms of promoting lung cancer (Gotts et al., 2019).

1.1.3.2.2 Ionising radiation

Ionising radiation can be either occupational or non-occupational; this exposure can be from ionising radiation from outside the body, as well as *in vivo* radiation caused

by inhalation of radioactive dust and gases. In the UK, ionising radiation causes approximately 5% of lung cancer cases (Bray et al., 2018, Brown et al., 2018). It is estimated that 9% of lung cancer deaths across Europe are associated with exposure to indoor radon (Bray et al., 2018, Darby et al., 2005).

1.1.3.2.3 Air pollution

a. Outdoor air pollution

Industrial waste gas, vehicle exhaust and road asphalt in cities all have carcinogens. In the UK, 8% of lung cancer patients are caused by air pollution (Bray et al., 2018, Brown et al., 2018). Studies have shown that for every 10µg/m³ of PM 2.5 (fine particulate matter, PM) air pollution, the risk of lung adenocarcinoma is 40% higher and the risk of lung adenocarcinoma is 29% higher per 10µg/m³ of PM 10 air pollution (Bray et al., 2018, Hamra et al., 2014).

b. Indoor air pollution

A meta-analysis primarily from China revealed that people who use coal for cooking or heating at home have double the risk of having lung cancer (Bray et al., 2018, Hosgood et al., 2011, Kurmi et al., 2012).

1.1.3.2.4 Occupational carcinogens

In the UK, 13% of lung cancer cases are related to workplace exposure (Bray et al., 2018, Brown et al., 2018). Asbestos, silica, diesel engine exhaust, TCDD (2,3,7,8-tetrachlorodibenzo-para-dioxin), radon, mineral oils, arsenic and inorganic arsenic compounds are all common occupational carcinogens associated with lung cancer and working as a painter or welder also carries an increased risk (Bray et al., 2018).

1.1.3.2.5 Family history

A meta-analysis showed that lung cancer risk is 82% higher in people whose sibling has/had lung cancer and 25-37% higher in people whose parent has/had lung cancer (Bray et al., 2018, Cote et al., 2012).

1.1.3.3 Classification of lung cancer

1.1.3.3.1 General classification

According to the distribution of tumours in the lungs, lung cancer may be allocated to three main types: central type, peripheral type and diffuse type.

- Central type lung cancer occurs in the main bronchus or lobar bronchus, forming a mass in the hilum. Central type cancer is the most common lung cancer, accounting for 60% -70% of the total numbers of lung cancer.
- Peripheral lung cancer originates from the segmental bronchi or distal bronchi, forming nodular or spherical tumours in the peripheral part of the lung close to the lung membrane. The relationship with the bronchus is not obvious. It accounts for 30%-40% of the total number of lung cancers.
- Diffuse lung cancer is rare, accounting for only 2% to 5% of lung cancers. It is easily confused with lung metastatic tumours (Travis, 2015).

1.1.3.3.2 Histopathological classification

The histopathological features of lung cancer are complex and diverse. Lung cancer can be divided into two major types: small cell lung cancer (SCLC) and non-small cell lung cancer (NSCLC). Any types of epithelial lung cancer other than SCLC belong to NSCLC, which accounts for more than 85% of all lung cancers. SCLC is less common but more aggressive than NSCLC. SCLC is usually lacking early symptom, which means once symptoms do appear, it often indicates that the cancer has metastasized. Consequently, the prognosis of SCLC is worse than NSCLC (Herbst et al., 2018,

Jamal-Hanjani et al., 2017).

According to the 2015 WHO classification of tumours of the lung, all the lung carcinoma can be subdivided into: adenocarcinoma, squamous cell carcinoma, neuroendocrine tumours, large cell carcinoma, adenosquamous carcinoma, sarcomatoid carcinoma, carcinosarcoma, pulmonary blastoma, papillomas, adenomas, *et al.* In addition to primary pulmonary carcinoma, tumours of the lung include mesenchymal tumours, lymphohistiocytic tumours, tumours of ectopic origin and metastatic tumours (Travis et al., 2015a, Travis et al., 2015b) (**Table 1.1**).

Table 1.1: WHO Classification of Tumours of the Lung, Pleura, Thymus and Heart. Fourth edition(Travis et al., 2015a).

Epithelial Tumours		Papillomas	
Adenocarcinoma	8140/3	Squamous cell papilloma	8052/0
Lepidic adenocarcinoma	8250/3*	Exophytic	8052/0
Acinar adenocarcinoma	8551/3*	Inverted	8053/0
Papillary adenocarcinoma	8260/3	Glandular papilloma	8260/0
Micropapillary adenocarcinoma	8265/3	Mixed squamous cell and glandular papilloma	8560/0
Solid adenocarcinoma	8230/3	Adenomas	
Invasive mucinous adenocarcinoma	8253/3*	Sclerosing pneumocytoma	8832/0
Mixed invasive mucinous and non-mucinous adenocarcinoma	8254/3*	Alveolar adenoma	8251/0
Colloid adenocarcinoma	8480/3	Papillary adenoma	8260/0
Fetal adenocarcinoma	8333/3	Mucinous cystadenoma	8470/0
Enteric adenocarcinoma	8144/3	Mucous gland adenoma	8480/0
Minimally invasive adenocarcinoma		Mesenchymal tumours	
Non-mucinous	8250/2*	Pulmonary hamartoma	8992/0
Mucinous	8257/3*	Chondroma	9220/0
Preinvasive lesions		PEComatous tumours	
Atypical adenomatous hyperplasia	8250/0*	Clear cell tumour	8005/0
Adenocarcinoma in situ		Lymphangioleiomyomatosis	9174/1
Non-mucinous	8410/2	PEComa, benign	8714/0
Mucinous	8253/2	Congenital peribronchial myofibroblastic tumour	8827/1
Squamous cell carcinoma	8070/3	Diffuse pulmonary lymphangiomatosis	
Keratinizing squamous cell carcinoma	8071/3	Inflammatory myofibroblastic tumour	8825/1
Non-keratinizing squamous cell carcinoma	8072/3	Epithelioid haemangioendothelioma	9133/3
Basaloid squamous cell carcinoma	8083/3	Pleuropulmonary blastoma	8973/3
Preinvasive lesion		Synovial sarcoma	9040/3
Squamous cell carcinoma in situ	8070/2	Pulmonary artery intimal sarcoma	9137/3
Neuroendocrine Tumours		Pulmonary myxoid sarcoma with EWSR1-CREB1 translocation	8842/3*
Small cell carcinoma	8041/3	Myoepithelial tumours	
Combined small cell carcinoma	8045/3	Myoepithelioma	8982/0
Large cell neuroendocrine carcinoma	8013/3	Myoepithelial carcinoma	8982/3
Combined large cell neuroendocrine carcinoma	8013/3	Lymphohistiocytic tumours	
Carcinoid tumours		Extranodal marginal zone lymphoma of mucosa-associated lymphoid tissue (MALT lymphoma)	9699/3
Typical carcinoid tumour	8240/3	Diffuse large B-cell lymphoma	9680/3
Atypical carcinoid tumour	8249/3	Lymphomatoid granulomatosis	9766/1
Preinvasive lesion		Intravascular large B-cell lymphoma	9680/3
Diffuse idiopathic pulmonary neuroendocrine cell hyperplasia	8040/0*	Pulmonary Langerhans cell histiocytosis	9751/1
Large cell carcinoma	8012/3	Erdheim-Chester disease	9750/1
Adenosquamous carcinoma	8560/3	Tumours of ectopic origin	
Sarcomatoid carcinoma	8033/3	Germ cell tumours	
Pleomorphic carcinoma	8022/3	Teratoma mature	9080/0
Spindle cell carcinoma	8032/3	Teratoma immature	9080/1
Giant cell carcinoma	8031/3	Intrapulmonary thymoma	8580/3
Carcinosarcoma	8980/3	Melanoma	8720/3
Pulmonary blastoma	8972/3	Meningioma, NOS	9530/0
Other and unclassified carcinomas		Metastatic tumours	
Lymphoepithelioma-like carcinoma	8082/3		
NUT carcinoma	8023/3*		
Salivary gland-type tumours			
Mucoepidermoid carcinoma	8430/3		
Adenoid cystic carcinoma	8200/3		
Epithelial-myoepithelial carcinoma	8562/3		
Pleomorphic adenoma	8940/0		

1.1.3.3.2.1 Lung adenocarcinoma (LUAD)

Adenocarcinomas have glandular differentiation, mucin production, or lung cell marker expression. LUAD Tumours usually have acinar, papillary, micropapillary, squamous, or solid growth, with mucin or lung cell marker expression such as TTF1 and Napsin A (Travis et al., 2015b, Travis et al., 2015a).

a. Invasive mucinous adenocarcinoma. Invasive mucinous adenocarcinoma is one type of adenocarcinoma including formerly classified as mucinous bronchioloalveolar carcinoma. The tumour cells are goblet or columnar morphologically with much intracytoplasmic mucin. The growth pattern could be lepidic (most common), acinar, papillary, or micropapillary, except solid.

b. Colloid adenocarcinoma. Colloid adenocarcinoma has abundant mucin pools intracellular covering air spaces.

c. Foetal adenocarcinoma. Foetal adenocarcinoma is an adenocarcinoma which resembles foetal lung. The tumours of lower grade are purer but high-grade tumours usually have more than 50% foetal morphology.

d. Enteric adenocarcinoma. Enteric adenocarcinoma is an adenocarcinoma that has some features resembling the adenocarcinomas arising in the colorectum.

e. Minimally invasive adenocarcinoma. Minimally invasive adenocarcinoma (MIA) is a small (less than 3cm, and invasion dimension less than 5cm), solitary adenocarcinoma. MIA is predominantly lepidic in pattern, solitary and discrete, but rarely mucinous.

f. Atypical adenomatous hyperplasia. Atypical adenomatous hyperplasia is a small (usually less than 0.5 cm in size) localized proliferation. Atypical adenomatous hyperplasia has atypical type II pneumocytes and/or Clara cells growing mildly to moderately lining the alveolar walls and sometimes respiratory bronchioles.

g. Adenocarcinoma in situ. Adenocarcinoma in situ (AIS) is a small (usually less than 3 cm in size), localized adenocarcinoma with pure lepidic growth limited to neoplastic cells along pre-existing alveolar structures. Generally, AIS lacks stroma, vascular or pleural invasion, meanwhile the acinar, papillary, solid or micropapillary invasion and intra-alveolar tumour cells are usually absent. AIS is mostly non-mucinous, but rare mucinous cases occur.

1.1.3.3.2.2 Squamous cell carcinoma (LUSC)

Squamous cell carcinoma has features of either keratinization and/or intercellular bridges, or is a morphologically undifferentiated NSCLC with squamous cell differentiation markers under immunohistochemical test (Travis et al., 2015b, Travis et al., 2015a).

a. Basaloid squamous cell carcinoma. Basaloid squamous cell carcinoma is a poorly differentiated malignant epithelial tumour. Basaloid squamous cell carcinoma proliferates as small cells with lobular architecture and peripheral palisading, and normally lacking squamous morphology but expressing typical immunohistochemical squamous markers. Basaloid squamous cell carcinoma usually contains keratinizing or non-keratinizing squamous cell components. This type used to be considered as a variant of large cell carcinoma, but was recognized as a different type after the 2nd version WHO classifications in 1999 (Travis et al., 2015b, Travis et al., 2015a).

b. Squamous cell carcinoma in situ. Squamous dysplasia is a precursor lesion of squamous cell carcinoma existing in the bronchial epithelium. Squamous dysplasia as well as the carcinoma in situ are continuous parts of recognizable histological changes in the large airways. Dysplasia can be found as single or multifocal lesions throughout the whole tracheobronchial tree (Travis et al., 2015b, Travis et al., 2015a).

1.1.3.3.2.3 Neuroendocrine tumours

a. Small cell carcinoma (Small Cell Lung Cancer, SCLC). Small cell carcinoma is a poorly differentiated type of neuroendocrine lung cancer, which is a malignant epithelial tumour consisting of small cells with scant cytoplasm, ill-defined cell borders finely dispersed granular nuclear chromatin, and absent or inconspicuous nucleoli. Morphologically, the cells are round, oval, or spindle-shaped. Nuclear moulding is prominent. Extensive necrosis is typically found in SCLC, and the mitotic count is high. Most small cell carcinomas express neuroendocrine markers. Combined small cell carcinoma can have an additional component, which could be any of the

histological types of NSCLC, such as adenocarcinoma, squamous cell carcinoma, large cell carcinoma, or large cell neuroendocrine carcinoma, or less commonly spindle cell carcinoma or giant cell carcinoma (Travis et al., 2015b, Travis et al., 2015a).

b. Large cell neuroendocrine carcinoma (LCNEC). Large cell neuroendocrine carcinoma belongs to NSCLC with typical histological neuroendocrine morphology features like rosettes and peripheral palisading, and immunohistochemical neuroendocrine markers. Like SCLC, there also exists combined LCNEC with components of adenocarcinoma, squamous cell carcinoma, or spindle cell carcinoma, and/or giant cell carcinoma (Travis et al., 2015b, Travis et al., 2015a).

c. Carcinoid tumour. Carcinoid tumours are neuroendocrine epithelial malignancies, which can be divided into two subtypes: typical and atypical carcinoids. typical carcinoids are tumours with less than 2 mitoses per 2 mm², and lacking necrosis. The size usually measures more than 0.5 cm. Atypical carcinoids require tumours having 2–10 mitoses per 2 mm², and/or foci of necrosis (Travis et al., 2015b, Travis et al., 2015a).

1.1.3.3.2.4 **Large cell carcinoma**

Large cell carcinoma is an undifferentiated non-small cell lung cancer lacking the cytological, architectural, and immunohistochemical features of small cell carcinoma, adenocarcinoma, or squamous cell carcinoma. The diagnosis requires a thoroughly sampled resected tumour, and cannot be made on non-resection or cytology specimens such as free cancer cells (Travis et al., 2015b, Travis et al., 2015a).

1.1.3.3.2.5 **Adenosquamous carcinoma**

Adenosquamous carcinoma is a carcinoma showing components of both LUSC and LUAD, with each component constituting at least 10% of the tumour. A resection

specimen is required for definitive diagnosis(Travis et al., 2015b, Travis et al., 2015a).

1.1.3.3.3 Molecular classification and biomarkers

With the successive identification of a series of cancer-driver genes for lung cancer, multiple studies have shown that targeted therapy and immunotherapy drugs have greatly improved prognosis and prolonged the survival of lung cancer patients carrying the corresponding driver genes. The classification of lung cancer is also further subdivided into molecular subtypes based on driver genes in addition to the previous simple histopathological classification (**Table 1.2**) (Herbst et al., 2018, Chen et al., 2014).

Table 1.2: Major genetic changes and molecular biomarkers work as check points for diagnosis and molecular classification in SCLC and two major type of NSCLC(Travis et al., 2015b).

Alterations	Small cell carcinoma (%)	Adenocarcinoma (%)	Squamous cell carcinoma (%)
Mutation			
<i>BRAF</i>	0%	< 5%	0%
<i>EGFR</i> Caucasian	< 1%	10–20%	< 1%
Asian	< 5%	35–45%	< 5%
<i>ERBB2/HER2</i>	0%	< 5%	0%
<i>KRAS</i> Caucasian	< 1%	15–35%	< 5%
Asian	< 1%	5–10%	< 5%
<i>PIK3CA</i>	< 5%	< 5%	5–15%
<i>RB</i>	> 90%	5–15%	5–15%
<i>TP53</i>	> 90%	30–40%	50–80%
Amplification			
<i>EGFR</i>	< 1%	5–10%	10%
<i>ERBB2/HER2</i>	< 1%	< 5%	< 1%
<i>MET</i>	< 1%	< 5%	< 5%
<i>MYC</i>	20–30%	5–10%	5–10%
<i>FGFR1</i>	< 1%	< 5%	15–25%
Gene rearrangement			
<i>ALK</i>	0%	5%	< 1%
<i>RET</i>	0%	1–2%	0%
<i>ROS1</i>	0%	1–2%	0%
<i>NTRK1</i>	0%	< 1%	0%
<i>NRG1</i>	0%	< 1%	0%

All NSCLC patients, regardless of their clinical characteristics (history of smoking, gender, race, etc), should be routinely tested for EGFR (epidermal growth factor receptor) mutations, ALK (anaplastic lymphoma kinase) fusions, and ROS1 (ROS proto-oncogene 1) fusions. EGFR mutation detection should cover EGFR 18, 19, 20, and 21 exons. Other gene mutations that can be used as therapeutic targets include KRAS (KRAS proto-oncogene) mutation, HER2 (human epidermal growth factor receptor 2) mutation, BRAF (B-Raf proto-oncogene) mutation, RET (RET proto-oncogene) mutation, MET (MET proto-oncogene) mutation and amplification, etc.

(Figure 1.9)(Collisson et al., 2014, Hammerman et al., 2012, Sharma et al., 2007).

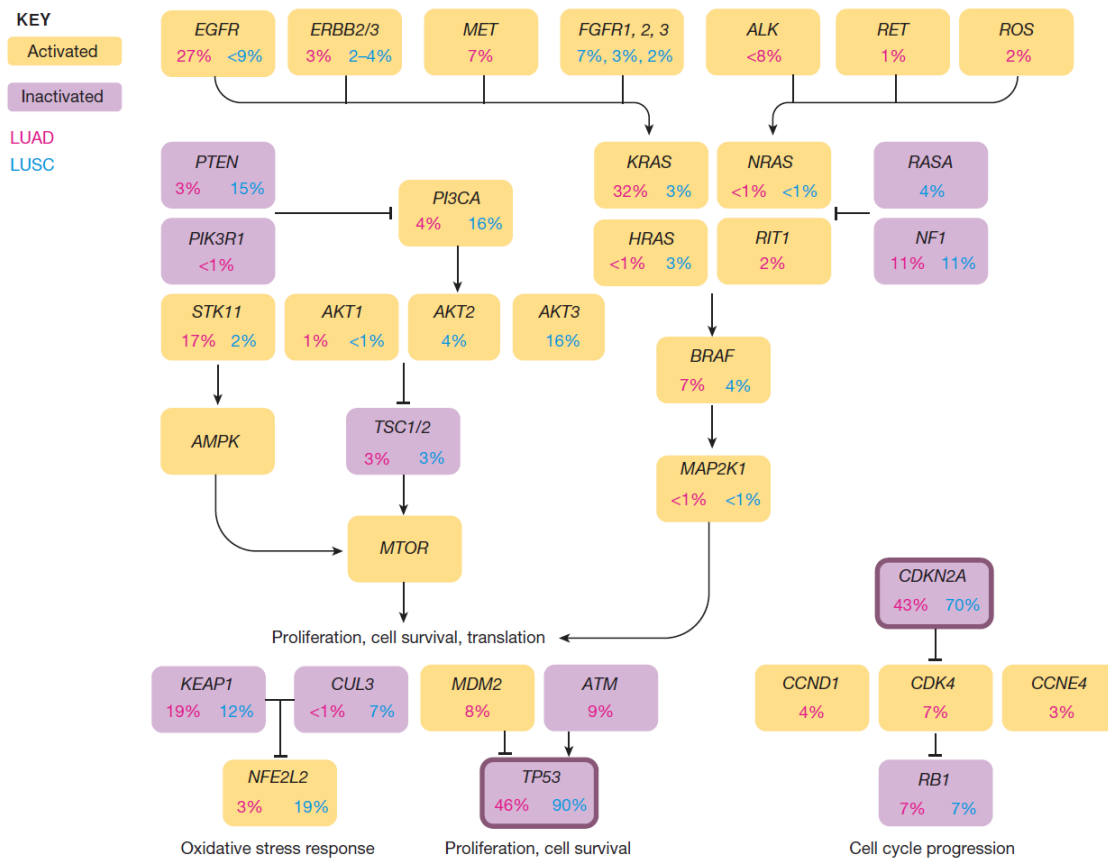


Figure 1.9: Alterations in targetable oncogenic pathways in LUAD (pink) and LUSC (blue) (Herbst et al., 2018). The activated mutation (yellow box) in EGFR, KRAS, ALK, MET and inactivated mutation (purple box) in PTEN, CDKN2A and TP53 are most common genetic changes in NSCLC.

Programmed death 1 (PD-1) is a key immune-checkpoint receptor which is expressed by activated T cells, and mediates immunosuppression. PD-1 functions primarily in peripheral tissues, where T cells may encounter the immunosuppressive PD-1 ligands PD-L1 and PD-L2, which are expressed by tumour cells. Inhibition of the interaction between PD-1 and PD-L1 can enhance T-cell responses *in vitro* and mediate preclinical antitumor activity. Immunotherapy checkpoints PD-1 and/or PD-L1 have been shown to be useful for the treatment of local or metastatic NSCLC. The detection of immunotherapy checkpoints could provide useful information for treatment (Sacher and Gandhi, 2016).

Tumour mutational burden (TMB) may predict the efficacy of immune checkpoint

inhibitors. It is feasible to estimate TMB using NGS (Next Generation Sequencing technology). When tissue specimens are insufficient, the use of cDNA (circulation DNA) to estimate TMB is a potentially feasible technique (Altorki et al., 2019, Herbst et al., 2018).

1.1.3.4 Staging of lung cancer

Accurate staging is one of the most important factors influencing the choice of treatment and prognosis of lung cancer. At the 16th World Lung Cancer Congress in Denver, USA, in September 2015, the International Association for The Study of Lung Cancer (IASLC) announced the newly revised TNM staging system for lung cancer (**Table 1.3, Table 1.4**) (Rami-Porta et al., 2015, Asamura et al., 2015, Eberhardt et al., 2015, Rami-Porta et al., 2014).

Table 1.3: Proposed T, N, and M descriptors for the eighth edition of TNM classification for lung cancer (Goldstraw et al., 2016).

T: Primary tumor	
Tx	Primary tumor cannot be assessed or tumor proven by presence of malignant cells in sputum or bronchial washings but not visualized by imaging or bronchoscopy
T0	No evidence of primary tumor
Tis	Carcinoma in situ
T1	Tumor ≤ 3 cm in greatest dimension surrounded by lung or visceral pleura without bronchoscopic evidence of invasion more proximal than the lobar bronchus (i.e., not in the main bronchus) ^a
T1a(mi)	Minimally invasive adenocarcinoma ^b
T1a	Tumor ≤ 1 cm in greatest dimension ^a
T1b	Tumor > 1 cm but ≤ 2 cm in greatest dimension ^a
T1c	Tumor > 2 cm but ≤ 3 cm in greatest dimension ^a
T2	Tumor > 3 cm but ≤ 5 cm or tumor with any of the following features ^c : <ul style="list-style-type: none"> - Involves main bronchus regardless of distance from the carina but without involvement of the carina - Invades visceral pleura - Associated with atelectasis or obstructive pneumonitis that extends to the hilar region, involving part or all of the lung
T2a	Tumor > 3 cm but ≤ 4 cm in greatest dimension
T2b	Tumor > 4 cm but ≤ 5 cm in greatest dimension
T3	Tumor > 5 cm but ≤ 7 cm in greatest dimension or associated with separate tumor nodule(s) in the same lobe as the primary tumor or directly invades any of the following structures: chest wall (including the parietal pleura and superior sulcus tumors), phrenic nerve, parietal pericardium
T4	Tumor > 7 cm in greatest dimension or associated with separate tumor nodule(s) in a different ipsilateral lobe than that of the primary tumor or invades any of the following structures: diaphragm, mediastinum, heart, great vessels, trachea, recurrent laryngeal nerve, esophagus, vertebral body, and carina
N: Regional lymph node involvement	
Nx	Regional lymph nodes cannot be assessed
N0	No regional lymph node metastasis
N1	Metastasis in ipsilateral peribronchial and/or ipsilateral hilar lymph nodes and intrapulmonary nodes, including involvement by direct extension
N2	Metastasis in ipsilateral mediastinal and/or subcarinal lymph node(s)
N3	Metastasis in contralateral mediastinal, contralateral hilar, ipsilateral or contralateral scalene, or supraclavicular lymph node(s)
M: Distant metastasis	
M0	No distant metastasis
M1	Distant metastasis present
M1a	Separate tumor nodule(s) in a contralateral lobe; tumor with pleural or pericardial nodule(s) or malignant pleural or pericardial effusion ^d
M1b	Single extrathoracic metastasis ^e
M1c	Multiple extrathoracic metastases in one or more organs

Table 1.4: Proposed stage groupings for the eighth edition of the TNM classification for lung cancer (Goldstraw et al., 2016).

Occult carcinoma	TX	N0	M0
Stage 0	Tis	N0	M0
<u>Stage IA1</u>	<u>T1a(mi)</u>	<u>N0</u>	<u>M0</u>
	<u>T1a</u>	<u>N0</u>	<u>M0</u>
<u>Stage IA2</u>	<u>T1b</u>	<u>N0</u>	<u>M0</u>
<u>Stage IA3</u>	<u>T1c</u>	<u>N0</u>	<u>M0</u>
Stage IB	T2a	N0	M0
Stage IIA	T2b	N0	M0
Stage IIB	<u>T1a-c</u>	<u>N1</u>	<u>M0</u>
	<u>T2a</u>	<u>N1</u>	<u>M0</u>
	T2b	N1	M0
	T3	N0	M0
Stage IIIA	<u>T1a-c</u>	<u>N2</u>	<u>M0</u>
	T2a-b	N2	M0
	T3	N1	M0
	T4	N0	M0
	T4	N1	M0
Stage IIIB	<u>T1a-c</u>	<u>N3</u>	<u>M0</u>
	T2a-b	N3	M0
	<u>T3</u>	<u>N2</u>	<u>M0</u>
	T4	N2	M0
<u>Stage IIIC</u>	<u>T3</u>	<u>N3</u>	<u>M0</u>
	<u>T4</u>	<u>N3</u>	<u>M0</u>
<u>Stage IVA</u>	<u>Any T</u>	<u>Any N</u>	<u>M1a</u>
	<u>Any T</u>	<u>Any N</u>	<u>M1b</u>
<u>Stage IVB</u>	<u>Any T</u>	<u>Any N</u>	<u>M1c</u>

1.1.3.5 Treatment of lung cancer

1.1.3.5.1 Surgery

In early stage lung cancer, surgery usually achieves an effective outcome. Indications for surgical treatment are for non-small cell lung cancers of stage I , II and selected stage IIIa (e.g. T3N1M0) (NCCN.org, 2020a). In patients with mediastinal lymph node metastasis (N2), surgery may be considered after chemotherapy or chemoradiotherapy. In stage IIIb and stage IV lung cancer, surgery should not be classified as the main treatment (NCCN.org, 2020a). In addition to tumour factors,

vital organs such as the heart and lungs of the patient must have sufficient functional reserves to withstand surgery. Anatomical lobectomy and lymph node dissection are the preferred surgical methods for lung cancer (Rami-Porta et al., 2005, NCCN.org, 2020a). Most small cell lung cancer has metastasis at the time of consultation, and surgical treatment is still controversial. Surgery should only be considered for patients with stage I (T1N0 or T2N0) SCLC where it has been confirmed that there is no involvement with the mediastinal lymph nodes. While stage 1 patients accounted for only 5% of all patients. Evidence suggests that SCLC patients with clinical stages of disease over T2N0 cannot benefit from surgery (NCCN.org, 2020b).

1.1.3.5.2 Chemotherapy

Chemotherapy includes neoadjuvant chemotherapy (preoperative chemotherapy), adjuvant chemotherapy (postoperative chemotherapy), maintenance chemotherapy, and palliative chemotherapy. Commonly used chemotherapeutic drugs include the platinum (carboplatin, cisplatin), gemcitabine, pemetrexed, taxanes (paclitaxel, docetaxel), vinorelbine, etoposide and camptothecin analogues (Irinotecan)(NCCN.org, 2020b, NCCN.org, 2020a). Non-small cell lung cancer is not sensitive to chemotherapy. The recommended first-line regimen for chemotherapy is a combination of two drugs containing cisplatin (NCCN.org, 2020a). Small cell lung cancer is very sensitive to chemotherapy and chemotherapy is the basic treatment for all SCLC patients. Many single-agent chemotherapy and combination chemotherapy regimens are effective in treating SCLC. Etoposide and cisplatin (EP) are the most commonly used initial combination chemotherapy regimens (NCCN.org, 2020b).

1.1.3.5.3 Radiotherapy

Radiation has a wide killing effect on cancer cells. Radiotherapy can be generally divided into radical radiotherapy and palliative radiotherapy. And the radical

radiotherapy contains adjuvant radiotherapy and neoadjuvant radiotherapy. Radiotherapy is usually combined with chemotherapy to treat lung cancer. Because of the differences in the stage of cancer and general condition for individual patients, the combined regimen can be concurrent chemoradiotherapy or sequential chemoradiotherapy. For NSCLC patients, all drugs can be used for sequential chemoradiotherapy regimens. However regimens for concurrent chemoradiotherapy may include cisplatin with etoposide or vinorelbine (NCCN.org, 2020a). For SCLC, combined chemoradiotherapy should comprise etoposide with cisplatin (NCCN.org, 2020b). Small cell lung cancer is most sensitive to radiotherapy, followed by squamous cell carcinoma and adenocarcinoma. Therefore, the dose of radiotherapy for SCLC should be the smallest and that for adenocarcinoma should be the largest (NCCN.org, 2020b, NCCN.org, 2020a).

1.1.3.5.4 Targeted therapy

Cytotoxic chemotherapy works as the historical standard treatment for NSCLC, but it has now faced a therapeutic bottleneck recently (Schiller et al., 2002). Molecular targeted drugs that inhibit the abnormal activation of signalling pathways which promote tumorigenesis have a significant role in the treatment of NSCLC and improvement of the prognosis of patients, and have gradually become a research hotspot (Herbst et al., 2008, Herbst et al., 2018). Therefore, accumulated trails in NSCLC targeted therapy are focusing on the use of drugs that inhibit various targets, especially epidermal growth factor receptor (EGFR) and anaplastic lymphoma kinase (ALK).

EGFR (epidermal growth factor receptor) gene mutation. EGFR belongs to the receptor tyrosine kinase (RTK) super-family on the surface of cells working as a mediators of extra-cellular signalling triggered by different growth factors (Sharma et al., 2007, Wu et al., 2017). The EGFR receptor consists of four domains in the extracellular region, a short extracellular juxtamembrane (eJM) region, a

transmembrane domain and a short intracellular juxtamembrane (iJM) region, following a tyrosine kinase domain with at least five tyrosine autophosphorylation sites, and a carboxy tail (Lemmon et al., 2014). EGFR binds to its activating ligands epidermal growth factor (EGF) and transforming growth factor- α (TGF α) leading to the dimerization of EGFR and trans-phosphorylation of the tyrosine residues in the carboxy tail, which could activate the downstream signalling pathways and correlates with malignant proliferation, survival, invasion, angiogenesis and metastasis of cancer (Hynes and Lane, 2005, Wheeler et al., 2010). Overexpression of EGFR was found in tumours of head and neck, ovary, cervix, bladder, oesophagus, stomach, brain, breast, colon and often associated with poor prognosis (Nicholson et al., 2001, Krause and Van Etten, 2005). In lung cancer, especially in NSCLC, retrospective analysis revealed EGFR overexpression was found in 40-85% of NSCLC cases and a high level of EGFR was associated with poor outcome (Fuster and Sandler, 2004, Nicholson et al., 2001, Ohsaki et al., 2000, Hirsch et al., 2003). In addition to amplification, various EGFR mutations also contribute to the development of NSCLCs which are seen in about 30-40% of Asian NSCLC patients and in about 10% of Caucasian NSCLC patients (Shigematsu et al., 2005). Heterozygous mutations in the tyrosine kinase domain clustering around the ATP binding pocket can activate EGFR and its downstream signalling independently, without the binding of the ligand. In NSCLC The most common mutations in EGFR are the exon 19 deletion (EGFR del19) and point missense mutations on exon 21 (EGFR L858R), which are also the target of EGFR inhibitors (EGFR tyrosine kinase inhibitors, TKI) (Sharma et al., 2007, Mitsudomi and Yatabe, 2007, Shi et al., 2014). Other mutations such as exon 19 insertion are also sensitive to TKI. Exon 20 insertion and p.T790M predict resistance to TKI. Commonly used TKIs include the first generation of TKI gefitinib, erlotinib, erlotinib, second generation TKI afatinib and third generation TKI osimertinib (NCCN.org, 2020a).

ALK (anaplastic lymphoma kinase, ALK) gene rearrangements. ALK is a receptor tyrosine kinase in NSCLC, with the most common fusion partner with ALK being

echinoderm microtubule-associated protein-like 4 (EML4). ALK-TKIs such as crizotinib, ceritinib, alectinib and brigatinib can be used for ALK rearrangement positive NSCLC (NCCN.org, 2020a).

Other mutations. ROS 1 (ROS proto-oncogene 1) gene rearrangements, BRAF(B-Raf proto-oncogene) point mutation and KRAS(KRAS proto-oncogene) point mutation are also seen in NSCLC, TKIs such as crizotinib, ceritinib, trametinib, dabrafenib can be used as targeted therapy (NCCN.org, 2020a).

1.1.3.5.5 Immunotherapy

In NSCLC tumours with programmed death ligand (PD-L1) positively expressed , an inhibitor such as pembrolizumab, nivolumab and atezolizumab can be used to block the binding of PD-1 and PD-L1 (NCCN.org, 2020a).

1.2 Metastasis of cancer

Tumour metastasis is a complex, multistage process in which cancer cells have to separate from the primary tumour, invade into adjacent tissue, migrate and travel through the circulatory system and then settle and proliferate in the distant tissue or organ forming the secondary disease (Cheung and Ewald, 2016, Talmadge and Fidler, 2010, Massague and Obenauf, 2016). Once formed, tumours begin the process of metastasis in order that malignant cancer cells can enter the vasculature which may occur well before the tumour is diagnosed (Massague and Obenauf, 2016). This is a major important cause of the high mortality in patients with cancer (Valastyan and Weinberg, 2011).

1.2.1 The invasion-metastasis cascade

The process of cancer metastasis consists of a succession of complex cellular

biological events collectively termed the metastatic cascade (**Figure 1.10**) (Valastyan and Weinberg, 2011):

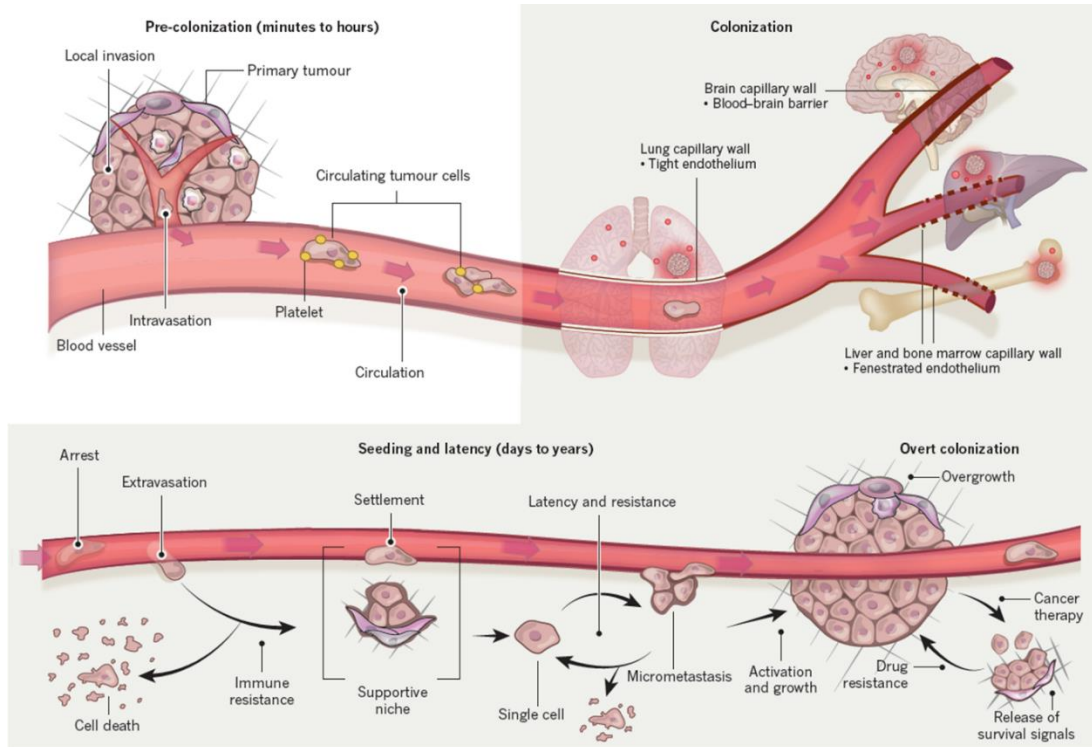


Figure 1.10. The main steps in the formation of metastatic cascade (Massague and Obenauf, 2016). The primary tumour cancer cells invade into the local ECM, promote angiogenesis; then invade into the blood vessels and circulate throughout the blood. Once the circulating tumour cells extravasate the blood vessel and settle at a distant organ, the cancer cells proliferate and survive in the new site to form micrometastases.

1.2.2 Local invasion through extracellular matrix (ECM) and stromal cells.

Local invasiveness refers to the entry of cancer cells from primary tumour into the surrounding stroma and thereafter into the adjacent normal tissue (Valastyan and Weinberg, 2011). To achieve this cancer cells must enter the basement membrane (BM), a specialized extracellular membrane. The tight junction (TJ) in epithelial cells works as an intrinsic wall to separate the epithelial and stromal compartments and is the first barrier to prevent cancer invasion (Bissell and Hines, 2011, Tsukita et al., 2001). To overcome the epithelial tissue barrier, including TJs and E-cadherin mediated intercellular adherens junctions (AJs) and desmosomes (Cavallaro and

Christofori, 2004, Tsukita et al., 2001), cancer cells have to conduct a cell-biological program known as epithelial mesenchymal transition (EMT) (Valastyan and Weinberg, 2011, Ye and Weinberg, 2015, Thiery et al., 2009), which is managed by a group of transcription factors (EMT-TFs) including Slug, Snail, Twist, E47, KLF8 and Zeb family (Thiery et al., 2009). The ECM also contains growth factor molecules that can be liberated by carcinoma-secreted proteases such as the matrix-degrading metalloproteinases (MMPs) family and cathepsins. (Valastyan and Weinberg, 2011, Kessenbrock et al., 2010) Moreover the BM is also involved in signal transduction with cancer cells via integrin signalling pathways initiating alterations in cell polarity, proliferation, invasion and apoptosis (Hood and Cheresch, 2002).

Once invading cancer cells have dissolved the BM, they enter the stroma, consequently encountering fibroblasts, myofibroblasts, endothelial cells, adipocytes, mesenchymal stem cells, as well as immune cells such as macrophages (Quail and Joyce, 2013). These stromal cells can enhance the aggressive behaviours of cancer cells through various signalling pathways. For instance, interleukin-6 (IL6) secreted by adipocytes can stimulate breast cancer cells (Dirat et al., 2011); and CD4⁺ T cells can stimulate tumour associated macrophages (TAMs) to activate epidermal growth factor receptor (EGFR) signalling in the breast cancer cells (DeNardo et al., 2009).

1.2.3 Intravasation into the lumina of blood vessels.

Intravasation involves cancer cells entering into the lumina of lymphatic or blood vessels after locally invasion (Gupta and Massague, 2006, Valastyan and Weinberg, 2011). The spread of cancer cells in lymphatic tissue is an important prognostic marker for disease progression, and metastatic carcinoma cells in hematogenous circulation represents a major mechanism of cancer spread (Gupta and Massague, 2006). Microvessel walls formed by endothelial cell can be invaded by cancer cells with various molecular changes such as activating of the Notch signalling pathway (Sonoshita et al., 2011, Meurette and Mehlen, 2018) and the cytokine-transforming

growth factor- β (TGF β) signalling pathway (Giampieri et al., 2009, Seoane and Gomis, 2017), epidermal growth factor (EGF) (Wyckoff et al., 2007, Lemmon and Schlessinger, 2010b) and colony-stimulating factor 1 (CSF-1) (Wyckoff et al., 2007). Intravasation is largely influenced by the structural features of tumour-associated blood vessels, so that cancer cells can stimulate the formation of new blood vessels within their local microenvironment via a variety of mechanisms such as the activation of vascular endothelial growth factors (VEGFs). This process is termed neoangiogenesis (Carmeliet and Jain, 2011).

1.2.4 Survival and transport within the circulatory system.

Once cancer cells have intravasated into the lumen of the vasculature, they can disseminate widely throughout the body. In recent years, advanced technologies have been developed to aid in the detection of circulating tumour cells (CTCs) in the circulatory system of cancer patients (Nagrath et al., 2007).

1.2.5 Extravasation and arrest at a distant site to form a secondary focus.

In the circulation system, CTCs have to arrest and settle at a distant organ site, and brain, liver, lung and bone are some of the most common sites for metastasis. (Valastyan and Weinberg, 2011). Once lodged in the microvasculature of distant organs, the CTCs can initiate intraluminal growth to form a microcolony followed by breaking through or extravasation of the walls of surrounding vessels. Thereby cancer cells directly contact with stromal tissue cells. In order to overcome the barriers preventing extravasation in tissues with low microvessel permeability, cancer cells are able to secrete factors which can induce vascular hyperpermeability, including the protein Fascin-1 and other components of invading protrusions known as invadopodia, along with autocrine enhancers of cancer-cell motility such as epiregulin and WNT ligands (Minn et al., 2005, Massague and Obenauf, 2016). For example, the secreted protein angiopoietin-like-4 (Angptl4), as well as the

pleiotropically acting factors EREG, COX-2, MMP1 and MMP2 dissolve the pulmonary vascular endothelial cell junctions during the extravasation of breast cancer cells in lung metastases (Gupta et al., 2007, Minn et al., 2005). Similarly angiopoietin2 (Angpt2), MMP3, MMP10, placental growth factor, and VEGF secreted by various types of primary tumours are also capable of inducing pulmonary hyperpermeability to welcome the arrival of carcinoma cells in the lungs leading to the extravasation of CTCs (Weis et al., 2004). Platelets associated with CTCs can stimulate extravasation by activating TGF- β signalling triggered EMT in cancer cells (Labelle et al., 2011).

1.2.6 Formation of micrometastases.

In order to form micrometastases, extravasated cancer cells have to survive in the foreign microenvironment in the distant organ (Massague and Obenauf, 2016). Primary tumours can release systemic signals such as lysyl oxidase (LOX) (Erler et al., 2009) which changes the distant microenvironments into more hospitable sites for disseminated cancer cells to form micrometastases (Valastyan and Weinberg, 2011). At the same time, extravasated cancer cells must adapt to foreign tissues. For instance, during the development of lung and bone metastasis, the extravasated breast cancer cells survival and metastatic colonization are achieved through the activating the Src-dependent CXCL12 activation of Akt signalling (Zhang et al., 2009).

1.2.7 Proliferation at secondary foci - metastatic colonization.

Disseminated cancer cells are still not guaranteed to form a macroscopic metastasis even when the extravasated cancer cells have survived their initial encounter with the microenvironment of a foreign organ tissue. In breast cancer metastases, the disseminated cancer cells may stay in quiescence for a considerable time, which is related to an inability to trigger the focal adhesion kinase (FAK), integrin β 1, and Src pathways (Barkan et al., 2008). When considering the “seed-and-soil” hypothesis,

specific organ microenvironments are more or less hospitable for the proliferation and survival of certain types of cancer cells (Massague and Obenauf, 2016, Fidler, 2003).

1.3 SIPA1 and metastasis of cancer

1.3.1 SIPA1 (Signal Induced Proliferation Associated 1)

Since Dr. Stephen Paget proposed the "seed and soil" theory of metastasis in 1889 (Paget, 1889), research regarding the mechanism of cancer metastasis has been a keen area of interest for over 100 years (Fidler, 2003). People gradually recognized that cancer metastasis is a complex process involving multiple factors including sustaining proliferative signalling and evading growth suppressors, resisting cell death, enabling replicative immortality, inducing angiogenesis recurrence, activating invasion/migration and drug resistance (Hanahan and Weinberg, 2011, Valastyan and Weinberg, 2011). All these factors lead to a poor prognosis. Increasing numbers of oncogenes, such as ErbB2, PI3KCA, MYC, CCND1 and tumour suppressor genes, such as p53, and Rb were identified as being related to tumour metastasis (Lee and Muller, 2010). Additionally, many more signalling pathways were found to play an essential role in the development and progress of cancer including TGF- β (Seoane and Gomis, 2017), MAPK (Dhillon et al., 2007), Wnt (Logan and Nusse, 2004), NOTCH (Ranganathan et al., 2011), FAK (Sulzmaier et al., 2014), PI3K/Akt (Vanhaesebroeck et al., 2010, Goncalves et al., 2018) etc. In this project, we focus on signal-induced proliferation-associated protein 1 (SIPA1), which has been found to participate in the metastasis process of malignant tumours and to play an important role in the metastatic process.

1.3.2 Cloning and identifications of the gene of SIPA1

The gene SIPA1, also called as SPA1 (suppressor of phyA-105), was first cloned from

a murine lymphoid cell line, LFD 14, after IL-2 stimulation in 1995 by M. Hattori (Hattori et al., 1995). SIPA1 in mice was originally described as 3518 bp long with a long open reading frame (ORF) (from position 1199 to 3280) and several short ORFs in the 5'-end (Hattori et al., 1995). In 1997, the same research team cloned the human SIPA1 cDNA from human peripheral blood lymphocytes (PBL) after stimulation with phytohemagglutinin and TPA (Kurachi et al., 1997). The human SIPA1 gene was mapped to chromosome 11q13.1, spanning 12.8 kb. The human SIPA1 gene is highly homologous to the murine gene, containing 16 exons, amongst which exon 1, 91 bp of exon 2 (considered as 5'-UTR) and the 3'-region 205 bp of exon 16 are untranslated (Hattori, 2011). The human SIPA1 genome contains a much longer ORF of 1042 residues (from position 297 to 3425) (Kurachi et al., 1997). In the 5' terminal region of SIPA1 gene, residues from position 192 to 539 (containing part of the exon 5, exon 6, 7 and part of exon 8 in human) were found to be highly homologous to human Rap1-GAP (Gap related domain, GRD), both in human and murine. Upstream of the GRD encoded a proline-rich domain with the potential ability to bind SH3 and downstream of GRD there is the PDZ domain which consists of part of exon 9. In the 3' region, part of exon 14, exon 15 and translated part of exon 16 encoded a leucine zipper (LZ)-like domain, which were also found to be conserved in both humans and mice (**Figure 1.11**) (Kurachi et al., 1997, Hattori, 2011).

1.3.3 The structure and expression of SIPA1 protein

In mice, the SIPA1 gene encodes a 68-KDa protein (P68) with 693 amino acids, mostly located in the nuclei (Hattori et al., 1995), whilst the human SIPA1 protein contains 1042 amino acids with a molecular mass 130-KDa (Kurachi et al., 1997). Three domains were identified in the SIPA1 protein: a RapGTPase-activating protein (GAP) related domain (GRD) (350-539), a PSD-95/discs-large/ZO-1 Homology (PDZ) domain (685-759) and a leucine zipper like (LZ) domain (964-1042) which is similar to myosin tail (Hattori, 2011). There was a proline-rich domain including possibly SH3-binding motifs located in the N terminal to the GRD and upstream the LZ domain

had a probable PEST (P, Pro; E, Glu; S, Ser; T, Thr) sequence (**Figure 1.11**) (Kurachi et al., 1997). The GRD domains are key catalytic functional regions of those large proteins, involving in variety of interactions with other proteins, lipids, and regulatory molecules (Bos et al., 2007). The PDZ domain is more commonly known as the protein binding domain, especially for proteins with scaffold functions (Manjunath et al., 2018). Ligand selection and ligand interactions are relatively complex and conservative. The PDZ domain can resist the effects of mutations to maintain its unique structure (Alber, 1992). The leucine zipper (LZ) mediates dimerization, juxtaposing two basic regions to form the DNA-binding site. Lastly PEST sequences are regarded as target sites for phosphorylation and/or degradation (Ghose et al., 2001).

Expression levels and localization of SIPA1 protein vary in different human tissues and cells. SIPA1 protein is most highly expressed in a lymphohematopoietic system such as the spleen, bone marrow and thymus and SIPA1 may be located in the cytoskeleton, plasma membranes and possibly nuclei resting with the type of cell and interaction with other proteins (Hattori, 2011).

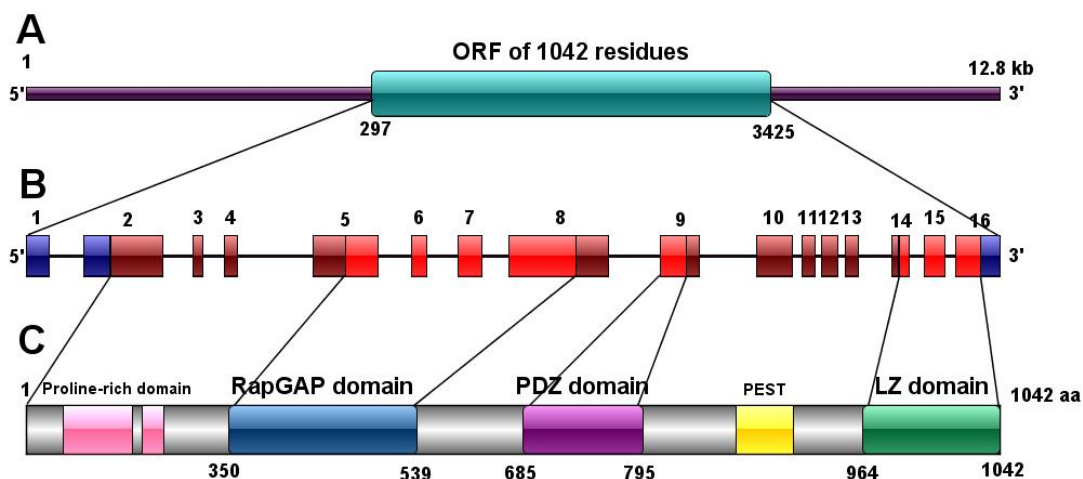


Figure 1.11. The structure of human SIPA1 gene and protein. (A) Schematic representation of the SIPA1 gene structure. **(B)** 16 exons of SIPA1 gene. **(C)** Schematic representation of the SIPA1 protein structure.

1.3.4 Germline polymorphisms in SIPA1

There exist thousands of single-nucleotide polymorphisms in the SIPA1 gene, in which seven SNPs located in the promoter region or encoding region of SIPA1 have been identified as being associated with tumorigenesis, metastasis and prognosis in previous research (Roberts et al., 2013, Crawford et al., 2006, Gaudet et al., 2009, Hsieh et al., 2009a, Brooks et al., 2010). Amongst them, most research has focused on three SNPs: G>A SNP rs931127 located in the promoter region; rs3741378 a C>T or C>G SNP that encodes for the replacement of a serine (Ser) to phenylalanine (Phe) amino acid in exon 3; and rs746429, a G>A SNP that encodes for a synonymous amino acid (Alanine, Ala) transformation in exon14. These three SNPs are considered to be related to the development, metastasis and prognosis of breast, lung and cervical cancer (Pei et al., 2013, Roberts et al., 2013, Ugenskiene et al., 2016, Hsieh et al., 2009a, Gaudet et al., 2009, Crawford et al., 2006, Brooks et al., 2010, Hsieh et al., 2009b, Gdowicz-Klosok et al., 2015, Xie et al., 2013). Other SNPs were shown to be involved in breast cancer: rs2306364, a G>A SNP rs2448490, a G>A, G>C or G>T SNP, both of which encode for a synonymous amino acid (Alanine, Ala) transformation (Roberts et al., 2013, Hsieh et al., 2009a, Xie et al., 2013) In addition, rs75894763, a G>A SNP also encoding for a synonymous amino acid (Valine, Val) transformation (Roberts et al., 2013) and rs75894763 are also related to lung cancer (Xie et al., 2013). The G>T SNP, rs3741379, encoding for the replacement of an Ala to Ser amino acid have been indicated to be involved in the process of lung cancer metastasis (Xie et al., 2013).

1.3.5 SIPA1 family and Rap1-GTPase activating proteins

The initial function of SIPA1 was believed to be specific GAP activity for Ras-related mediating proteins, Rap1, Rap2, Rsr1 and nuclear Ran (Kurachi et al., 1997). Although recent research suggested that SIPA1 cannot work as a GAP for Ran or other small GTPases (Kurachi et al., 1997). SIPA1 overexpression induced rounding

and eventual detachment of inherently adherent cells from extracellular matrix by inhibiting endogenous Rap1 activation, indicating that Rap1 signals are involved in the regulation of cell adhesion and SIPA1 functions as a negative regulator of cell adhesion (Hattori et al., 1995).

Human RapGTPase activating protein mainly consists of two subfamilies: SIPA1 family and rapGAP family. In addition, the SIPA1 family also has SIPA1-like1 (SIPAL1, also called E6TP1 or SPAR), SIPAL2, and SIPAL3 except SIPA1 and the rapGAP family contains rapGAP1 and rapGAP2 (Hattori, 2011). All the RapGAPs share homologous catalytic GRD domain in addition to an analogous PDZ domain (Kurachi et al., 1997, Hattori, 2011).

1.3.6 SIPA1 interacting molecules (Figure 1.12)

1.3.6.1 Nuclear SIPA1 and integrin β 1

Nuclear SIPA1 have been shown to interact with and activate the integrin β 1 promoter in breast cancer cells (Zhang et al., 2015). After SIPA1 knock down in MDA-MB-231 cell, mRNA levels of SIPA1 were significantly downregulated. Chromatin immunoprecipitation experiments revealed nuclear SIPA1 could interact with the ITGB1 promoter and increase its transcription activity, causing further phosphorylation changes in the integrin-mediated FAK/Akt signalling pathway, thereby affecting the adhesion and invasion capability of cancer cells (Zhang et al., 2015).

1.3.6.2 Association of SIPA1 and AF6

Co-immunoprecipitation experiments demonstrated that SIPA1 bonded specifically with AF6 (afadin) in 293T cells transfected with both SIPA1 and AF6, with further studies revealing that binding occurred between the GRD domain of SIPA1 and the PDZ domain of AF6. AF6 was reported to localize at the cell adhesion sites and have

an association with the tight junction (TJ) protein ZO1 (Zonula Occludens 1). SIPA1 also co-localized with AF6 in the similar cell to cell adhesion site, so it was suggested that SIPA1 may also regulate TJs via AF6, although evidence remained fragmentary (Su et al., 2003).

1.3.6.3 **SIPA1 colocalizes with AQP2 in renal collecting ducts**

Studies in renal collecting ducts have shown that SIPA1 directly binds to aquaporin 2 (AQP2) and is involved in the regulation of trafficking AQP2 to the apical membrane. AQP2 has the ability to bind to molecules containing a PDZ domain, so SIPA1 with a PDZ domain can combine with AQP2 and play a role in the intracellular transport of AQP2. Studies also demonstrated that the Rap1 signalling pathway was involved in the AQP2 intracellular transport system. As a regulation factor of Rap1, SIPA1 can control the transport process by inhibiting Rap1. Therefore, the interaction between SIPA1 and AQP2 may be both direct and indirect (Noda et al., 2004).

1.3.6.4 **Brd4 interacts with SIPA1**

In HeLa cells, the bromodomain protein Brd4 was found to bind to the GRD domain of SIPA1 directly and this interaction is mainly located in the cell nucleus, especially near or at the inner face of the nuclear membrane, and enhances the RapGTPase activity of SIPA1 for Rap1 and Rap2 (Alsarraj et al., 2013, Farina et al., 2004). The combination of SIPA1 and Brd4 promotes the cell cycle through M to G1 phases, which may also regulate cancer development (Farina et al., 2004).

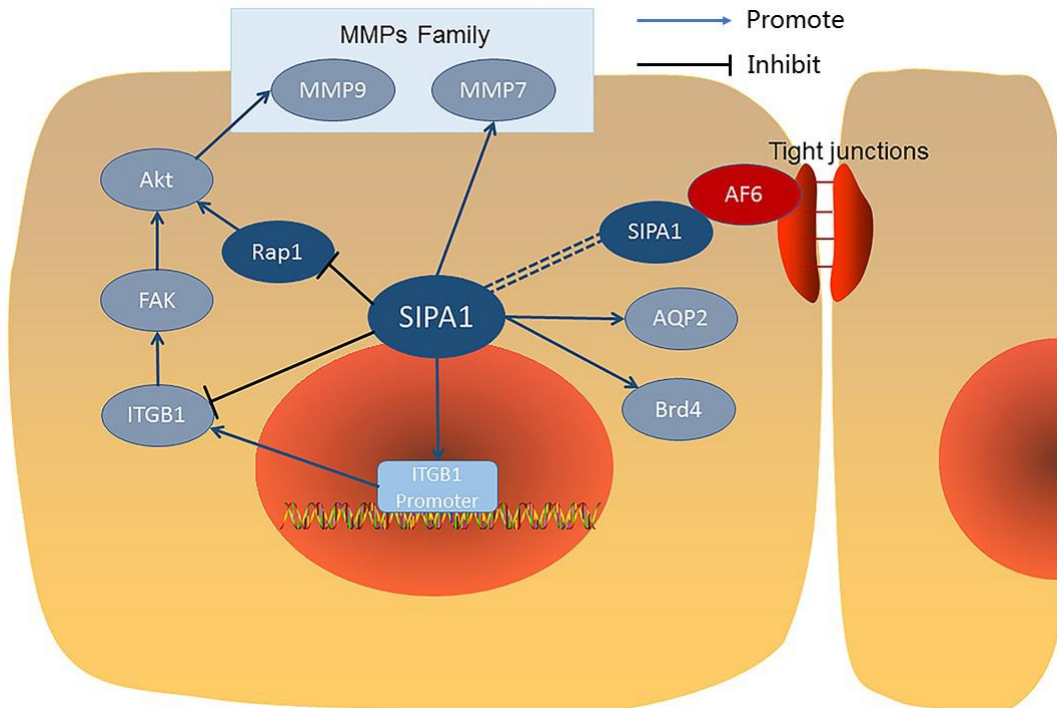


Figure 1.12: Schematic diagram of the SIPA1 interacting molecules. SIPA1 is in the centre of the interaction. SIPA1 can regulate the transcription of ITGB1, and then control the MMP family. Also, the inhibition of Rap1 could modulate the MMP through Akt signalling by contraries. AF6 showed in the red is the key molecule which SIPA1 could affect directly and adjust the tight junction proteins, further maintain the cell-to cell barrier function.

1.3.7 Multiple roles of SIPA1 in cancer and the mechanisms thereof

1.3.7.1 Breast cancer

The role of SIPA1 in cancer and cancer metastasis has mostly been studied in breast cancer. Immunohistochemical staining has shown that in breast cancer patients, SIPA1 is localized to the nuclear region, where the expression level might be a predictive factor for lymph node metastatic status. Similarly, in breast cancer cells, SIPA1 is mainly localized to the nucleus in the aggressive breast cancer cell line MDA-MB-231 cells after transgenic overexpression of SIPA1 (Zhang et al., 2015). *In vitro* cell function experiments demonstrated that knock down of SIPA1 reduced the potential of for adhesion, migration and invasion in the MDA-MB-231 cell line, but promoted cells to proliferate (Zhang et al., 2015). These changes may be due to the

fact that nuclear SIPA1 interacts with the integrin β 1 promoter (ITGB1) and activated it, thereby regulating the adhesion and invasion of breast cancer cells. Knock down of SIPA1 in the MDA-MB-231 cell line suppressed the integrin mediated FAK/Akt-MMP9 signal pathway by markedly decreasing the phosphorylation levels of FAK and Akt and extracellular secretion of MMP9 (Zhang et al., 2015). Thus the mechanism of SIPA1 promoting breast cancer cell adhesion, invasion and metastasis may occur by regulating the integrin β 1/FAK/Akt-MMP9 signalling pathway.

1.3.7.2 Prostate cancer

In human prostate cancer (CaP) patients, high expression of SIPA1 was associated with poor disease prognosis and tumour metastasis (Shimizu et al., 2011). Similarly in the human CaP cell lines, LNCaP with low metastatic capacity inoculated into SCID mice was accompanied with undetectable levels of SIPA1, while PC3 cells with high metastatic capacity in SCID mice was accompanied with by high levels of SIPA1 expression (Shimizu et al., 2011). After transduction of SIPA1, the low metastatic LNCaP cells inoculated into the testis of SCID mice exhibited a high metastatic capacity to the abdominal lymph nodes. Following knock down of SIPA1, the highly metastatic PC3 cells exhibited reduced metastatic capacity and there was no significant change in the size of primary tumour in both groups (Shimizu et al., 2011). Thus, the effect of SIPA1 on prostate metastasis is greater than the effect on proliferation. *In vitro*, after transduction of SIPA1 in LNCaP cells, expression of SIPA1 resulted in decreased adhesion of CaP cells to the extracellular matrix (ECM). Nuclear Brd4 and ECM-related gene expression were down-regulated, which was regulated by Rap1 activation (Shimizu et al., 2011). A meta-analysis of human gene expression data (Oncomine website: <https://www.oncomine.org/resource/login.html>) from prostate, lung and a variety of solid tumours showed overexpression of SIPA1 in human primary prostate cancer tissues which was related to cancer metastatic progress.

1.3.7.3 Oral squamous cell carcinoma

Expression of SIPA1 in both human oral squamous cell carcinoma (OSCC) and OSCC cells is higher than in normal tissue and is related to regional lymph node metastasis in OSCC patients. In the OSCC cell line HSC-3 and HSC-4, knockdown of SIPA1 reduced the ability of cells to invade and migrate, but increased the adhesion of cells and had no significant effect on proliferation compared with the control group. In the same cell line, knockdown of SIPA1 down-regulated the cytosolic expression of BRD4, but abundant BRD4 protein was still expressed in the nucleus (Takahara et al., 2017). The interaction between SIPA1 and BRD4 may promote OSCC metastasis. The expression of ITGB1, an integrin which is known to be an important marker of cell invasion and adhesion, was significantly higher in SIPA1 knock down cells than control cells. However, the expression of MMP7 (membrane metalloproteinase 7) which has an essential role in tumour invasion, growth and metastasis, was markedly reduced after knock down of SIPA1 (Takahara et al., 2017). Therefore, SIPA1 and its interaction with BRD4 may impact the development and metastatic progression of OSCCs by regulating ITGB1 and MMP7.

1.3.7.4 Colorectal cancer

In human colorectal adenocarcinoma patients, there was increased expression of SIPA1 in tumour, especially in the well-differentiated and moderately differentiated tumours as compared to poorly-differentiated tumours. Those patients with a higher expression level of SIPA1 were associated with poor prognosis. *In vitro* experiments demonstrated that after knock down of SIPA1 in HT115 and Caco-2 colorectal cancer cell lines, the potential of cancer cells to invade, adhere and migrate was increased compared to the control group, while the ability to proliferate was decreased (Ji et al., 2012). This suggested SIPA1 may have an active role during progression of colorectal adenocarcinoma.

1.3.7.5 Cervical cancer

Two SNPs in SIPA1 (rs931127, 313G>A and rs746429, 2760G>A) were potentially related to an increased risk of nodal metastasis in cervical cancer. The G allele at both rs931127 and rs746429 in SIPA1 was associated with nodal disease in overall cases and controls. In terms of the tumour size, patients with smaller stage I B1 tumours having the G allele showed an increased risk of nodal metastases at SIPA1 rs746429 and at rs931127. However, the correlation between polymorphisms in SIPA1 and nodal metastasis was not significant in I B2 tumours (which are larger lesions). The G allele in SIPA1 at both rs746429 and rs931127 was significantly related to nodal disease in patients without lymph vascular space invasion (LVSI), which was considered as an independent poor prognostic factor for cervical cancer patients. The GG genotype was associated with a markedly higher risk of nodal disease in both SNPs of SIPA1 in patients without LVSI. Histologically, SNPs in SIPA1 rs746429 and rs931127 were not related to histology types (adenocarcinoma or squamous cancer). Moreover, SNPs of SIPA1 made no difference to the survival of cervical cancer patients (Brooks et al., 2010).

1.3.7.6 Lung Cancer

Previous studies focused on polymorphisms in SIPA1 in lung cancer development and metastasis. Three SNPs were found to be involved in lung cancer, rs931127 A>G, rs2448490 G>A and rs3741379 G>T (Gdowicz-Klosok et al., 2015, Xie et al., 2013). In a previous study, researchers genotyped these SNPs in the southern Chinese population. High frequency of the G allele at rs931127 was significantly correlated with the risk of lung cancer, but no significant connection was observed in the other two SNPs. From the perspective of tumour staging and grading, the fusion of the G allele in rs931127 was also associated with poor clinical stages, nodal metastasis and distal metastasis. The SNP rs931127 A>G in the promoter of SIPA1 was highly

associated with tumour genesis and metastasis of lung cancer (Xie et al., 2013). Another study suggested that G allele fusion in SNP rs931127 A>G was significantly correlated with more serious progression free survival (PFS) in patients with non-small cell lung cancer (NSCLC) (Gdowicz-Klosok et al., 2015). Therefore the SIPA1 SNP rs931127 A>G may be identified as an independent prognostic predictive factor for PFS in NSCLC patients (Gdowicz-Klosok et al., 2015, Xie et al., 2013).

1.3.7.7 Gastric cancer

There is scant previous research regarding the role of SIPA1 in gastric cancer. A single study demonstrated both mRNA level (detect by qPCR) and protein expression (detect by western blotting) of SIPA1 in gastric tumour tissues was lower than tumour-adjacent normal tissues. On the contrary, IHC of gastric tumour tissues revealed that positive staining of SIPA1 was significantly higher than in tumour adjacent normal tissue (Li et al., 2017). Positive staining of SIPA1 in the tumour from gastric cancer patients tumour tissue was markedly associated with the degree of differentiation, lymph node metastases and clinical grading (Li et al., 2017). The expression and function of SIPA1 in gastric cancer and its mechanism remains to be explored.

1.3.7.8 Melanoma

There is little known regarding the role of SIPA1 in melanoma and limited research conducted previously. One study indicated that in fast-growing melanoma there was significant overexpression of the SIPA1, resulting in the inactivation of Rap1 and aggressive melanoma cell models. When knockdown of SIPA1 in these melanoma models was carried out, adhesion capability was enhanced but chlorogenic potential and migration ability were reduced (Mathieu et al., 2012). These data suggested that SIPA1 interacted with Rap1 and may have a complex role in the regulation of melanoma development and metastasis.

1.3.8 Summary of SIPA1 in cancer

Although it has been nearly 30 years since the discovery of SIPA1, there has been a scarcity of research carried out as regards to the role of SIPA1 in cancer. However, the mechanism of SIPA1's role in human cancer and cancer metastasis warrants further exploration. Clinical data showed SIPA1 is upregulated in tumour tissue compared with normal tissue. In addition, studies of SIPA1 in different cancers demonstrated that SIPA1 promotes cancer cell invasion, migration and proliferation. In almost all types of cancers, SIPA1 was associated with lymph node metastasis, which suggests that SIPA1 might be a judgment indicator of cancer metastasis and patients' prognosis. Interaction of SIPA1 with molecules and signalling pathways such as ITGB1, MMP, AF6, AQP2, Brd4, FAK/Akt may be involved in cancer development and metastasis. moreover, the classical function of SIPA1 in Rap1 signalling pathway may also be closely related to cancer and cancer metastasis. Meanwhile SIPA1's direct or indirect interaction with various types of molecules may also be involved in development and metastasis of cancer, the importance of which is yet to be revealed.

1.4 HGF/MET signalling pathway

1.4.1 Hepatocyte growth factor

Hepatocyte growth factor (HGF), also called scatter factor (SF), is a paracrine cellular growth factor, with both motility and morphogenic effects (Weidner et al., 1991, Gherardi and Stoker, 1990). HGF is synthesized and secreted by mesenchymal cells as a single-chain precursor and activated by HGFAC (Hepatocyte Growth Factor Activator, HGFA or HGFAC) in the extracellular stroma, forming an active α - and β -chain heterodimer and targeting epithelial cells and endothelial cells. HGF contains six domains, an amino-terminal hairpin loop (HL), four kringle domains (K1–K4) and a serine protease homology (SPH) domain lacking proteolytic activity (**Figure 1.13**)

(Trusolino et al., 2010). HGF-induced cell scatter may increase the motility and invasiveness of the cells, which is essential for embryonic development but may also result in the metastasis of cancer (Wen-Sheng Wu, 2010, Martin et al., 2004, Martin et al., 2001, Jiang et al., 1999).

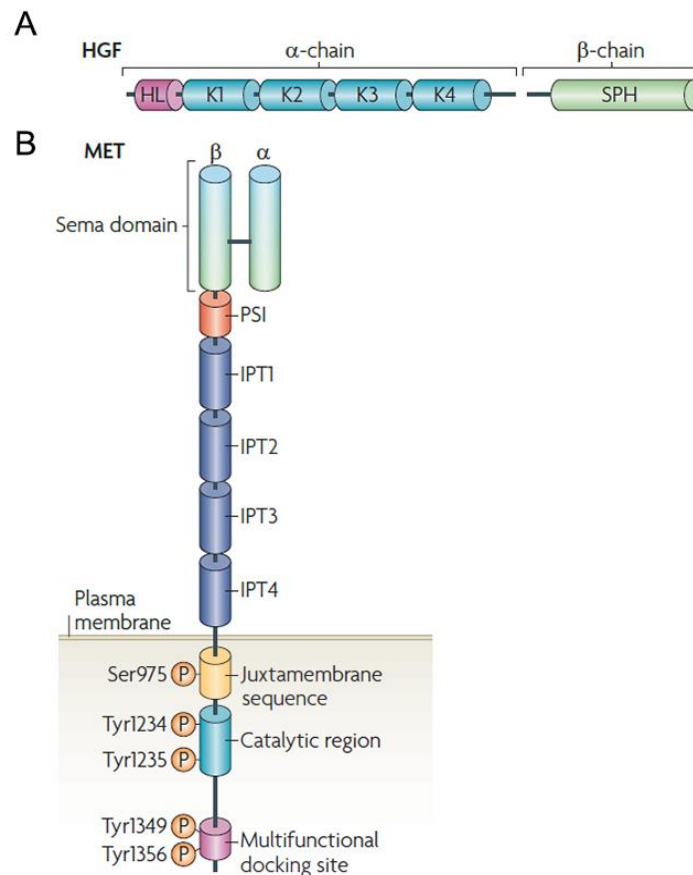


Figure 1.13: The schematic diagram of domain structures of HGF and MET-RTK (Trusolino et al., 2010). (A) The schematic diagram of the HGF structure. HGF consists of six domains: one hairpin loop (HL), four kringle domains (K1–K4) and a serine protease homology (SPH) domain. **(B) The schematic diagram of the MET structure.** MET consists of a transmembrane β chain and an extracellular α chain. The Sema domain, PSI domain with a transmembrane helix and four IPT domains, the juxtamembrane domain, catalytic domain, C-terminal docking site are shown in the figure.

1.4.2 The HGF/MET pathway and receptor tyrosine kinase (RTK) families

The receptor of HGF is the tyrosine-protein kinase receptor MET, also called hepatocyte growth factor receptor (HGFR), was first identified in the 1980s as an

oncogene (Bottaro et al., 1991, Cooper et al., 1984, Birchmeier et al., 2003a). MET belongs to the receptor tyrosine kinase (RTK) family. All RTKs have conservative molecular structure, with extracellular ligand binding domains, transmembrane domain, and cytoplasmic region that contains the protein tyrosine kinase (TK) domain, additional carboxyterminal and juxtamembrane regulatory regions (**Figure 1.13**) (Lemmon and Schlessinger, 2010a). Similarly, the MET receptor consists of a 140kDa transmembrane β chain and a 50kDa extracellular α chain. These two subunits are disulfide-bonded to form a heterodimeric complex of 185kDa. The extracellular amino-terminal (N-terminal) portion of MET binds to the ligand. The extracellular β subunit contains the Sema domain (whole α chain plus part of β chain), PSI domain which contains a transmembrane helix and four IPT (immunoglobulin-like fold shared by plexins and transcriptional factors) domains. The intracellular segment has three regions: a juxtamembrane domain, a catalytic domain, and a carboxy-terminal (C-terminal) multifunctional docking site (**Figure 1.14**) (Cooper et al., 1984, Trusolino et al., 2010).

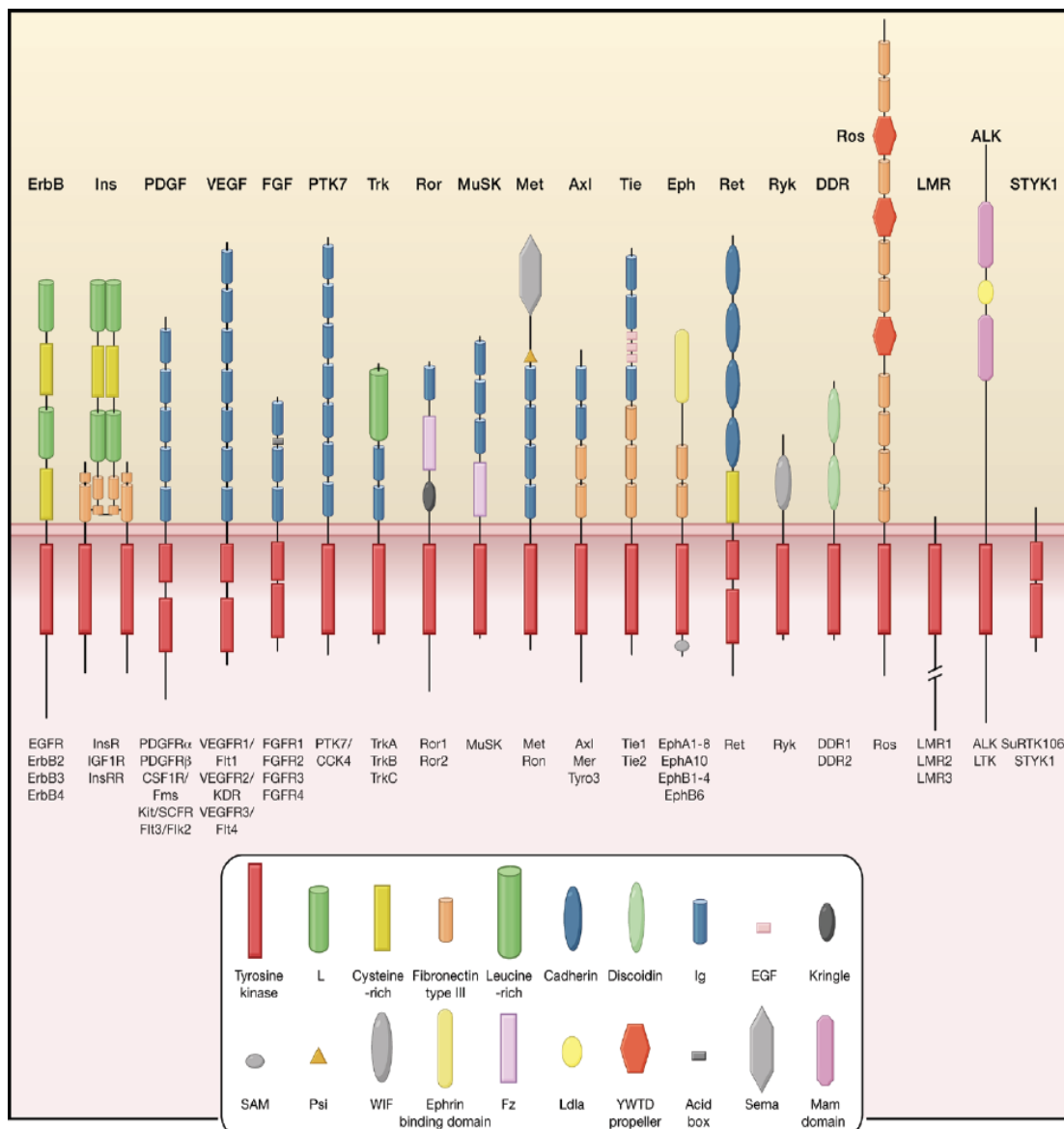


Figure 1.14: Introduction of the Human receptor tyrosine kinases (RTKs) Family Members. Human RTKs contain 20 subfamilies, each subfamily together with their members names was shown under the receptors' schematic diagram. The extracellular and intracellular domains of the RTK family are noted respectively (Lemmon and Schlessinger, 2010a).

Binding to HGF/SF triggers autophosphorylation of the cytoplasmic domain of MET. Phosphorylation of two tyrosine residues Y1234 and Y1235 in the catalytic region is important for the activation of MET to work as a tyrosine kinase, while phosphorylating the Y1349 and Y1356 tyrosine residues in the C-terminal docking site is crucial for adaptor protein recruiting. The adaptor proteins always contain a Src homologous 2

(Sh2) domain, which can interact with MET and a Src homologous 3 (Sh3) domain which is used for binding to downstream signal molecules (Gao and Vande Woude, 2005, Ferracini et al., 1991). Many adaptor proteins such as Shc, Src, Grb2, p85 regulatory subunit of PI3K and Gab1 could bind with the met receptor directly or indirectly (Wen-Sheng Wu, 2010, Birchmeier et al., 2003a). Numerous downstream signalling pathways can be triggered by HGF/MET, such as Raf-ERK/MAPK signalling pathway, PI3K/MAPK signalling pathway, Jun amino-terminal kinase (JNK) signalling pathway, signal transducer and activator of transcription-3 (STAT3) signalling pathway, nuclear factor κ B (NF- κ B) signalling pathway and the β -catenin signalling pathway (**Figure 1.15, 1.16**) (Birchmeier et al., 2003a, Cavallaro and Christofori, 2004, Meurette and Mehlen, 2018, Goncalves et al., 2018, Pylayeva-Gupta et al., 2011, Morikawa et al., 2016).

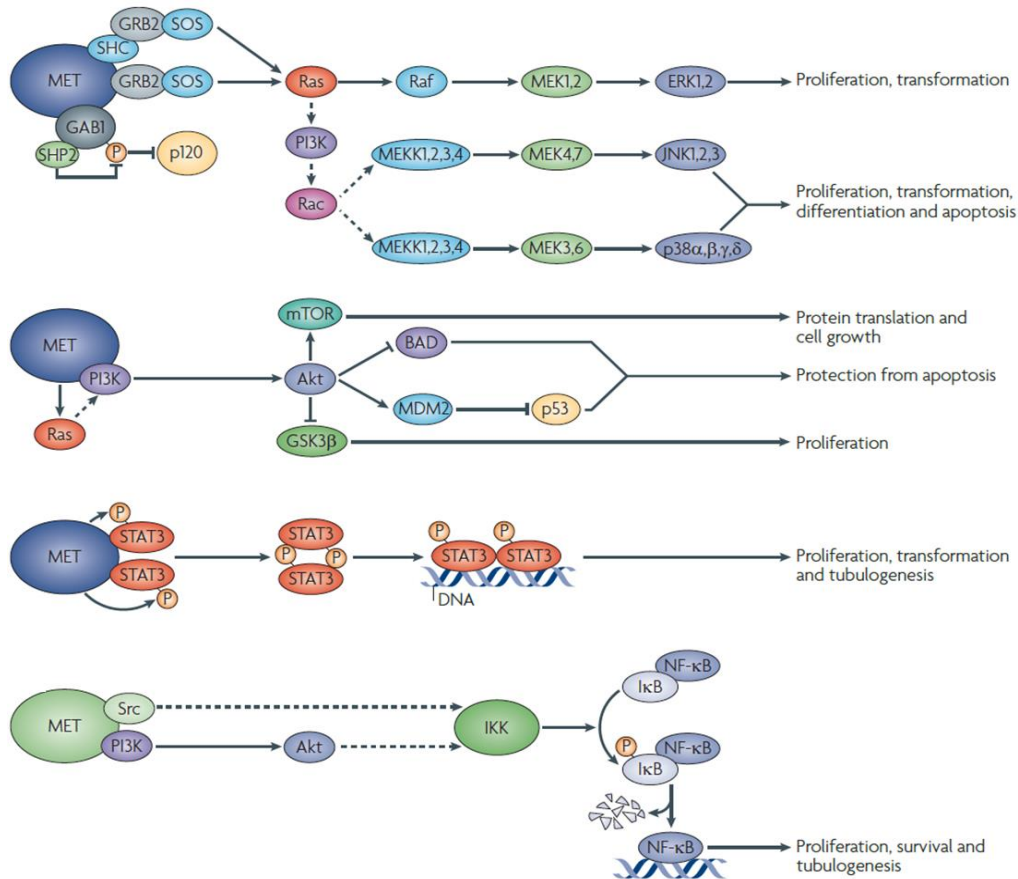


Figure 1.15: Schematic diagram of the major MET downstream signalling pathways and the regulation of cellular function (Trusolino et al., 2010). Cell proliferation is regulated by MET signalling via control the Ras/ERK, PI3K/Akt, STAT3 and NF- κ B signalling pathway. MET could also modulate the apoptosis, differentiation and transformation via ERK, MEK, PI3K/Akt and STAT3 signalling pathway.

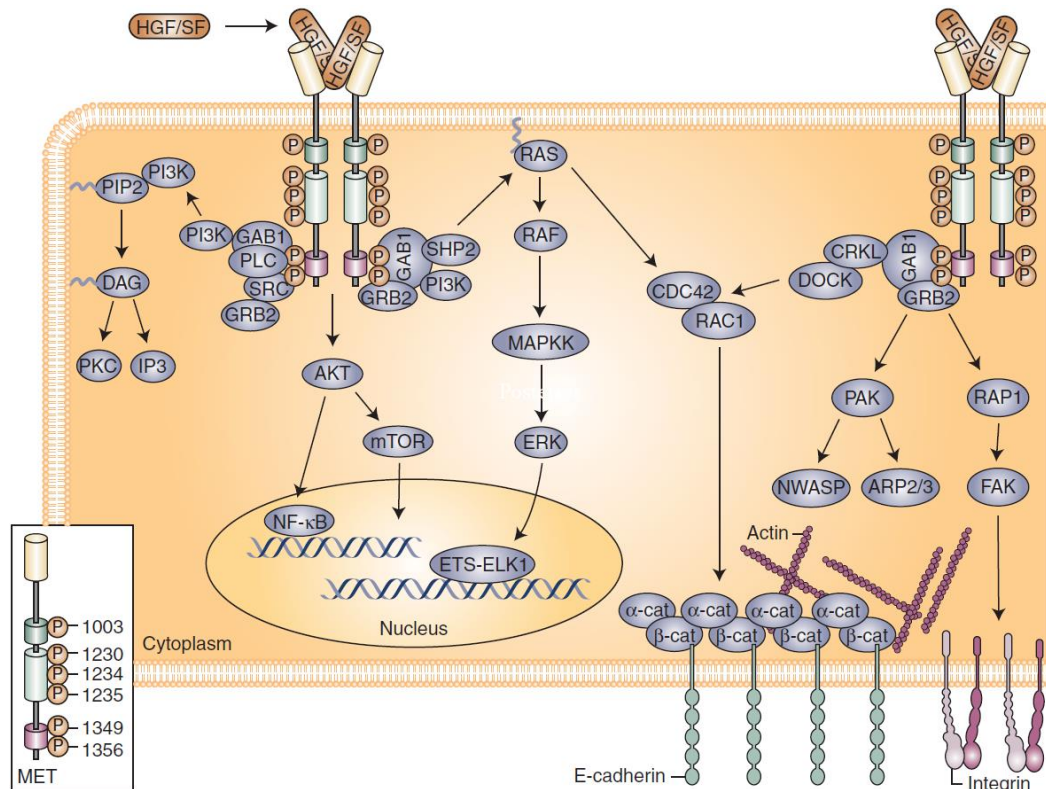


Figure 1.16: Schematic diagram of intracellular downstream signalling pathways activated by HGF/MET RTK(Graveel et al., 2013). The activation of MET recruits of scaffolding proteins like Gab1 and Grb2, then downstreaming activates Ras-ERK-MAPK. Activated Ras leading the activation of Rac1/CDC42- α / β -cat to regulate the cell adhesion junction. And Gab2-Rap1-FAK activation also regulates cytoskeletal and cell adhesion via integrins. Gab1-PI3K-Akt activation controls cell survival and DNA transcription through NF- κ B and mTOR.

1.4.3 The regulation of MET

Like many RTKs, the regulation of MET is a very complex process which never stops during the whole process from production to final degradation of the MET receptor (**Figure 1.17**). MET expression is modulated by DNA methylation and histone acetylation/methylation, which are catalysed by DNA methyltransferases (DNMT) and histone acetylases (HATs) respectively. Various transcription factors could modulate MET gene expression at the transcript level. After transcription, alternative splicing of MET mRNA precursors into mature mRNAs of various lengths takes place. The mature mRNA is recognized and regulated by micro-RNAs in the cytoplasm leading to inhibition of MET mRNA translation. MET mRNA translation is also regulated by

multiple modifiers such as glycosylation in the Golgi apparatus and ligand binding dependent kinases phosphorylation or auto-phosphorylation. Internalization leading to degradation and recycling regulates the activity of MET signalling (Zhang and Babic, 2016).

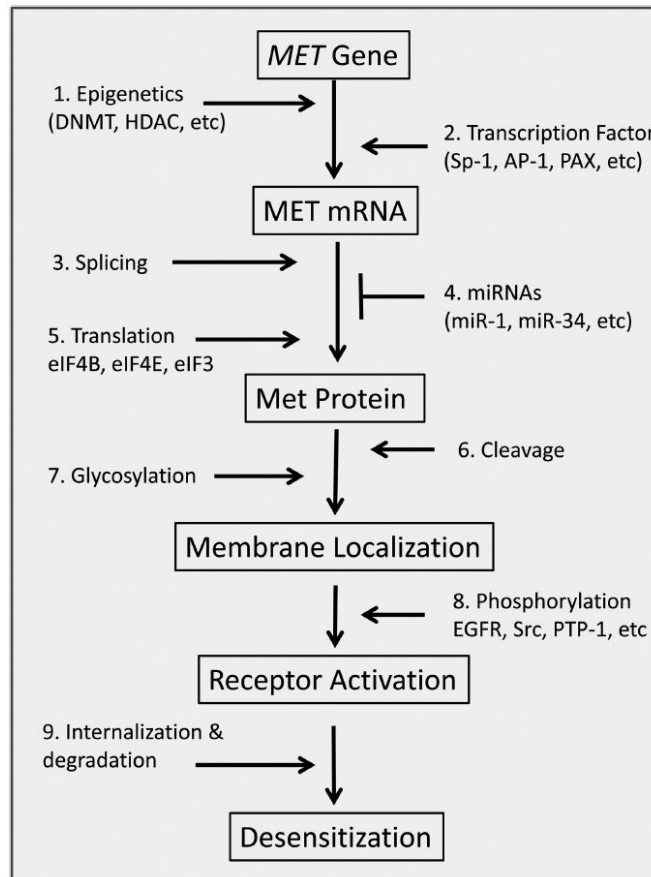


Figure 1.17: Simplified scheme of regulation of MET (Zhang and Babic, 2016). The regulation of MET is multifaceted and in several different levels, which occurs in the DNA, mRNA, and protein levels, and involves multiple processes including transcription, translation, modification, splicing, internalization, and degradation, etc.

1.4.4 Internalization and recycling of MET

The Cbl E3 ubiquitin ligase mediates ubiquitination of MET, providing a signal for MET internalization, which has been shown to be clathrin- or caveolin- dependent. Internalization can be enhanced by Grb2, CIN85, SNX2, CD44 and PTP1B. Once internalized, the MET receptor can be delivered to lysosomes to be degraded or it

can be recycled back to the plasma membrane through the endosomal compartments. PKC ϵ is important for e delivery towards the endosomes, from which the c-Met receptor can signal to specific signalling routes, including STAT3. Recycling back to the plasma membrane has been shown to be dependent on RCP, GGA3 and/or TSN4 (**Figure 1.18**) (Viticchiè and Muller, 2015).

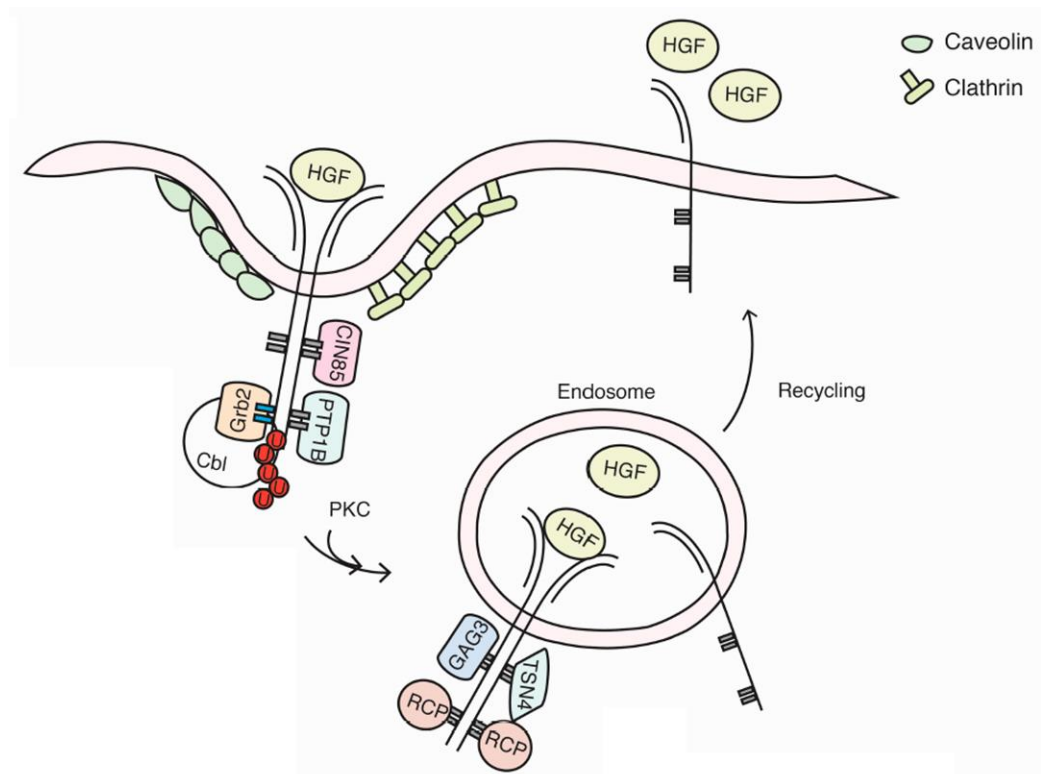


Figure 1.18: Simplified scheme of the internalization and recycling of MET (Viticchiè and Muller, 2015). The internalization and recycling are initiated by ubiquitination MET mediated by Cbl E3 ubiquitin ligase. Grb2, CIN85, SNX2, CD44v6 and PTP1B could all enhance the internalization and recycling. And the PKC is required for the endosome delivery and RCP, GGA3 and/or TSN4 is important for the recycling of MET back to the membrane.

1.4.5 HGF/MET activation in cancer.

HGF/SF is produced by surrounding mesenchymal cells and interacts with MET which is expressed in epithelial cells (Martin et al., 2004, Martin et al., 2001). This ligand/receptor-mediated association between the stroma and epithelium is essential for normal physiological processes such as organogenesis during embryonic

development and hepatocyte repair after injury and is tightly regulated (Gao and Vande Woude, 2005, Wen-Sheng Wu, 2010). However, HGF/MET activation is also observed in cancer and many tumours constitutively express HGF and/or MET (Birchmeier et al., 2003a, Wen-Sheng Wu, 2010, Martin et al., 2002). In many tumours, high expression of MET has been shown to be necessary to maintain tumour growth and survival (Shinomiya et al., 2004). In tumour cells, MET can also be overexpressed or mutated, thereby activating the downstream pathway without the need for a ligand (**Figure 1.19**) (Birchmeier et al., 1997, Duplaquet et al., 2018). MET gene amplification was found in gastric cancer and NSCLC, which is regarded as the driving factors for tumorigenesis and an essential resistance mechanism (Duplaquet et al., 2018). MET mutations in the tyrosine kinase domain have been found in both sporadic and hereditary forms of human papillary renal carcinomas (Schmidt et al., 1997). In both gastric (Lee et al., 2000) and small cell lung cancer (Ma et al., 2003), exon 14 skipping mutation encoding the juxtamembrane domain of MET were found. Mutations in this domain can continuously activate the MET signalling pathway (Peschard et al., 2001, Duplaquet et al., 2018).

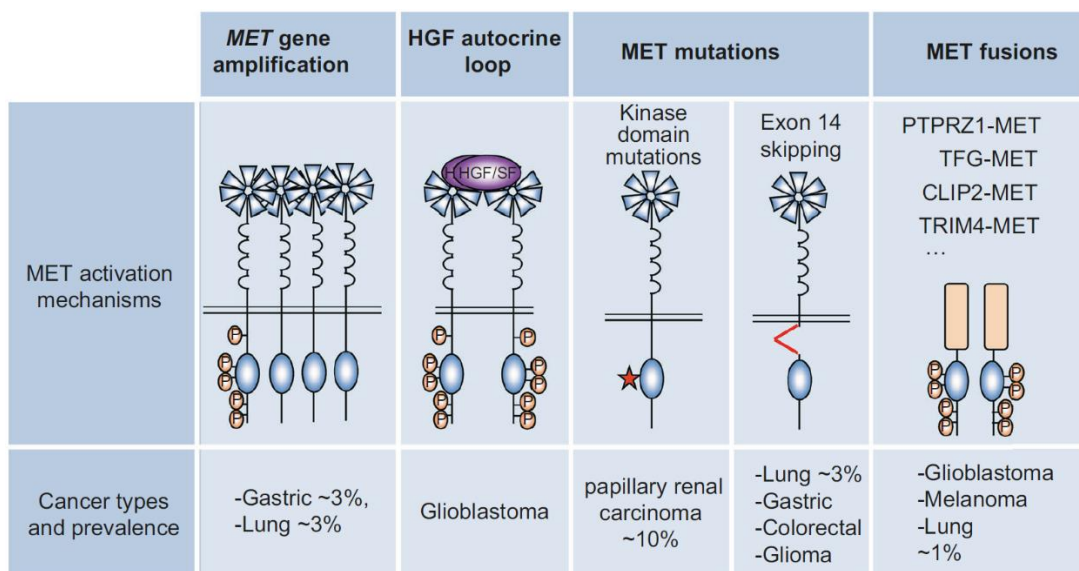


Figure 1.19: Schematic diagram of different molecular mechanisms activating MET in cancer (Duplaquet et al., 2018). Figure shows the MET gene amplification, HGF autocrine loop, MET mutations, and generation of MET fusion proteins through chromosomal rearrangement.

1.4.6 HGF/MET in NSCLC

High expression of MET can be observed in 61% of NSCLC patients and is closely related to poor prognosis (Ma et al., 2005).

a. In NSCLC, MET may be a driver of tumorigenesis, but not commonly (Wu et al., 2017). MET exon 14-skipping mutations could be found in only about 3% of NSCLCs and MET inhibitor monotherapy has a significant effect on such tumours (Frampton et al., 2015). Amplification of MET may be a 1-7% carcinogenic driver of NSCLC, and similarly this tumour may be inhibited by MET inhibitor monotherapy (Collisson et al., 2014).

b. MET may be the cause for drug resistance to other therapies (Wu et al., 2017). The largest group of NSCLC patients likely to benefit most from MET inhibitor therapy (in combination with an EGFR TKI) are patients with abnormal MET activity and resistance to EGFR-TKI. Combination of MET inhibitor with EGFR inhibitor may restore sensitivity to EGFR-TKIs (Raghav et al., 2012). Abnormal MET activity may be the second most common cause of acquired/secondary resistance to EGFR-TKI treatment, after EGFR T790M mutation. Previous research has revealed that in NSCLC, MET amplification occurs in 5-22% cases of acquired/secondary resistance to EGFR-TKI therapy (Wu et al., 2017).

1.5 Tight junctions

1.5.1 The Tight Junction (TJ) structure and function

In addition to connective tissue in human and multicellular animals, cells in other tissues are arranged and interconnected via various structures on the surface of adjacent cell membranes. These connections function to strengthen the mechanical connection between cells, maintain the integrity of tissue structure and coordinate the function of the cells. These structures are called cell junctions. Cell junctions, together

with cell adhesions, are the basic structural forms in which tissue remain intact and functionally distinct and which regulate multiple functional activities of cells such as growth, proliferation, differentiation and migration (Tracey A. Martin, 2013).

Cell junctions are divided into three groups based on difference in structure and function: tight junction (TJ), anchoring junctions and communicating junctions. Tight junctions are the areas between the cell membranes of adjacent cells, which can completely occlude the space between cells and isolate the extracellular space, thereby creating an intercellular barrier (Tracey A. Martin, 2013, Martin and Jiang, 2009). TJs maintain the permeability of epithelial cells and endothelial cells. Molecules and inflammatory cells can pass through the barrier of TJs in endothelial cells, whereas in epithelial cells, TJ acts in an adhesive manner and prevents cell dissociation (Martin and Jiang, 2009).

1.5.2 The structure of tight junctions

Tight junctions have a characteristic structure. They are located on the apical side of the epithelium and endothelial cells close to the external surface. Under electron microscopy, the TJ can be seen to be intermittently fused between the outer plasma membrane of adjacent cells and the cell gap disappeared at the fusion site. There remains a cell gap of 10-15nm in the non-fusion site (Tracey A. Martin, 2013, Martin, 2014). TJs appear as continuous intramembrane particle strands in the protoplasmic side, which completely circumscribe the apices of the cells as a network. The TJ structure is representative of the conglomerate of molecules that constitute, associate with or regulate TJs (Martin, 2014).

1.5.3 The tight junction proteins

In short, the TJ proteins consist of three major components (Martin, 2014, Tracey A. Martin, 2013):

- Integral transmembrane proteins
- Peripheral or plaque anchoring proteins
- TJ associated or regulatory proteins

The integral transmembrane protein includes the TAMP (transmembrane adhesion membrane proteins) such as Occludin, Tricellulin (also called Marvel D2), Marvel D3, the Claudin family, junctional adhesion molecules (JAMs), Nectins and other CTX (Cholera toxin) family members. Most peripheral or plaque anchoring proteins contain PDZ motifs which participate in protein-protein interactions, such as the Zonula Occludens (ZO) family ZO1, ZO2 and ZO3, MAGI-1 (membrane-associated guanylate kinase1), s-afadin, Par3 and Par6. The TJ associated or regulatory proteins include α -catenin, Cingulin and Rho-GTPases (**Table1.5**) (Martin, 2014, Tracey A. Martin, 2013, Martin and Jiang, 2009).

Table 1.5: Proteins involved in TJ structure, function and regulation.

Integral transmembrane proteins	Peripheral or plaque anchoring proteins	TJ-associated/regulatory proteins.
the TAMP proteins: Tricellulin (Marvel D2) Marvel D3 Occludin	ZO family: ZO1 ZO2 ZO3	Cingulin, 7H6, Symplekin, ZONAB, Rab-13, 19B1, ponsin, Rab 3B, PKC, I-afadin,
Claudin family	MAGI-1, -2, -3	c-src, Gai-2, Gai-12,
JAMs	s-afadin/AF6	α -catenin, Pals, PATJ,
Nectins	Par3/ASIP	PKA, JEAP, Pilt, PTEN,
CTX family: Coxsackie adenovirus receptor (CAR)	Par6 MUPP-1 CAROM CASK	ZAK, SCRIB, ITCH, Rho-GTPases, WNK4, vinculin

1.5.4 The function of tight junctions

The four main functions of the epithelial/endothelial TJs are (Martin, 2014, Martin and Jiang, 2009):

a. The TJ seals the intercellular space and the separation of apical and basolateral fluid compartments of epithelia and endothelia. The TJ works as a diffusion barrier to plasma membrane lipids and proteins, and those polarized epithelial and endothelial cells require TJs to define apical and basolateral membrane domains. Therefore in the epithelium, the TJ is essential to maintain the chemical and electrical gradients across the cell monolayer, which is requisite for vectorial transport processes such as absorption and secretion.

b. TJ molecules are intermediates and transducers of cell signalling that play a role in polarity, cell differentiation, cell growth and proliferation.

c. TJs mediate cell to cell adhesion between adjacent cells.

d. The TJ is a barrier to cell migration and motility.

Scientists have a better understanding of the barrier function of TJs, but as a complex multi-protein structure, understanding of the role of TJs in cell processes, proliferation, differentiation, as well as the development and metastasis of tumours is limited (Martin, 2014). It has become increasingly obvious that human cancer is frequently associated with the failure of epithelial cells to form TJ and to establish correct apicobasal polarity (Martin and Jiang, 2009). Changes in the expression and/or distribution of the TJ protein may result in complete loss of the TJ structure due to cancer cell invasion and ultimately cancer cell evaluation. Therefore, TJs could be an important factor in the progression of tumours (Martin, 2014).

1.5.5 Tight junctions are barriers to cancer metastasis

It is clear that the interaction and penetration of tumour cells with the endothelium is a critical step in tumour metastasis. Early studies demonstrated that TJ molecule reduction is associated with tumour development and it has become evident that TJs are the structure that cancer cells must overcome in order to metastasize successfully (Sato et al., 1996, Ren et al., 1990, Hoevel et al., 2002, Martin, 2014). Gradually, it

has been discovered that both up- regulation and down-regulation of TJ proteins can lead to loss of cell-cell binding, inhibition of cell contact, uncontrolled growth and loss of adhesion to basement membrane, eventually lead to tumourigenesis (Martin, 2014). Meanwhile, it is not only the change of cancer cell TJs, but the change of TJs in endothelial cells that is also very important for cancer metastasis (Martin, 2014). TJs occur between cancer cells and endothelial cells and may be the primary structure that hinders the transfer of cancer cells successfully (Martin and Jiang, 2009). TJs in vascular endothelial cell acts as a barrier between blood and tissue against metastatic cancer cells (Martin et al., 2002). Consequently, cancer cells must destroy the TJ structure in order to penetrate the endothelium. The regulation and functional changes of TJs form a vicious cycle in cancer progression, where changes in TJ function/structure are not only the consequence but also the cause of cancer progression. TJs are also critical to cancer development and sustainability, which ultimately leads to metastasis and secondary disease (Martin, 2014). Thus, studying the role of TJs in cancer is critical to understanding cancer metastasis and creating new diagnostic and therapeutic methods.

1.5.6 Changes in TJs in lung cancer

Previously it has been shown that a statistically significant association exists between tumours and Claudin1 or Claudin5 in lung cancer patients (Paschoud et al., 2007). Squamous cell carcinoma and normal bronchial basal cells are Claudin1 positive, Claudin5 negative, while adenocarcinoma, normal columnar epithelium and alveolar cells are Claudin5 positive, Claudin1 negative, suggesting different progression of lung cancer development. Claudin4 and ZO1 were positive in both lung squamous cell carcinoma and adenocarcinoma, whereas Cingulin was not detected in squamous cell carcinoma. In squamous cell carcinoma, the transcription level of JAM1, Occludin, Claudin3, Claudin4, Claudin7, Cingulin, ZO2 and ZO3 was significantly decreased, but Claudin1 was increased. In adenocarcinoma, the transcription levels of Claudin1, Claudin3, Claudin4, Claudin7, ZO2 and ZO3 were

also found to be significantly reduced compared to normal bronchial cells (Paschoud et al., 2007). Quantitative real-time reverse transcription PCR analysis revealed differential expression of Claudin1 occurs in 82.1% of tumours in small cell lung cancer (Liu et al., 2007). An early study of 68 lung cancers and adjacent normal lung tissue showed that Occludin stained strongly in normal lung tissue. IHC found Occludin is strongly stained in spots and short lines at the apex of bronchial epithelial cells and bronchial gland cells, and strongly stained continuously in the membrane of the alveolar epithelium (Tobioka et al., 2004). In all adenocarcinomas, regardless of typing and staging, Occludin exhibits similar staining in the luminal cancer cells as the normal tissue mentioned above. However, Occludin staining was not obvious in squamous cell carcinoma, large cell carcinoma, small cell carcinoma or neuroendocrine cancer (Tobioka et al., 2004). Therefore, it has been suggested that Occludin can be used as a molecular marker for determining the histological classification of lung cancer (Martin and Jiang, 2009, Tobioka et al., 2004).

1.6 Hypothesis and aims of this study

SIPA1 has been considered to play a positive role in the invasion and migration of breast cancer (Zhang et al., 2015). Previous work from the host laboratory showed that SIPA1 was involved in the regulation of HGF on TJs in breast cancer cell lines (unpublished data). However, there are limited studies investigating the function of SIPA1 in lung cancer (Gdowicz-Klosok et al., 2015, Xie et al., 2013) and the mechanism of SIPA1 in cancer development and metastasis still remains largely unknown especially the mediation of SIPA1 in regulating the TJs and reacting to HGF signalling pathway in lung cancer cells.

This thesis will test the hypothesis that SIPA1 plays a role as an important tumour promoter and a key modulator of the regulation of HGF in TJs in human lung cancer, and that it is linked to poor disease progression in the patients with lung cancer.

The aims of the study were as follows:

a. To determine the expression of SIPA1 in human lung cancer tissue and its

implications in cancer development and metastasis and disease progression.

b. To generate cell models from human lung cancer cell lines with various expression of SIPA1.

c. To assess the impact of differentially expressed SIPA1 on human lung cancer cell lines.

d. To investigate the underlying mechanism of SIPA1 in regulating tight junctions in human lung cancer cell lines.

e. To investigate the underlying mechanism of SIPA1 involved in the HGF/MET signalling pathway on the regulation of tight junctions in human lung cancer cell lines.

f. To investigate the underlying mechanism of SIPA1 in the regulation of human lung cancer cell behaviours including growth, invasion, migration and adhesion.

Chapter-2 Materials and methods

2.1 General materials

2.1.1 Cell lines

The cell lines used throughout the study were three lung cancer cell lines: A549, SK-MES-1 and COR-L23. A549 and SK-MES-1 cell lines were purchased from the American Type Culture Collection (ATCC) (LGC standard, Salisbury, England) and COR-L23 was purchased from the European Collection of Animal Cell Cultures (ECACC) through ECACC Salisbury, England. All cell lines were verified at the source for identity and were at low passage throughout the study. Further detailed information of these cell lines is listed in **Table 2.1**.

Table 2.1: Details of lung cancer cell lines used in this study

Cell line	A549	SK-MES-1	COR-L23
Species	<i>Homo-sapiens</i> , Human	<i>Homo-sapiens</i> , Human	<i>Homo-sapiens</i> , Human
Tissue	Lung	Lung; Derived from Metastatic Site: pleural effusion	Lung
Disease	Adenocarcinoma	Squamous cell carcinoma	Large cell carcinoma
Gender	Male	Male	Male
Age	58 years	65 years	62 years
Morphology	Epithelial-like	Epithelial	Epithelial
Growth properties	Adherent	Adherent	Adherent
Country	UK	UK	UK

2.1.2 Collection of human cancer tissues

A clinical cohort consisting of lung tumours (n=148) together with adjacent background tissues (n=148) was obtained immediately after surgery and stored in a freezer at -80°C until used. The cohort was the result of two consecutive collections, of which the protocol of collection, the procedure for tissue storage and processing including materials used to process the tissues was identical. Informed, written

consent was obtained from the patients at Peking University Cancer Hospital. All protocol and procedures were approved by the Peking University Cancer Hospital Research Ethics Committee (Appendix). The frozen tissues were sectioned using a Leica CM1900 Cryostat (Leica Microsystems Ltd, Bristol, UK) at 8-10µm thickness. These sections (n>50) were aliquoted into three portions. Firstly, some of the sections were mounted on glass slides immediately and fixed for routine histology assessment. Secondly, part of the sections were mounted on slides and fixed using Superfrost®Plus microscopic slides and stored at -20 °C for further immunohistochemical analysis. Thirdly the remaining sections were merged together and homogenized to extract RNA for genetic analysis.

2.1.3 General compounds

Chemicals material and reagents used throughout the study together with their suppliers are shown in **Table 2.2**.

2.1.4 General plastic consumables, hardware and software

General plastic consumables, the instruments, various hardware and software used throughout the study together with their suppliers are listed in **Table 2.3**.

Table 2.2: Chemicals and reagents

Material/Reagent	Supplier
10% Foetal calf serum (FCS)	Sigma-Aldrich, Poole, Dorset, UK
A/G protein agarose beads	Insight Biotechnology, Wembley, UK
Acetic acid	Fisher Scientific, Leicestershire, UK
Acrylamide mix (30%)	Sigma-Aldrich, Poole, Dorset, UK
Agarose	Melford Laboratories Ltd, Suffolk, UK
Ammonium persulphate (APS)	Sigma-Aldrich, Poole, Dorset, UK
Amphotericin B	Sigma-Aldrich, Poole, Dorset, UK
Ampicillin	Sigma-Aldrich, Poole, Dorset, UK
Bio-Rad DC™ Protein Assay	Bio-Rad Laboratories, Watford, London,

	UK
Blasticidin S	Melford Laboratores Ltd., Suffolk, UK
Boric acid	Melford Laboratories Ltd, Suffolk, UK
Bovine serum albumin (BSA)	Sigma-Aldrich, Poole, Dorset, UK
Bromophenol Blue	Sigma-Aldrich, Poole, Dorset, UK
Calcium chloride (CaCl ₂)	Sigma-Aldrich, Poole, Dorset, UK
Chloroform	Sigma-Aldrich, Poole, Dorset, UK
Coomassie Blue	Sigma-Aldrich, Poole, Dorset, UK
Crystal violet	Sigma-Aldrich, Poole, Dorset, UK
Diethylpyrocarbonate (DEPC)	Sigma-Aldrich, Poole, Dorset, UK
Dimethylsulphoxide (DMSO)	Sigma-Aldrich, Poole, Dorset, UK
Disodium phosphate (Na ₂ HPO ₄)	BDH Chemicals Ltd, Poole, Dorset, UK
Dithiothreitol	Sigma-Aldrich, Poole, Dorset, UK
Dulbecco's Modified Eagles' Medium (DMEM)/Nutrient mixture F-12 Ham's	Sigma-Aldrich, Poole, Dorset, UK
Ethylenediaminetetraacetic acid (EDTA)	Sigma-Aldrich, Poole, Dorset, UK
Ethanol	Fisher Scientific, Leicestershire, UK
Formalin	Sigma-Aldrich, Poole, Dorset, UK
Glycine	Melford Laboratories Ltd, Suffolk, UK
GoTaq® Green Master Mix	Promega (Southampton, UK)
Hydrochloric acid (HCl)	Sigma-Aldrich, Poole, Dorset, UK
Isopropanol	Sigma-Aldrich, Poole, Dorset, UK
Matrigel®	Corning Incorporated, Flintshire, UK
Methanol	Fisher Scientific, Loughborough, UK
PVDF membrane	EMD Millipore Corporation, Watford, London, UK
Penicillin	Sigma-Aldrich, Poole, Dorset, UK
Ponceau S Stain	Sigma-Aldrich, Poole, Dorset, UK
Precision qScript™ RT PCR kit	Primerdesign Ltd, Southampton, UK
Potassium chloride (KCl)	Fisons Scientific Equipment, Loughborough, UK
GI-1640	Sigma-Aldrich, Poole, Dorset, UK
Sodium azide (NaN ₃)	Sigma-Aldrich, Poole, Dorset, UK
Sodium chloride (NaCl)	Sigma-Aldrich, Poole, Dorset, UK
Sodium dodecyl sulphate (SDS)	Melford Laboratories Ltd, Suffolk, UK
Sodium fluoride (NaF)	Sigma-Aldrich, Poole, Dorset, UK
Sodium hydroxide (NaOH)	Sigma-Aldrich, Poole, Dorset, UK
Sodium nitrate (NaNO ₃)	Sigma-Aldrich, Poole, Dorset, UK
Sodium orthovanadate (Na ₃ VO ₄)	Sigma-Aldrich, Poole, Dorset, UK
Sodium pyrophosphate (Na ₄ P ₂ O ₇)	Sigma-Aldrich, Poole, Dorset, UK
Streptomycin	Sigma-Aldrich, Poole, Dorset, UK
Sucrose	Fisons Scientific Equipment, Loughborough, UK

SYBR®Safe DNA gel stain	Invitrogen, Paisley, UK
Tetramethylethylenediamine (TEMED)	Sigma-Aldrich, Poole, Dorset, UK
TRI Reagent	Sigma-Aldrich, Poole, Dorset, UK
Tris-Cl	Melford Laboratories Ltd, Suffolk, UK
Triton X-100	Sigma-Aldrich, Poole, Dorset, UK
Trypsin	Sigma-Aldrich, Poole, Dorset, UK
Tween 20	Melford Laboratories Ltd, Suffolk, UK
Vectastain Universal ABC kit	Vector Laboratories Inc, Peterborough, UKA
Zinc chloride (ZnCl)	Sigma-Aldrich, Poole, Dorset, UK

Table 2.3 Instruments, hardware and software

Hardware/Software	Supplier
0.4 µm and 8 .0 µm cell culture inserts	EMD Millipore Corporation, Watford, London. UK
25 cm ² and 75 cm ² cell culture flasks	CELLSTAR, Greiner bio-one, Stonehouse, Gloucester, UK
6 well, 24 well, 48 well, 96 well cell culture plate.	CELLSTAR, Greiner bio-one, Stonehouse, Gloucester, UK
8-well glass chamber slide (for immunofluorescence)	EMD Millipore Corporation, Watford, London. UK
Neubauer haemocytometer counting chamber	Mod-Fuchs Rosenthal, Hawksley, UK
Lecia DM IRB microscope	Lecia GmbH, Bristol, UK
ACCUspIN Micro 17R	Thermo Fisher Scientific, Germany
EVOS FL Auto 2 imaging system	Thermo Fisher Scientific, Waltham, MA USA
Electrical Cell-Substrate Impedance Sensing (ECIS)	Applied BioPhysics Inc, Troy, New York, USA
ECIS array plate 96W1E+	Ibidi Mannheim, Germany
Image J	Public Domain
GraphPad Prism	
Microsoft Excel	Microsoft In., Redmond, WA, USA
UV light chamber	Germix, UK
Class II laminar flow cabinet	Wolflabs, York, UK

2.1.5 Primers

All primers used in this study were designed using the Beacon Design Programme (Biosoft International, Palo Alto, California, USA) and were synthesized by either

Invitrogen (Paisley, UK) or Sigma (Poole, Dorset, UK). Details of the primers used for conventional RT-PCR and real time quantitative PCR (QPCR) are provided in **Table 2.4**.

Table 2.4 Primers for conventional RT-PCR, QPCR and ribozyme synthesis

PRIMER NAME	PRIMER SEQUENCE(5'-3')
GAPDHF8	GGCTGCTTTTAACTCTGGTA
GAPDHR8	GACTGTGGTCATGAGTCCTT
GAPDHF1	AAGGTCATCCATGACAACCT
GAPDHZR1	ACTGAACCTGACCGTACAGCCATCCACAGTCTTCTG
SIPA1F1	AGAACTCGCTGTCACCAC
SIPA1ZR	ACTGAACCTGACCGTACATACTGATGGCTTGGCTGT
CLDN1F	GAAGTGTATGAAGTGCTTGG
CLDN1ZR	ACTGAACCTGACCGTACAGACCTGCAAGAAGAAATA
CLDN2F1	AAGTCTTTGACTCCTTGCTG
CLDN2ZR	ACTGAACCTGACCGTACAGCCACAAAGATTGCTATCAC
CLDN3F1	ACTGCCACAGGACCTTCA
CLDN3ZR	ACTGAACCTGACCGTACAATGGTGATCTTGGCCTTG
CLDN4F1	GCAGCAACATTGTCACCT
CLDN4ZR	ACTGAACCTGACCGTACAGTACACCTTGCACCTGCATC
CLDN 5F1	TTCCTGGACCACAACATC
CLDN5ZR1	ACTGAACCTGACCGTACACACCGAGTCGTACACTTTGC
CLDN5F2	TTCCTGGACCACAACATC
CLDN5ZR2	ACTGAACCTGACCGTACACACCGAGTCGTACACTTTGC
CLDN6F1	ACGTGCCCTCTGTGTCAT
CLDN6ZR	ACTGAACCTGACCGTACACTCCACACAGGTGGTACACT
CLDN7F1	ATAACCCTTTGATCCCTACC
CLDN7ZR	ACTGAACCTGACCGTACAACAGGAACAGGAGAGCAGT
CLDN8F1	GCTTGGAGAAGCTCTCTACTT
CLDN8ZR	ACTGAACCTGACCGTACAAGCTACTGCTCTTTTCGTTG
CLDN9F1	GTGCCCTCTGTGTCATTG
CLDN9ZR	ACTGAACCTGACCGTACATCCACACACGTGGTACACT
CLDN10F1	GTCTCCAACCTGCAAGGACT
CLDN10ZR	ACTGAACCTGACCGTACAGCAAATATGGAACCAAAGAA
CLDN11F1	CCGGTGTGGCTAAGTACA
CLDN11ZR	ACTGAACCTGACCGTACACACAGGGAACCAAGATG
CLDN12F1	CTCTGCCTGATTGGAATG
CLDN12ZR	ACTGAACCTGACCGTACAACCTGCACTATTGACCAGAC
CLDN14F1	CACCCTACAGGCCCTACC
CLDN14ZR	ACTGAACCTGACCGTACAGTCTTTGTAGGCAGCTGGT

CLDN15F1	CCTGGGCGTCTACAACCTG
CLDN15ZR	ACTGAACCTGACCGTACAATAGACATCAGCCGGACA
CLDN17F1	CTGCTTATTGGCATCTGTG
CLDN17ZR	ACTGAACCTGACCGTACATGAAGTTCCCAGAAGGTATG
CLDN18F1	GGATCATGTTTATTGTCTCA
CLDN18ZR	ACTGAACCTGACCGTACACATCCAGAAGTTAGTCACCAG
CLDN19F1	GGAGCCCTCTTCATCCTG
CLDN19ZR	ACTGAACCTGACCGTACAGTGCTTGGGTTGAAGAACT
CLDN20F1	AGCAAACCTTTCTGGATCTGA
CLDN20ZR	ACTGAACCTGACCGTACACAGAAAATCATGCCAGAGAT
CLDN22F1	CAGGCTCTTGTAACCTCAAC
CLDN22ZR	ACTGAACCTGACCGTACATTGGATGACACAGGTTTG
CLDN23F1	CCGCCATCAAGTACTACAG
CLDN23ZR1	ACTGAACCTGACCGTACACCACCGAGTTGGTGTAGG
CLDN24F1	GTGGACGCACATGACTGT
CLDN24ZR	ACTGAACCTGACCGTACACAGGAGGAAGGTGAGCTG
JAM1F2	AACAAGATCACAGCTTCCTA
JAM1ZR	ACTGAACCTGACCGTACAACAAGTGTATGTCCCAGTGT
JAM2F1	CTGATAGGGGCTGTAAATCT
JAM2ZR	ACTGAACCTGACCGTACATAATGATGCAAGACAGTTCC
JAM3F1	TTGATGAGATTGTGATCGAG
JAM3ZR	ACTGAACCTGACCGTACAATCTTGCCTACTGGTACAGC
ZO1ZF2	TGGGTATGACACACATGGTA
ZO1ZR2	ACTGAACCTGACCGTACAGGTGGTACTTGCTCGTAA
ZO2F1	CAAAAGAGGATTTGGAATTG
ZO2ZR1	ACTGAACCTGACCGTACAGAGCACATCAGAAATGACAA
ZO3F1	CTGACATGGAGGAGCTGA
ZO3ZR1	ACTGAACCTGACCGTACAGCTTAGCTTCCCTTCTGACT
AF6F	ATCATCCACCACTGGAAC
AF6ZR	ACTGAACCTGACCGTACATCATCACTCCATGGAACCTC
OCLNZF	G AATTCAAACCGAATCATTG
OCLNZR	ACTGAACCTGACCGTACATGAAGAATTTTCATCTTCTGG

Z sequence 'ACTGAACCTGACCGTACA' highlighted in blue. Z-sequence presents on the specific primers containing a 5' hairpin structure labelled with a fluorophore (FAM).

2.1.6 Antibodies

2.1.6.1 Primary antibodies

Full detailed information of primary antibodies used in the current study are supplied in **Table 2.5**.

2.1.6.2 Secondary antibodies

The secondary antibodies used for western blotting were horseradish peroxidase (HRP) conjugated anti-goat IgG, goat anti-rabbit IgG, and rabbit anti-mouse IgG antibodies, all these antibodies are purchased from Sigma (**Table 2.5**) (Poole, Dorset, UK).

Table 2.5 Primary and secondary antibodies used in this study

Antibodies	Molecular weight (kDa)	Supplier	Product code
Mouse anti SIPA1	112	Abcam	ab219085
Mouse anti GAPDH	37	Insight Biotechnology	sc-32233
Mouse anti AF6	200	Insight Biotechnology	sc-74433
Rabbit anti ZO1	220	Thermo Fisher Scientific	61-7300
Goat anti ZO2	160	Insight Biotechnology	sc-12386
Goat anti ZO3	80-160	Insight Biotechnology	sc-11475
Goat anti Claudin1	22	Insight Biotechnology	sc-17658
Rabbit anti Claudin5	23	Insight Biotechnology	sc-28670
Goat anti Claudin7	24	Insight Biotechnology	sc-17670
Goat anti Claudin9	23	Insight Biotechnology	sc-17672
Rabbit anti Claudin10	23/19	Insight Biotechnology	sc-25710
Rabbit anti Claudin11	20	Insight Biotechnology	sc-25711
Goat anti Claudin15	23	Insight Biotechnology	sc-17683
Rabbit anti Claudin19	22	Insight Biotechnology	sc-134618
Rabbit anti Claudin20	23.5	Novusbio	H00049861-D01P
Goat anti Claudin23	32	Insight Biotechnology	sc-87047
Mouse anti JAM1	36	Insight Biotechnology	sc-53623
Goat anti JAM2	54	Insight Biotechnology	sc-23002
Goat anti JAM3	38	Insight Biotechnology	sc-23006
Goat anti Occludin	60-82	Insight Biotechnology	sc-8145
Rabbit anti-mouse (whole molecule) IgG peroxidise conjugate	Dependent on primary	Sigma-Aldrich	A5278
Goat anti-rabbit	Dependent	Sigma-Aldrich	A0545

(whole molecule) IgG peroxidise conjugate	on primary		
Rabbit anti-goat (whole molecule) IgG peroxidise conjugate	Dependent on primary	Sigma-Aldrich	A5420

2.1.7 Preparation of Reagents, Buffers and Standard solutions

2.1.7.1 Solutions for molecular biology experiments

- *Tris-Boric-Acid (TBE) electrophoresis buffer*

TBE buffer 10X concentrate (T4415) was purchased from Sigma-Aldrich (Poole, Dorset, UK), and diluted with distilled water into 1X stock and stored at room temperature for further use.

- *Diethylpyrocarbonate (DEPC) water*

500µl of diethyl pyrocarbonate (DEPC) (Sigma-Aldrich, Poole, Dorset, UK) was dissolved in 9,500µl distilled water to make the stock solution of DEPC water and autoclaved before use.

- *Loading buffer (used for DNA electrophoresis)*

25mg bromophenol blue (Sigma-Aldrich, Poole, Dorset, UK) and 4g sucrose (Fisons Scientific Equipment, Loughborough, UK) was dissolved in 10ml of H₂O to prepare the loading buffer and stored at 4°C until use.

Solutions for use in cell culture

- *Preparation of Complete Cell Culture Medium*

A549, SK-MES-1 lung cancer cells were cultured in Dulbecco's Modified Eagle's medium supplemented with 50ml heat inactivated foetal calf serum (FCS) (Sigma-Aldrich, Pooled, Dorset, UK) and 5ml of an antibiotic cocktail comprising penicillin, streptomycin and amphotericin B (Sigma-Aldrich, Pooled, Dorset, UK). COR-L23 lung cancer cells were cultured in GI 1640 containing 2mM glutamine with 50ml of heat inactivated FCS and 5ml of an antibiotic cocktail comprising penicillin, streptomycin and amphotericin B. The prepared medium was stored at 4°C for no more than one month.

- *Preparation of 0.05M EDTA*

The buffer was prepared by dissolving 40g NaCl, 1g KCl, 5.72g Na₂HPO₄ (BDH Chemical Ltd., Poole, England, UK), 1g KH₂PO₄ (BDH Chemical Ltd., Poole, England, UK) and 1.4g EDTA (Sigma-Aldrich, Pooled, Dorset, UK) in 5 litres of dH₂O to prepare the stock solution. The pH was adjusted to 7.4 using Sodium hydroxide (NaOH) and was autoclaved before use.

- *Trypsin (25mg/ml)*

Dissolving 500mg trypsin in 20ml 0.05M EDTA to prepare the 25mg/ml stock solution. The solution was filtered through a 0.2µm Minisart filter Sigma-Aldrich (Pooled, Dorset, UK) and stored at -20°C. The working solution was prepared by further dissolving 250µl of the stock trypsin/EDTA solution in 10ml of 0.05M EDTA to detach cells, and was stored at 4°C until use.

- *Phosphate buffered saline (PBS)*

PBS buffer 10X concentrate was purchased from Sigma-Aldrich (Poole, Dorset, UK), and diluted with distilled water into 1X stock and stored at room temperature for further use.

- *Antibiotics*

Antibiotic Antimycotic Solution (100X) was purchased from Sigma-Aldrich (Poole, Dorset, UK). 5ml of the antibiotic solution was added to a 500ml DMEM to obtain a final 1X concentration.

2.1.7.2 Solutions for use in cloning

- *Luria Bertani (LB) broth*

LB broth buffered capsules were purchased from Melford Laboratories Ltd (Bildeston Road, Chelsworth, Ipswich, Suffolk). The pH value was adjusted to 7.2 at 20°C and then the broth was sterilized by autoclaving and stored at room temperature until use.

- *LB agar*

LB agar was prepared by the addition of 25 LB broth capsules and 15g agar dissolved in 1L of distilled water at 37°C. The pH value was adjusted to 7.2 at 20°C and then the broth was sterilized by autoclaving and stored at room temperature until use. LB agar was melted in a microwave to make a LB agar dish. Adding appropriate antibiotic when the agar solution was cooled down to about 65°C. The agar solution was then poured into 10 cm² Petri dishes. The LB agar dishes were stored at 4°C.

2.1.7.3 Solutions for use in protein work

- *Lysis Buffer*

Lysis buffer was prepared by dissolving NaCl 150mM (8.76g), Tris 50mM (6.05g), sodium azide 0.02% (200mg), sodium deoxycholate 0.5% (5g), Triton X-100 1.5% (15ml), Aprotinin 1µg/ml (1mg), Na₃VO₄ 5mM (919.5mg) and Leupeptin 1µg/ml (1mg)

in 1 litre of dH₂O, and was stored at 4°C until use.

- *Tris Buffered Saline (TBS)*

Tris Buffered Saline 10X solution (T5912), 1L, was purchased from (Sigma-Aldrich, Poole, Dorset, UK) and diluted in 9L of distilled water. The pH was adjusted to 7.4 using HCl and stored at room temperature until use.

- *Ammonium persulphate (APS), 10%*

The solution was prepared by dissolving 1g APS in 10ml dH₂O and then stored at 4°C for future use.

- *Running buffer*

Tris-Glycine-SDS Buffer 10X concentrate (T7777), 1L, (Sigma-Aldrich, Poole, Dorset, UK) was diluted in 9L of distilled water and stored at room temperature for further use.

- *Transfer buffer*

Tris-Glycine Buffer 10X concentrate (T4904) (Sigma-Aldrich, Poole, Dorset, UK) , 1L, was diluted in 9L of distilled water containing 2L methanol (Fisher Scientific, Loughborough, UK) and stored at room temperature for further use.

2.2 Cell Culture

2.2.1 Cell Culture, maintenance and Storage

A549, SK-MES-1 and COR-L23 lung cancer cell lines were cultured in Dulbecco's Modified Eagle's Medium/Nutrient F-12 Ham (DMEM-F12, Sigma-Aldrich, Poole,

Dorset, UK). This medium contains 2mM L-glutamine and 4.5mM NaHCO₃ and supplemented with 10% heat inactivated Foetal Bovine Serum (Sigma-Aldrich, Poole, Dorset, England, UK) and antibiotics in PH 7.3.

All cell lines were cultured in 25 cm² and 75 cm² flasks (Greiner Bio-One Ltd, Gloucester, UK) depending on the required application with a loose cap in an incubator at 37°C, 95% humidification and 5% CO₂.

Confluency and viability of cells were visually assessed with an inverted phase contrast microscope. The confluency of cells was estimated based on the percentage of cells covering the surface of the tissue culture flasks. Cells were left to grow until they reached sub-confluency (80-95%) for experiments. All handling of cells was carried out using a Class II laminar flow cabinet with autoclaved and sterile equipment. Cells were passaged when they reached 80%-90% confluency.

2.2.2 Trypsinization and Counting of cell lines

The tissue culture flask was taken out from the incubator and the waste medium was aspirated using a glass pipette. Following this, the flask was briefly washed with sterile 5ml EDTA BSS buffer to remove remaining serum which would inhibit the action of trypsin.

Approximately 1-2ml of trypsin/EDTA solution (Trypsin 0.01% (w/v) and EDTA 0.05% (w/v) in BSS buffer) was added to the tissue culture flask. The adherent cells were detached after the flask was returned to the incubator for 5-10 minutes at 37°C. Flasks were inspected visually under the light microscope to make sure the cells were detached completely.

Once detached, 5ml DMEM containing 10% FCS was added to the flask to neutralise the trypsin and the detached cells were washed from the surface of the flask. The cell mixture was then transferred to a 30ml universal container (Greiner Bio-One Ltd, Gloucestershire, UK) and centrifuged at 1,800g for 10 minutes.

The supernatant was aspirated and the cell pellet was re-suspended in medium for re-culturing or used in experimental work immediately.

Cell counting was carried out using a Neubauer haemocytometer counting chamber under a light microscope using the x10 objective lens. The haemocytometer calculated the number of cells in a predetermined volume of fluid in order to obtain the quantity of cells per millilitre. The haemocytometer chamber was divided into 9 squares with dimensions of 1mm x 1mm x 0.2mm. For consistency of cell density and error reduction, four corners of 9 squared areas were counted. The number of cells was calculated using the following equation:

$$\text{Cell number/ml} = (\text{the sum of the number of cells in four corners}/8) \times (1 \times 10^4)$$

2.2.3 Storage of cell lines in liquid nitrogen and cell resuscitation

Cells were detached with trypsin from the flask as described in section 2.3.2. After centrifugation, the cells were re-suspended in medium with 10% dimethyl sulfoxide (DMSO) at a density of 1×10^6 cells/ml.

The cell suspension was transferred into 1ml pre-labelled CRYO.STM tubes (Greiner Bio-One, Germany) wrapped in protective tissue paper and then frozen down to -80°C . For longer term storage, the cells were transferred and stored at -196°C in a liquid nitrogen tank.

In order to resuscitate the frozen cells, the CRYO.STM tube was taken from the liquid nitrogen and thawed in a 37°C water bath rapidly. The cell suspension was then transferred into a 30ml universal container containing 5ml of pre-warmed medium and then centrifuged at 1,800g for 5 minutes. The medium was removed by aspiration. The cells were then resuspended in 5ml medium. The cells were incubated at 37°C , 95% humidification, and 5% CO_2 for further experiment.

2.3 Methods for RNA detection

2.3.1 RNA extraction

There are three main types of Ribonucleic acid (RNA) within the cytoplasm of all living eukaryotic cells:

- ribosomal RNA (rRNA)
- transfer RNA (tRNA)
- messenger RNA (mRNA)

Cellular mRNA was used in this study based on its important role of carrying genetic information and encoding corresponding protein products. At the transcript level, the presence of specific mRNA can indicate which proteins are likely to be produced by the cell. RNA isolation was performed using the Tri Reagent (Sigma-Aldrich, Poole, Dorset, UK) as outlined below.

After cells were cultured in a monolayer to a confluence of approximately 90% (5-10x10⁵ cells), the medium was removed and replaced with RNA reagent (1ml per 5-10x10⁵ cells) to produce cell lysate. The homogenous lysate was then transferred into a sterile microfuge tube, and left at room temperature for 5 min.

Chloroform was added to the homogenate at 0.2ml per 1ml of RNA reagent (Sigma-Aldrich, Poole, Dorset, UK) and the tube capped and shaken vigorously for 15 seconds. The resulting homogenate was then centrifuged at 12000g for 15 minutes at 4°C (Boece, Wolf laboratories, York, UK). Centrifugation resulted in separation of the lysate into three phases in the acidic environment - a red organic phase containing protein, an interphase containing DNA and a colourless upper aqueous phase containing RNA.

The upper aqueous phase containing RNA was carefully transferred to a fresh microfuge tube. Following this, 500 µl of 2-propanol (per 1ml TRI Reagent®) was added to the sample, shaken and incubated on ice for 10 minutes before centrifugation, for pelleting precipitated RNA, at 12,000 x g for 10 minutes at 4°C.

Subsequently, an RNA pellet was observed at the bottom of the microfuge tube.

The supernatant was discarded and the RNA pellet was washed with 1ml 75% ethanol (made with DEPC water) twice with vortexing and centrifuging at 7,500g for 5 minutes at 4°C.

The RNA pellet was briefly dried at 55°C for 5-10 min in a Techne, Hybridiser HB-1D drying oven (Wolf laboratories, York, UK), in order to remove any remaining ethanol.

Finally, the RNA pellet was dissolved in 50-100µl (depending on RNA pellet size) of DEPC water by vortexing. DEPC is used as a histidine specific alkylating agent to inhibit the hydrolysis of RNA by RNAases.

2.3.2 RNA Quantification

Once RNA isolation was completed, the concentration and purity of the resulting single stranded RNA were quantified by measuring its absorbance at a wavelength of 260nm using a UV 1101 Biotech spectrophotometer (WPA, Cambridge, UK). The RNA samples were measured with a Starna glass cuvette (Optiglass limited, Essex, UK). The A260nm/ A280nm ratio was used to estimate the purity of RNA sample by measuring the different absorbance between the RNA sample and DEPC water (as a blank control). The concentration of RNA samples was then standardised using DEPC water for reverse transcription (RT) or stored at -80°C for future use.

2.3.3 Reverse Transcription of RNA for production of cDNA

To determine transcript expression, an mRNA template was used to generate complementary DNA (cDNA) using reverse transcription (RT). Transcripts of a particular gene were then determined using RT-PCR and QPCR.

RT was performed by converting 500 ng of RNA into cDNA using the GoScript™ Reverse Transcription System kit (Promega, Southampton, UK) Based on the

instruction provided by the manufacture, each reaction was set up in 200µl PCR tubes as follows in **Table 2.6**:

Table 2.6: The system of RT-PCR.

Component Volume	Each reaction
GoScript™ 5X Reaction Buffer	4µl
MgCl ₂	1.2µl
PCR Nucleotide Mix	1µl
Recombinant RNasin Ribonuclease Inhibitor	0.5µl
GoScript™ Reverse Transcriptase	1µl
RNA template (0.5µg/µl)	1µl
Nuclease-Free Water	7.3µl

The reaction was carried out in a 2720 Thermal Cycler (Applied Biosystems, Paisley, UK). The reaction condition is listed as following in **Table 2.7**:

Table 2.7: The reaction condition of RT-PCR

Time	Temperature
5 minutes	25°C
60 minutes	42°C
15 minutes	70°C

After the reaction completed, the cDNA was diluted by 1:4 with PCR water as a template for PCR or store at -20°C for future use.

2.3.4 Polymerase chain reaction

Polymerase chain reaction (PCR) was first devised by Kary Mullis in 1983. It is a simple technique that is used to detect and amplify a single target DNA and produce thousands or millions of copies of the DNA sequence (Bartlett and Stirling, 2003). In this reaction, two short DNA sequences (oligonucleotides- *i.e.* forward and reverse

primers), which bind to the template DNA by base pairing, are required and are complementary to a defined sequence on each of the two strands of the DNA. These primers are aligned with the 3' ends facing each other.

The components of a PCR reaction include a DNA template containing the target DNA that is to be amplified, a heat resistant DNA polymerase such as Taq polymerase which synthesises DNA from nucleotides, short DNA fragments called primers which contain complementary sequences to the 3' ends of the sense and anti-sense strand of the target DNA and which act as a starting point for DNA formation by the DNA polymerase, deoxynucleotide triphosphates (dNTPs) from which the polymerase can synthesise new DNA strands and a thermal cycler, which provides repeated cycles of heating and cooling to provide the required temperatures for each step of the reaction. The DNA produced by PCR acts as a further template for replication resulting in a chain reaction and the exponential amplification of DNA.

In the current study, target genes were amplified using the GoTaq Green master mix (Promega, Southampton, UK). The reaction in aliquots of 16 μ l was set up in PCR tubes as described in **Table 2.8**:

Table 2.8: The system of PCR.

Component	Volume
cDNA template	2 μ l
Forward primer (working concentration of 1 μ M)	1 μ l
Reverse primer (working concentration of 1 μ M)	1 μ l
2X GoTaq Green master mix	8 μ l
PCR H ₂ O	4 μ l

A test sample containing PCR water instead of cDNA template was run alongside to detect any contamination of the reaction.

The PCR samples were briefly mixed and placed in a 2720 Thermo Cycler (ThermoFisher Scientific, Altrincham, UK). The condition of reaction was set as

described in **Table 2.9**:

Table 2.9: The reaction condition of PCR.

Step	Temperature	Time	Cycles
Initialisation	94°C	5min	1
Denaturation	94°C	20sec	32 cycles
Annealing	55°C	20 sec	
Extension	72°C	30 sec	
Final extension	72°C	10min	1
Final hold	4°C	∞	1

2.3.5 Agarose gel electrophoresis and DNA visualization

Agarose gel electrophoresis is the most common method to separate and analyse DNA fragments. It works by using electrical current to separate negatively charged DNA to a positive electrode through an agarose gel matrix, with the speed of migration depending on the size of DNA fragments. Agarose gels containing either 0.8% (1-10kb DNA fragments) or 1-2% (smaller fragments less than 1kb) agarose were prepared for running DNA samples.

The required amount of agarose powder (Melford Chemicals, Suffolk, UK) was added to 100ml (1X) TBE buffer and heated in a microwave oven until the agarose was completely dissolved. After cooling down for 5 minutes, the solution was stained with SYBR®Safe DNA gel stain (Invitrogen, Paisley, UK) and poured into electrophoresis cassettes (Scie-Plas Ltd, Cambridge, UK). Well forming combs were gently inserted and the gel was left to set at room temperature for 30-40 minutes until completely solidified.

Once the gel had set, the well forming combs were removed after 1xTBE was poured over and exceed 5mm of the gel surface. 8µL DNA ladder (GenScript®, Piscataway, USA) was loaded into the first lane of the gel and then 8-10µL of DNA samples were loaded into additional wells of the gel by placing the gel loading tips just over the well.

The gel was run with an electrophoresis power supply (Gibco BRL, Life Technologies Inc.) at 120V, 100mA and 50W for approximately 30-50 minutes. When the visible dye line had moved the desired distance required for the product size, the electrodes were disconnected.

The gel was then removed, and the DNA fragments visualised using Syngene U: Genius3 fluorescence UV transilluminator (Synoptics Ltd, Cambridge, UK). Images were saved electronically and printed using a thermal printer.

2.3.6 Quantitative RT-PCR (QPCR)

Real-time (or quantitative) PCR is a sensitive technique for gene analysis. It measures PCR amplification in real-time as the reaction proceeds instead of at the end of the reaction in comparison with conventional PCR. This method works by detecting a fluorescent reporter probe which is increased during PCR amplification (PCR product is proportional to the level of fluorescence detected). The fluorescence level is continuously recorded by a sensitive camera attached to the system.

In this study, the Ampliflour™ Uniprimer™ Universal system (Intergen company®, New York, USA) was used to quantify transcript copy number. The ampliflour probe consists of a 3' region specific to the Z-sequence ([ACTGAACCTGACCGTACA](#)) present on the target specific primers and a 5' hairpin structure labelled with a fluorophore (FAM). In this hairpin structure, the fluorophore is linked to an acceptor moiety (DABSYL) which acts to quench the fluorescence emitted by the fluorophore, preventing any signal from being detected.

During PCR, the probe becomes incorporated and acts as a template for DNA polymerisation in which DNA polymerase uses its 5'-3' exonuclease activity to degrade and unfold the hairpin structure, thereby disrupting the energy transfer between fluorophore and quencher, allowing sufficient fluorescence to be emitted and hence detected. The fluorescent signal emitted during each PCR cycle can then be directly correlated to the amount of DNA that has been amplified. This process is

Each sample was loaded into a 96 well plate (Applied Biosystems™, Life Technologies Ltd, Paisley, UK), covered with MicroAmp® Optical Adhesive film (ThermoFisher Scientific, Life Technologies Ltd, Paisley, UK) and run alongside a podoplanin (PDPL) standard of a known transcript number (ranging from 10⁸ to 10). PDPL is a lymphangiogenesis marker, which is employed as a reference control gene for a standard curve to ensure any differences observed were not due to technical errors and allowed normalization of results. It is also used to calculate relative copy numbers of target genes. The 96 well plate was placed in an iCycler Thermal Cycler which uses a light source to excite the fluorescent molecules in the wells and an image intensifier and a 350,000-pixel charge-coupled device (CCD) detector to image all 96 wells every second and detect fluorescent light at the annealing stage. The conditions used for QPCR are shown as described in **Table 2.11**:

Table 2.11: The reaction condition of real time quantitative PCR.

Step	Temperature (°C)	Time (minutes:seconds)	Number of cycles
Initial denaturation	94	05:00	1
Denaturation	94	00:10	100 cycles
Annealing	55	00:35	
Extension	72	00:20	

The fluorescent signal is detected at the annealing stage by a camera where its geometric increase directly correlates with the exponential increase of product. This is then used to determine a threshold for quantification of genes amplified in each reaction. Copy number of a target transcript is determined using the cycle number of a reaction when its fluorescence signal reaches the threshold.

The degree of fluorescence emitted by a range of standards with a known copy number of a reference gene (PDPL) are used to compare the amount of fluorescence emitted by each sample, allowing for the transcript copy number of a target gene in each sample to be accurately calculated.

Furthermore, the transcript copy number of each sample was normalized against the detection of GAPDH copy numbers. The procedure was repeated at least three times, and representative data is demonstrated.

How transcript levels are quantified is shown in **Figure 2.2**.

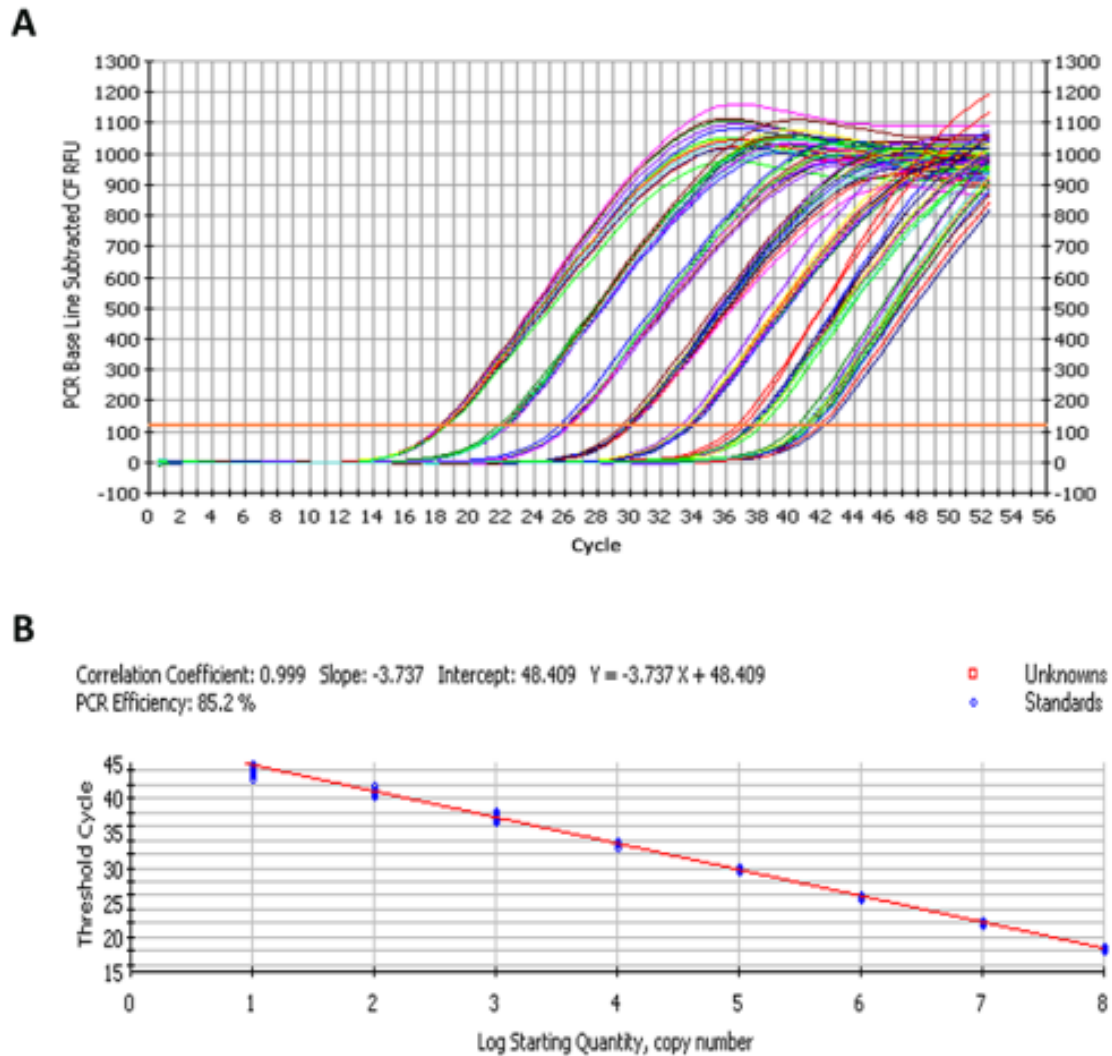


Figure 2.2: Diagram of standard curve generation. (A) Reaction curves for serial diluted standard samples (10^8 to 10 copy number) using Step One plus Real-Time PCR System; **(B)** The standard curve generated based on the threshold cycle and copy number of the serial diluted standard samples. Red line indicates the standard curve generated and blue dots stand for different standard samples with known copy number.

2.4 Methods for protein detection

2.4.1 Protein extraction and preparation of cell lysates

When cells reached sufficient confluence, the medium was removed and the cell monolayer was washed twice with PBS buffer. 5ml PBS was then added to the flask and the cells were scraped with a sterile cell scraper from the flask surface and transferred to a universal tube.

The cell suspension was centrifuged at 1,800g for 10 minutes to obtain a cell pellet. After removal of the supernatant with a vacuum aspirator, 200-300 μ l (depending on pellet size) of lysis buffer was added to the universal tube and the cell suspension was transferred to a 1.5ml microfuge tube. In order to extract protein from cell lysate, the sample was incubated at 4°C for 1 hour with continuous rotation on a Labinoco rotating wheel (Wolf laboratories, York, UK) (25g and 4°C). After 1 hour, the resulting lysate was centrifuged at 13,000g for 15 minutes. The supernatant containing proteins was then transferred to a fresh tube. The pellet containing insoluble and any unwanted cell debris was discarded. The protein sample was then either quantified for western blot or stored at -20°C until further use.

2.4.2 Protein quantification and preparation of samples for SDS-PAGE

In order to standardize their concentration before they were analysed using sodium dodecyl-polyacrylamide gel electrophoresis (SDS-PAGE) and western blotting, the protein samples were quantified using the Bio-Rad DC Protein Assay kit (Bio-Rad Laboratories, Hemel-Hempstead, UK). The kit utilised a colorimetric assay based on the reaction of protein with an alkaline copper tartrate solution (Reagent A) and Folin reagent (Reagent B), which is used for the determination of protein concentration following detergent solubilisation. The protein reacts with copper in the alkaline medium resulting in the subsequent reduction of the Folin reagent and the production of a characteristic blue colour (with an absorbance between 405-750nm). Bovine serum albumin (BSA) was used as a standard for this protein quantification.

In a 96 well plate, 50mg/ml BSA standard (Sigma-Aldrich, Poole, Dorset, UK) was diluted in lysis buffer to produce a concentration gradient from 0.78mg/ml to 50 mg/ml. These were used to generate a standard curve for determining concentration of the protein samples. Either protein samples or standards (5 μ l) were added into each well on a 96-well plate and 25 μ l of Reagent A' (prepared by adding 20 μ l of reagent S to every 1ml of reagent A) was added to each well followed by 200 μ l of Reagent B.

After the sample was mixed, the plate was left at room temperature for 30-45 minutes for the colorimetric reaction to occur. The absorbance for each well was then measured at a wavelength of 630nm using the ELx800 plate reading spectrophotometer (Bio-Tek, Wolf Laboratories, York, UK).

The standard curve was set up using the absorbance of the standards. Protein concentration of the test samples was determined according to the standard curve. Appropriate amounts of lysis buffer was used to standardise the protein samples to a final concentration of 1-2mg/ml depending on the lowest concentration of the same collection.

This sample was finally diluted 1:1 with 2x Lamelli sample buffer concentrate (Sigma-Aldrich, Poole, Dorset, UK) and then denatured by boiling at 100°C for 5-10 minutes. The boiled samples were either used immediately for SDS-PAGE or stored at -20°C until further use.

2.4.3 Sodium Dodecyl Sulphate Polyacrylamide Gel Electrophoresis (SDS-PAGE)

Four glass plates were prepared and assembled in two gel cassettes on a casting stand. Once assembled, ethanol was used to fill the space between the glass plates to test for leakages.

The system used to conduct SDS-PAGE in this study was an OmniPAGE VS10 vertical electrophoresis system (Clever Scientific Ltd., Rugby, Warwickshire, UK).

The required percentage of resolving gel was dependant on the protein size. A mixture of 15ml (enough for 2 gels) was prepared by adding all the constituents listed in **Table 2.12**:

Table 2.12: Component of the 10% resolving gel

Component of 10% Resolving gel	
Distilled water	5.9ml
30% acrylamide mix (Sigma-Aldrich, Poole, Dorset, UK)	5.0ml
1.5 M Tris (pH8.8)	3.8ml
10% SDS	0.15ml
10% Ammonium persulphate	0.15ml
TEMED (Sigma-Aldrich, Poole, Dorset, UK)	0.006ml

The resolving mixture was then added into space between the two glass plates carefully until it reaches a level about 1cm below the comb. In order to prevent gel oxidation, 1ml 2-propanol was added to cover the top of resolving gel.

The gels were then left to polymerise at room temperature for about 30 minutes, or until set completely. The excess 2-propanol was poured off before a sufficient amount of stacking gel was added. The ingredients for staking gel are listed in **Table 2.13**.

Table 2.13: Component of the stacking gel

Component of Stacking gel	
Distilled water	3.4ml
30% acrylamide mix (Sigma-Aldrich, Poole, Dorset, UK)	0.83ml
1.0M Tris (PH 6.8)	0.63ml
10% SDS	0.05ml
10% Ammonium persulphate	0.05ml
TEMED (Sigma-Aldrich, Poole, Dorset, UK)	0.005ml

A well forming Teflon comb was inserted immediately after adding the stacking gel,

and the gel was left at room temperature for around 20 minutes for polymerisation to occur.

After the gel was set, the loading cassette was transferred into an electrophoresis tank and covered with 1X running buffer before the well comb was removed. 10 μ l of Broad range markers (Santa Cruz Biotechnology, UK) were loaded into the first well of the gel, followed by 10-15 μ l of the required protein samples.

The proteins were then separated at 80-120V, 50mA, and 50W for a period up to 3 hours depending on the degree of separation required for target proteins according to their molecular weight.

2.4.4 Western blotting: transferring proteins from gel to nitrocellulose membrane

After SDS-PAGE, the gel containing protein samples was electrically transferred onto a PVDF membrane. Following SDS-PAGE separation, the electrophoresis cassettes were disassembled and the gels were taken out. The stacking gel on each gel was cut off and discarded. The resolving gel was then placed on the lower graphite base electrode in a SD20 SemiDry Maxi System blotting unit (SemiDRY, Wolf Laboratories, York, UK) on top of 3 pieces of 1X transfer buffer pre-soaked filter paper (Whatman International Ltd., Maidstone, UK), and 1 sheet of PVDF membrane.

An additional 3 sheets of pre-soaked filter paper were placed on top of the gel to form a sandwich arrangement in the order of filter papers, gel, membrane, filter papers (from cathode to anode) (**Figure 2.3**). Electroblothing was then conducted at 15V, 500mA, and 8W for 40-90 minutes according to protein size. Once the proteins had been transferred sufficiently, the membranes were blocked with 5% milk solution (5% milk skimmed powder and 0.1% polyoxyethylene (20) sorbitan monolaurate (Tween 20) in TBS for at least one hour at room temperature. This step aims to reduce background, *i.e.* non-specific binding to the membrane before subsequent probing with antibodies.

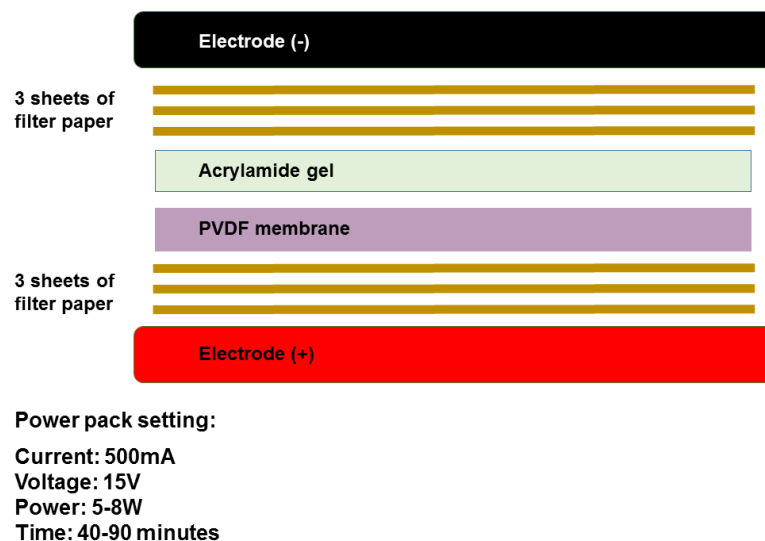


Figure 2.3: Diagram of the electrophoresis equipment transferring proteins from gel to membrane. The ‘sandwich’ structure from upper to lower: electrode (-) → filter paper → acrylamide gel → PVDF membrane → filter paper → electrode (+). To make sure the negatively charged protein move towards the positive electrode.

2.4.5 Protein detection using specific Immuno-probing

Once the blocking was completed, the membrane was transferred into 50ml falcon tubes (Nunc, Fisher-Scientific, Leicestershire, UK) with the membrane surface facing upwards. Then the membrane was incubated overnight at 4°C in 10ml 1% milk solution (1% milk powder, 0.1% Tween 20 in TBS) with primary antibody diluted 1:500.

After probing with the primary antibody, the membrane was washed with 5ml TBST (TBS with 0.1% Tween 20) for three times (10 mins each) to remove remaining unbound antibodies. The membrane was subsequently incubated for one hour with continuous rotation with 5ml of 1:1000 horseradish peroxidase (HRP) conjugated secondary antibody diluted in 3% milk. The membrane was subsequently washed three times (10 mins each) with 5ml TBST before undertaking chemiluminescent detection.

2.4.6 Chemiluminescent protein detection

Chemiluminescent protein detection was carried out using a luminol/peroxide based enhanced chemiluminescence (EZ-ECL) kit (Biological Industries Israel Beit Haemek Ltd., Israel). This solution consists of a highly sensitive chemiluminescent substrate and is used to detect HRP for visualising the probed protein bands under X ray film or imaging system. The protocol was undertaken as follows: 100 μ L of ECL reagent was required per cm² of membrane area with a 5-minute incubation at room temperature. The chemiluminescent signal was detected using G: Box (Syngene, Cambridge, UK) which contains both an illuminator and a camera linked to a computer. The exposure time was adjusted as necessary until the protein bands were sufficiently visible and the image was captured and analysed (ImageJ) for the protein band quantification.

In this study, GAPDH was used as a loading control and run alongside when detecting any other proteins for additional normalisation of the sample. GAPDH was used because of its high abundance and conserved nature within eukaryotic cells and is one of the most widely employed and accepted internal controls in determining mRNA and protein expression.

2.4.7 Immunohistochemical staining

This was based on paraffin embedded sections in the form of tissue microarray. After dewaxing and rehydration in each solution for 5 minutes sequentially: 100% xylene, 50% ethanol with 50% xylene, 100% ethanol, 90% ethanol, 70% ethanol, 50% ethanol, the tissue section was treated with 3% H₂O₂ for 15 mins to inactivate endogenous enzymes was . Antigens on the tissue section were repaired by heating the tissue section in the microwave for 20 mins. Horse serum (1-2 drops) was added into 5ml of 1 \times OptiMax Wash Buffer (BioGenex, San Ramon, USA) to prepare the blocking solution, and the tissue section was blocked in the blocking solution for 30 minutes at room temperature. After blocking, the slide was washed three times with

wash buffer, and then incubated overnight in 4°C with primary antibody (diluted to a concentration of 10µg/ml in blocking solution). Any unbound antibody was subsequently removed after washing in buffer for 10 mins repeated three times. The corresponding secondary antibody diluted 1:1000 in blocking solution was added and incubated for 30 minutes in room temperature. After three washes with wash buffer, the sections were incubated with 200µl of VECTASTAIN® Universal ABC complex (Vector Laboratories Inc., Burlingame, USA) for 30 minutes. The ABC complex must be prepared ready at least 30 minutes before using by mixing 4 drops of the supplied reagent A, with 4 drops of reagent B. The ABC solution was removed by washing three times with wash buffer, then 3,3'-Diaminobenzidine (DAB) chromogen (Vector Laboratories Inc., Burlingame, USA) were added on the tissue section and incubated for 5 minutes in the dark. The DAB was made up as a mixture of 2 drops of the provided buffer (pH 7.5), 4 drops of DAB, and 2 drops of hydrogen peroxide in 5ml of distilled water. A brown colouration showed the presence of the target protein and then the DAB was washed off using distilled water and the sections were co-stained with Mayer's haematoxylin for approximately 5 minutes. The tissue section was then washed with distilled water three times, and the tissue section slide was dehydrated for 5 minutes in each solution sequentially: 50% ethanol, 70% ethanol, 90% ethanol, 100% ethanol, 50% ethanol with 50% xylene, 100% xylene. After dehydration, slides were mounted with DPX mount and left to dry.

2.4.8 Protein for Kinexus™ microarrays

2.4.8.1 Sample preparation

Before protein extraction, each cell type was cultured in two T75 flasks until approximately 80% confluent. Cells were left in serum free medium for 24 hours and treated with/without HGF (hepatocyte growth factor) (50ng/ml) for one hour. Cells were washed with PBS in 4°C twice and scraped from the flask in 5ml sterile PBS. The cell suspension was centrifuged at 2,500g for 10 minutes to pellet the cells. The

pellet of cells was lysed in 500µl lysis buffer and placed on a Labinoco rotating wheel (Wolf laboratories, York, UK) (25g and 4°C) for 60 minutes to make a sufficient extract. Then after centrifugation at 13000g for 15 minutes, the protein lysate was used for protein quantification described as before. Following this, 350µl of the solution was prepared and stored at -20°C until sending to Kinexus™ microarray analysis (Kinexus Bioinformatics, Vancouver, British Columbia, Canada).

2.4.8.2 Antibody microarrays

This study employed a recent protein kinase array, namely KAM1325. The array has 1325 antibody spots (Kinexus Bioinformatics Ltd, Vancouver, Canada). A representative image for each of the antibody is as follows:

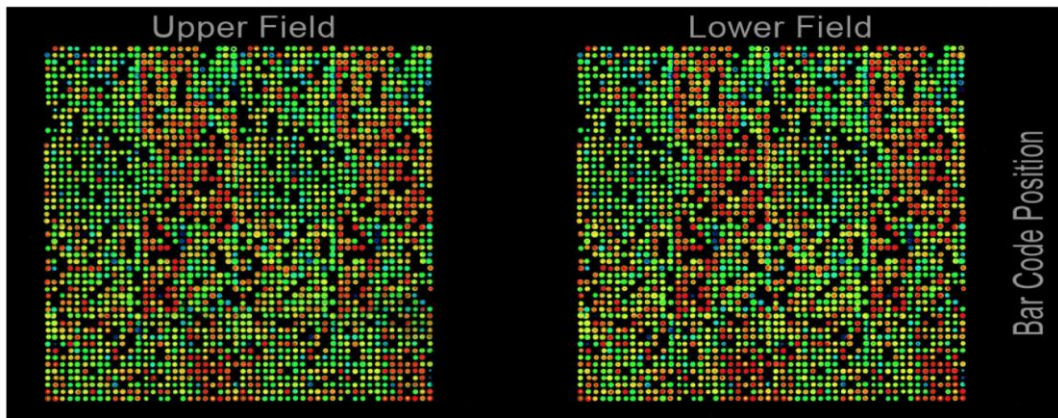


Figure 2.4: Antibody layout on a typical KAM1325 protein array, image supplied by Kinexus Inc. Using the protein microarray to compare the difference in these key signalling molecules between the control cells and SIPA1 knockdown cells. The different sites in the figure show different colours (red and green) because different antibodies are recognized and stained with different colour dyes, and black means the stain intensity is very low.

2.4.8.3 Key information derived from KAM1325.

The following are the key parameters collected and used for the data analyses:

Globally Normalized Signal Intensity - Background corrected intensity values are globally normalized. The Globally Normalized Signal Intensity is then calculated by summing the intensities of all the net signal median values for a sample.

Flag - An indication of the quality of the spot, based on its morphology and background. The flagging codes used in the reports are as follows:

0: acceptable spots

1: spots manually flagged for reasons and may not be very reliable

3: poor spots defined by various parameters

%CFC (change from control) - The percent change of the treated sample in Normalized Intensity from the specified control.

Calculation = (Globally Normalized Treated – Globally Normalized Control)/Globally Normalized Control) * 100

% Error Range - A parameter to show how tightly the “Globally Normalized Net Signal Intensity” for adjacent duplicate spots of the same protein in the sample compare to each other.

Calculation = ABS (Globally Normalized Spot 1 - Globally Normalized Spot 2)/Globally Normalized Spot 2*100

Log2 (Intensity Corrected) - Spot intensity corrected for background is log transformed with the base of 2.

Calculation = LOG (Average Net Signal Median, 2)

Z Scores - Z score transformation corrects data internally within a single sample.

Z Score Difference - The difference between the observed protein Z scores in samples in comparison.

Z Ratios - Divide the Z Score Differences by the SD of all the differences for the

comparison.

2.4.8.4 Antibody array analysis of SIPA1 interacting proteins

The immunoprecipitates from normal and tumour tissues from the same patient was applied to the same slide, to reduce the inter-assay variance. The proteins samples were labelled, applied to the microarray, and image subsequently scanned using Perkin-Elmer Scan Array Reader laser array scanner, according to manufacturer's instructions. Analysis was carried out using the *ImaGene 9.0* from BioDiscovery (El Segundo, CA).

Here our analyses focused on the Globally Normalized Signal Intensity, %CFC and the Z-scores.

2.4.9 Immunofluorescence staining.

Cells were seeded into 8 or 16 well glass chamber slides and allowed to reach about 90% confluency in an overnight culture. After brief washing, the cells were exposed to 2% FCS media for 2 hours, before treatments were given. At the conclusion of the treatment, cells were fixed with 5% formaldehyde prepared in a neutral buffer for long than 2 hours. Following washing with PBS buffer, the cells were treated with a permeabilisation buffer (PBS with 0.1% Triton X100) for 5 minutes, before additional washing. Block the cells with horse serum. The primary antibody or antibodies (in the case of dual staining), diluted to the pre-determined concentration in PBS with 1% BSA, were added to each well, followed by incubation for overnight at 4°C in dark (by wrapping in kitchen foil). After 5 extensive washings with the same buffer, secondary antibodies tagged with either FITC (fluorescein isothiocyanate) or TRITC (tetramethylrhodamine isothiocyanate) were added to the wells and allowed for a further 2 hours. After brief washing, DAPI (4',6-diamidino-2-phenylindole, for nucleus staining) was added to the well for 30 minutes, followed by extensive washing.

After carefully removing silicon sealant surrounding the wells, Fluosave™ was added to the slides and coverslips were carefully laid over the slides. The procedures were carried out in dark and slides always stored in dark at 4°C. The slides were subsequently examined under a fluorescent microscope and images photographs using a Hamamatsu Orca digital camera.



Figure 2.5: Olympus Fluorescence Microscope equipped with a Hamamatsu digital camera.

2.5 Targeting SIPA1 gene expression

2.5.1 Knock down of SIPA1 using Ribozyme Transgenes

Hammerhead ribozyme transgenes were used to knockdown the expression of SIPA1 by specifically targeting and cleaving the SIPA1 transcript. Hammerhead ribozymes targeting SIPA1 were designed based on the secondary structure of

SIPA1 mRNA (Figure 2.6).

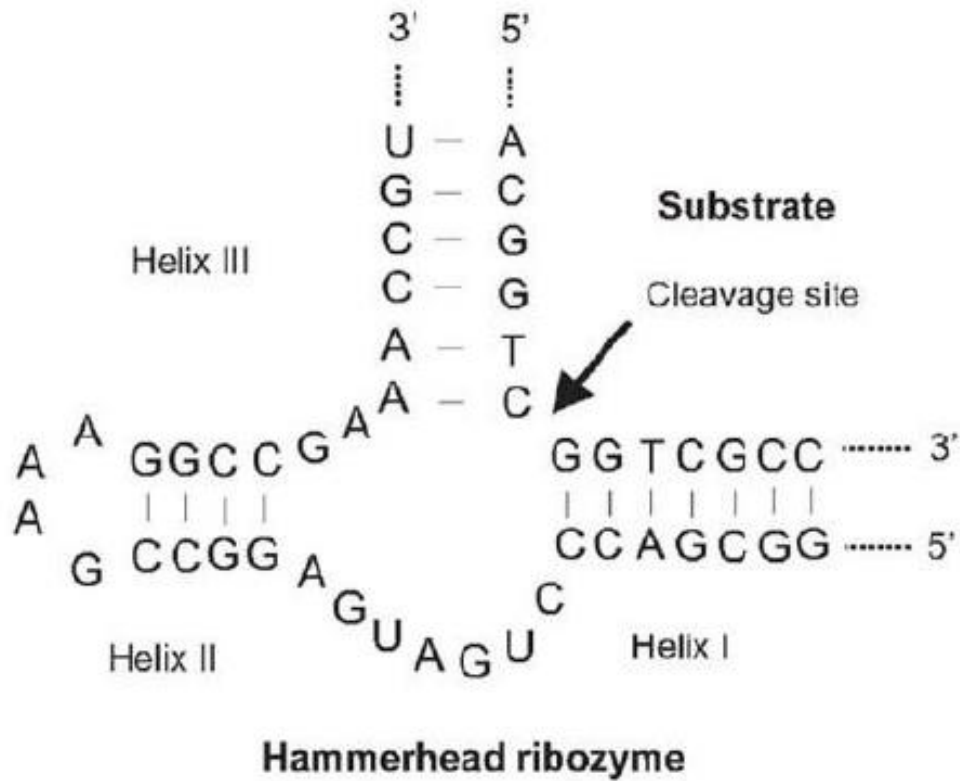


Figure 2.6 A: Schematic diagram of the secondary structure of hammerhead ribozyme. Helix I and helix III are the binding site, which could recognize and bind to the specific sequence, then the cleavage site is able to cut the mRNA to knock down the gene expression in transcript level.

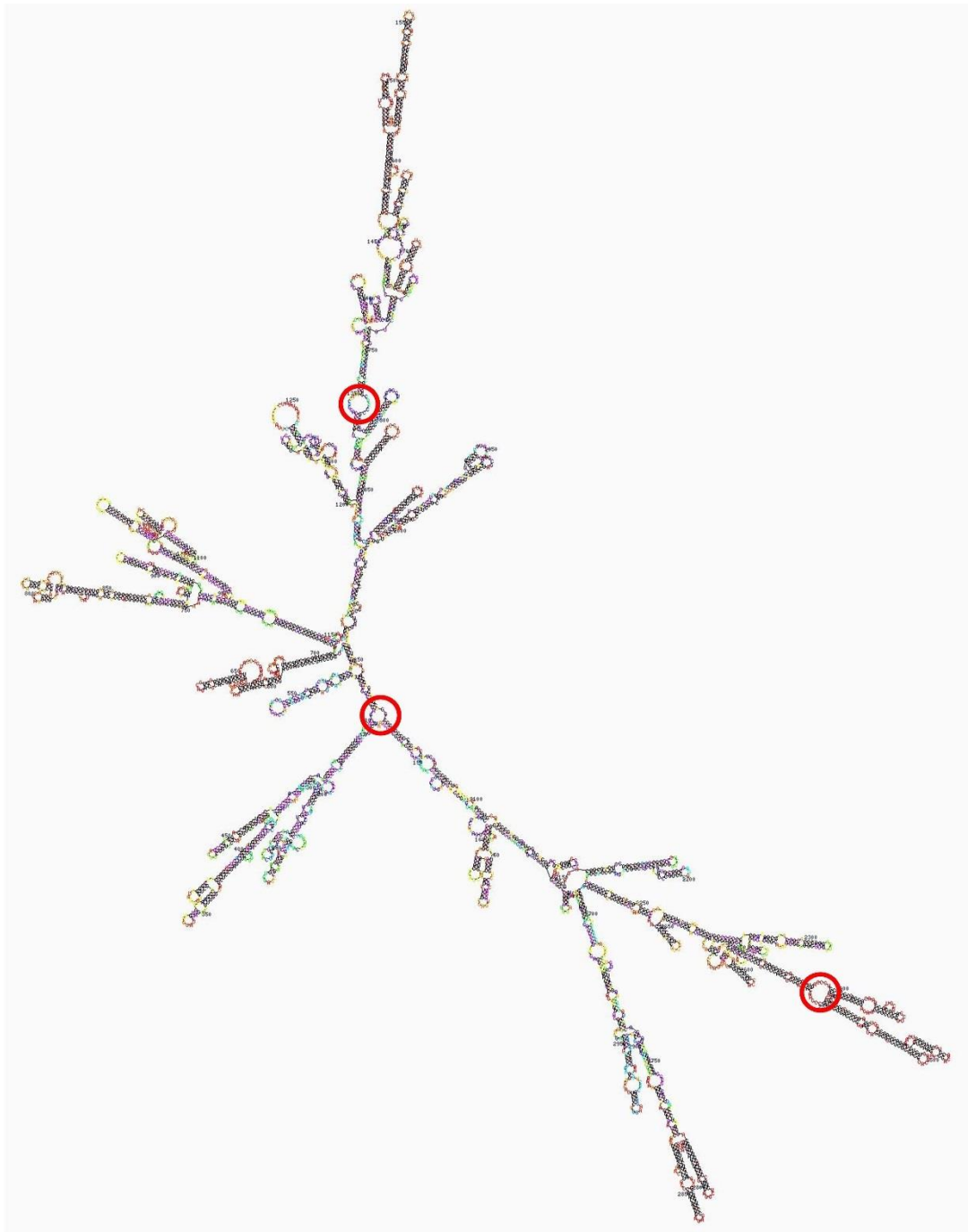


Figure 2.6 B: Schematic diagram of the secondary structure of SIPA1 mRNA. Generated from The mfold Web Server: <http://unafold.rna.albany.edu/?q=mfold/RNA-Folding-Form>. The loop region in the mRNA was chosen to be the site of action of the ribozyme (typical examples are marked in red).

The transgenes were synthesised using touchdown PCR and the products were then

run on a 2% agarose gel to verify their presence and size before being cloned into the pEF6/His plasmid vector (**Figure 2.7**). Subsequently, the ribozymes obtained from the above procedure were cloned into the pEF6/V5-His-TOPO vector, and this was followed by transferring the reaction mixture to a vial of TOP10 chemically competent *Escherichia Coli* (*E. coli*). After 30 minutes on ice, the bacteria were subject to heat shock at 42°C for 30 seconds, before being placed on ice for 2 minutes. The bacterial mixture was added to S.O.C. medium (Super broth with Catabolite repression, a rich culture media used for *E. coli*) and placed on an orbital shaker for 1 hour, at a speed of 200g. The bacterial solution was plated on agar plates containing 100µg/ml ampicillin and allowed to grow overnight. As the pEF plasmid has antibiotic resistance genes to ampicillin and blasticidin, only the cells containing the plasmid were able to grow on the agar. Colonies of transformed *E. coli*, transgenes of SIPA1 cloned into pEF6/V5-His-TOPO plasmids (Invitrogen Inc., Paisley, UK) were analysed using RT-PCR with the T7F primer coupled either with RbBMR and RbTPF primers. After amplifying the correct colonies, the plasmids were extracted using the Promega Plasmid MidiPrep Kit. Control plasmid and the plasmid containing the ribozyme transgene were used to transfect A549, SKMES1 and CORL23 cell lines respectively. The transfected cells were cultured in selection medium containing 5-10µg/ml blasticidin for around 1-2 weeks so that only those cells containing the plasmid would survive. Following selection, the cells were transferred into maintenance medium containing 0.5µg/ml blasticidin. To verify the knockdown of SIPA1, RT-PCR, QPCR and western blot procedures were carried out as previously described.

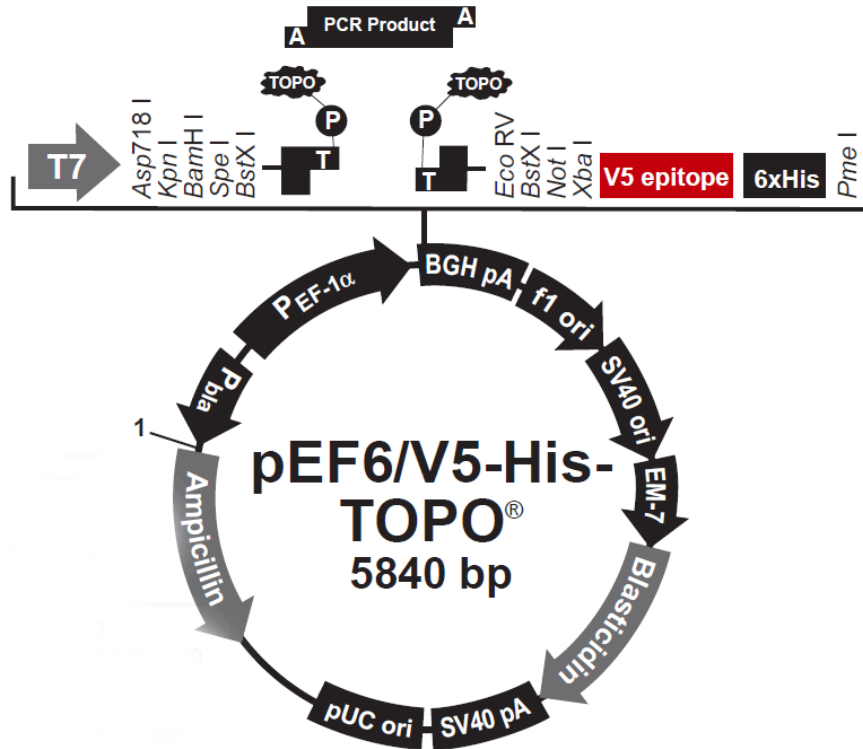


Figure 2.7: Schematic of the pEF6 plasmid (From pEF6/V5-His TOPO TA Expression Kit protocol).

2.6 *In vitro* Function assay

2.6.1 *In vitro* cell growth assay

Medium (200µl) containing 3,000 cells was seeded into 96 well plates. These plates were incubated at 37°C, with 5% CO₂, for periods of 24, 48, 72, and 120 hours respectively.

After incubation, the medium was aspirated, and the cells were fixed with 4% formaldehyde for 10-20 minutes before being stained with 0.5% crystal violet for 10 minutes. The plate was then rinsed with tap water and left to air dry.

The crystal violet was then solubilised using 200µl of 10% acetic acid and the amount of cells was assessed by measuring the absorbance of the resulting solution at 540nm using a spectrophotometer (BIO-TEK, ELx800, UK). The growth rate was calculated as a percentage, using the absorbance from the corresponding plate

collected at 24 hours as a baseline.

2.6.2 *In vitro* thiazolyl blue tetrazolium bromide (MTT) cell growth assay

MTT (3-(4,5-dimethylthiazol-2-yl)-2,5-diphenyltetrazolium bromide) tetrazolium has been widely adopted in a variety of cell functional assays, especially cell viability assay. MTT can be converted into a purple coloured formazan product with absorbance near 570nm by viable cells with active metabolism. Such formazan product, soluble in DMSO, accumulates as precipitate and distributes inside the cell as well as the culture medium near the cell surface. The amount of formazan product corresponds to the number of viable cells following linearity. Thus, the absorbance of formazan solution is comparable to the number of viable cells. MTT stock solution (5.5mg/ml) was made by adding 110mg thiazolyl blue tetrazolium bromide powder (MTT) (Sigma-Aldrich, Inc., Dorset, UK) in 20ml PBS into a foil wrapped 30ml universal container, and the tube was then placed on a roller mixer (Stuart, Wolf-Laboratories, York, UK) until the powder was dissolved thoroughly. Once the powder was dissolved completely, the solution was filtered through a 0.2µm filter on top of a fresh foil wrapped sterile universal tube in a biosafety cabinet and stored at 4°C in a fridge for further use.

Once 90% confluency was obtained, cells were trypsinised, centrifuged and re-suspended with normal medium. Cell number was then counted manually and an appropriate amount and cell density of cell solution was prepared for cell seeding. 200µl of the cell suspension (2000 cells/200µl) was then pipetted into three 96-well plates in six replicates followed by incubation for 24 (1 day), 72 (3 days) and 120 hours (5 days) at 37.0°C, 5% CO₂ and 95% humidity respectively. 20µl of sterile MTT stock solution was added at 24, 72 and 120 hours after cell seeding (working concentration of 0.5mg/ml MTT) and the plates were incubated at 37°C, 5% CO₂ and 95% humidity for 4 hours. The MTT medium solution was then aspirated gently, using a glass aspirator, followed by the addition of 200µl of DMSO. After 10 minutes

incubation at 37.0°C, 5% CO₂ and 95% humidity, the plate was taken out and tapped gently to thoroughly mix the DMSO solution.

The absorbance of each well was read at 540nm using an ELx800 plate reading spectrophotometer (Bio-Tek, Wolf laboratories, York, UK). Experiments were repeated for a minimum of three times. The cell number in each well was determined by the absorbance and a percentage increase at each time point was calculated as follows:

Percentage increase = [(day 3 or day 5 absorbance - day 1 absorbance)/(day 1 absorbance-background absorbance)] x 100%

2.6.3 *In vitro* transwell cell invasion assay

8µm pore transwell inserts (Millicell, Merck KGaA, Darmstadt, Germany) were placed into wells of a 24 well plate, using sterile forceps in order to prevent contamination.

Each insert was coated with 100µl of serum free medium containing 50µg Matrigel® Basement Membrane Matrix (Corning Incorporated, Flintshire, UK, stock concentration 0.5µg /µl) and left to dry for 2 hours at 55°C. The Matrigel was then rehydrated with 200µl serum free medium at room temperature for 45 minutes. After the water was carefully discarded, 20,000-40,000 cells in 200µl medium were seeded into each insert. Medium (600µl) was then added to the bottom chamber of each well. The cells were incubated for 72 hours, with 5% CO₂ at 37°C (**Figure 2.8**).

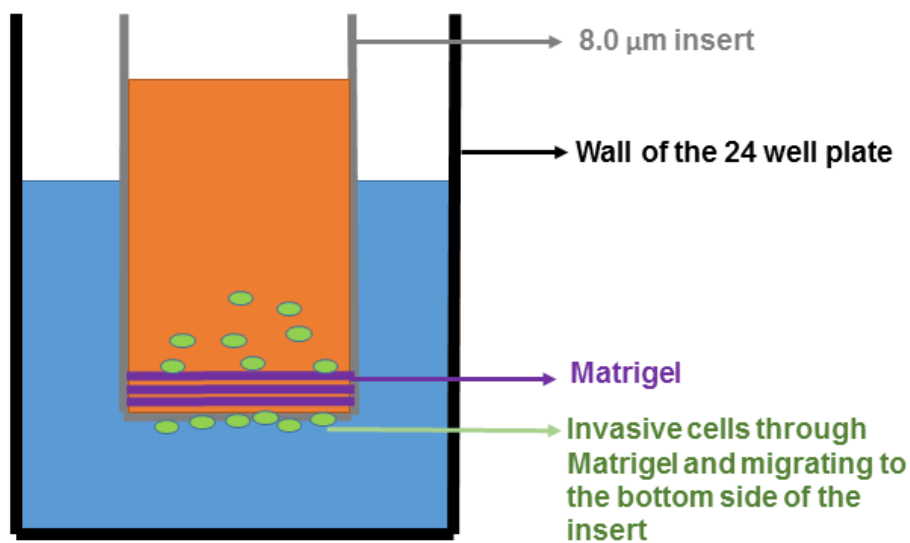


Figure 2.8: Schematic diagram of *in vitro* invasion assay showing double chamber arrangement that is separated by a semi-permeable membrane (8.0 µm pore size).

After 72 hours incubation, the Matrigel layer and the non-invasive cells were then removed from the insert using a cotton bud. Both the Matrigel layer and the non-invasive cells were thoroughly removed as they can also be stained with crystal violet, impacting quantification of invasive cells that had invaded the Matrigel and porous membrane and established on the underside of the insert. The invasive cells were then fixed with 4% formalin for 10-20 minutes and stained with 0.5% crystal violet for 10 minutes. The crystal violet was then washed off and the plate was left for air dry. The stained cells were subsequently counted and photographed under the microscope.

2.6.4 *In vitro* cell adhesion assay

Serum free medium (100µl) containing 5µg Matrigel (Matrigel® Basement Membrane Matrix (Corning Incorporated, Flintshire, UK)) was added to a 96-well plate. The

Matrigel was then left to dry for 2 hours at 55°C. Following this, 200µl of sterile water

was added to each well and left for at least 45 minutes at room temperature to rehydrate the Matrigel. The medium was aspirated and 20,000 cells, diluted in 200 μ l medium, were seeded into each well and left to adhere at 37°C, with 5% CO₂ for 40 minutes.

After incubation, the medium was discarded and the cells were washed with BSS to remove any non-adherent cells. The remained adhered cells were then fixed with 4% formalin for 10-20 minutes, and then stained with 0.5% crystal violet for 10 minutes. Following substantial washes, the plates were left to dry before counting adherent cells and capturing images under the microscope. Due to the fluid dynamics within the small size wells of 96 well plate, the unevenly set Matrigel can lead to the cell aggregation around the edges of the well. In order to avoid this issue, only the cells that adhered to the central area of the well were counted.

2.6.5 *In vitro* MTT cell adhesion assay

Cell adhesion assays were used to examine cell initial adhesive ability to Matrigel matrix. Matrigel was diluted with serum free medium (SFM) to 50 μ g/ml and 5 μ g of Matrigel was added to the wells of 96-well plate under sterile conditions followed by dehydration at 55°C for 1 to 2 hours. The Matrigel matrix coated wells were rehydrated by gently pipetting 100 μ l SFM and incubating at room temperature for at least 30 minutes before aspirating the SFM. Cells (40,000 cells in 200 μ l normal medium) were seeded on the rehydrated Matrigel matrix in six replicates and the plate was incubated for 45 minutes. Subsequently, the medium was gently aspirated by glass aspirator and 100 μ l of PBS was used to gently wash the wells twice. MTT in 200 μ l normal medium (0.5mg/ml working concentration) was added to each well and the plate was incubated at 37.0°C, 5% CO₂ and 95% humidity for 4 hours. The medium containing MTT was then aspirated followed by the addition of 200 μ l DMSO. After 10 minutes of incubation in DMSO at 37.0°C, 5% CO₂ and 95% humidity, the plate was taken out and tapped gently to let the DMSO solution mix thoroughly.

The absorbance of each well was detected at 540nm using ELx800 plate reading spectrophotometer (Bio-Tek, Wolf laboratories, York, UK). Initially attached cell numbers in each well was determined by the absorbance. Experiments were repeated a minimum of three times.

2.6.6 *In vitro* cell transwell migration assay

Transwell inserts (Millicell®, pore size 8.0µm, 24 well format, Greiner Bio one, Germany) were placed into wells of a 24 well plate (NUNC™, Greiner Bio one, Stonehouse, Glos, UK), using sterile forceps in order to prevent contamination. 20,000 cells, in 200µl medium, were seeded into each insert. 600µl medium was then added to the bottom chamber of each well (**Figure 2.9**). The cells were incubated for 72 hours, with 5% CO₂ at 37°C. After 24 hours incubation, non-invasive cells were then removed from the insert using a cotton bud. Cells which had migrated through the insert were then fixed with 4% formalin for 10-20 minutes and then stained with 0.5% crystal violet for 10 minutes. The crystal violet was then washed off and the plate was left to air dry. The stained cells were subsequently counted and photographed under the microscope.

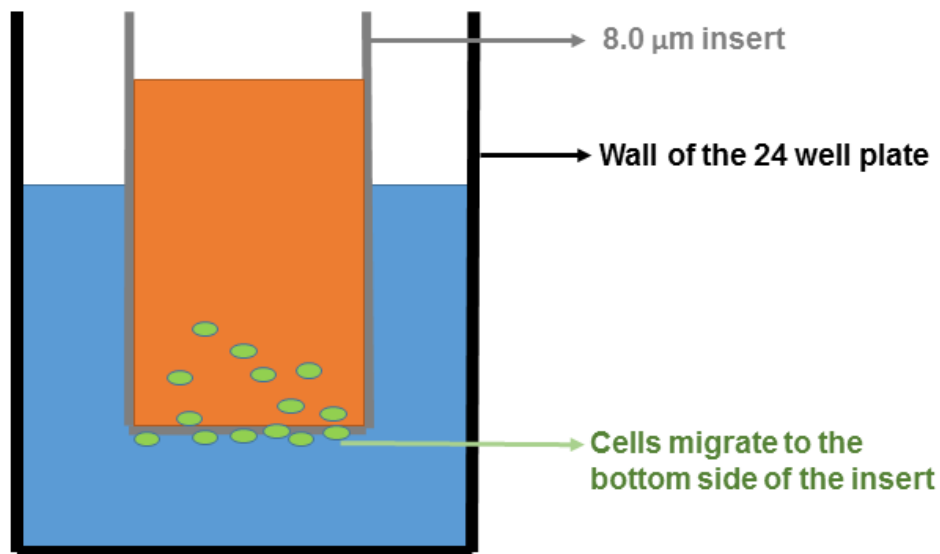


Figure 2.9: Schematic diagram of *in vitro* transwell migration assay showing double chamber arrangement allowing the passage of cells through the 8.0μm pores in the semi-permeable membrane.

2.6.7 *In vitro* cell migration assay (wound healing assay)

An EVOS® FL2 Auto Imaging System (Life technologies, CA, USA) equipped with EVOS® Onstage Incubator (Life technologies, CA, USA) were used the *in vitro* cell migration assay. Such a system was used to capture images at certain time intervals at the same location in each monitored well and continuously maintain culture conditions for the cells being investigated.

Cells in 1ml of normal medium were pre-seeded with appropriate density of 400,000-600,000 cells/well in a 24-well plate and incubated until the formation of a monolayer on the next day. The cell monolayer was scraped by a 200μl pipette tip producing an approximately straight wound. The medium was aspirated by glass aspirator and the well was washed by pipetting and aspirating PBS twice to remove the detached cell debris. 2ml of normal medium was then gently pipetted into the well followed by 10 minutes of incubation at 37°C, 5% CO₂ and 95% humidity for cell recovery. The 24-well plate was then placed in an EVOS® Onstage Incubator (Life technologies, CA, USA) equipped in an EVOS® FL2 Auto Imaging System (Life technologies, CA, USA)

(Figure 2.10). Integrated EVOS® FL2 Auto Imaging System Software was used to set up and adjust the chamber environment condition at 37°C, 5% CO₂. Views on each wound were set up to be captured in every 60 minutes interval until the 24th hour. The distance between two wound edges was measured using Image J v1.50c in pixels, and the distance change at every time interval was calculated by wound edge distance at minute zero subtracting wound edge distance at each time point. The mean and standard deviation was calculated using the three measurements per each wound and was plotted on a scatter line chart. Experiments were repeated a minimum of three times.



Figure 2.10: EVOS® FL2 Auto Imaging System with EVOS® Onstage Incubator, which provide the environment condition at 37°C, 5% CO₂ for cells, and record the cells via the various zoom of microscope.

2.6.8 Electric cell-substrate impedance sensing (ECIS)

Electric cell-substrate impedance sensing (ECIS) instruments (Applied Biophysics Inc., NJ, USA) were applied to investigate cell behaviour based on the impedance parameter detected from gold electrodes coated on the bottom of a 96-well plate

(Applied Biophysics Inc., NJ, USA) (**Figure 2.11**). ECIS is an *in vitro* assay used to quantify cell behaviour through detection of impedance variation based upon the current flow change on the electrode that is cultured with cells. Such a technique enables the measurement of impedance over a range of frequencies to study different functional and structural cell properties, based on cell-cell junctional contacts and cell-substrate interactions, during the same period of time. Moreover, there are two parameters, resistance and capacitance, derived from impedance measurements. Resistance, consisting para- and trans-cellular current flow (**Figure 2.12**), is more likely to represent the quality and function of the cell barrier, whereas capacitance stands for the overall coverage of the electrodes. In this project, resistance measured in 1,000-4000Hz were chosen to analyse cell resistance referring to the function of tight junctions.

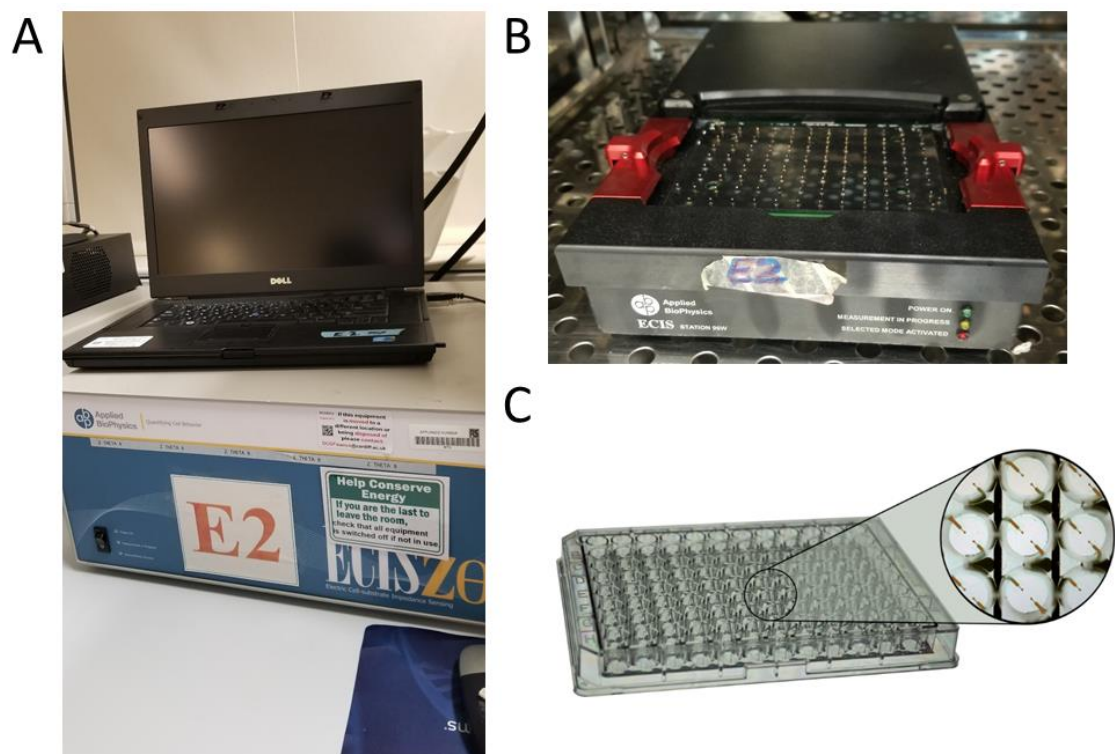


Figure 2.11: Electric cell-substrate impedance sensing (ECIS). **A.** Electric cell-substrate impedance sensing (ECIS) instruments (Applied Biophysics Inc., NJ, USA). **B.** ECIS 96-channel array station. **C.** 96W1E+ electrode array with two electrodes on the bottom of the well (available from: <http://www.biophysics.com/cultureware.php>).

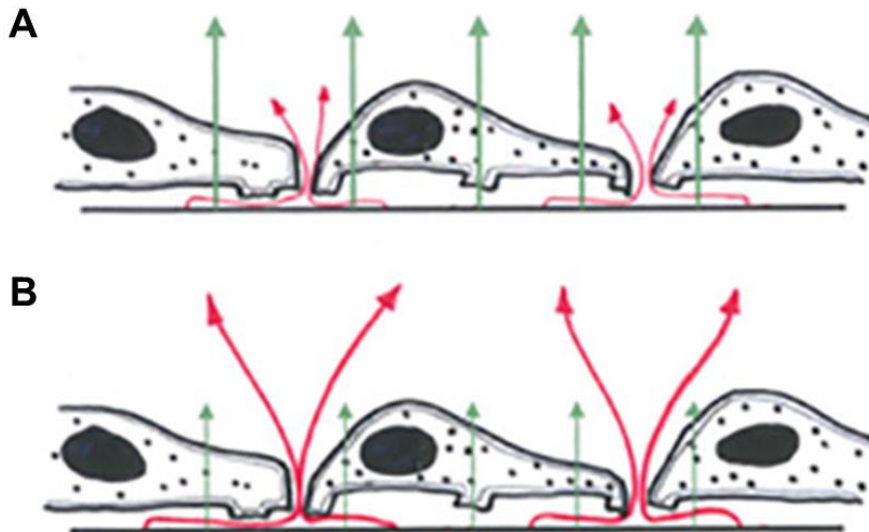


Figure 2.12: Diagram of current flow following cell attachment to the gold electrode (available from: <http://www.biophysics.com>). **A.** At high frequencies (e.g. 40,000Hz), most current flows capacitively through the cell membranes. **B.** At lower frequencies (e.g. 2000Hz), the membrane impedance increases, and more current finds an easier route going under and between the cells.

The 96-channel array station was connected to the ECIS instruments pre-warmed at 37°C, 5% CO₂ and 95% humidity in an incubator. 200µl of serum free medium was pipetted into each well of the 96-well ECIS plate, and the 96-well ECIS plate was connected to the 96-channel array station followed by connection check and stabilisation using Applied BioPhysics-ECIS Software V1.2.135 (Applied Biophysics Inc., NJ, USA).

During the time required to complete stabilisation, the cell suspension solution with appropriate cell density was prepared based on the cell type. Once the array stabilisation was completed, the 96-well ECIS plate was removed from the array station and transferred into the biosafety hood where the medium was aspirated using a glass aspirator and replaced with 200µl of prepared cell suspension solution with the cells at an appropriate density. Each sample was seeded in at least six replicates. After the cell seeding, the 96-well ECIS plate was connected to ECIS station in the incubator.

Following inoculation at time zero, resistance increases as the cells attach to the

electrode and begin spreading and the resistance will continue to increase until the cells reach confluence. For the initial functional analysis of our cells, the resistance was measured at multiple frequencies, and the first four hours of data, obtained at 4,000Hz was taken to analyse the initial adhesion.

A lethal electroporation (electrical wounding) was applied to the cells covering the gold electrodes for 30 seconds at the conditions of 3000 μ A and 60,000Hz to generate a uniform lesion (250 μ m diameter). The resistance was measured following electrical wounding and used to analyse cell migratory function over a four-hour period following wounding. The electrical wounding and the subsequent measurements were repeated twice. The resistance obtained for each hour was used to subtract the initial value at hour zero to display the resistance change which represents the cell re-coverage of the electrodes from the starting point. Experiments were repeated for at least three times.

2.6.9 Transepithelial Resistance (TER)

Transwell inserts (Millicell, MerckMillipore, Watford, UK) with 0.4 μ m pores were placed into wells of a 24 well plate, using sterile forceps in order to prevent contamination. 5×10^4 cells were seeded into inserts in 500 μ l medium with 1ml medium in the well outside of the insert (**Figure 2.13**). Cells were incubated at 37 °C, 5 % CO₂ for 24-48 hours until confluent. Medium was then replaced and resistance across the membrane was then measured in triplicate immediately afterwards using the EVOM² Epithelial Volt/Ohm Meter (World Precision Instruments, Hitchin, Hertfordshire, UK) (**Figure 2.14**). Various treatments were carried out and resistance was also measured every hour after the initial measurement for 12 hours. Change of the resistance was used as the measurement of the change of the TJ function of the cells.

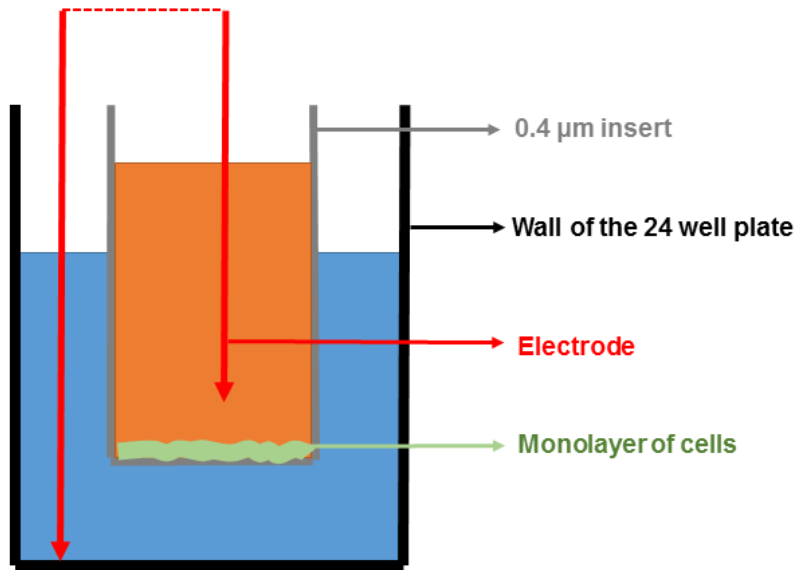


Figure 2.13: Schematic diagram of transepithelial resistance assay showing double chamber arrangement preventing the passage of cells through the 0.4 μm pores in the semi-permeable membrane.



Figure 2.14: EVOM² Epithelial Volt/Ohm Meter with chopstick electrode for measuring the resistance between the two electrodes (World Precision Instruments, Hitchin, Hertfordshire, UK).

Chapter-3 Expression of SIPA1 in lung cancer and its clinical relevance

3.1 Introduction

Over the past two decades, there have been limited literature reports, indicating that SIPA1 participates in the metastasis process of cancer. The initial function of SIPA1 was thought to be that of having a specific GAP activity for Ras-related mediating proteins, Rap1, Rap2, Rsr1 and nuclear Ran (Kurachi et al., 1997). SIPA1 overexpression induced rounding and eventual detachment of inherently adherent cells from the extracellular matrix by inhibiting endogenous Rap1 activation, indicating that Rap1 signals are involved in the regulation of cell adhesion and that SIPA1 functions as a negative regulator of cell adhesion (Kurachi et al., 1997, Hattori, 2011). In addition to the functions originally discovered, SIPA1 was also found to have the ability to bind with a few molecules such as AQP2, BRD4, AF6, by so doing, play different roles in a variety of tumour types (Alsarraj et al., 2013, Brooks et al., 2010, Noda et al., 2004, Su et al., 2003, Ugenskiene et al., 2016, Zhang et al., 2015).

Our previous work has found that the invasive human breast cancer cell line MDA-MB-231 and the PC-3 human prostate cancer cell line exhibited significantly reduced response to HGF during both transepithelial resistance (TER) and paracellular permeability (PCP) assays, as well as cell adhesion, after knockdown of SIPA1 ($p < 0.001$) (Jiang, 2013, Jiang, 2006).

Studies on SIPA1 in human lung cancer are very sparse. There has been one report on the function of SIPA1 SNP polymorphism, in which it was shown that G allele at rs931127 was significantly correlated with the risk of lung cancer, as well as with poor clinical staging (Xie et al., 2013). G allele fusion in SNP rs931127 A>G was associated with worse progression free survival (PFS) in the patients with NSCLC (Gdowicz-Klosok et al., 2015). The role of SIPA1 in cancer is most focused on breast cancer. There is a very well-designed study showing the mechanism of SIPA1 in breast cancer carried out by Zhang *et al.* (Zhang et al., 2015). It revealed that nuclear SIPA1 affects ITG β 1 (integrin beta1) in breast cancer cells and activates the Alk signalling pathway, leading to a more invasive phenotype of breast cancer. There are also a few studies on the role of SIPA1 in prostate cancer. High expression of SIPA1

was associated with poor disease prognosis and metastases in human prostate cancer patients (Shimizu et al., 2011). SIPA1 increases the invasion and metastasis potential of prostate cancer cells both *in vitro* and *in vivo* in mice (Shimizu et al., 2011). SIPA1's expression in both human oral squamous cell carcinoma (OSCC) and OCSS cells are higher than normal tissue, which is linked with metastasis to regional lymph nodes in OSCC patients (Takahara et al., 2017).

In the light of the limited information about SIPA1 in human lung cancers and the potential link between SIPA1 and the clinical outcome of patients with cancer, this current chapter of the study aimed to establish the pattern of expression of SIPA1 in human non-small cell lung cancer (NSCLC), at both messenger RNA and protein levels, using QPCR and immunohistochemistry (IHC) and to determine the relationship, if any between SIPA1 expression and the clinical pathological features of these patients.

3.2 Materials and methods

3.2.1 Lung cancer tissues

Lung tumours (n=148) together with adjacent normal tissue (n=148) were collected immediately after surgery and stored at -80°C until use, with written consent from the patients at Peking University Cancer Hospital. All protocols and procedures were approved by Peking University Cancer Hospital Research Ethics Committee (Appendix 1). RNA was extracted and converted to complementary DNA (cDNA) for subsequent quantification using real time quantitative PCR (QPCR).

3.2.2 Primers and antibody

All the primers used were synthesised and provided by Invitrogen (Paisley, UK). Primer sequences are shown in **Table 2.3, 2.4**. Mouse anti-SIPA1 antibody (ab219085) was obtained from ABCAM (Cambridge, UK). The name, molecular

weight, supplier, and the product code of the primary and secondary antibodies used in this chapter is shown in **Table 2.5**.

3.2.3 RNA extraction, reverse transcription, PCR and QPCR

Total RNA was isolated using TRI Reagent (Sigma-Aldrich, Poole, Dorset, UK), first strand cDNA was then synthesis using the GoScript™ Reverse Transcription System kit (Thermo Fisher Scientific, Life Technologies Ltd, Paisley, UK). And QPCR was carried out as described in section 2.4.

3.2.4 Immunohistochemistry (IHC) for lung tissue microarray

Immunohistochemical staining was carried out on a lung disease spectrum tissue microarray (TMA) (LC1201, Biomax, Maryland, US). Staining intensity and positive percentage of SIPA1 staining was determined independently by three researchers (CL, YXC and YZC). The IHC scoring was calculated based on both staining intensity and positive percentage of SIPA1. IHC score = staining intensity (0-3) + positive percentage (0-3).

3.2.5 Statistical analysis

One-way ANOVA test, Two-way ANOVA test, *t*-test, paired *t*-test, Mann-Whitney test and chi-square tests were performed, where appropriate, to analysis the expression level of SIPA1 in tumours. SPSS was used to carry out the survival analysis. Differences were considered to be statistically significant when $p < 0.05$.

3.3 Result

3.3.1 Transcript level of SIPA1 in lung cancer

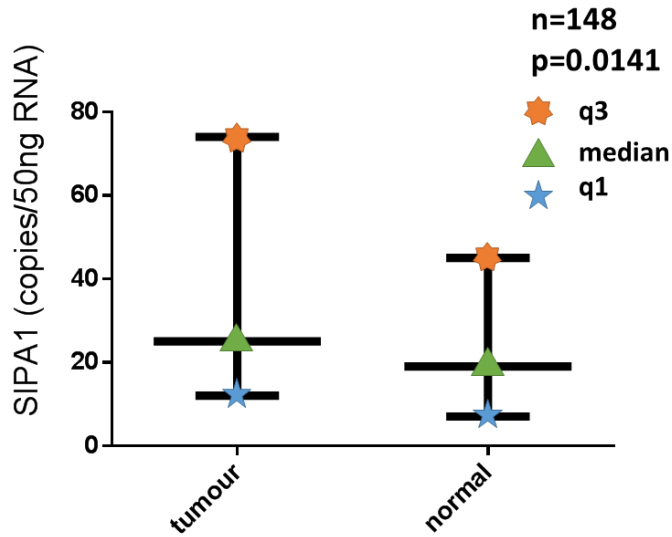
Expression of SIPA1 in lung cancer was determined by evaluating the transcript levels of SIPA1 in two clinical cohorts, collected sequentially at the Peking University Cancer Hospital, using QPCR. Patients' clinical and pathological features, as well as the levels of expression of the SIPA1 transcript are summarized in **Table 3.1 A**. Median levels of SIPA1 transcript levels in tumour and normal tissue are shown in **Table 3.1 B**, **Figure 3.1** and **Figure 3.2**. Data was analysed using the Mann-Whitney test. It can be observed that SIPA1 was significantly upregulated in lung tumour tissues compared with adjacent normal lung tissues ($p=0.0141$). The same rise was also found when paired tissues were analysed ($p=0.0358$) (**Figure 3.1, 3.2**).

Table 3.1 A: Clinical and pathological demographics of the cohort and the level of expression of SIPA1 transcripts. We compared the SIPA1 transcript level between lung tumour tissue and normal tissue, also we look through the different expression of SIPA1 in each sub-group respectively like histology type, degree of differentiation, T Staging, nodal staging, TNM staging, TNM substaging and smoking history.

	Parameters	Sample number	Median	Interquartile range	
				Q1	Q3
Entire cohort	Tumour	148	25	12	74
	Normal	148	19	7	45
Histology type	Squamous Cell Carcinoma	50	25	14	62
	Adenocarcinoma	67	19.8	9.1	73.8
	Others	18	24	6	121
					21.8
Degree of differentiation	High	7	14.88	3.05	8
	High to moderate	16	24.2	15.9	63.5
	Moderate	50	25	9	67
	Moderate to Low	23	26.9	12.2	96.7
	Low	14	17.9	7.5	42.5
T Staging	T-1	21	17.3	4.2	63
	T-2	57	21	9	65
	T-3	29	50	20	168
	T-4	16	18.3	6.1	65.3
Nodal staging	N-0	70	24.1	9	63.7
	N-1	22	31	11	82
	N-2	38	19	10	78
TNM staging	TNM1	39	17.3	6.9	59.7
	TNM2	31	52	20	189
	TNM3	51	19	12	63
	TNM4	1	0.113	*	*
TNM substaging	TNM1A	17	15.5	4.1	63
	TNM1B	22	21.9	8.2	60.3
	TNM2A	2	135	*	*
	TNM2B	29	52	20	189
	TNM3A	37	20	14	63
	TNM3B	14	18.3	6.4	77.1
Smoking history	Non smokers	59	28.5	9.7	63.8
	Smokers	77	20	11	71

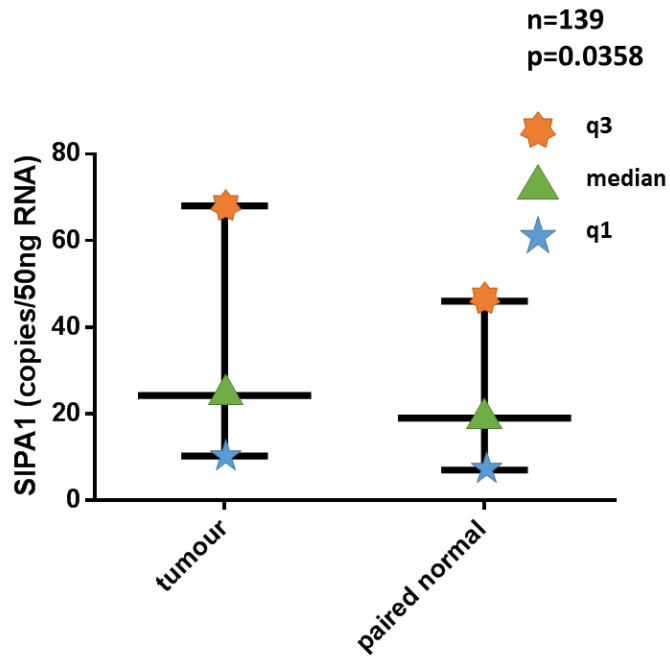
Table 3.1 B: Expression of SIPA1 transcripts in the clinical cohort of NSCLC lung cancers. SIPA1 transcript level was significant higher in lung tumour tissue, whether compared to normal tissue or paired normal tissue. *Mann-Whitney U test.

	N	Median (copy numbers/50ng RNA)	p-value*
All tissues			
Tumour	148	25	0.0141
Normal	148	19	
Paired tissues			
Tumour	139	24.2	0.0358
Paired Normal	139	19	



Statistic	Tumour tissue	Normal tissue
median	25	19
Q1-Q3	12-74	7-45
Min-max	0-12482	0-8475

Figure 3.1: Transcript level of SIPA1 between lung cancer and adjacent normal lung tissue. SIPA1 transcript level was significantly higher in lung tumour tissue, whether compared to normal tissue. SIPA1 level was evaluated by copy numbers/50ng RNA. Statistical method: Mann-Whitney U test.



Statistic	Tumour tissue	Paired normal tissue
Median	24.2	19
Q1-Q3	10.3-68	7-46
Min-Max	0.1-6104.6	0-84756

Figure 3.2: Transcript level of SIPA1 between lung cancer and paired adjacent normal lung tissue. SIPA1 transcript level was significantly higher in lung tumour tissue, whether compared to paired normal tissue. SIPA1 level was evaluated by copy numbers/50ng RNA. Statistical method: Mann-Whitney U test.

3.3.2 Protein level of SIPA1 in lung cancer

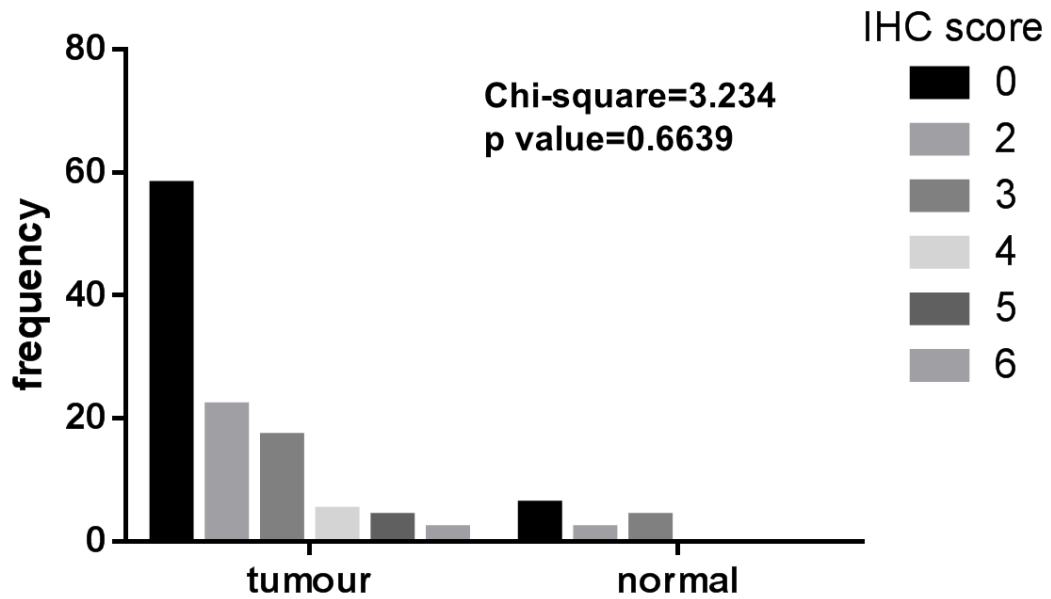
To examine the protein expression level of SIPA1 in patients with lung cancer, immunohistochemical staining was performed using a commercial lung cancer tissue microarray (**Figure 3.3**). Samples included primary tumours of adenocarcinoma, squamous cell carcinoma, papillary adenocarcinoma, small cell carcinoma, atypical carcinoid, bronchioloalveolar carcinoma, giant cell carcinoma, large cell carcinoma, metastatic squamous cell carcinoma, metastatic adenocarcinoma and normal lung tissues. Summative pathological information of the TMA can be seen in **Table 3.2** and **Figure 3.4**. The IHC scoring did not show a significant difference of SIPA1 staining in lung tumours compared with all normal pneumonic tissue, neither did it show differences with normal tissue and adjacent normal tissue (**Figures 3.4, 3.5, shows representative sections of the typical staining observed**).



Figure 3.3: Overall look of the IHC staining of SIPA1 on lung cancer TMA (LC1201, Biomax, Maryland, US). The TMA slide contains lung tumours tissue, normal lung tissue and a positive control tissue. Image was scanned using a high resolution EVOS scanner after IHC stained using anti-SIPA1 antibody. Detailed information was seen in the appendix.

Table 3.2: Pathological information summary of lung cancer TMA (LC1201, Biomax, Maryland, US). Detailed information of each sample was seen in the appendix.

Pathological characteristic	Numbers of samples
Normal tissue	12
Normal pneumonic tissue	6
Cancer adjacent normal pneumonic tissue	6
Malignant tumour	108
Adenocarcinoma	27
Squamous cell carcinoma	27
Papillary adenocarcinoma	8
Small cell carcinoma	8
Atypical carcinoid	8
Bronchioloalveolar carcinoma	8
Giant cell carcinoma	2
Large cell carcinoma	8
Metastatic squamous cell carcinoma	4
Metastatic adenocarcinoma	8
All	120



Score	0	2	3	4	5	6	all
tumour	58	22	17	5	4	2	108
normal	6	2	4	0	0	0	12
all	64	24	21	5	4	2	120

Figure 3.4: Frequency analysis of the each IHC score in lung cancer tumour and normal tissue samples by chi-square test. Table attached showed the exact frequency of each score sub-group in tumour and normal tissue group.

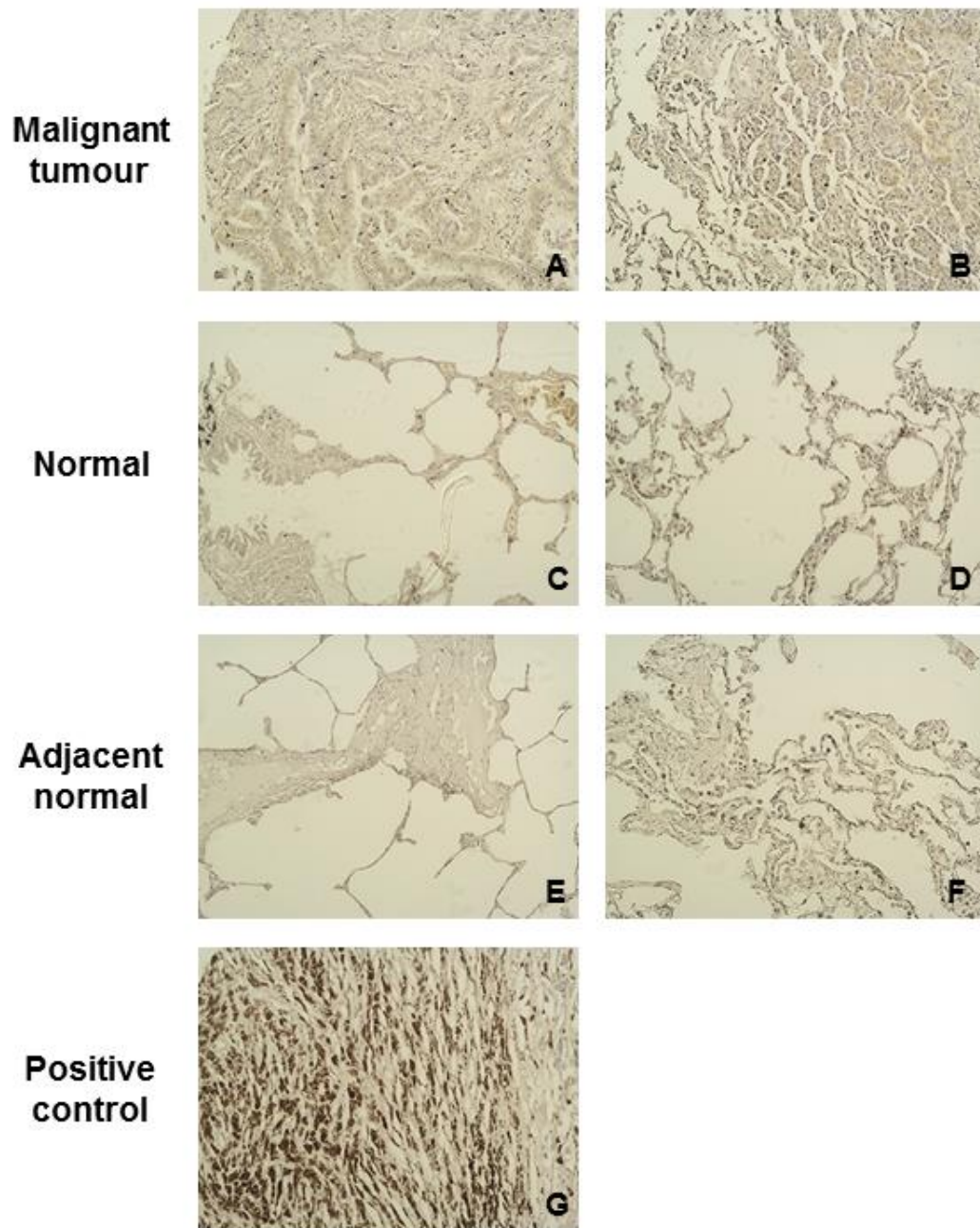


Figure 3.5: representative IHC SIPA1 staining images in the TMA. A-B are malignant tumour tissues, **C-D** are normal pneumonic tissues, **E-F** are cancer adjacent normal pneumonic tissues, **G** is the positive control from skin malignant melanoma. All the images were captured at 200× objective magnification.

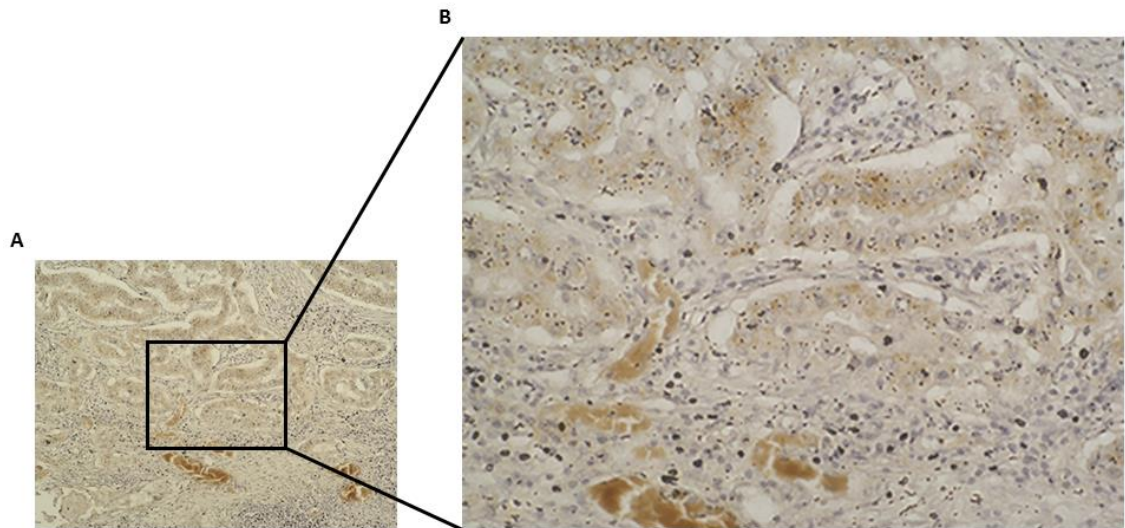


Figure 3.6: Representative IHC SIPA1 staining images in the malignant tumour tissues. The expression of SIPA1 in tumour tissue under **(A)** 200× magnification. **(B)** 400× magnification. Dark brown colour represents a higher SIPA1 expression level seen in the staining image.

3.3.3 SIPA1 transcript and protein expression and histological type of lung cancer

Both transcript and protein levels of SIPA1 from different histology types of lung cancer were measured. In the clinical cohort, the main types of lung cancer were adenocarcinoma and squamous cell carcinomas. The levels of SIPA1 were then compared between these two types and the remaining patients which were small in number. As shown in **Figure 3.7**, the difference in transcript levels of SIPA1 among adenocarcinoma, squamous cell carcinoma and other types of lung cancer is not statistically significant (**Figure 3.7**). However, it was noted that adenocarcinoma tissues of the lung showed a trend towards higher levels of SIPA1 transcript than that in squamous cell carcinoma and other types of lung cancer (**Figure 3.8**).

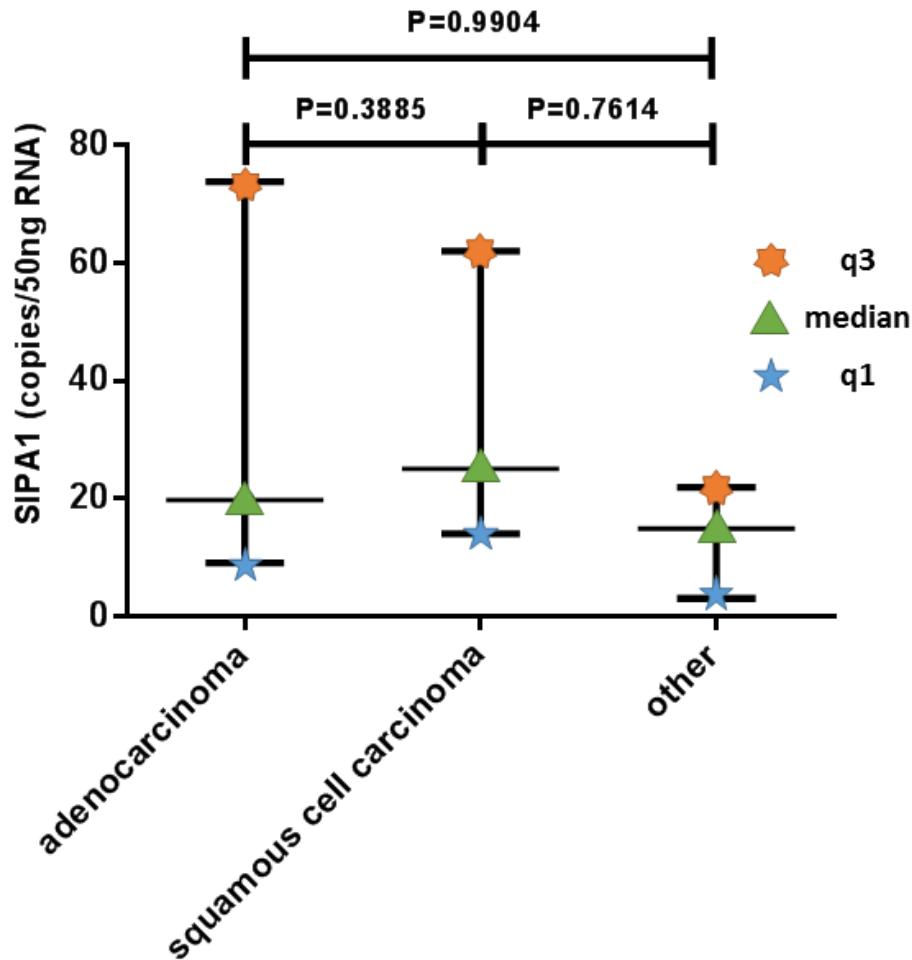
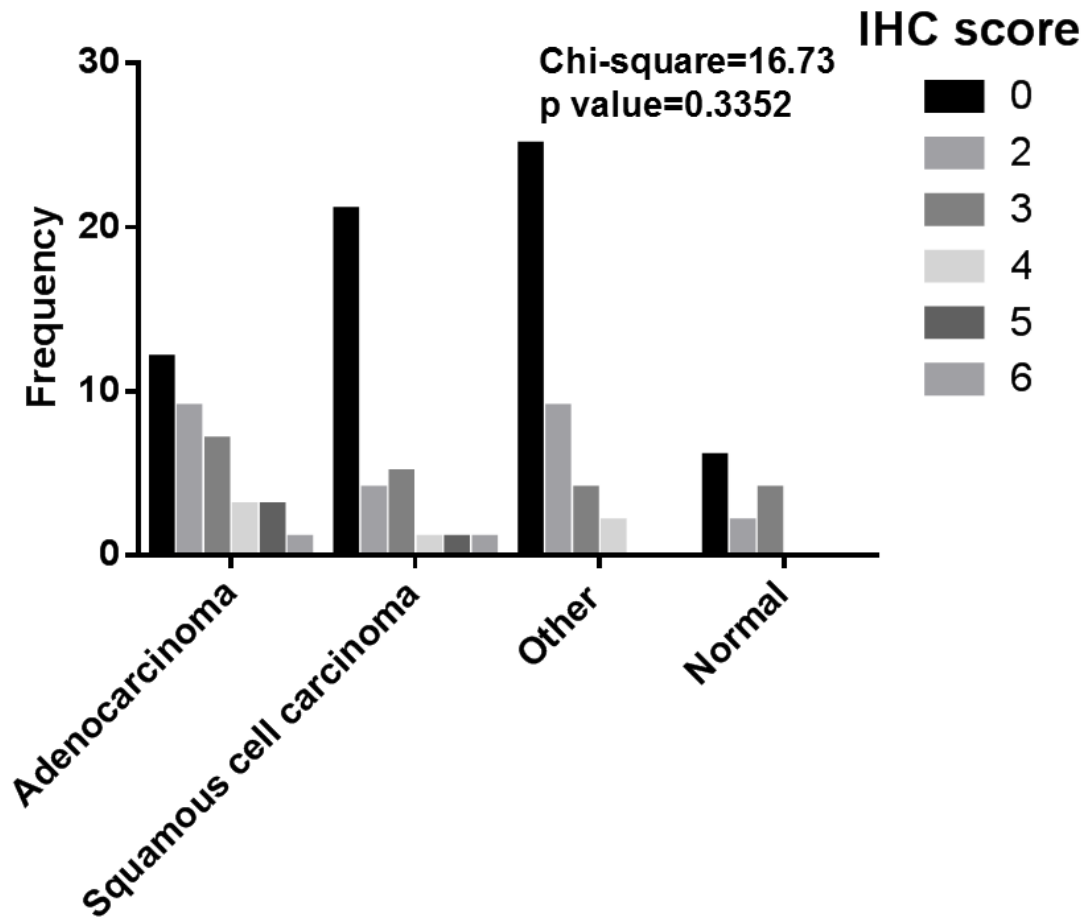


Figure 3.7: Transcript level of SIPA1 in different histology of lung cancer. The transcript level of SIPA1 among the adenocarcinoma, squamous cell carcinoma and others are shown. (SIPA1 level was evaluated by copy numbers/50ng RNA).



Score	0	2	3	4	5	6	all
Adenocarcinoma	12	9	7	3	3	1	35
Squamous cell carcinoma	21	4	5	1	1	1	33
Other	25	9	4	2	0	0	40
Normal	6	2	4	0	0	0	12
all	64	24	20	6	4	2	120

Figure 3.8.1: Frequency analysis of the IHC scores in various histology of tumour samples and normal samples by chi-square test. The protein level of SIPA1 among the adenocarcinoma, squamous cell carcinoma and others are shown.

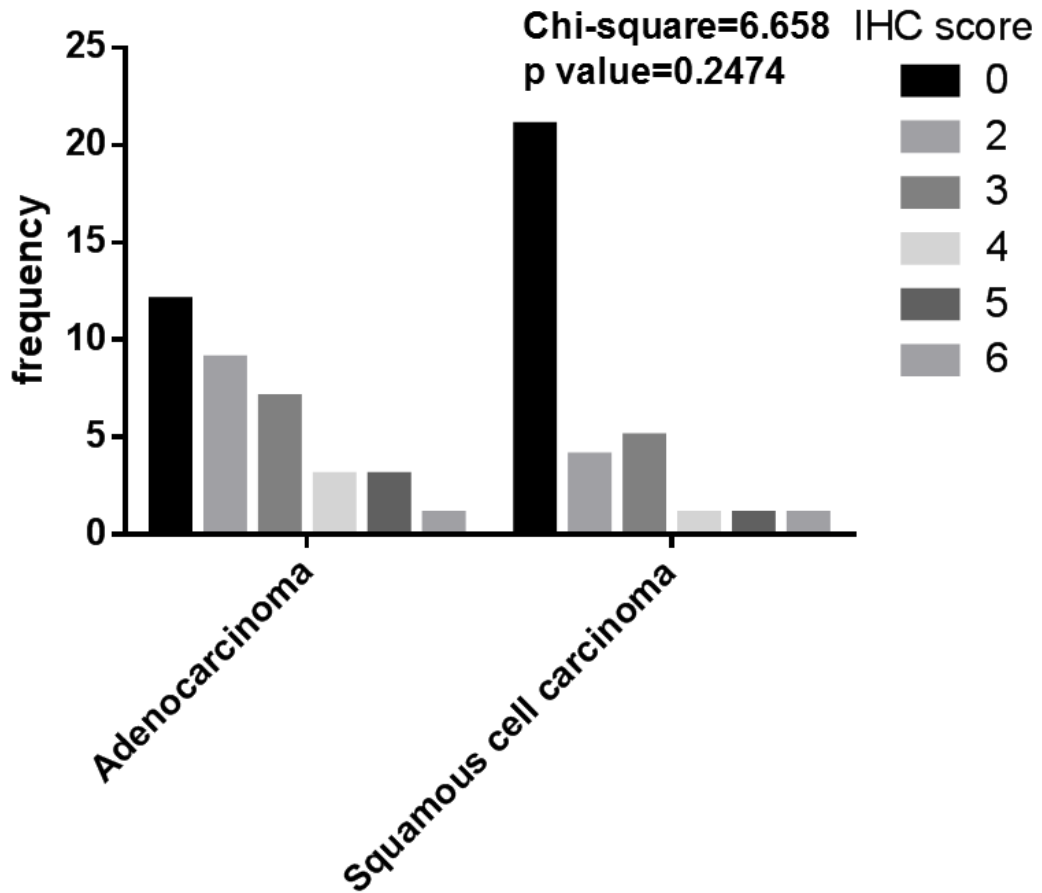
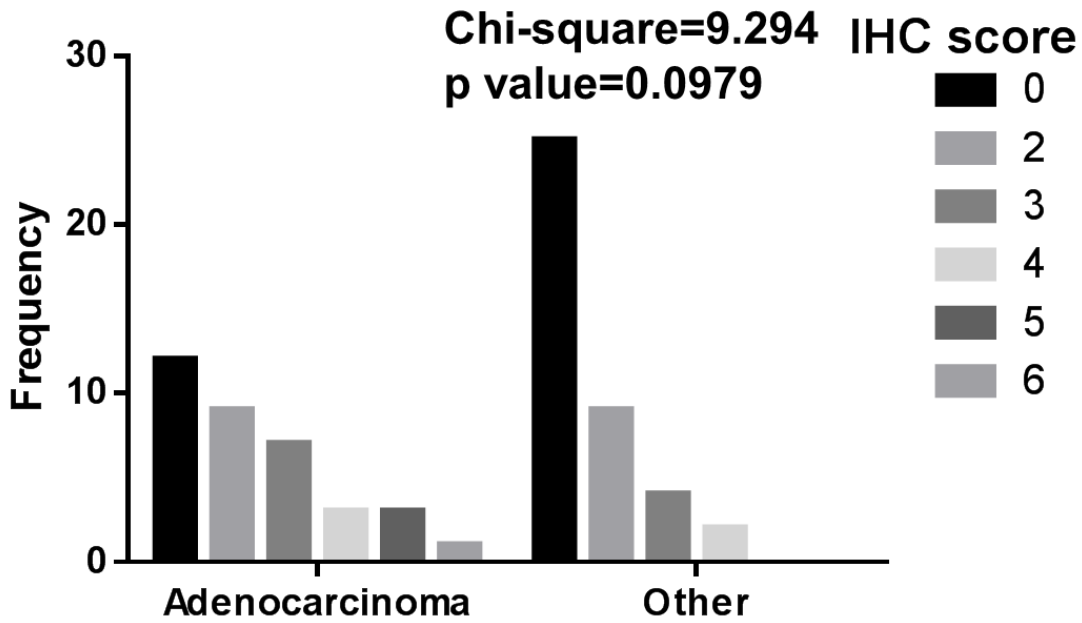
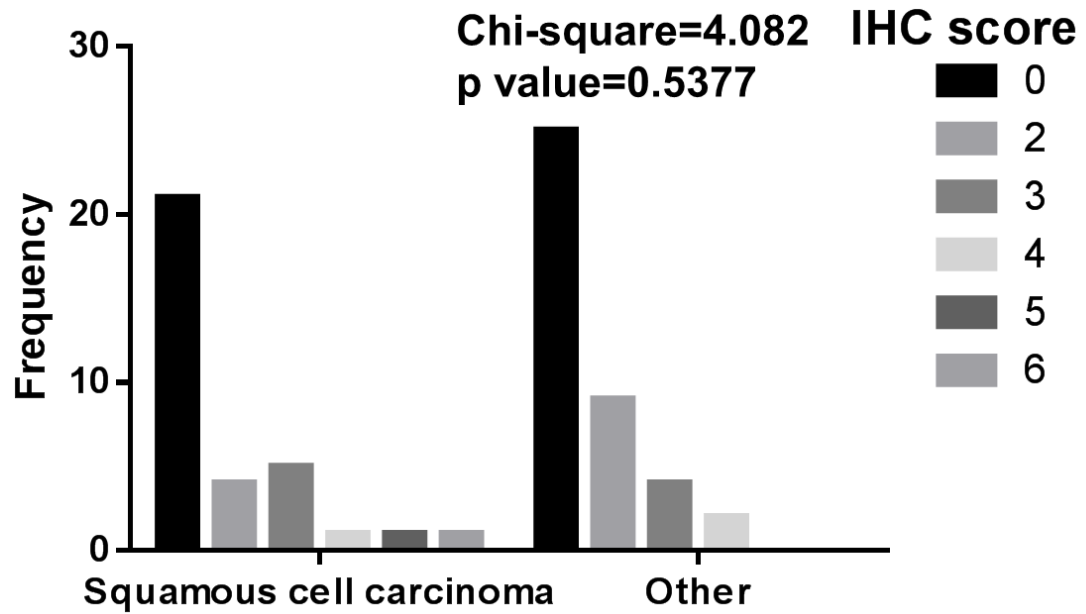


Figure 3.8.2: Frequency analysis of each IHC score in adenocarcinoma and SCC samples by chi-square test. The protein level of SIPA1 between the adenocarcinoma and squamous cell carcinoma are shown.



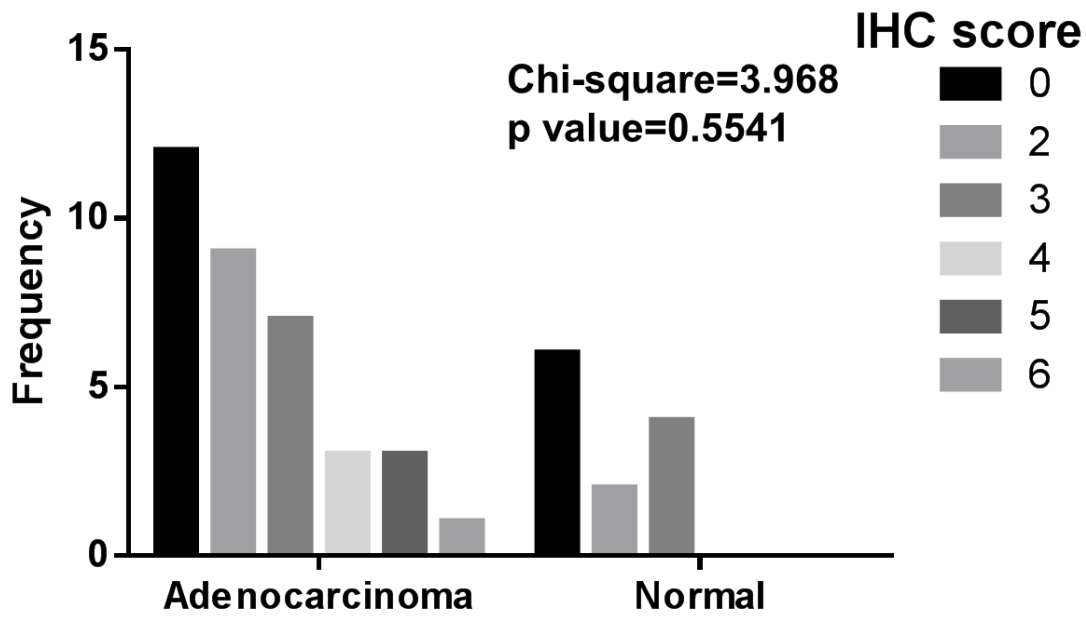
Score	0	2	3	4	5	6	all
Adenocarcinoma	12	9	7	3	3	1	35
Other	25	9	4	2	0	0	40
all	37	18	11	5	3	1	75

Figure 3.8.3: Frequency analysis of each IHC score in adenocarcinoma samples and other lung cancer samples by chi-square test. The protein level of SIPA1 between the adenocarcinoma and others are shown.



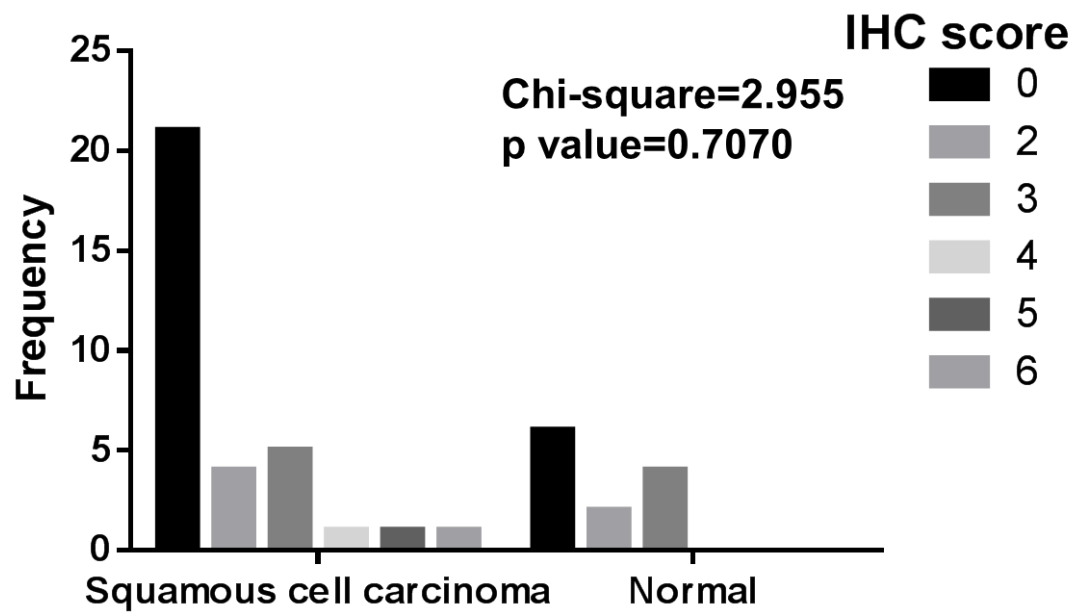
Score	0	2	3	4	5	6	all
Squamous cell carcinoma	21	4	5	1	1	1	33
Other	25	9	4	2	0	0	40
all	46	13	9	3	1	1	73

Figure 3.8.4: Frequency analysis of each IHC score in SCC samples and other lung cancer samples by chi-square test. The protein level of SIPA1 between the squamous cell carcinoma and others are shown.



Score	0	2	3	4	5	6	all
Adenocarcinoma	12	9	7	3	3	1	35
Normal	6	2	4	0	0	0	12
all	18	11	11	3	3	1	47

Figure 3.8.5: Frequency analysis of each IHC score in adenocarcinoma samples and normal samples by chi-square test. The protein level of SIPA1 between the adenocarcinoma and normal tissue are shown.



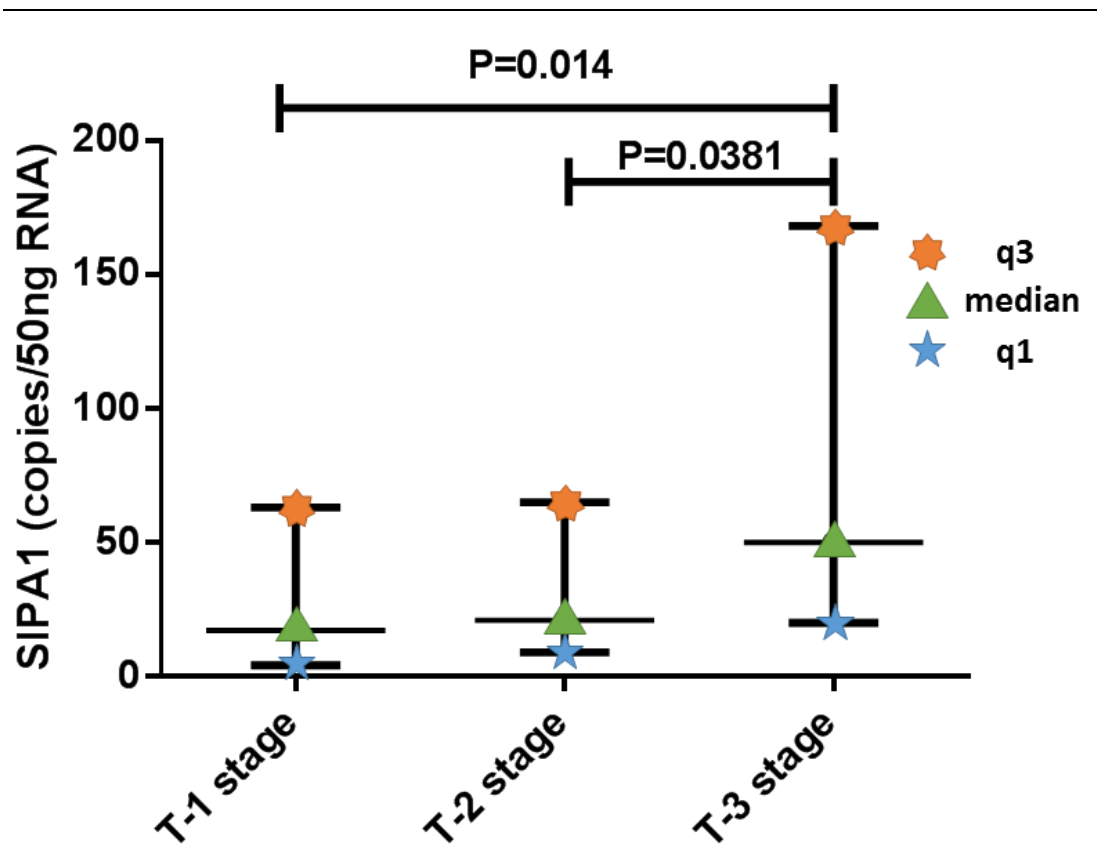
Score	0	2	3	4	5	6	all
Squamous cell carcinoma	21	4	5	1	1	1	33
Normal	6	2	4	0	0	0	12
all	27	6	9	1	1	1	45

Figure 3.8.6: Frequency analysis of each IHC score in SCC samples and normal samples by chi-square test. The protein level of SIPA1 between the squamous cell carcinoma and normal are shown.

3.3.4 SIPA1 in relation to the pathological tumour staging and clinical features of lung cancer

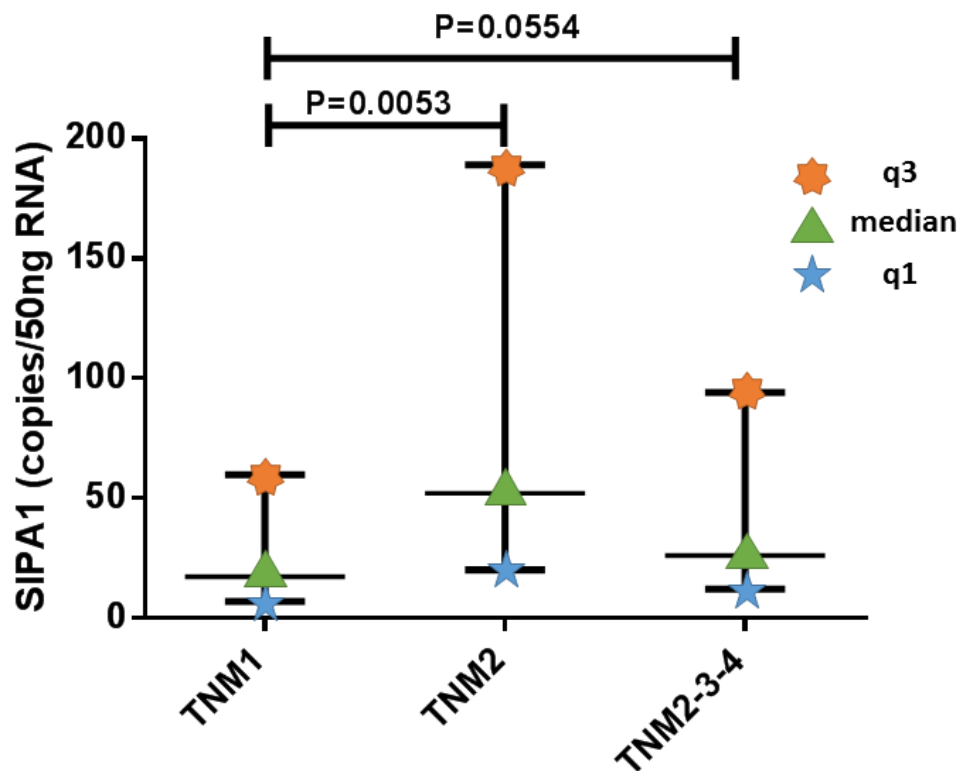
The transcript level of SIPA1 in stage T-3 lung cancer was statistically significantly higher than that in stage T-1 and T-2 tumours (**Figure 3.9**). Comprehensive analysis of the TNM stage of the lung cancers, showed that TNM2 tumours had higher SIPA1 transcript levels than for stage TNM1 tumours (**Figure 3.10**). SIPA1 transcript levels in TNM2-3-4 stage was comprehensively higher than in the TNM1 tumours, but the difference was not statistically significant. SIPA1 levels in Stage 1A and 1B tumours were lower than those in stage 2B which had increased metastasis; and the difference was statistically significant (**Figure 3.11**).

To evaluate the protein level of SIPA1 in different stages of lung cancer, IHC was carried out and scored using a lung cancer TMA. Results showed that differences in SIPA1 levels did not reach statistical significance amongst T-1 to T-4 tumours (**Figure 3.12**).



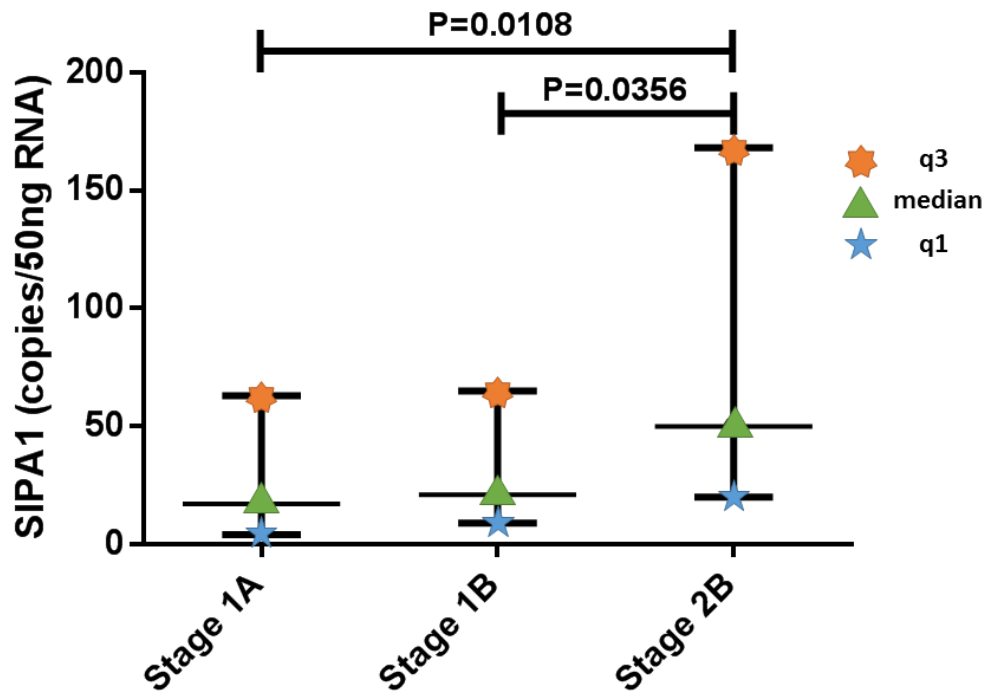
Stage	T-1	T-2	T-3
Sample numbers	21	57	29
Median	17.3	21	50
MIN-Max	2.9-260.6	2-6023	2-5151
Q1-Q3	4.2-63	9-65	20-168
p value to T-3	0.014	0.0381	NA

Figure 3.9: Transcript level of SIPA1 in different T stage lung cancer. The transcript level of SIPA1 among the T-1, T-2 and T-3 stage of lung cancer are shown. (SIPA1 level was evaluated by copy numbers/50ng RNA). * $p < 0.05$ by Mann-Whitney U test.



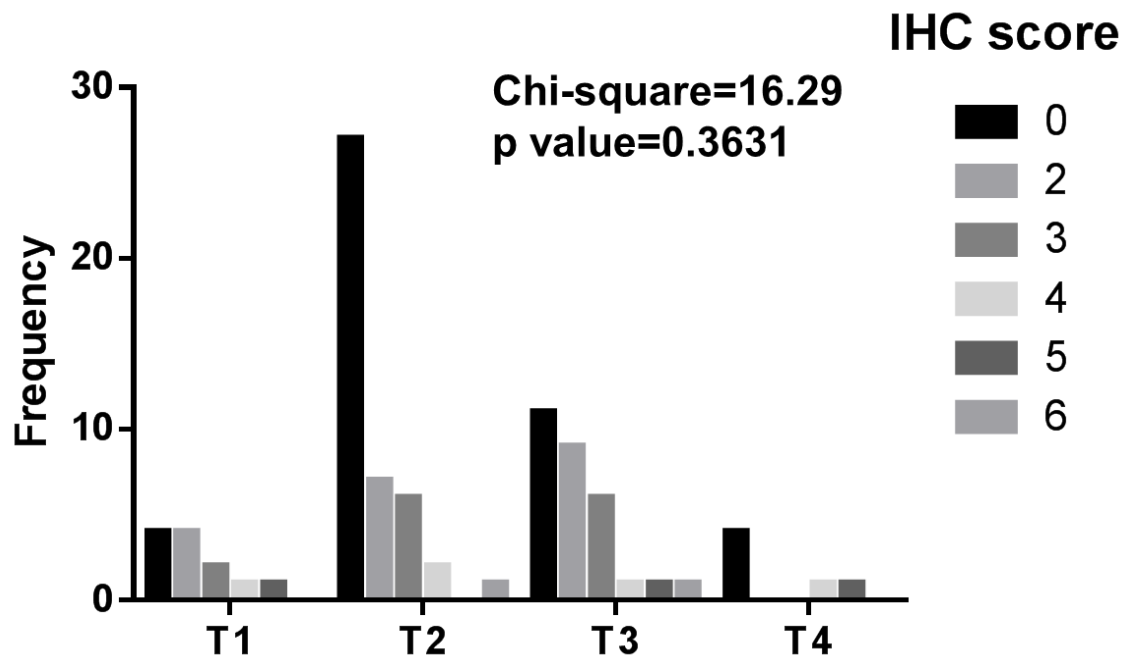
Stage	TNM1	TNM2	TNM2-3-4
Sample numbers	39	31	83
Median	17.32	52.1	26.34
MIN-Max	2.4-1185.2	4-5151	0-6023
Q1-Q3	6.9-59.7	20-189	12-94
p value to TNM1*	NA	0.0053	0.0554

Figure 3.10: Transcript level of SIPA1 in different TNM stage lung cancer. The transcript level of SIPA1 among the TNM1, TNM2 and TNM2-3-4 stage of lung cancer are shown. (SIPA1 level was evaluated by copy numbers/50ng RNA). * $p < 0.05$ by Mann-Whitney U test.



Stage	TNM1A	TNM1B	TNM2B
Sample numbers	21	57	29
Median	17.3	21	50
Max	2.9-260.6	2-6023	2-5151
Q3	4.2-63	9-65	20-168
P value to TNM2B	0.0108	0.0356	

Figure 3.11: Transcript level of SIPA1 in different stage lung cancer. The transcript level of SIPA1 among the stage 1A, 1B and 2B of lung cancer are shown. (SIPA1 level was evaluated by copy numbers/50ng RNA). * $p < 0.05$ by Mann-Whitney U test.

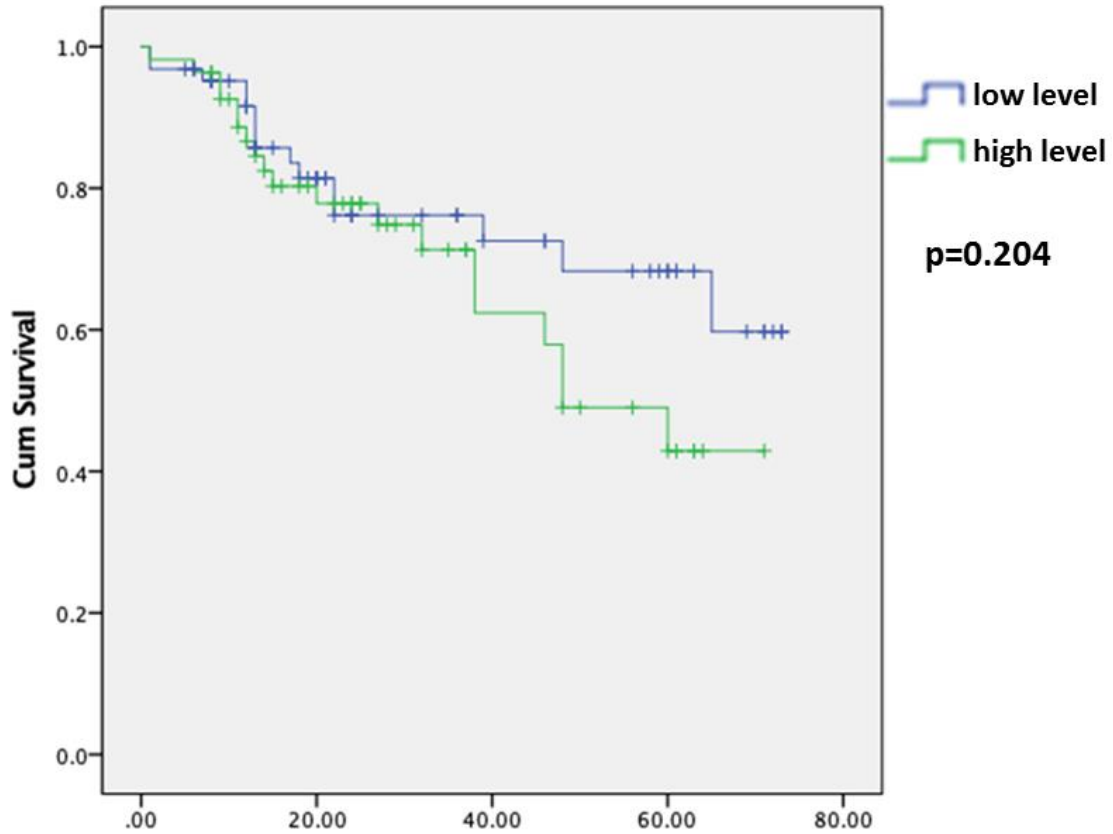


Score	0	2	3	4	5	6	all
T1	4	4	2	1	1	0	12
T2	27	7	6	2	0	1	43
T3	11	9	6	1	1	1	29
T4	4	0	0	1	1	0	6
ALL	46	20	14	5	3	2	90

Figure 3.12: Frequency analysis of the each IHC score various T stage samples by chi-square test. The protein level of SIPA1 among the stage T1, T2, T3 and T4 of lung cancer are shown.

3.3.5 Correlation between SIPA1 expression and clinical outcome of the patients in the Peking cohorts

Patients were divided into two groups according to the transcript expression level of SIPA1, with a cut-off at 25 copy numbers/50ng RNA, the median level of the tumour group. Overall survival was analysed using SPSS and the result is shown in **Figure 3.13**. Kaplan-Meier survival analysis revealed that patients with a high expression level of SIPA1 had lower overall survival of 48.3 months (95%C.I. 40.7 – 55.9 months), compared to 55.9 months (95%C.I. 48.5 - 63.2 months) of patients with low expression level of SIPA1. However, the data did not reach statistical significance (p=0.204).



	Total N	Events N	Censored N	Percent	Mean ^a (months)			
					Estimate	Std. Error	95% C.I. Lower Bound Upper Bound	
Low level	55	19	48	76.2%	55.874	3.748	48.529	63.219
High level	118	34	36	65.5%	48.307	3.892	40.678	55.936
Overall	118	34	84	71.2%	52.635	2.786	47.175	58.095

Figure 3.13: The Kaplan-Meier survival model of correlation between SIPA1 transcript levels and overall survival. Using 25, the median in the tumour group, as the cut-off to divide patients into two groups with high and low SIPA1 level.

Here, we carried out another analysis using a publicly available database, *kmplot*, that allows comparisons of tissue gene transcript information of patients from various cohorts available from (<http://kmplot.com/analysis/index.php?p=background>). In line with the analysis of our cohort, the analysis has also used the median as the cut-off to divide the patients into two groups. In all of the lung cancer patients, SIPA1 was statistically correlated with post-progression survival (PPS) ($p=0.02$) (**Figure 3.14**). Patients with higher SIPA1 levels correlated with poor prognosis in terms of post progression survival (PPS). There was no statistical correlation of SIPA1 expression level with overall survival (OS) ($p=0.46$) or progression-free survival (PFS) ($p=0.071$) (**Figure 3.15**).

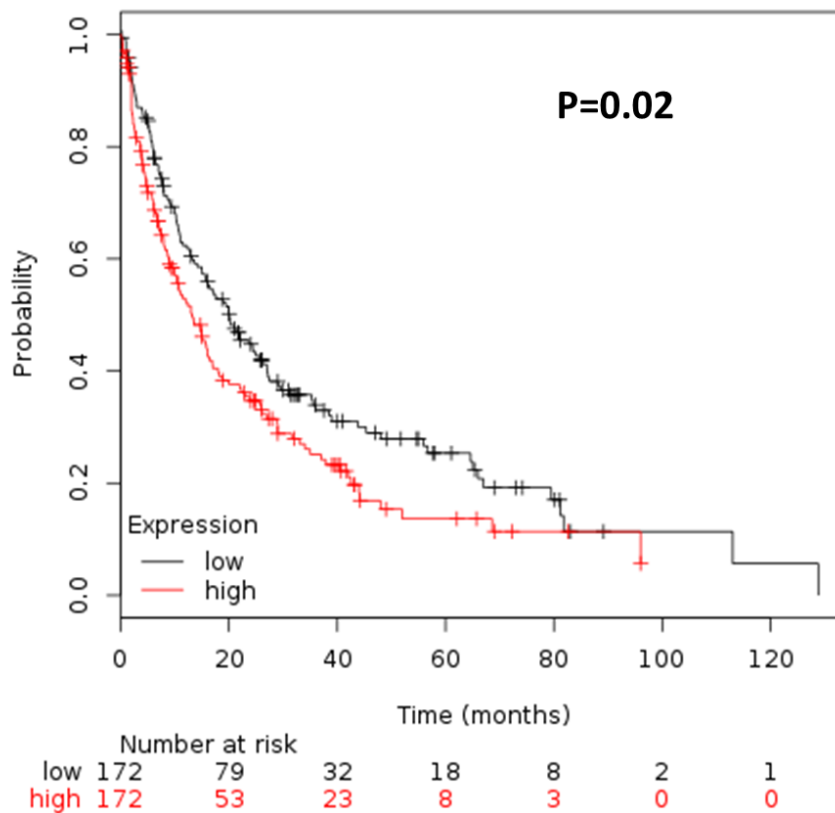


Figure 3.14: The Kaplan-Meier survival model of correlation between SIPA1 transcript levels and post-progression survival (PPS) in all lung cancer patients (available from <http://kmplot.com/analysis/index.php?p=background>). The median was chosen as the cut-off to divide the patients into high and low groups.

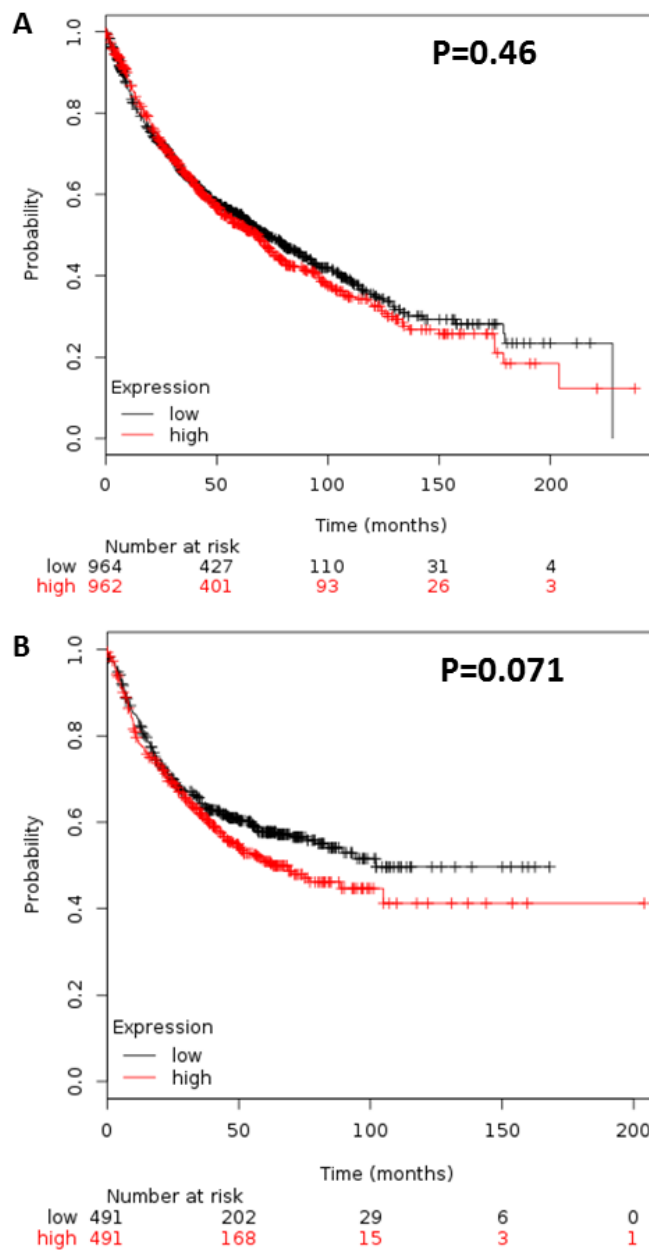
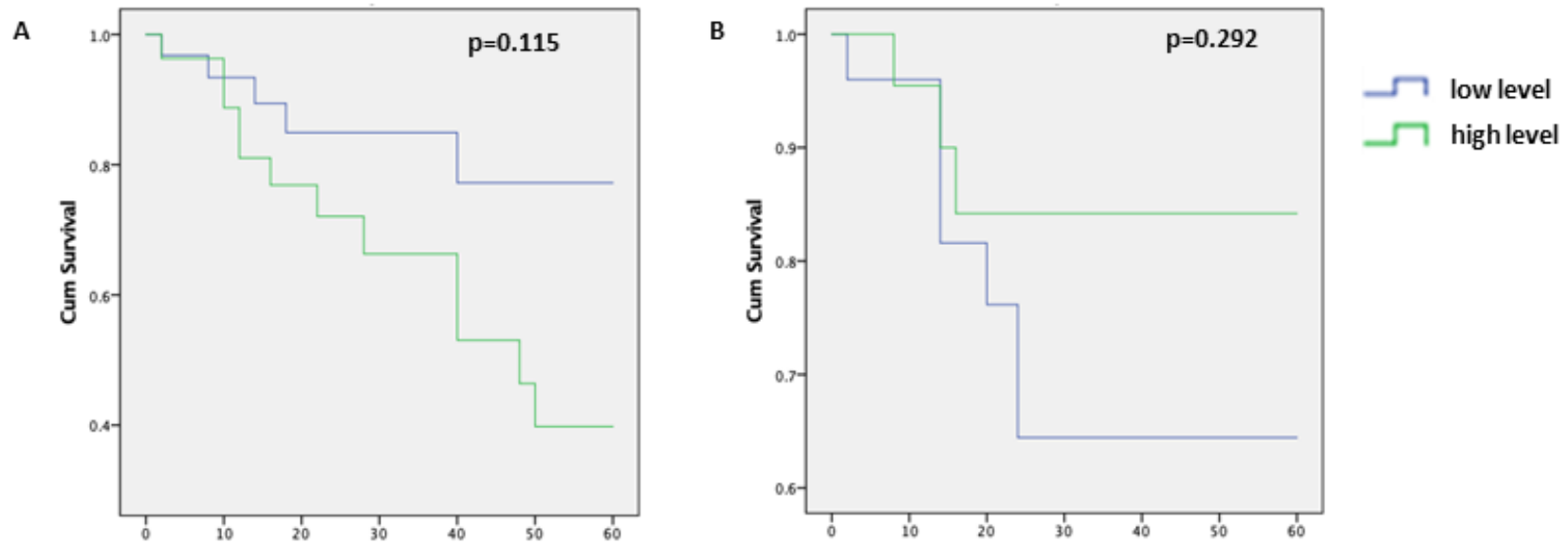


Figure 3.15: The Kaplan-Meier survival model of correlation between SIPA1 transcript levels and prognosis: overall survival (OS), progression-free survival (PFS) in all lung cancer patients (available from <http://kmplot.com/analysis/index.php?p=background>). (A) Overall survival (OS) (B) progression-free survival (PFS). The median was chosen as the cut-off to divide the patients into high and low groups.

Analysis was carried out to explore the correlation between SIPA1 levels and lung cancer patient prognosis in regards to the main histological types of lung cancer, namely adenocarcinoma and squamous cell carcinoma using the data from the Peking cohort. The result based on the Peking cohort showed that in patients with adenocarcinoma, those with a low level of SIPA1 tended to have longer survival, whilst in squamous cell carcinoma patients, those with a low level of SIPA1 tended toward a worse prognosis (**Figure 3.16**). However, due to the limitation of the sample size and the loss of follow-up data, neither of the subgroups showed statistical significance ($p=0.115$ and 0.292 in adenocarcinoma and squamous carcinoma respectively).

To further explore the relationship between SIPA1 and lung cancer prognosis, survival data of patients with different histological lung cancers from the Kaplan Meier plotter website (<http://kmplot.com/analysis/index.php?p=background>) were analysed. In lung adenocarcinoma patients (**Figures 3.17-3.19**), high SIPA1 level was accompanied by a poor outcome of cancer in terms of both OS ($p=0.0021$) and PFS ($p=0.0065$). However, according to PPS, the trend was the same but the result was not statistically significant ($p=0.17$). In lung squamous cell carcinoma, the correlation between SIPA1 level and patients' prognosis was established (**Figure 3.20**).



A	Total		Events		Censored		B	Total		Events		Censored	
	N	N	N	Percent	N	Percent		N	N	N	Percent		
0 (low level)	31	5	26	83.90%	0	25	7	18	72.00%				
1 (high level)	27	13	14	51.90%	1	22	3	19	86.40%				
Overall	58	18	40	69.00%	Overall	47	10	37	78.70%				

Figure 3.16: The Kaplan-Meier survival model of correlation between SIPA1 transcript levels and overall survival in various histology of lung cancer. (A) The correlation in adenocarcinoma. (B) The correlation in squamous cell carcinoma. a. Estimation is limited to the largest survival time if it is censored. Using 25, the median in the tumour group, as the cut-off to divide patients into two groups with high and low SIPA1 level.

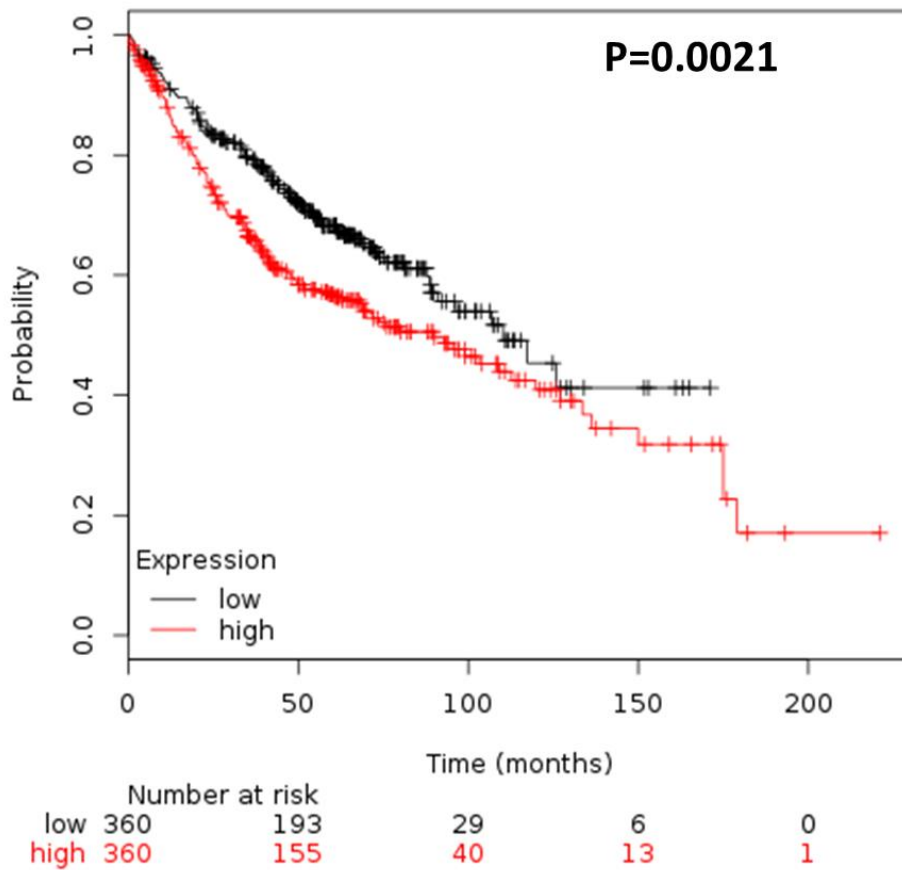


Figure 3.17: The Kaplan-Meier survival model of correlation between SIPA1 transcript levels and overall survival (OS) in lung adenocarcinoma patients (available from <http://kmplot.com/analysis/index.php?p=background>). The median was chosen as the cut-off to divide the patients into high and low groups.

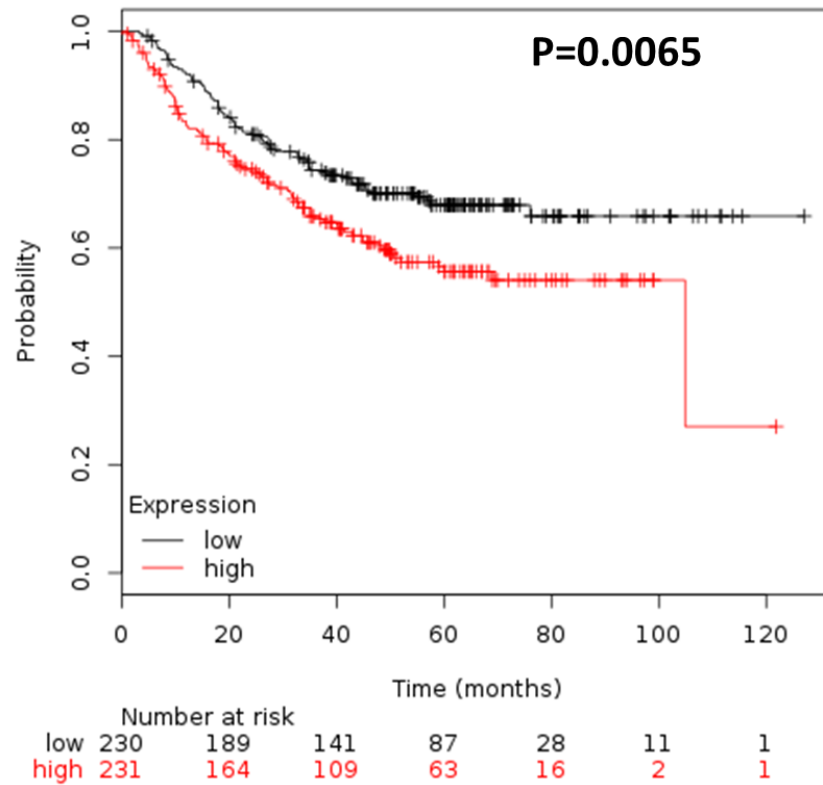


Figure 3.18: The Kaplan-Meier survival model of correlation between SIPA1 transcript levels and progression-free survival (PFS) in lung adenocarcinoma patients (available from <http://kmplot.com/analysis/index.php?p=background>). The median was chosen as the cut-off to divide the patients into high and low groups.

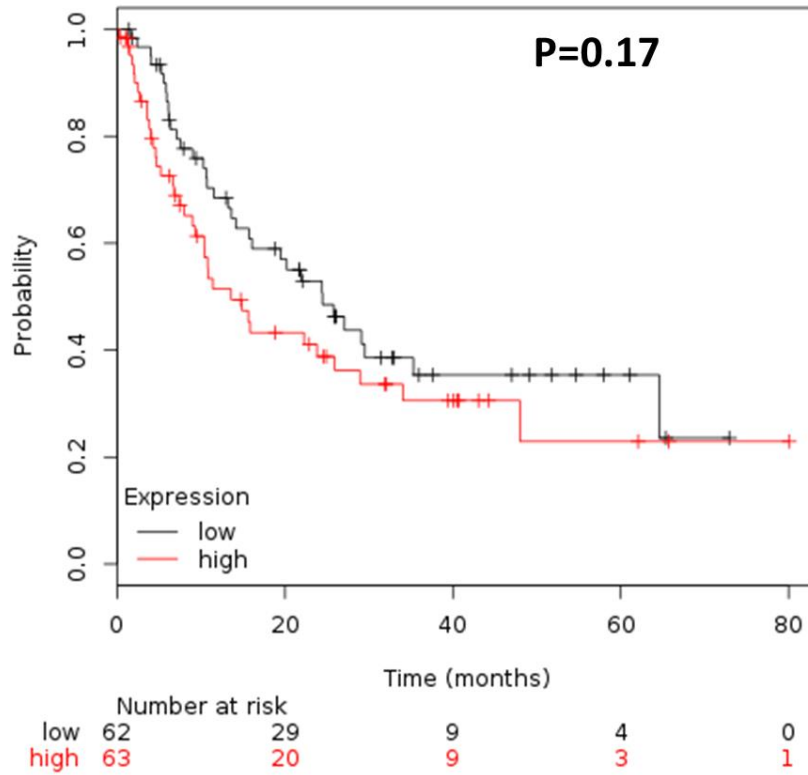


Figure 3.19: The Kaplan-Meier survival model of correlation between SIPA1 transcript levels and post-progression survival (PPS) in lung adenocarcinoma patients (available from <http://kmplot.com/analysis/index.php?p=background>). The median was chosen as the cut-off to divide the patients into high and low groups.

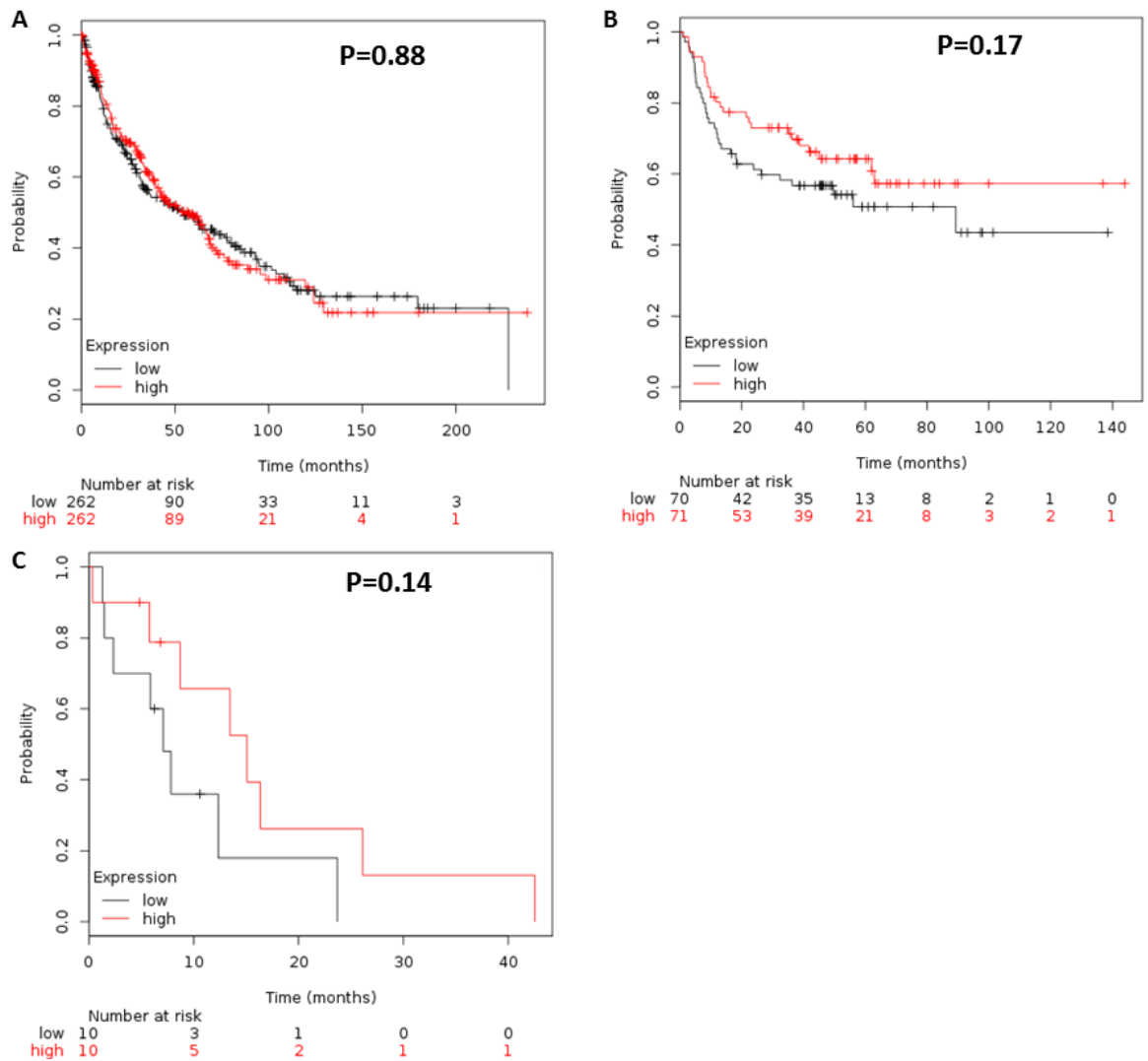


Figure 3.20: The Kaplan-Meier survival model of correlation between SIPA1 transcript levels and overall survival (OS), progression-free survival (PFS) and post-progression survival (PPS) in lung squamous cell carcinoma patients (available from <http://kmplot.com/analysis/index.php?p=background>). (A) Overall survival (OS). (B) Progression-free survival (PFS). (C) Post-progression survival (PPS). The median was chosen as the cut-off to divide the patients into high and low groups.

3.4 Discussion

During the past decade, it was revealed, within the scope of limited literature, that SIPA1 may have a role to play in the progression of various cancers (Takahara et al., 2017, Zhang et al., 2015, Brooks et al., 2010). A small number of studies investigated the expression level of SIPA1 in human tumours. Previous research by Takahara et al., demonstrated that SIPA1 level was upregulated in human oral squamous cell carcinoma compared with normal tissue by using IHC staining of the SIPA1 protein (Takahara et al., 2017). In prostate cancer, Gleason scores of IHC staining of SIPA1 was found to be positively correlated with tumour progression and metastasis (Shimizu et al., 2011). Detecting the nuclear expression of SIPA1 in breast cancer tissue by IHC staining was also shown to predict lymph node metastasis (Zhang et al., 2015). These are very important indicators of a potential role for SIPA1 in human tumours.

However, studies examining the role of SIPA1 in lung cancer are very few and the correlation between SIPA1 and clinical outcome in lung cancer is not at all clear. In this study we evaluated SIPA1 expression level in a clinical cohort consisting of 148 lung tumour tissue samples with 148 adjacent normal tissue samples, of which 139 tumour tissues were paired. SIPA1 transcript levels were higher in 148 tumour tissues compared with normal tissue ($p=0.0141$), and the same was seen in 139 tumour tissues compared with the paired normal tissue ($p=0.0358$). Thus, this dataset established that at the message RNA level, SIPA1 is more highly expressed in tumours compared with normal lung tissues.

IHC staining and scoring of the lung tumour TMA was far less convincing. The protein level of SIPA1 in tumour tissue samples was higher than that in normal lung tissues and adjacent normal lung tissues, but the difference was not statistically significant. There are some possible reasons which can account for why the SIPA1 gene transcripts analysis result and the SIPA1 protein analysis result cannot be completely matched.

-
- Firstly, cohorts and composition of the cohort. Our clinical cohort is larger and most importantly has substantially more normal tissues than the TMA cohort (148 vs 12, our cohorts vs TMA). This would undoubtedly contribute to the statistical power of the TMA cohorts, making it difficult to draw a solid conclusion.
 - Secondly, the nature of the samples. Whilst our cohort is fresh frozen and we were able to determine SIPA1 message quantitatively, the TMA however is an archival collection and only allows qualitative analysis. Of course, the size of the cohort and in particular that of the normal tissues in the cohort makes it less than ideal to appraise.
 - Thirdly, the present study cannot exclude the possibility of discrepancies between gene transcription and protein translation for SIPA1.
 - Fourthly, the evaluation of protein in this project is performed by IHC staining and scoring, which is more subjective whereas RNA extraction and analysis is a more specific, robust and reproducible laboratory technique.

Nonetheless, in terms of tumorigenesis, clinical cohort data demonstrated that the transcript level of SIPA1 was higher in advanced T stage, TNM stage and stage grouping with statistical significance. Scoring of IHC staining showed a statistically significant result in T stage but there was not a clear trend between SIPA1 level and tumour development. It is very interesting to note that the present study and those from the independent cohort (*KMplot*) were able to establish a clear correlation between SIPA1 transcript expression and the clinical outcome of the patients with lung cancer. Kaplan-Meier survival model from the data of our clinical cohort showed that patients with highly expressed SIPA1 had a lower overall survival of 48.3 months compared to 55.9 months of patients with low level of SIPA1. While the result did not reach statistical significance, this is highly likely due to the size of the cohort. The data available from the KM-plotter website (<http://kmplot.com/analysis/index.php?p=background>), with a larger cohort, showed the same statistically significant trend between SIPA1 and the post-

progression survival (PPS) of lung cancer statistically. Collectively, these data show that SIPA1 transcript levels *are* linked to the disease progression and clinical outcome of the patients with lung cancer.

The role of SIPA1 in different histological types of lung cancer is of great interest. Overall, both cohorts have indicated that SIPA1 has a significant role to play in the progression of adenocarcinoma of the lung. In lung adenocarcinoma, a high level of SIPA1 is associated with both shorter overall survival (OS) and shorter progression-free survival (PFS) statistically significantly. The correlation of SIPA1 and patient prognosis in lung squamous cell carcinoma is not clear and lacked statistical significance.

Taking all the data together, we found that in lung cancer, especially in adenocarcinoma, the expression of SIPA1 was increased and that high expression level of SIPA1 correlated with prognosis of lung cancer patients. Moreover, SIPA1 levels were upregulated in advanced developed tumour compared with initially developed tumours, which demonstrated that SIPA1 may have an essential role in tumorigenesis.

After analysing the data from the clinical cohorts, we are now left with a new set of questions:

- Why SIPA1 was upregulated in lung cancer?
- Why was SIPA1 correlated with the development of lung tumour?
- What is the mechanism of SIPA1 involved in the tumorigenesis and metastasis?
- How do SIPA1 and the HGF/MET connect in the intracellular signalling?

The subsequent work in this thesis will aim to answer these questions.

**Chapter-4 Impact of SIPA1
expression on the cellular function
behaviour of human lung cancer
cells**

4.1 Introduction

SIPA1 was first cloned from a murine lymphoid cell line (Hattori et al., 1995) and human peripheral blood lymphocytes (PBL) (Kurachi et al., 1997) and is highly expressed in lymphohematopoietic tissues (Hattori, 2011). In recent years, SIPA1 was found to be abundantly expressed in solid tumours, although the levels of SIPA1 expression level varies in different tumour cell lines. In breast cancer, expression of SIPA1 is highly expressed in MDA-MB-231 cells compared with MCF7 cells both at mRNA level and protein level (Zhang et al., 2015). The two human colorectal cancer cell line, HT115 and Caco-2, have high expression level of SIPA1 in terms of mRNA (Ji et al., 2012). Nine human oral squamous cell carcinoma (OCSS) HSC-2, HSC-3, HSC-4, Sa3, Ca9-22, SAS, KOSC-2, Ho-1-u-1 and Ho-1-N-1 all have a high expression level of SIPA1 compared to human normal oral keratinocytes HNOKs (Takahara et al., 2017). In prostate cancer, PC3 cells which have a high invasive potential showed highly upregulated expression of SIPA1 when compared with that in LNCaP cells which have a lower SIPA1 level and are less invasive (Shimizu et al., 2011). SIPA1 knockdown or over-expression models in tumour cell lines have been established by distinct methods. In previous studies, shRNA was used to knockdown SIPA1 in human breast cancer MDA-MB-231 cells (Zhang et al., 2015), human prostate cancer PC-3 cells (Shimizu et al., 2011) and human OSCC HSC-3 and HSC-4 cells (Takahara et al., 2017). SiRNA was used to suppress SIPA1 in the aggressive human melanoma cell line VM-1 (Mathieu et al., 2012) and ribozyme technology was used to target SIPA1 in the human colorectal cancer cell lines HT115 and Caco-2 (Ji et al., 2012).

It has been shown that overexpression and knockdown of SIPA1 in cancer cell lines resulted in changes in the cellular function of these cancer cells. *In vitro* cell function experiments showed that knocking down of SIPA1 reduced adhesion, migration and invasion in the human breast cancer MDA-MB-231 cell line (Zhang et al., 2015). *In vivo* metastasis experiments revealed that SIPA1 was positively correlated with the invasion potential of prostate cancer cells (Shimizu et al., 2011). In the OSCC cell

line HSC-3 and HSC-4, knocking down SIPA1 reduced the invasion and migration ability of cells but increased the adhesion of cells, with no significant change on proliferation potential (Takahara et al., 2017).

The number of studies on the mechanism of SIPA1 in cancer is insufficient to provide a categorical theory as to its role, with most studies being focused on the effect of SIPA1 on the invasion potential of cancer cells. In the host laboratory and at the preliminary phase of the present study, it was noted causal changes of barrier junction function following SIPA1 knock down in breast cancer cells, in that loss of SIPA1 in breast cancer cells resulted in a marked alteration of barrier electric resistance in these cells (Martin and Jiang 2013). Tight junctions have an essential role in cancer development and metastasis. In chapter 3, we found the intimate link between SIPA1 and its clinical relevance in lung cancer. In this present chapter we explore the influence of SIPA1 on cellular functions related to cancer cell metastasis as well as to the function of TJs, following the establishment of SIPA1 knock-down lung cancer cell models.

4.2 Material and methods

4.2.1 Cell lines

A549, SKMES1 and CORL23 lung cancer cell lines were used in this study to set up the SIPA1 knockdown cell model. A549 and SKMES1 cell lines were cultured in DMEM medium with 10% FBS and antibiotics and CORL23 cell line was cultured in RPMI-1640 medium with 10% FBS and antibiotics. Detailed information of these cell lines is described in section 2.1.1. Cell culture, maintenance and storage is described in section 2.3.

4.2.2 Knockdown of SIPA1 by using ribozyme transgene

Anti-SIPA1 ribozyme transgenes were constructed as described in section 2.6. Briefly,

SIPA1 ribozymes were amplified using 2× GoTaq G2 Green PCR master mix (Promega, Southampton, UK). The ribozyme sequence was then cloned into the pEF6/V5-His TOPO TA plasmid to produce the SIPA1-KD plasmid utilising the pEF6/V5-His TOPO TA expression kit (Invitrogen, Life technologies, Paisley, UK). The plasmid was transferred into the TOP10 Chemically Competent Escherichia. coli. The colonies for amplification and purification were selected by ampicillin. Correct colonies of the plasmids detected by RT-PCR using T7F primer coupled either with RbBMR and RbTPF primers were extracted utilising the Promega Plasmid MidiPrep Kit. Anti-SIPA1 ribozyme knockdown (SIPA-KD) plasmid together with pEF6/V5-His TOPO TA control (pEF-CT) plasmid were transformed into lung cancer cell lines via electroporation. The transfected cells were selected in medium containing 5-10µg/ml blasticidin and maintained in medium containing 0.5µg/ml blasticidin for further experimentation.

4.2.3 Primers and antibody

All the primers used were synthesised and provided by Invitrogen (Paisley, UK). Primer sequences are shown in **Table 2.3** and **2.4**. Mouse anti-SIPA1 antibody (ab219085) was obtained from ABCAM (Cambridge, UK). The name, molecular weight, supplier, and the product code of the primary and secondary antibodies used in this chapter is shown in **Table 2.5**.

4.2.4 RNA extraction, RT-PCR, and QPCR

The RNA was extracted by using Tri Reagent as described in section 2.8.1. After the isolation of RNA was completed, the quantification of RNA was carried out as described in section 2.8.2, followed by RT-PCR to obtain the cDNA. The cDNA could then be used for PCR and QPCR as describes in section 2.4.3 to 2.4.6.

4.2.5 Protein extraction, SDS-PAGE, and western blot analysis

The extraction of protein was carried out as the description in section 2.5.1. Proteins were extracted using lysis buffer and then quantified using the Bio-Rad DC Protein Assay kit (Bio-Rad Laboratories, Hemel-Hempstead, UK). After separation in the SDS-PAGE gel, proteins were transferred onto PVDF membranes as described in section 2.5.2. The membranes with protein were subsequently blocked and probed with various primary antibody and a corresponding peroxidase-conjugated secondary antibody. The antibodies' information in this study is showed in **Table 2.5**. Finally, the protein bands on the membrane were visualised using the chemiluminescence detection kit (Luminata, Millipore).

4.2.6 *In vitro* cell growth assay

Due to the difference growth speed between different cell lines, 3,000 - 5,000 cells were seeded into 200 μ l medium in three 96-well plates appropriately. After incubation for 1, 3, and 5 days respectively, the cells were fixed and stained by crystal violet. The absorbance was measured after dissolving the crystal violet with acetic acid (10% v/v) and the absorbance was determined at a wave length of 560nm using a spectrophotometer (BIO-TEK, Elx800, UK).

4.2.7 *In vitro* cell invasion assay

20,000-40,000 cells were seeded into transwell inserts (pore size, 8 μ m, Millicell, Merck KGaA, Darmstadt, Germany) coated with 50 μ g Matrigel. After the incubation of three days, cells that had invaded through the Matrigel and migrated on to the other side of the insert were fixed and stained with crystal violet and then counted. The absorbance was measured after dissolving the crystal violet with acetic acid (10% v/v) and the absorbance was determined at a wave length of 560nm using a spectrophotometer (BIO-TEK, Elx800, UK).

4.2.8 Transepithelial Resistance (TER) and Paracellular Permeability (PCP) assay

The Transepithelial Resistance (TER) and Paracellular Permeability (PCP) assay were performed as described in section 2.7.9. Approximately 50,000 cells in 100 μ l medium were seeded into transwell inserts (pore size, 0.4 μ m, Millicell, Merck KGaA, Darmstadt, Germany) with 1ml medium in the well outside of the insert, following the incubation of three days. Resistance across the membrane was measured using the EVOM² Epithelial Voltohmmeter (World Precision Instruments, Hitchin, Hertfordshire, UK).

4.2.9 Electric Cell-Substrate Impedance Sensing (ECIS)

ECIS assay to detect the resistance of cells was performed as described in section 2.7.8. 50,000 cells were seeded in the 96W1E+ electrode array plate after stabilization, following with measurement over different frequencies were to study different functional and structural cell properties. Resistance was measured between 1,000-4000Hz. Increased resistance of confluent cell monolayers implies increased cell-cell adhesion and hence increased barrier function.

4.2.10 Statistical Analysis

In this session, *t*-tests and Mann-Whitney test were performed using the Graphpad Prism 6 software. Image J software was used to analyse the PCR and western blotting bands. The results of the ECIS assay was analysed using the ECIS software. Differences were considered to be statistically significant when $p < 0.05$.

4.3 Result

4.3.1 Knockdown of SIPA1 in lung cancer cell lines

Anti-SIPA1 ribozyme transgenes were used to knockdown SIPA1 in SKMES1, CORL23 and A549 lung cancer cell lines. PCR, QPCR and western blot were performed to detect the knockdown of SIPA1 in both mRNA level and protein level. As shown in **Figures 4.1-4.3**, SIPA1 was successfully knocked down at both message RNA (**Figures 4.1 and 4.2**) and protein levels (**Figure 4.3**) in all three cell lines.

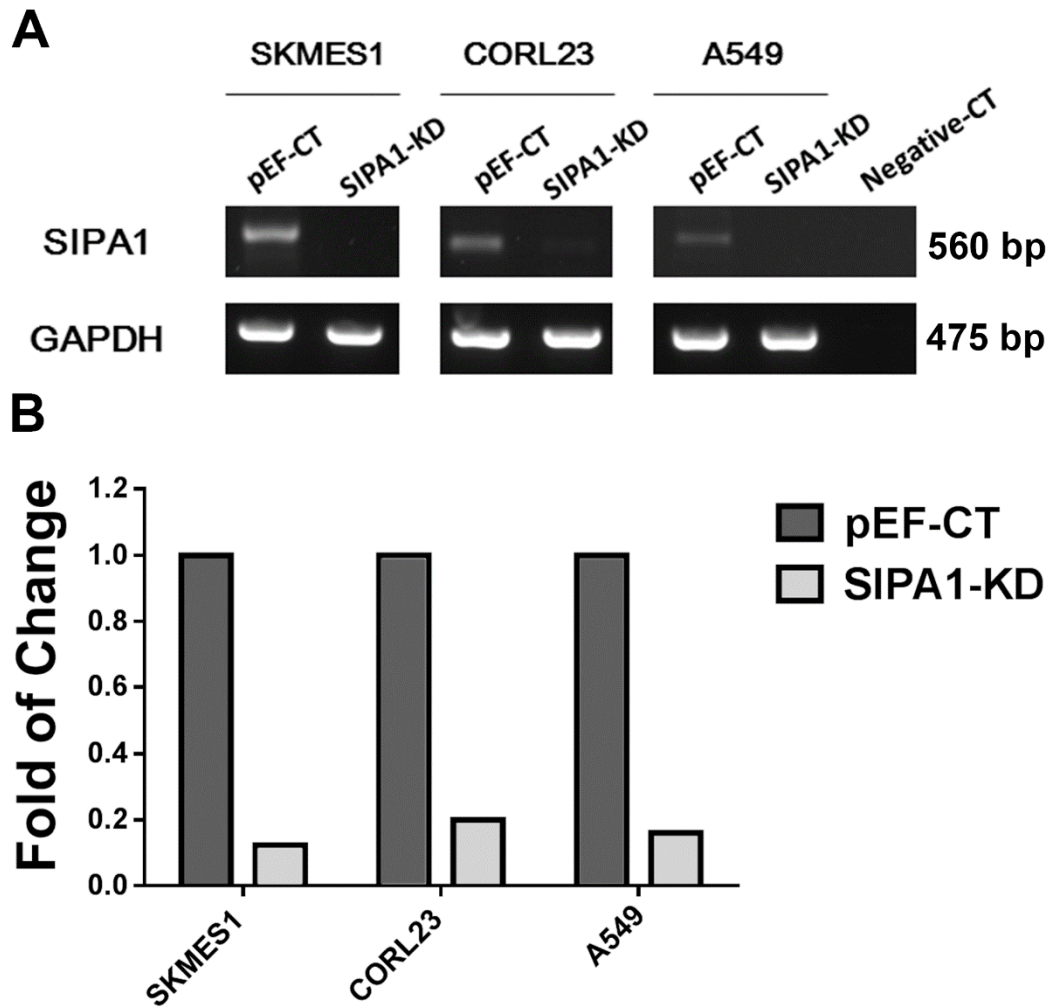


Figure 4.1: Verification of the knockdown of SIPA1 in SKMES1, CORL23 and A549 cell lines in mRNA level using PCR. A. The mRNA level of SIPA1 knockdown in SKMES1, CORL23 and A549 lung cancer cell lines was examined using conventional PCR. **B.** Quantitative analysis of the PCR bands.

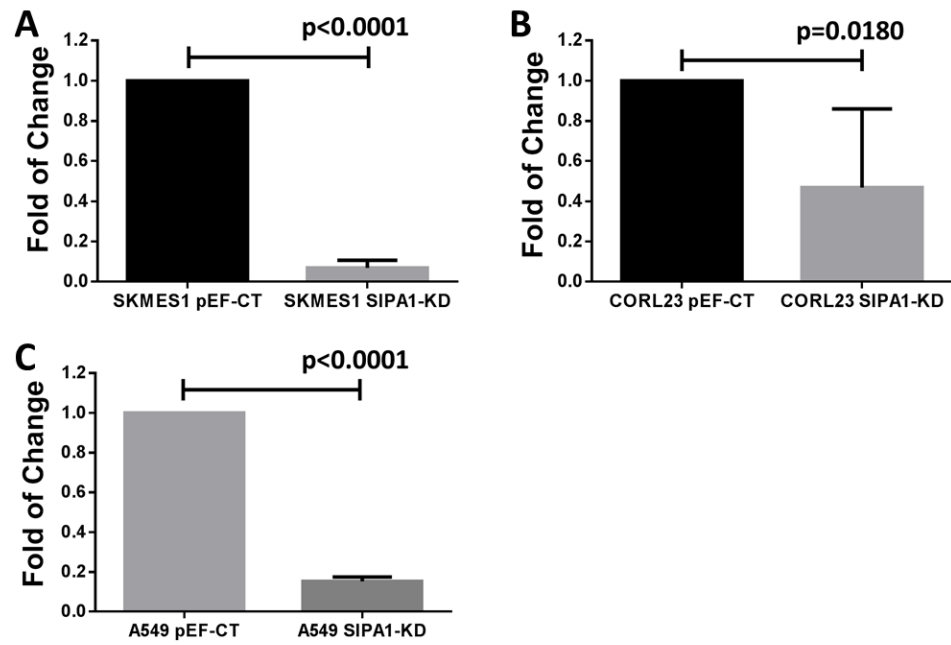


Figure 4.2: Verification of the knockdown of SIPA1 in SKMES1, CORL23 and A549 cell lines in mRNA level using QPCR. A. The mRNA level of SIPA1 knockdown in SKMES1 cell lines was examined using QPCR. **B.** The mRNA level of SIPA1 knockdown in CORL23 cell lines was examined using QPCR. **C.** The mRNA level of SIPA1 knockdown in A549 cell lines was examined using QPCR. Error bars show SD.

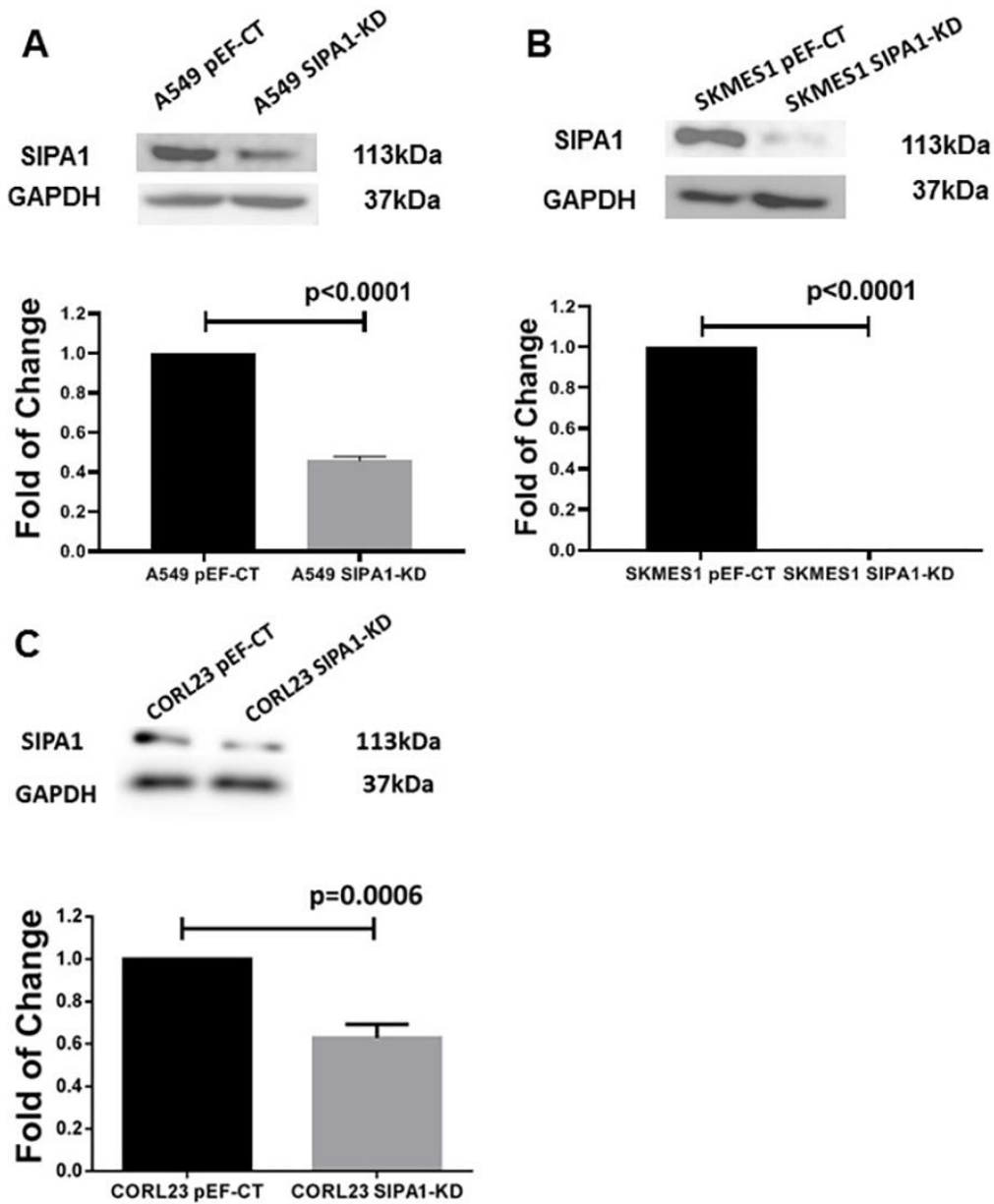


Figure 4.3: Verification of the knockdown of SIPA1 in A549, SKMES1, and CORL23 cell lines in protein level using western blot. A. The protein level of SIPA1 knockdown in A549 cell lines was examined using western blot. **B.** The protein level of SIPA1 knockdown in SKMES1 cell lines was examined using western blot. **C.** The protein level of SIPA1 knockdown in CORL23 cell lines was examined using western blot. Image J software was used to analyse the bands quantitatively. Error bars show SD.

4.3.2 Impact of SIPA1 on proliferation potential of lung cancer cells

The effect of SIPA1 knockdown on the proliferation of A549 cell lines was first evaluated by an *in vitro* growth assay (**Figure 4.4**). Results both after 3 days and 5 days indicated that SIPA1 knockdown significantly decreased the proliferation potential of the A549 cells.

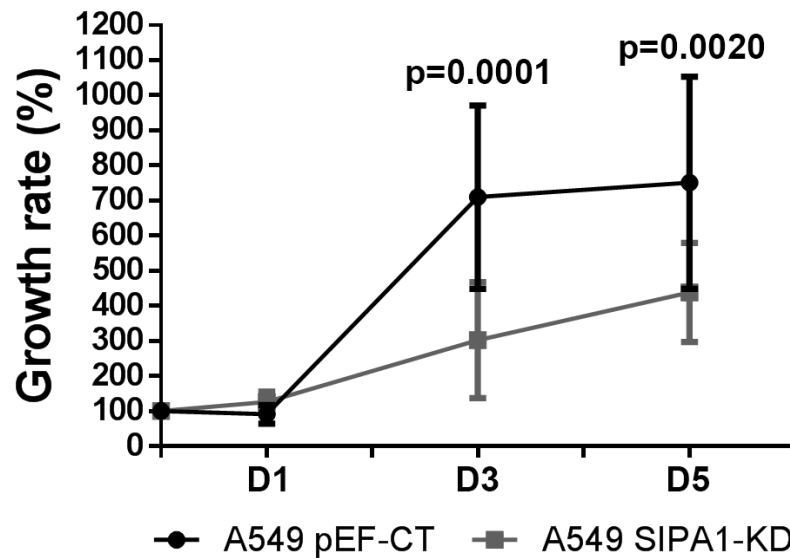


Figure 4.4: Knockdown of SIPA1 decreased the growth of the A549 cells significantly. Cells were incubated for 1, 3, and 5 days respectively and eight-well repeats were included. Growth rate (%) = Absorbance (Day 1, 3, 5) / Absorbance (Day 0) × 100. Error bars show SD.

4.3.3 Impact of SIPA1 on invasion potential of lung cancer cells

In vitro trans-well invasion assay was performed to investigate the effect of SIPA1 on the invasion function of lung cancer cell lines. Result showed the invasion potential was markedly reduced after knockdown SIPA1 in A549 and SKMES1 lung cancer cell lines (**Figure 4.5**).

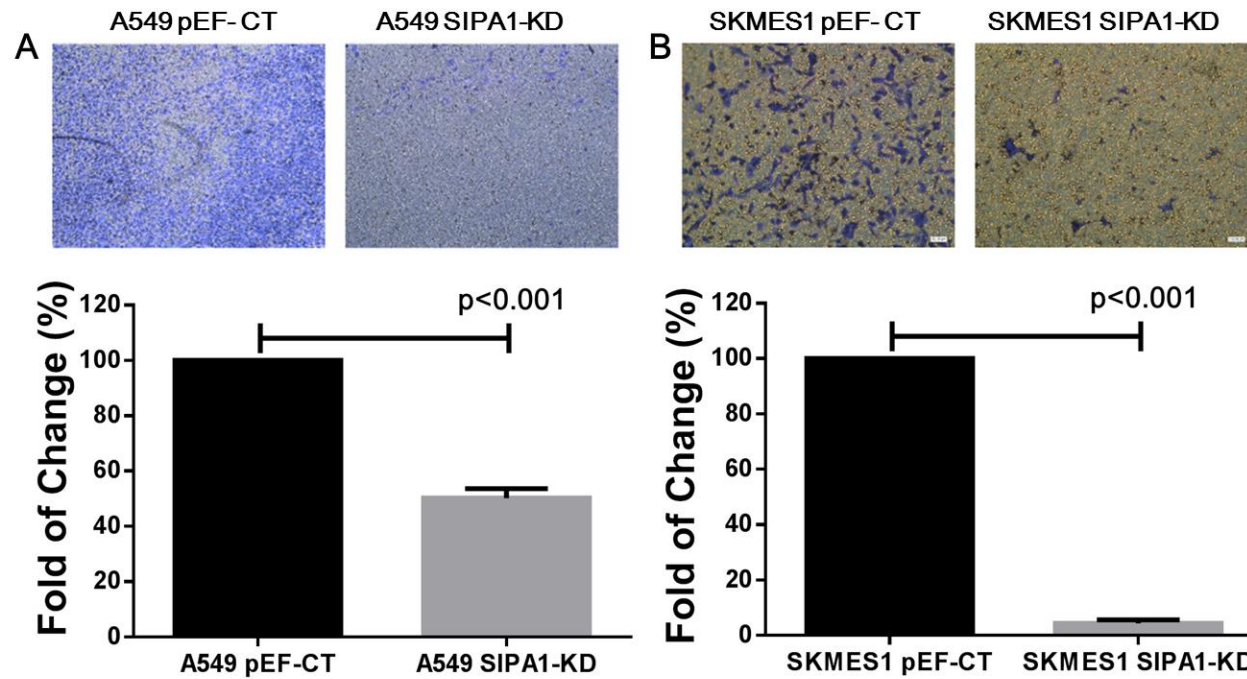


Figure 4.5: Knockdown of SIPA1 decreased the invasion of the A549 and SKMES1 cells significantly. Representative images of A549 invaded cells after staining (upper) and the absorbance measured by dissolving the crystal violet from stained invaded cells. **(B)** Representative images of SKMES1 invaded cells after staining (upper), bar graph shows the measurement of numbers of invaded cells. Error bars show SD.

4.3.4 Impact of SIPA1 on tight junction of lung cancer cells

To measure the change of barrier and TJ function on lung cancer cells after knockdown of SIPA1, two independent methods were employed, namely electric cell-substrate impedance sensing (ECIS) assay and trans-epithelial electric resistance (TER). ECIS can provide data on barrier function of a confluent cell monolayer; TER is a well-known method for investigating resistance across cell layer that is directly related to TJ function. The data from the ECIS assay showed knockdown SIPA1 in A549 cells enhanced cell-cell barrier function significantly (**Figure 4.6.A**). 3D figure showed the impact of SIPA1 on TJ via various frequencies (**Figure 4.6.B**), and quantitative analysis of the resistance when cells formed the monolayer between time point 1.5 to 2.5 hours showed that SIPA1 knockdown effected statistically significant differences in the barrier function of these cells (**Figure 4.6.C**). The TER experiment results showed similar findings: knockdown of SIPA1 enhanced cell-cell TJ compared to WT-CT and pEF-CT group in the A549 cell line (**Figure 4.7**).

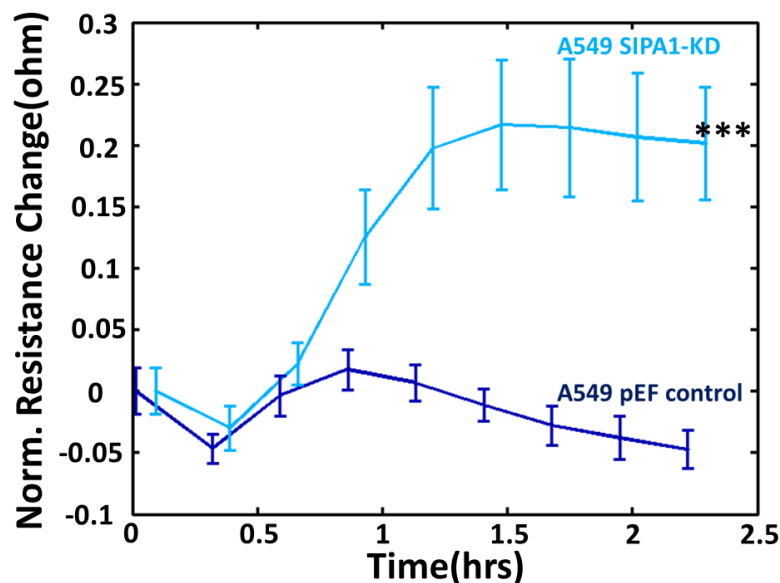


Figure 4.6.A: Knockdown of SIPA1 increased the cell-cell tight junction of the A549 cells significantly. Measurement the change of the resistance during a period of 2.5 hours after cells seeded in the plate. 1000Hz frequency was chosen to analyse cell resistance referring to the function of tight junction. *** represents $p < 0.001$, Error bars show SD.

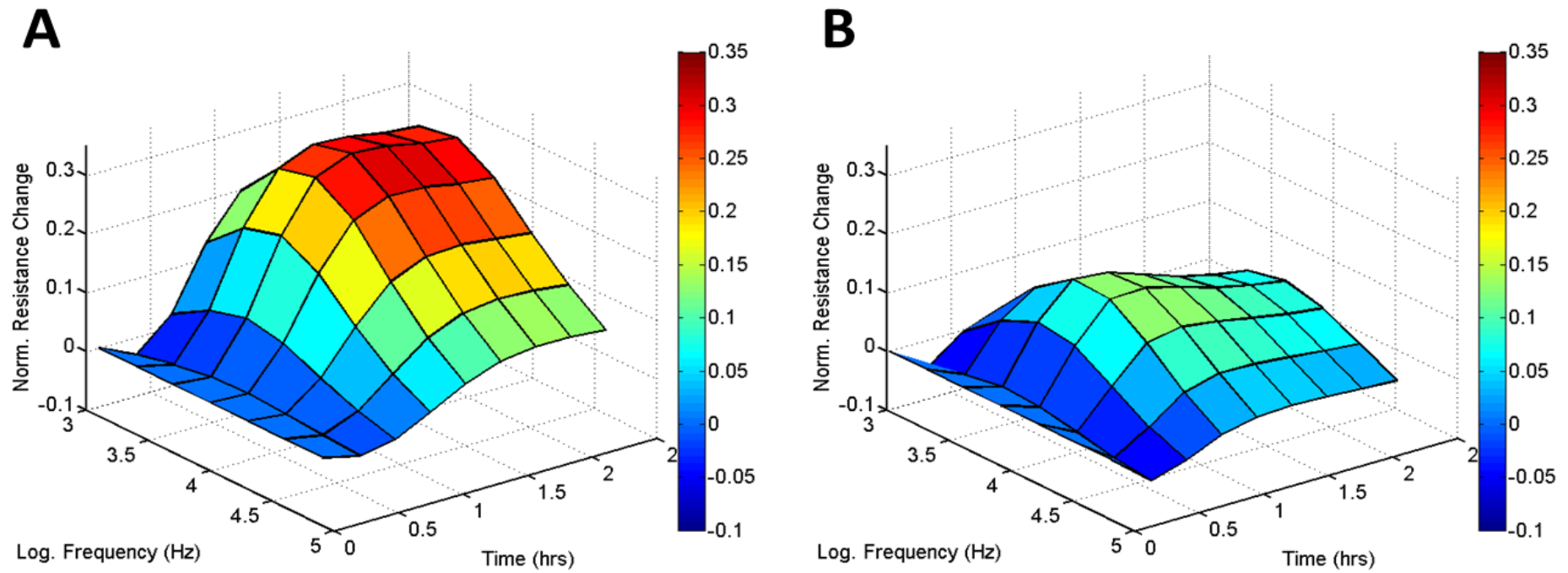


Figure 4.6.B: 3D figure showed knockdown of SIPA1 increased the cell-cell tight junction in different frequencies. Left: A549 SIPA1-KD cells. Right: A549 pEF-CT cells. The change of normalised resistance of A549 SIPA1-KD cells was significantly higher than that in A549 pEF-CT cells.

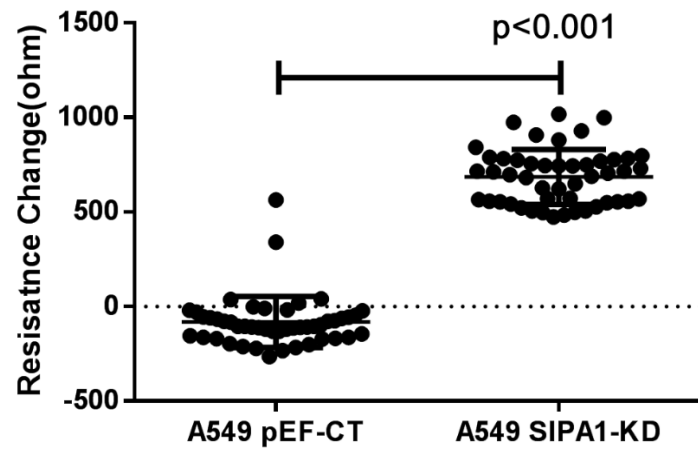


Figure 4.6.C: The effect of SIPA1 in enhancing tight junction is statistically significant. Quantitative analysis of the change of resistance of the data from 4 time points between 1.5 and 2.5 hours showed the change of TJ was significant statistically ($p < 0.001$).

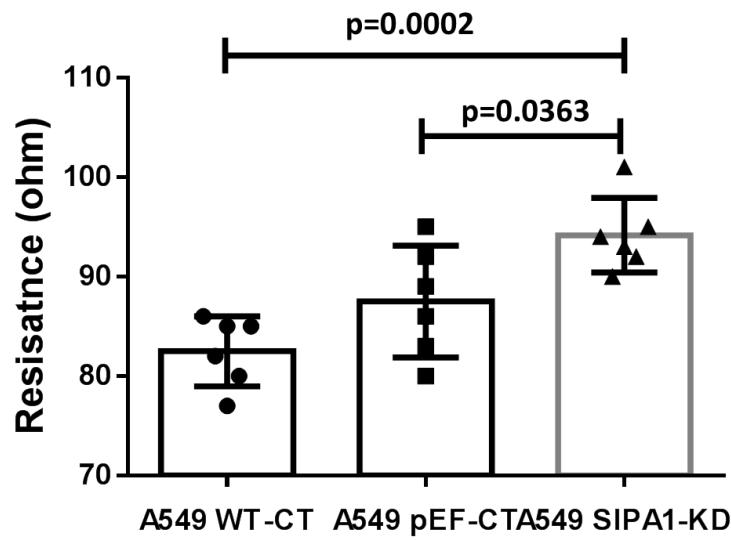


Figure 4.7: The Effect of SIPA1 Knockdown on A549 cell line detected using Transepithelial Resistance (TER). Knockdown of SIPA1 enhanced cell-cell TJ significantly. Error bars show SD.

4.4 Discussion

As mentioned above, expression of SIPA1 was higher in lung tumour tissue and the high level was correlated to the malignant phenotype of tumours and poor prognosis in lung cancer patients. We therefore determined to investigate the impact of SIPA1 on the function of lung cancer cells, as well as on tight junction function and component expression. Similarly to the knockdown of SIPA1 in breast cancer (Zhang et al., 2015), prostate cancer (Shimizu et al., 2011) and OSCC (Takahara et al., 2017), knockdown SIPA1 in lung cancer cells decreased the invasive potential of cancer cells. Invasion is an essential part of tumour metastasis and is one of the main causes of secondary disease and poor prognosis (Hanahan and Weinberg, 2011, Valastyan and Weinberg, 2011). The correlation between the high expression level of SIPA1 in lung cancer and the malignancy of the tumour and poor prognosis may be related to the demonstration that SIPA1 promotes the invasion of lung cancer, resulting in a poor patient outcome. Meanwhile, SIPA1 increases the propensity of lung cancer cells to grow and tumour growth is another crucial feature of malignant disease. In breast cancer or OSCC, previous studies showed that the promotion of SIPA1 for tumour growth and invasion was correlated with ITGB1, Brd4 and MMP (Takahara et al., 2017, Zhang et al., 2015).

Gradually, increasing studies demonstrated the essential role of TJs in cancer metastasis and the function of TJ proteins was not only pertinent in forming the structure of TJs but in various aspects such as extracellular signal transduction, cell morphology maintenance, participating intracellular signalling pathway, *etc.* (Martin, 2014, Tracey A. Martin, 2013, Chiba et al., 2008). Previous studies showed that the expression patterns of Claudin1 and Claudin5 were highly disparate between lung squamous cell carcinomas and lung adenocarcinomas: Claudin1 was positive in lung squamous cell carcinomas and Claudin5 was negative, whereas adenocarcinomas were positive for Claudin5 and negative for Claudin1 (Paschoud et al., 2007). Claudin1 had confirmed expression in small cell lung cancer in more than 80% of tumour tissues assessed (Liu et al., 2007). An early study of 68 lung cancers and

adjacent normal lung tissue showed that Occludin stained strongly in normal lung tissue (Tobioka et al., 2004).

In this current study, barrier and TJ function of the cells was evaluated using ECIS and TER and PCP assays, with all the results from these assays showing that SIPA1 knockdown enhanced the TJs of lung cancer cells both at total barrier function (ECIS) and at the transcellular and paracellular pathways. The TJ is the first barrier during cancer metastasis to overcome. The TJ provides the barrier to which cancer cells must overcome in order to (a) dissociate from the primary tumour; (b) intravasate; (c) extravasate at a secondary tumour site. If the TJ is either weak (so-called 'leaky' barriers) or dismantled (either by down regulation of vital TJ components, erroneous gene expression leading to truncated TJ proteins or changes in phosphorylation status) then cancer cells are able to undergo cancer spread. Conversely, strengthening of the TJ's can lead to less cancer spread. The enhanced function of TJs in cancer cells after knockdown of SIPA1 indicates a decrease in cancer cell metastatic phenotype and was consistent with the correlation of SIPA1 with poor prognosis in patients with lung cancer. In essence, we can deduct from these data that SIPA1 is an essential driver in lung cancer development and metastasis, which can promote the proliferation, invasion of lung cancer and may accomplish this by mediating decreases in integrity of the TJs of lung cancer cells.

Thus, the findings presented in this chapter strongly indicate that expression of SIPA1 in lung cancer cells is closely related to the expression of TJ molecules and the barrier functions of the cells. This leads us to a new set of questions:

- How does SIPA1 participate in the signalling events inside lung cancer cells and in particular to the events involved in the TJ signalling and indeed signalling that regulate cell migration and invasion?
- Does SIPA1 form an integral part of the chain events of TJs/cell migration triggered by external factors, such as hepatocyte growth factor (HGF), a factor known to disrupt TJs and be one of the most powerful mitogens and indeed

indicated to have a role to play in SIPA1 related cell functions (Jiang, 2006, Jiang, 2013).

These further investigations will be presented in the following chapter.

**Chapter-5 SIPA1 and its
intracellular signalling pathways in
human lung cancer cells**

5.1 Introduction

SIPA1 has been shown to play an important role in many kind tumours, like breast, gastric, cervical cancer, OSCC, colorectal cancer, and prostate cancer (Takahara et al., 2017, Li et al., 2017, Yi and Li, 2014, Pei et al., 2013, Ji et al., 2012, Shimizu et al., 2011). Our *in vitro* function research confirmed that knockdown of SIPA1 could inhibit the proliferation, invasion and increase the barrier function of lung cancer cells, which is consistent with the high expression of SIPA1 in tumour tissues compared to normal lung tissue in our clinical cohorts. Therefore, the specific mechanism of SIPA1 knockdown on cell function is worthy of deeper investigation to help study the mechanism of tumour metastasis and guide future clinical solutions. Correlation of SIPA1 and HGF/MET signalling pathway in breast cancer and prostate cancer was demonstrated by the host lab. Based on the previous study we found that in breast cancer cells SIPA1 is involved in the regulation of HGF on tight junctions (Jiang, 2013, Jiang, 2006). Lacking SIPA1, the breast cancer cell line MDA-MB-231 showed low reaction to the stimulation of HGF compared to wide type control cells. Therefore, we hypothesized that in lung cancer, SIPA1 also regulates cell aggressive behaviours through the interaction with HGF/MET signalling pathway to cause lung cancer development and metastasis.

HGF is known as a typical mitogen which could promote the motility, proliferation and invasion of the cells during the embryonic development, liver regeneration and cancer metastasis (Gherardi et al., 2012, Trusolino et al., 2010, Martin et al., 2004). Many studies have shown that the HGF/MET signalling pathway is constantly high expressed in primary cancer and their metastases and this aberrant expression correlates with poor prognosis (Martin et al., 2001, Jiang et al., 1999). In cancer, MET signalling pathway activation most often occurs through the ligand-dependent binding mechanism of HGF. Many types of cancer often overexpress MET, but the ligand is not expressed by the tumour cells, but in the extracellular matrix. Therefore, HGF/MET signalling pathway is often paracrine activated (Birchmeier et al., 2003b, Martin et al., 2001). The binding of activated HGF to MET induces

autophosphorylation of the Tyr residues Y1234 and Y1235 on the MET protein, then the kinase domain of the dimerized receptor is activated as a consequence, resulting in increasing the catalytic activity. Subsequently, phosphorylation of the Tyr residues Y1349 and Y1356 at the C-terminal fragment produces a binding site for those proteins which contain a Src homology 2 (SH2) domain (Trusolino et al., 2010). Signal effector proteins such as phosphatidylinositol 3-kinase (PI3K), phospholipase C gamma (PLCγ), the non-receptor tyrosine kinase Src and signal transducer and activation of transcription 3 (STAT3) can attach to the binding domain of MET. Meanwhile, some scaffolding adapters such as growth factor-bound protein (GRB2), GRB2-associated binding protein 1 (GAB1), and SH2 domain-containing transforming protein (SHC) can also be recruited by MET and linked to the binding site, becoming the new binding sites for other molecules (Trusolino et al., 2010). The downstream of HGF/MET includes RAS-RAF-MEK-ERK/MAPK, PI3K-Akt, Rap, and Rac-Pak signalling pathways, resulting in changes of cancer cell proliferation, survival, with complex cell mitogenic and morphogenic features (Trusolino et al., 2010, Birchmeier et al., 2003b).

Since SIPA1 can regulate the function of tumour cells and the response to HGF, HGF/MET signalling pathway may be the key point for SIPA1 regulation of tumour cells. HGF/MET signalling is an essential part of the control of tight junction function (Martin, 2014). HGF/MET signalling is also an important member of the receptor tyrosine kinase (RTK) signalling pathway, which also includes EGFR, VEGFR, IGFR, FGFR, etc. The RTKs family are a large and extremely complex family with similar functions, in which the interactions between family members, and the positive and negative feedback adjustments are particularly complicated (Trusolino et al., 2010). The complex interactions among the RTKs have been suggested to be potential causes of resistance to targeted therapy for lung cancer patients. The abnormal activity of MET is one of the most common causes of acquired resistance to EGFR-TKI treatment, and MET amplification can be found in more than 5-22% EGFR targeted therapy secondary resistance cases (Wu et al., 2017). Therefore, the

regulation of HGF/MET signalling pathway by SIPA1 may be more than just a simple regulation but a complex process. Revealing more detail of the regulation of SIPA1 is particularly important for a better understanding of the process of cancer metastasis and then providing clear clinical applications.

In this chapter, the markers known to be co-expressed with SIPA1 were investigated in both our Peking lung cancer cohort and TCGA database. Meanwhile, we analysed the intracellular signalling pathway regulated by SIPA1 and HGF/MET to find out the key markers and pathways involving in the interaction between SIPA1 and MET, aiming to find out the intracellular signalling pathways regulated by SIPA1 in human lung cancer cells.

5.2 Methods

5.2.1 Protein extraction

The extraction of protein was carried out as the description in section 2.5.1. Proteins were extracted using lysis buffer and then quantified using the Bio-Rad DC Protein Assay kit (Bio-Rad Laboratories, Hemel-Hempstead, UK).

5.2.2 Kinexus™ protein microarray in SIPA1 knockdown A549 cancer cells treat with/without HGF

Protein samples were collected from A549 lung cancer cells of PEF control and SIPA1 knockdown using anti-SIPA1 ribozyme transgene, respectively. After protein extraction and subsequent quantification, 350µl lysis (4mg/ml) was prepared and being stored at -20°C before sending for an analysis using the Kinexus™ antibody microarray (Kinexus Bioinformatics, Vancouver, British Columbia, Canada).

5.2.3 TCGA database acquirement and statistical analysis

In this session, The TCGA-LUAD database was obtained from the website <https://www.cancer.gov/about-nci/organization/ccg/research/structural-genomics/tcga>. T-tests, Mann-Whitney test and one-way ANOVA test were performed using the Graphpad Prism 6 software. Spearman correlation was calculated using SPSS software. Key signalling pathways were obtained from the *Reactome* website: www.reactome.org. Differences were considered to be statistically significant when $p < 0.05$, *represents $p < 0.05$, **represents $p < 0.01$, *** represents $p < 0.001$. Correlation was considered to be rather high when $R^2 > 0.3$ or < -0.3 .

5.3 Results

5.3.1 Potential connection among SIPA1, HGF signalling pathway and tight junctions' components

As discussed in the introduction, there is some evidence to indicate SIPA1 may be a potential downstream effector or interaction modulator of HGF and its receptor, MET signalling pathway (Kurachi et al., 1997, Birchmeier et al., 2003a). In this chapter, we delved deeper into HGF/MET-SIPA1 links and deciphered a potential link between SIPA1 and MET at the cellular level. Here we analysed the correlation between SIPA1, HGF, MET and PTK2 (Protein Tyrosine Kinase 2, or focal adhesion kinase, FAK), together with the MST1 (Macrophage Stimulating 1, or HGF-like Protein, HGFL, or Macrophage-Stimulating Protein, MSP) and its receptor, MST1R (or RON), in order to establish if a potential connection is present in the Peking lung cancer cohort. To investigate the regulation of HGF/MET-SIPA1 link on TJs, we also performed correlation analysis between SIPA1 and relevant TJ proteins. The dataset for HGF, MET, MST1, MST1R and PTK2 was only available in one of the two cohorts and the analysis was based on the Peking lung cancer cohort only (n=148). As shown in **Figure 5.1**, it was interesting to note that SIPA1 is highly correlated with transcript levels of the HGF, MET and PTK2, as well as with some TJ proteins such as JAM2, Marvel D2, Marvel D3, Nectin2 and some TJ regulating proteins such as RHOC,

ROCK1 and ROCK2. The correlation between SIPA1 and MST1/MST1R was not significant.

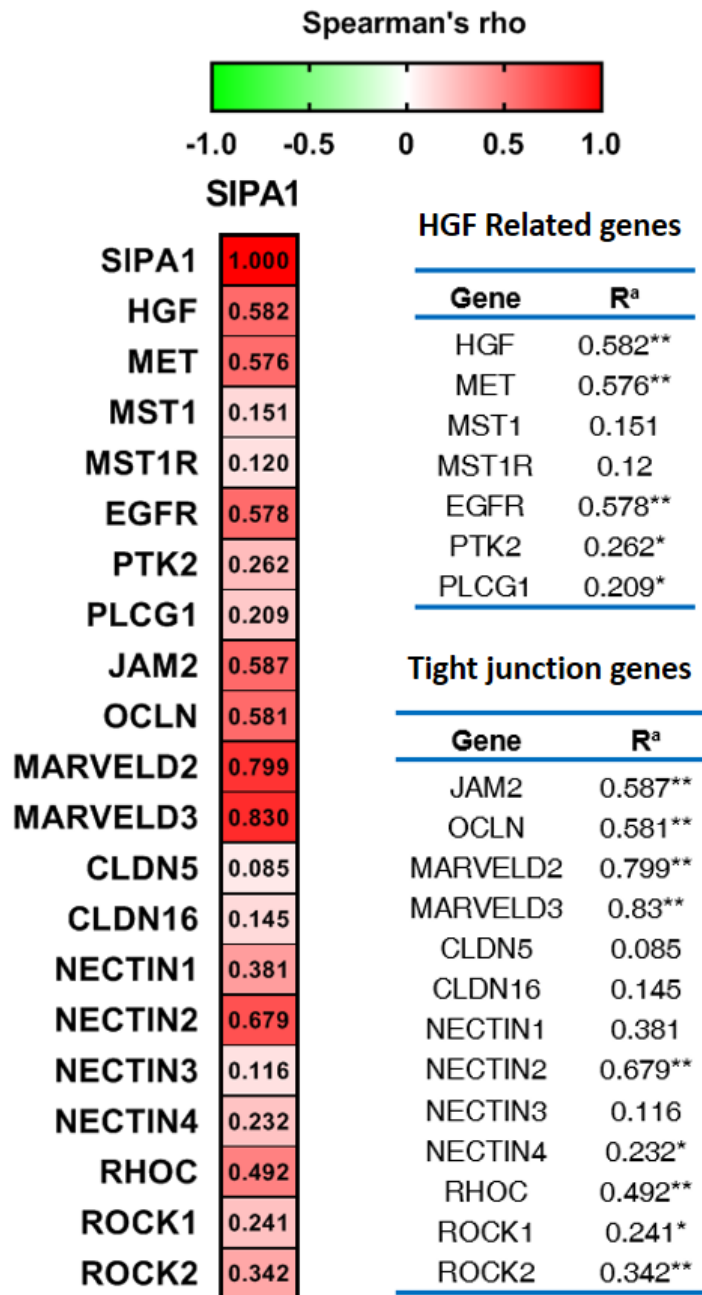


Figure 5.1: Spearman's rank correlation coefficient between SIPA1, HGF related genes and tight junction component genes analysed from the lung cancer cohort (n=148). a. Correlation coefficients, by Spearman ranked correlation method. *represents $p < 0.05$, **represents $p < 0.01$ in 2-tailed significance test. High correlation was considered when $R^2 > 0.3$ or < -0.3 . All the detected genes were described using their official name from NCBI (<https://www.ncbi.nlm.nih.gov/gene>).

To further investigate the potential interaction between SIPA1 and the HGF-MET signalling pathway, RTK family, and their effect on TJs, we carried out the analysis based on the TCGA-LUAD database (Available from the website <https://www.cancer.gov/about-nci/organization/ccg/research/structural-genomics/tcga>). We selected HGF Activator (Hepatocyte Growth Factor Activator, HGFAC), HGF/MET, MST1/MST1R, ERF/EGFR, PKT2 and its antagonist PXN (Paxillin), together with PRKCA/PTEN, the regulator of PKT2, and SRC, the downstream protein of PKT2. We found all these genes were correlated with SIPA1 in the transcriptional level with statistically significance (**Figure 5.2**).

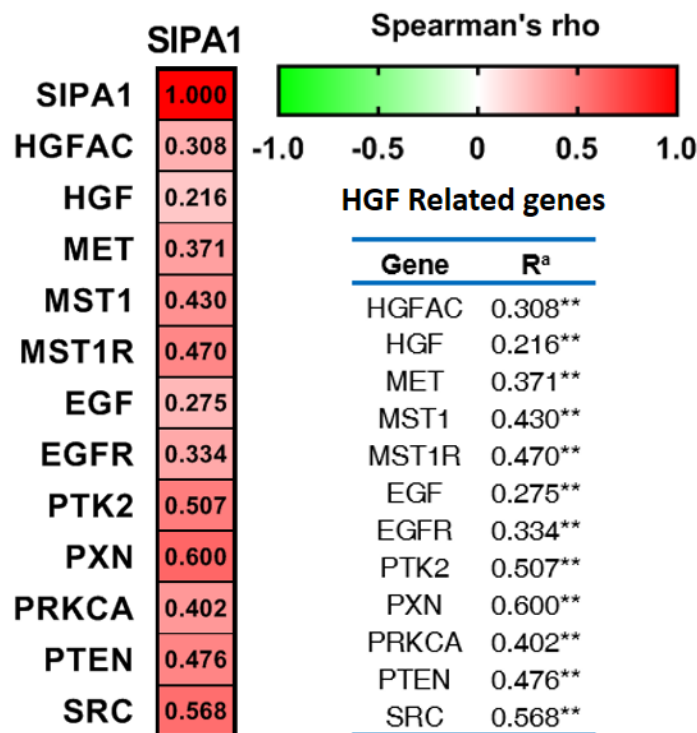


Figure 5.2: Spearman's rank correlation coefficient between SIPA1 and HGF related genes analysed from TCGA LUAD database (n=576). a. Correlation coefficients, by Spearman ranked correlation method. *represents $p < 0.05$, **represents $p < 0.01$ in 2-tailed significance test. High correlation was considered when $R^2 > 0.3$ or < -0.3 . All the detected genes were described using their official name from NCBI (<https://www.ncbi.nlm.nih.gov/gene>).

In another analysis on the correlation between SIPA1 and TJ components based on the TCGA-LUAD database (Available from the website: <https://www.cancer.gov/about-nci/organization/ccg/research/structural-genomics/tcga>), we focused on the JAM family, Claudin family, ZO family, TAMP proteins, and some regulating markers such as MAGI family and ROCK, *etc.* The gene F11R (encoding JAM1 protein), the ZO family encoding genes, Claudin proteins encoding genes such as CLDN4, CLDN7, CLDN12, CLDN15, Marvel D3 and MAGIX were all highly correlated with SIPA1 in the transcriptional level (**Figure 5.3**).

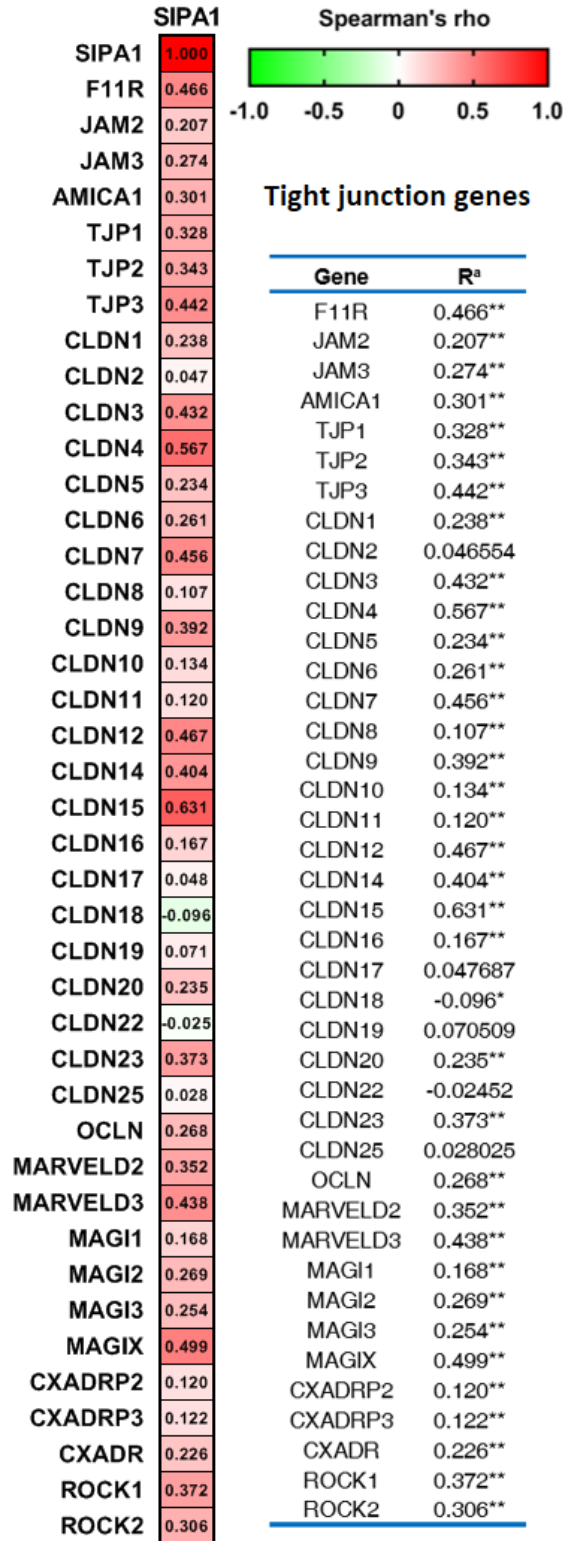


Figure 5.3: Spearman's rank correlation coefficient between SIPA1 and tight junction component genes analysed from TCGA LUAD database (n=576). a. Correlation coefficients, by Spearman ranked correlation method. *represents $p < 0.05$, **represents $p < 0.01$ in 2-tailed significance test. High correlation was considered when $R^2 > 0.3$ or < -0.3 . All the detected genes were described using their official name from NCBI (<https://www.ncbi.nlm.nih.gov/gene>).

We collected protein samples from A549 pEF control cells and SIPA1 knockdown cells treated with/without HGF for the protein kinase array analysis Kinexus™ platform. First, we obtained overall images of fluorescent-dye labelled antibody microarray slides, showing the overall phosphorylation intensity of the differently treated samples (**Figure 5.4**).

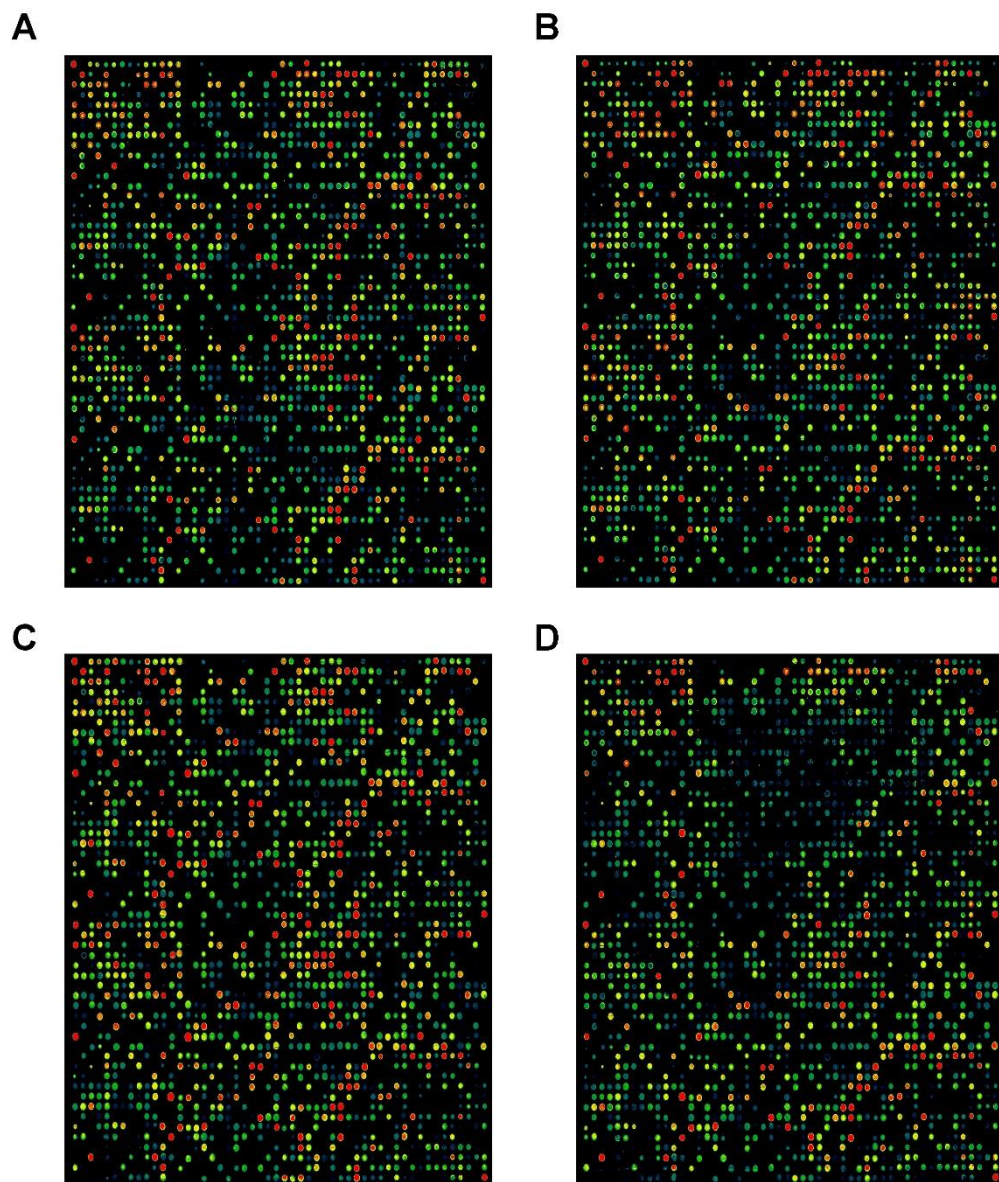


Figure 5.4: Overall images of a direct fluorescent-dye labelled KAM-1325 antibody microarray slide. A: detecting the protein sample from the A549 pEF control cells. **B:** detecting the protein sample from the A549 pEF control cells treat with HGF. **C:** detecting the protein sample from the A549 SIPA1 knockdown cells. **D:** detecting the protein sample from the A549 SIPA1 knockdown cells treat with HGF.

We then compared the phosphorylation status between A549 pEF control cells and the A549 SIPA1 knockdown cells. **Table 5.1** shows the markers whose phosphorylation status were most decreased after SIPA1 knockdown in the A549 cells, indicating the potential interaction markers with intercellular SIPA1. The website *Reacome* (www.reactome.org) was used to conduct the key pathway analysis report. The most downregulated markers after SIPA1 knockdown could be integrated to numbers of centralized signalling pathways, in which the top 25 signalling pathways are listed in **Table 5.2**. Also, the genome-wide overview schematic diagram of the signalling pathways was generated (**Figure 5.5**) to show the overall review of the main area in which the pathways downregulated by SIPA1 are located.

Table 5.1: Key markers whose phosphor-status were down regulated after SIPA1 knock down on A549 cells.

Target Name	P-Site	Full Target Protein Name	Average Normalized Net Signal		%CFC	Lead
			Control	SIPA1 KD		
Rb1	T821	Retinoblastoma-associated protein 1	902	323	-64	Possible
CRYAB	S19	Crystallin aB	1307	545	-58	Possible
GATA3	S369	Trans-acting T-cell-specific transcription factor GATA-3	1420	594	-58	Possible
GluR1	S849	Glutamate receptor 1	1261	536	-58	Possible
GCK (MAP4K2)	Pan-specific	Germinal centre protein-serine kinase	750	330	-56	Possible
PCK2 (PCTAIRE2, CDK17)	Pan-specific	Cell division protein kinase 17; Protein-serine kinase PCTAIRE-2	1844	861	-53	Possible
STAG2	Y433	Putative uncharacterized protein DKFZp781H1753	5391	2648	-51	Possible
DYRK2	Y382	Dual specificity tyrosine-phosphorylation-regulated kinase 2	2816	1424	-49	Possible
ARRB1	S412	Arrestin beta 1	800	409	-49	Possible
WNK2	Pan-specific	Serine/threonine-protein kinase WNK2	1215	623	-49	Possible
SRF	S224	Serum response factor	11435	5380	-53	
InsR (IR)	Pan-specific	Insulin receptor	1131	635	-44	
ASK1 (MAP3K5)	Pan-specific	Apoptosis signal regulating protein-serine kinase 1	2259	1414	-37	
Jun (c-Jun)	Y170	Jun proto-oncogene-encoded AP1 transcription	472	305	-35	

		factor				
JNK1 (MAPK8)	Y185	Jun N-terminus protein-serine kinase (stress-activated protein kinase (SAPK)) 1	5151	3362	-35	
Jun (c-Jun)	T91	Jun proto-oncogene-encoded AP1 transcription factor	937	639	-32	
HDAC5	S498	Histone deacetylase 5	1727	1192	-31	
ITK	Pan-specific	Tyrosine-protein kinase ITK/TSK	4223	2987	-29	
WNK1	Pan-specific	Serine/threonine-protein kinase WNK1	4291	3060	-29	
IGF1R	Y1280	Insulin-like growth factor 1 receptor protein-tyrosine kinase	1722	1237	-28	
IkBα	Pan-specific	Inhibitor of NF-kappa-B alpha (MAD3)	1324	956	-28	
STAT5	Y694	Signal transducer and activator of transcription 5	1745	1381	-21	
Yes	Y222+Y223	Yamaguchi sarcoma proto-oncogene-encoded tyrosine kinase	10235	8126	-21	
FAK (PTK2)	Y576+Y577	Focal adhesion protein-tyrosine kinase	404	324	-20	
TARDBP	S409+S410	TAR DNA-binding protein 43	4900	3996	-18	
AR	S310	Androgen receptor	8398	6996	-17	
Fyn	Pan-specific	Fyn proto-oncogene-encoded protein-tyrosine kinase	903	765	-15	
Vav	Y174	Vav 1 guanine nucleotide exchange factor	1659	1414	-15	

PKD1 (PRKCM, PKCm, PRKD1)	S910	Protein-serine kinase C mu (Protein kinase D)	619	564	-9	
MKK6 (MAP2K6, MEK6)	Pan-specific	MAPK/ERK protein-serine kinase 6 (MKK6); Dual specificity mitogen-activated protein kinase kinase 6	3719	3468	-7	
HSP90AB1 (HSP90; HSP84; HSP90B; HSPC2; HSPCB)	Pan-specific	Heat shock 90 kDa protein beta	1056	993	-6	
Lyn	Pan-specific	Yes-related protein-tyrosine kinase; Tyrosine-protein kinase Lyn	973	927	-5	
mTOR (FRAP)	Pan-specific	Mammalian target of rapamycin (FRAP); FKBP12-rapamycin complex-associated protein	6718	6460	-4	
CK2a1 (CSNK2A1)	T360+S362	Casein protein-serine kinase 2 alpha/ alpha prime	893	874	-2	
MLK1 (MAP3K9)	Pan-specific	Mixed-lineage protein-serine kinase 1; Mitogen-activated protein kinase kinase kinase 9	377	370	-2	
Chk1 (CHEK1)	S280	Checkpoint protein-serine kinase 1	10372	10176	-2	

Table 5.2: Top signalling pathways which were downregulated by SIPA1 knockdown on A549 cells. Generated from: www.reactome.org.

Pathway name	Entities				Reactions	
	found	ratio	p-value	FDR*	found	ratio
Signaling by SCF-KIT	6 / 51	0.004	4.86e-08	2.76e-05	21 / 36	0.003
CD28 co-stimulation	5 / 39	0.003	4.48e-07	1.27e-04	10 / 19	0.002
Interleukin-3, Interleukin-5 and GM-CSF signaling	5 / 50	0.003	1.50e-06	2.84e-04	10 / 38	0.003
Regulation of signaling by CBL	4 / 24	0.002	2.44e-06	3.44e-04	4 / 7	5.61e-04
ESR-mediated signaling	8 / 256	0.018	5.67e-06	6.26e-04	37 / 110	0.009
Signaling by Receptor Tyrosine Kinases	11 / 554	0.038	6.66e-06	6.26e-04	92 / 657	0.053
PECAM1 interactions	3 / 14	9.70e-04	2.31e-05	0.002	1 / 7	5.61e-04
Signaling by Interleukins	11 / 639	0.044	2.51e-05	0.002	52 / 490	0.039
Fc epsilon receptor (FCERI) signaling	7 / 235	0.016	3.10e-05	0.002	27 / 63	0.005
Costimulation by the CD28 family	5 / 97	0.007	3.61e-05	0.002	12 / 34	0.003
Generic Transcription Pathway	17 / 1,553	0.108	4.17e-05	0.002	61 / 824	0.066
EPHB-mediated forward signaling	4 / 51	0.004	4.60e-05	0.002	9 / 26	0.002
Regulation of KIT signaling	3 / 18	0.001	4.85e-05	0.002	3 / 8	6.41e-04
Signal Transduction	26 / 3,305	0.229	6.20e-05	0.002	240 / 2,303	0.184
Oxidative Stress Induced Senescence	5 / 114	0.008	7.70e-05	0.003	17 / 40	0.003
Fc gamma receptor (FCGR) dependent phagocytosis	6 / 193	0.013	9.45e-05	0.003	7 / 42	0.003
Signaling by Nuclear Receptors	8 / 385	0.027	1.02e-04	0.003	37 / 191	0.015
Cellular Senescence	6 / 199	0.014	1.12e-04	0.003	26 / 90	0.007
RNA Polymerase II Transcription	17 / 1,692	0.117	1.23e-04	0.004	61 / 885	0.071
CTLA4 inhibitory signaling	3 / 25	0.002	1.27e-04	0.004	2 / 5	4.00e-04
Developmental Biology	14 / 1,207	0.084	1.31e-04	0.004	109 / 511	0.041
PIP3 activates AKT signaling	7 / 316	0.022	1.95e-04	0.005	9 / 86	0.007
Cellular responses to stress	10 / 690	0.048	2.52e-04	0.006	45 / 227	0.018
EPHA-mediated growth cone collapse	3 / 33	0.002	2.87e-04	0.006	3 / 4	3.20e-04
Estrogen-dependent gene expression	5 / 154	0.011	3.09e-04	0.006	27 / 66	0.005

* False Discovery Rate

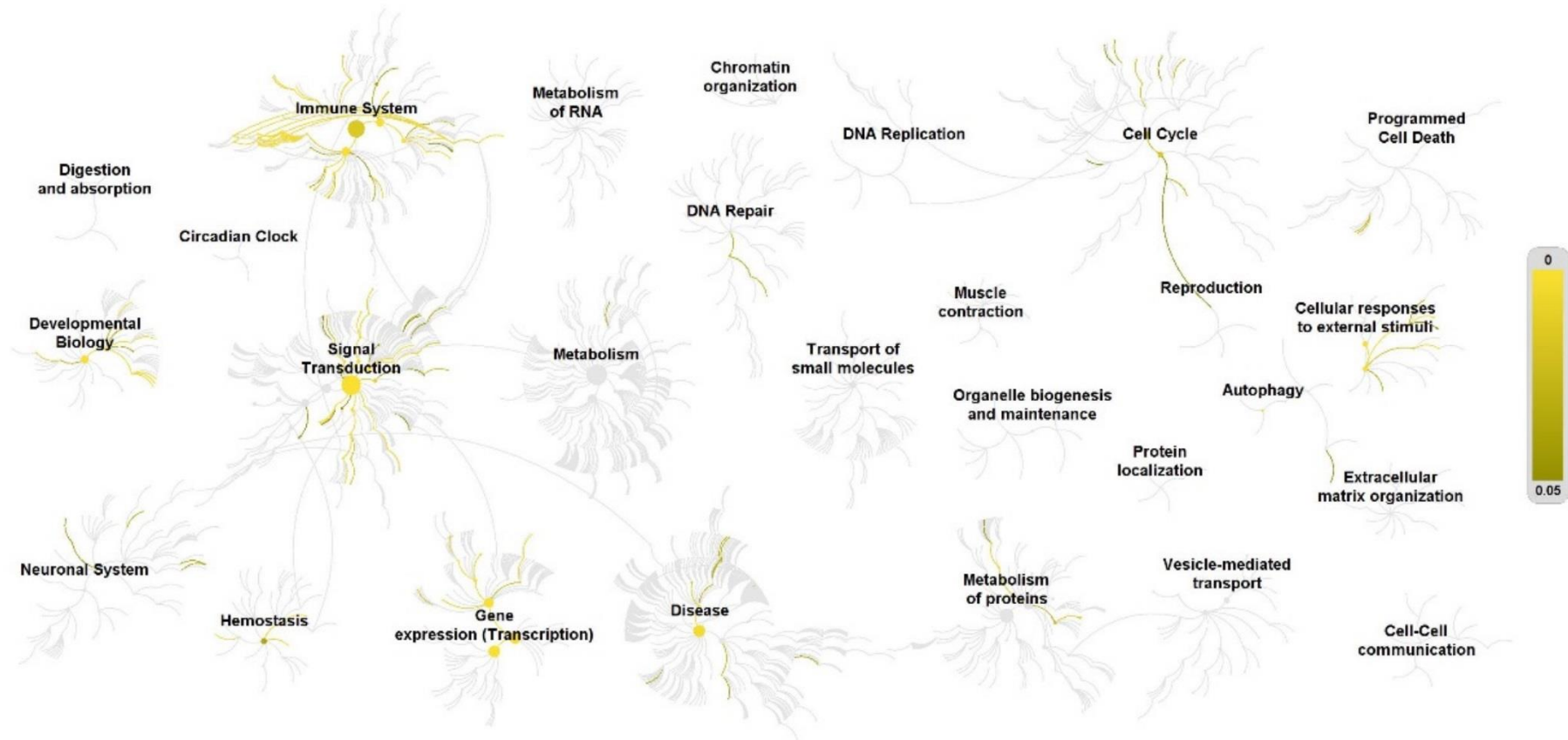


Figure 5.5: Genome-wide overview of the signalling pathway which were downregulated by SIPA1 knockdown on A549 cells. Pathways are arranged in a hierarchy. The centre of each of the circular represents the root of the top-level pathway. Each step away from the centre represents the next level lower in the pathway hierarchy. The light-yellow colour denotes over-representation of that pathway. Light grey signifies pathways which are not significantly over-represented. Generated from: www.reactome.org.

Similarly, **Table 5.3** shows the markers whose phosphorylation status were most increased after SIPA1 knockdown in the A549 cells, indicating the potential interaction markers with intercellular SIPA1, as well. The website Reacome (www.reactome.org) was used to conduct the key pathway analysis report. The most upregulated markers after SIPA1 knockdown could be integrated to numbers of centralized signalling pathways, in which the top 25 signalling pathways are listed in **Table 5.4**. Also, the genome-wide overview schematic diagram of the signalling pathways was generated (**Figure 5.6**) to show the overall review of the main area in which the pathways upregulated by SIPA1 are located.

Table 5.3: Key markers whose phosphor-status were up regulated after SIPA1 knock down on A549 cells.

Target Name	P-Site	Full Target Protein Name	Average Normalized Net Signal		%CF C	Lead
			Control	SIPA1KD		
Plk1 (PLK)	Pan-specific	Polo-like protein-serine kinase 1	756	11286	1393	Priority
EZH2	T487	Histone-lysine N-methyltransferase EZH2	1568	16728	967	Priority
MEF2A	T108	Myocyte-specific enhancer factor 2A	254	2636	939	Priority
ERK1 (MAPK3)	Y204+T207	Extracellular regulated protein-serine kinase 1 (p44 MAP kinase)	767	5502	618	Priority
Plk3 (CNK)	Pan-specific	Polo-like protein-serine kinase 3 (cytokine- inducible kinase (CNK))	417	2770	564	Priority
MARK2	Pan-specific	MAP/microtubule affinity-regulating protein-serine kinase 2	861	5695	561	Priority
RIPK2 (RICK; RIP2; CARD3)	S176	Receptor-interacting serine/threonine-protein kinase 2 (RIPK2)	3501	20283	479	Priority
TTK	T676	Dual specificity protein kinase TTK	561	3094	451	Priority
HePTP (PTPN7)	S44	Tyrosine-protein phosphatase non-receptor type 7	729	4009	450	Priority
PP1/Cb (PPP1CB)	T316	Serine/threonine-protein phosphatase PP1-beta catalytic subunit	2106	10875	416	Priority
mTOR (FRAP)	S2478+S2481	Mammalian target of rapamycin (FRAP); FKBP12-rapamycin complex-associated protein	399	1757	340	Priority
Pim2	T195	Serine/threonine-protein kinase Pim-2	2129	8764	312	Priority
TAK1 (MAP3K7)	T184+T187	TGF-beta-activated protein-serine kinase 1; Mitogen-activated protein kinase kinase kinase 7	733	2724	272	Priority

MPL	Y591	Thrombopoietin receptor	1317	4864	269	Priority
PKD2 (PRKD2)	S197+S198	Serine/threonine-protein kinase D2	2428	8686	258	Priority
PKD3 (PRKCN)	Pan-specific	Protein-serine kinase C nu; Serine/threonine-protein kinase D3	538	1746	225	Priority
MELK	Y438	Maternal embryonic leucine zipper kinase	508	1595	214	Priority
TBC1D7	Y14	TBC1 domain family member 7	499	1541	209	Priority
AurKC (Aurora C, AIK3)	Pan-specific	Aurora Kinase C (serine/threonine-protein kinase 13)	567	1732	205	Priority
RIOK1	Y466	Serine/threonine-protein kinase RIO1	1206	3527	192	Priority
AAK1	S637	AP2-associated protein kinase 1	5683	16337	187	Priority
RSK1 (RPS6KA1, p90RSK)	Pan-specific	Ribosomal S6 protein-serine kinase 1; Ribosomal protein S6 kinase alpha 2	701	1913	173	Priority
RIOK2	S332+S335+S337	Serine/threonine-protein kinase RIO2	3367	8853	163	Priority
MSK2 (RPS6KA4)	T687	Ribosomal protein S6 kinase alpha-4	4964	12958	161	Priority
p38a MAPK (MAPK14)	T180+Y182	Mitogen-activated protein-serine kinase p38 alpha; Mitogen-activated protein kinase 14	5219	12787	145	Priority
MST1 (STK4, Krs2)	T187	Mammalian STE20-like protein-serine kinase 1 (KRS2); Serine-threonine-protein kinase 4	926	2254	143	Priority
MST3 (STK24)	T184	Mammalian STE20-like protein-serine kinase 3; Serine-threonine-protein kinase 24	2079	4894	135	Priority
p38b MAPK (MAPK11)	T180+Y182	Mitogen-activated protein-serine kinase p38 beta; Mitogen-activated protein kinase 11	5425	12466	130	Priority
Met	Y1234	Hepatocyte growth factor (HGF) receptor-tyrosine kinase	4427	10046	127	Priority

FAK (PTK2)	Y397	Focal adhesion protein-tyrosine kinase	3460	7788	125	Priority
Nek7	T191+S195	NIMA (never-in-mitosis)-related protein-serine kinase 7	2552	5530	117	Priority
ErbB2 (HER2, Neu)	Y877	ErbB2 (Neu) receptor-tyrosine kinase	1441	3121	117	Priority
Fgr	Pan-specific	Gardner-Rasheed feline sarcoma viral (v-fgr) oncogene	4823	9945	106	Priority
BRSK1	T189	BR serine/threonine-protein kinase 1	21015	42125	100	Priority
Bmx (Etk)	Y40	Bone marrow X protein-tyrosine kinase	850	1669	96	Priority
CDKL5 (STK9)	Y171	Cyclin-dependent kinase-like 5; Serine-threonine-protein kinase 9	7007	13300	90	Priority
NDR1 (NDR, STK38)	S281+T282	Serine/threonine-protein kinase 38	7340	13894	89	Priority
MKK3 (MAP2K3, MEK3)	S218	MAPK/ERK protein-serine kinase 3 beta isoform (MKK3 beta); Dual specificity mitogen-activated protein kinase kinase 3	23383	43796	87	Priority
FOXO1A (FKHR)	S256	Forkhead box protein O1	3148	5840	86	Priority
PKCa (PRKCA)	Y195	Protein-serine kinase C alpha	1028	1885	83	Priority
NFAT5	T135	Nuclear factor of activated T-cells 5	6169	10954	78	Priority
Akt1 (PKBa)	Y326	RAC-alpha serine/threonine-protein kinase	269	1250	364	Possible
Btk	Y223+Y225	Bruton's agammaglobulinemia tyrosine kinase	192	765	298	Possible
NFkB p50 (NFKB1)	S337	Nuclear factor NF-kappa-B p105 subunit	192	762	296	Possible
STAT4	S721	Signal transducer and activator of transcription 4	289	1094	278	Possible
MEK1 (MKK1, MAP2K1)	S222	MAPK/ERK protein-serine kinase 1 (MKK1); Dual specificity mitogen-activated protein kinase kinase 1	321	1017	216	Possible
p38a MAPK	Pan-specific	Mitogen-activated protein-serine kinase p38 alpha;	241	749	211	Possible

(MAPK14)		Mitogen-activated protein kinase 14				
BCKD (BCKDK)	Pan-specific	[3-methyl-2-oxobutanoate dehydrogenase [lipoamide]] kinase, mitochondrial	300	920	207	Possible
ERK3 (MAPK6)	Pan-specific	Extracellular regulated protein-serine kinase 3	460	1221	165	Possible
GOLGA2 (GM130)	S25	Golgin subfamily A member 2	367	971	165	Possible
Abl2 (Arg)	Y439	Abelson murine leukemia viral oncogene homologue 2	462	1133	145	Possible
ATR	Pan-specific	Ataxia telangiectasia and Rad3 related protein-serine kinase	455	1050	131	Possible
TAO1 (TAOK1)	S181	Serine/threonine-protein kinase TAO1	365	823	125	Possible
Plk1 (PLK)	T210	Polo-like protein-serine kinase 1	1007	2236	122	Possible
MEK1 (MKK1, MAP2K1)	T286	MAPK/ERK protein-serine kinase 1 (MKK1); Dual specificity mitogen-activated protein kinase kinase 1	526	1126	114	Possible
Raf1 (RafC)	S296	Raf1 proto-oncogene-encoded protein-serine kinase	3787	8055	113	Possible
Bcr	Pan-specific	Breakpoint cluster region protein	373	770	107	Possible
SLK	S189	STE20-like serine/threonine-protein kinase; CTCL tumour antigen se20-9	631	1286	104	Possible
Rb1	S249+T252	Retinoblastoma-associated protein 1	407	827	103	Possible
GRK2 (BARK1, ADRBK1)	S670	Beta-adrenergic receptor kinase 1	1296	2245	73	Possible
mTOR (FRAP)	Pan-specific	Mammalian target of rapamycin (FRAP); FKBP12-rapamycin complex-associated protein	11143	19239	73	Possible
Rb1	T826	Retinoblastoma-associated protein 1	1264	2170	72	Possible
PAK1 (PAKa)	Pan-specific	p21-activated kinase 1 (alpha) (Protein-serine/threonine kinase PAK 1)	2786	4782	72	Possible
HIPK1	Y352	Homeodomain-interacting protein-serine kinase 1	4848	8286	71	Possible

PFTAIRE2 (ALS2CR7, CDK15)	Pan-specific	Amyotrophic lateral sclerosis 2 chromosomal region candidate gene 7 protein	1197	2035	70	Possible
NFKB p65 (Rel A)	Pan-specific	NF-kappa-B p65 nuclear transcription factor	955	1619	70	Possible
RSK2 (RPS6KA3)	T577	Ribosomal S6 protein-serine kinase 2; Ribosomal protein S6 kinase alpha-3	799	1341	68	Possible
p53 (TP53)	Pan-specific	Cellular tumor antigen p53	2880	4772	66	Possible
Raf1 (RafC)	S301+T303	Raf1 proto-oncogene-encoded protein-serine kinase	775	1274	64	Possible
ANXA2	Y238	Annexin A2	5030	8231	64	Possible
ULK1	Pan-specific	Unc-51-like kinase 1; Serine-threonine-protein kinase ULK1	466	762	63	Possible
PIK3R2	Y464	Phosphatidylinositol 3-kinase regulatory subunit beta	2688	4316	61	Possible
Raf1 (RafC)	S259	Raf1 proto-oncogene-encoded protein-serine kinase	3456	5512	59	Possible
Tyro3	Y685+Y686	Tyrosine-protein kinase receptor TYRO3	1851	2951	59	Possible
CTNNB1	Y489	Catenin (cadherin-associated protein) beta 1	14391	22502	56	Possible
CLK1	S337	Dual specificity protein kinase CLK1	1786	2791	56	Possible
CaMK2a	Pan-specific	Calcium/calmodulin-dependent protein kinase type II subunit alpha	3192	4957	55	Possible
IGF1R	Y1161+T1163	Insulin-like growth factor 1 receptor protein-tyrosine kinase	1844	2814	53	Possible
Plk1 (PLK)	Y217	Polo-like protein-serine kinase 1	3743	5672	52	Possible
CDK5	Y15	Cyclin-dependent protein-serine kinase 5	5122	7761	52	Possible
Abl2 (Arg)	Pan-specific	Abelson murine leukemia viral oncogene homologue 2	5641	8509	51	Possible
Chk1 (CHEK1)	Pan-specific	Checkpoint protein-serine kinase 1	1047	1550	48	Possible
GR(NR3C1)	S226	Glucocorticoid receptor	7219	10664	48	Possible

RPS6	S235+S236+S240	40S Ribosomal S6	3516	5172	47	Possible
SHIP2 (INPPL1)	Y886	Phosphatidylinositol-3,4,5-trisphosphate phosphatase 2	19347	28267	46	Possible

Table 5.4: Top signalling pathways which were up regulated by SIPA1 knockdown on A549 cells. Generated from: www.reactome.org.

Pathway name	Entities				Reactions	
	found	ratio	p-value	FDR*	found	ratio
MyD88:MAL(TIRAP) cascade initiated on plasma membrane	13 / 111	0.008	7.25e-11	5.41e-09	45 / 64	0.005
Toll Like Receptor TLR6:TLR2 Cascade	13 / 111	0.008	7.25e-11	5.41e-09	45 / 66	0.005
MAP kinase activation	11 / 69	0.005	9.09e-11	5.41e-09	24 / 32	0.003
Toll Like Receptor TLR1:TLR2 Cascade	13 / 114	0.008	1.00e-10	5.41e-09	45 / 66	0.005
Toll Like Receptor 2 (TLR2) Cascade	13 / 114	0.008	1.00e-10	5.41e-09	45 / 68	0.005
MyD88 cascade initiated on plasma membrane	12 / 94	0.007	1.53e-10	6.56e-09	30 / 58	0.005
Toll Like Receptor 5 (TLR5) Cascade	12 / 94	0.007	1.53e-10	6.56e-09	30 / 59	0.005
Toll Like Receptor 10 (TLR10) Cascade	12 / 94	0.007	1.53e-10	6.56e-09	30 / 59	0.005
Interleukin-17 signaling	11 / 77	0.005	2.85e-10	1.17e-08	24 / 35	0.003
Signaling by Interleukins	26 / 639	0.044	3.60e-10	1.30e-08	125 / 490	0.039
TRAF6 mediated induction of NFkB and MAP kinases upon TLR7/8 or 9 activation	12 / 102	0.007	3.81e-10	1.30e-08	30 / 48	0.004
Toll Like Receptor 3 (TLR3) Cascade	12 / 102	0.007	3.81e-10	1.30e-08	31 / 61	0.005
MyD88 dependent cascade initiated on endosome	12 / 103	0.007	4.25e-10	1.32e-08	30 / 63	0.005
Toll Like Receptor 7/8 (TLR7/8) Cascade	12 / 103	0.007	4.25e-10	1.32e-08	30 / 64	0.005
Signaling by Receptor Tyrosine Kinases	24 / 554	0.038	5.54e-10	1.61e-08	174 / 657	0.053
TRIF(TICAM1)-mediated TLR4 signaling	12 / 107	0.007	6.51e-10	1.76e-08	31 / 58	0.005
MyD88-independent TLR4 cascade	12 / 107	0.007	6.51e-10	1.76e-08	31 / 60	0.005
Toll Like Receptor 9 (TLR9) Cascade	12 / 107	0.007	6.51e-10	1.76e-08	30 / 67	0.005
Generic Transcription Pathway	41 / 1,553	0.108	7.51e-10	1.95e-08	279 / 824	0.066
Toll Like Receptor 4 (TLR4) Cascade	13 / 144	0.01	1.64e-09	4.10e-08	48 / 95	0.008
RNA Polymerase II Transcription	42 / 1,692	0.117	2.77e-09	6.64e-08	281 / 885	0.071
Gene expression (Transcription)	43 / 1,850	0.128	1.20e-08	2.88e-07	293 / 996	0.08
Nuclear Receptor transcription pathway	10 / 86	0.006	1.30e-08	2.99e-07	2 / 2	1.60e-04
Toll-like Receptor Cascades	13 / 184	0.013	2.89e-08	6.35e-07	53 / 182	0.015
VEGFA-VEGFR2 Pathway	11 / 126	0.009	4.33e-08	9.54e-07	37 / 77	0.006

* False Discovery Rate

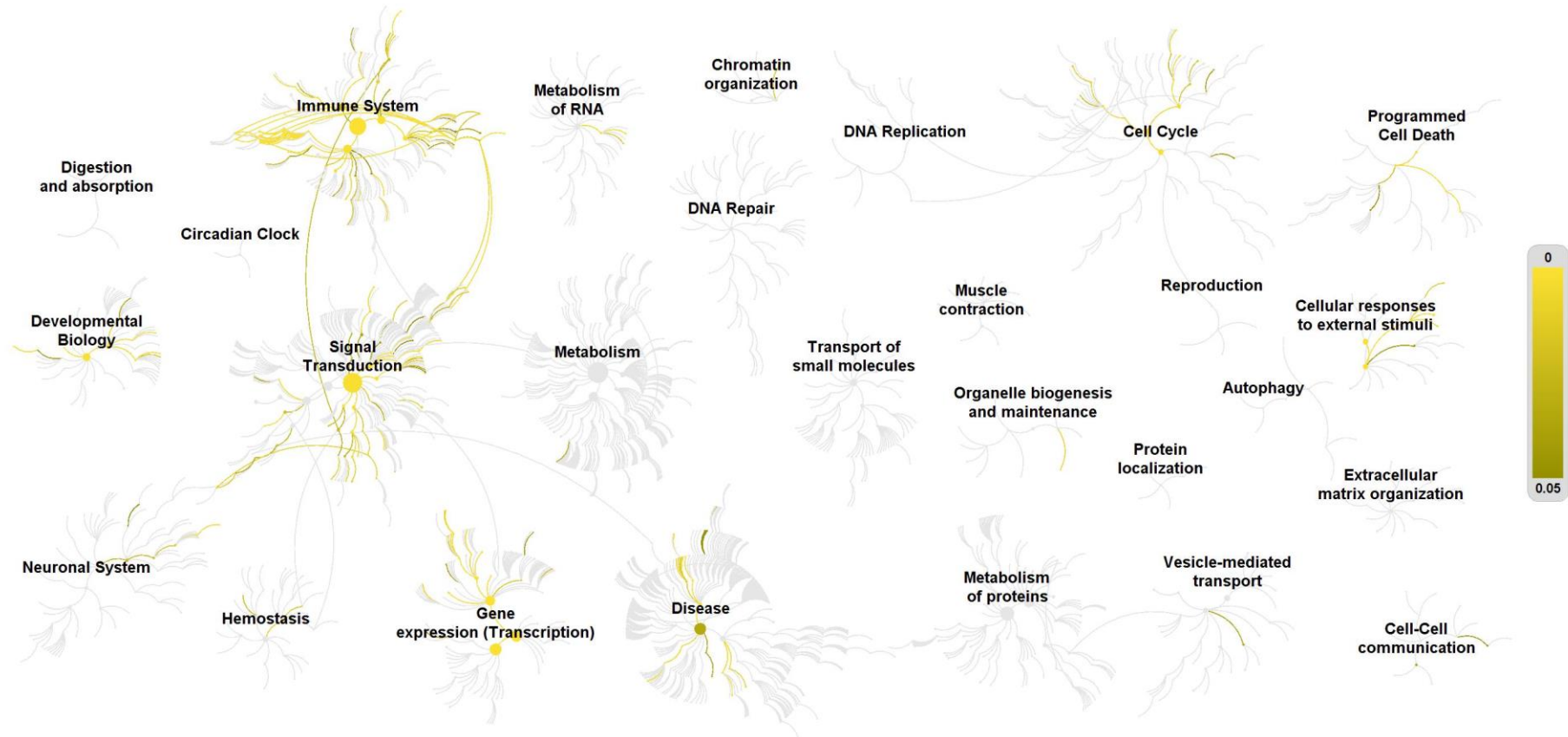


Figure 5.6: Genome-wide overview of the signalling pathway which were upregulated by SIPA1 knockdown on A549 cells. Pathways are arranged in a hierarchy. The centre of each of the circular represents the root of the top-level pathway. Each step away from the centre represents the next level lower in the pathway hierarchy. The light-yellow colour denotes over-representation of that pathway. Light grey signifies pathways which are not significantly over-represented. Generated from: www.reactome.org.

Besides the analysis of SIPA1 knockdown in A549 cells, we compared the phosphorylation status after the treatment of HGF on A549 pEF control cells. **Table 5.5** shows the markers whose phosphorylation status were most decreased after HGF treatment in the A549 pEF control cells, indicating the downstream markers of HGF/MET signalling. The website *Reacome* (www.reactome.org) was used to conduct the key pathway analysis report. The most downregulated markers after HGF treatment could be integrated to numbers of centralized signalling pathways, in which the top 25 signalling pathways are listed in **Table 5.6**. Also, the genome-wide overview schematic diagram of the signalling pathways was generated (**Figure 5.7**) to show the overall review of the main area in which the pathways downregulated by SIPA1 are located.

Table 5.5: Key markers whose phosphor-status were down regulated in A549 pEF control cells with treatment of HGF.

Target Name	P-Site	Full Target Protein Name	Average Normalized Net Signal		%CFC	Lead
			Control	Control+HGF		
SRF	S224	Serum response factor	11435	1214	-89	Priority
ITK	Pan-specific	Tyrosine-protein kinase ITK/TSK	4223	471	-89	Priority
STAT5A	Y694	Signal transducer and activator of transcription 5A	2786	217	-92	Possible
InsR (IR)	Pan-specific	Insulin receptor	1131	318	-72	Possible
TARDBP	S409+S410	TAR DNA-binding protein 43	4900	1470	-70	Possible
GCK (MAP4K2)	Pan-specific	Germinal centre protein-serine kinase	750	228	-70	Possible
HDAC5	S498	Histone deacetylase 5	1727	533	-69	Possible
Vav	Y174	Vav 1 guanine nucleotide exchange factor	1659	514	-69	Possible
ACTB	Y53	Actin, cytoplasmic 1; Beta-actin	1099	344	-69	Possible
PCK2 (PCTAIRE2, CDK17)	Pan-specific	Cell division protein kinase 17; Protein-serine kinase PCTAIRE-2	1844	659	-64	Possible
CRYAB	S19	Crystallin aB	1307	508	-61	Possible
AAK1	S637	AP2-associated protein kinase 1	5683	2342	-59	Possible
RPS6	S235+S236	40S Ribosomal S6	3861	1693	-56	Possible
Lyn	Pan-specific	Yes-related protein-tyrosine kinase; Tyrosine-protein kinase Lyn	973	467	-52	Possible
p70S6K (S6Ka, RPS6KB1)	Pan-specific	Ribosomal protein S6 kinase beta-1; Ribosomal protein S6 kinase 1	3889	1882	-52	Possible
Fyn	Y213+Y214	Fyn proto-oncogene-encoded protein-tyrosine kinase	1065	520	-51	Possible

CDKL1	Pan-specific	Cyclin-dependent kinase-like 1; Serine/threonine protein kinase KKIALRE	3147	1538	-51	Possible
Fyn	Pan-specific	Fyn proto-oncogene-encoded protein-tyrosine kinase	903	447	-50	Possible
ASK1 (MAP3K5)	Pan-specific	Apoptosis signal regulating protein-serine kinase 1	2259	1186	-47	Possible
MEF2A	T108	Myocyte-specific enhancer factor 2A	254	47	-82	
p38b MAPK (MAPK11)	T180+Y182	Mitogen-activated protein-serine kinase p38 beta; Mitogen-activated protein kinase 11	5425	1807	-67	
ANXA2	Y238	Annexin A2	5030	1900	-62	
GATA3	S369	Trans-acting T-cell-specific transcription factor GATA-3	1420	659	-54	
PAK1 (PAKa)	Pan-specific	p21-activated kinase 1 (alpha) (Protein-serine/threonine kinase PAK 1)	2786	1299	-53	
MEK1 (MKK1, MAP2K1)	T286	MAPK/ERK protein-serine kinase 1 (MKK1); Dual specificity mitogen-activated protein kinase kinase 1	526	260	-51	
PIK3 (CNK)	Pan-specific	Polo-like protein-serine kinase 3 (cytokine-inducible kinase (CNK))	417	212	-49	
MEK1 (MKK1, MAP2K1)	S222	MAPK/ERK protein-serine kinase 1 (MKK1); Dual specificity mitogen-activated protein kinase kinase 1	321	166	-48	
Raf1 (RafC)	S301+T303	Raf1 proto-oncogene-encoded protein-serine kinase	775	412	-47	
PIK3R2	Y464	Phosphatidylinositol 3-kinase regulatory subunit	2688	1486	-45	

		beta				
IGF1R	Y1161+T1163	Insulin-like growth factor 1 receptor protein-tyrosine kinase	1844	1058	-43	
CDK5	Y15	Cyclin-dependent protein-serine kinase 5	5122	3045	-41	
Abl2 (Arg)	Y439	Abelson murine leukemia viral oncogene homologue 2	462	276	-40	
BRSK1	T189	BR serine/threonine-protein kinase 1	21015	13148	-37	
p38a MAPK (MAPK14)	Pan-specific	Mitogen-activated protein-serine kinase p38 alpha; Mitogen-activated protein kinase 14	241	151	-37	
PFTAIRE2 (ALS2CR7)	Pan-specific	Amyotrophic lateral sclerosis 2 chromosomal region candidate gene 7 protein	1197	761	-36	
PKCa (PRKCA)	Y195	Protein-serine kinase C alpha	1028	666	-35	
ErbB2 (HER2, Neu)	Y877	ErbB2 (Neu) receptor-tyrosine kinase	1441	951	-34	
Plk1 (PLK)	T210	Polo-like protein-serine kinase 1	1007	676	-33	
RSK2 (RPS6KA3)	T577	Ribosomal S6 protein-serine kinase 2; Ribosomal protein S6 kinase alpha-3	799	546	-32	
Chk1 (CHEK1)	Pan-specific	Checkpoint protein-serine kinase 1	1047	722	-31	
ULK1	Pan-specific	Unc-51-like kinase 1; Serine-threonine-protein kinase ULK1	466	329	-29	
MSK2 (RPS6KA4)	T687	Ribosomal protein S6 kinase alpha-4	4964	3539	-29	
DYRK2	Y382	Dual specificity tyrosine-phosphorylation-regulated kinase 2	2816	2026	-28	
GRK2 (BARK1,	S670	Beta-adrenergic receptor kinase 1	1296	957	-26	

ADRBK1)						
CLK1	S337	Dual specificity protein kinase CLK1	1786	1336	-25	
Abl2 (Arg)	Pan-specific	Abelson murine leukemia viral oncogene homologue 2	5641	4301	-24	
Bmx (Etk)	Y40	Bone marrow X protein-tyrosine kinase	850	650	-23	
RSK1 (RPS6KA1, p90RSK)	Pan-specific	Ribosomal S6 protein-serine kinase 1; Ribosomal protein S6 kinase alpha 2	701	540	-23	
CDKL5 (STK9)	Y171	Cyclin-dependent kinase-like 5; Serine-threonine-protein kinase 9	7007	5451	-22	
SLK	S189	STE20-like serine/threonine-protein kinase; CTCL tumour antigen se20-9	631	500	-21	
Raf1 (RafC)	S259	Raf1 proto-oncogene-encoded protein-serine kinase	3456	2784	-19	
Rb	T821	Retinoblastoma-associated protein 1	902	777	-14	
ERK3 (MAPK6)	Pan-specific	Extracellular regulated protein-serine kinase 3	460	402	-13	
WNK2	Pan-specific	Serine/threonine-protein kinase WNK2	1215	1069	-12	
TAO1 (TAOK1)	S181	Serine/threonine-protein kinase TAO1	365	334	-8	
MST1 (STK4, Krs2)	T187	Mammalian STE20-like protein-serine kinase 1 (KRS2); Serine-threonine-protein kinase 4	926	858	-7	
GR	S226	Glucocorticoid receptor	7219	6801	-6	
NFAT5	T135	Nuclear factor of activated T-cells 5	6169	5913	-4	
HIPK1	Y352	Homeodomain-interacting protein-serine kinase 1	4848	4689	-3	
yro3	Y685+Y686	Tyrosine-protein kinase receptor TYRO3	1851	1798	-3	

Table 5.6: Top signalling pathways which were downregulated by treatment with HGF on A549 pEF control cells. Generated from: www.reactome.org.

Pathway name	Entities				Reactions	
	found	ratio	p-value	FDR*	found	ratio
Signaling by Receptor Tyrosine Kinases	21 / 554	0.038	1.92e-11	1.36e-08	142 / 657	0.053
Signaling by SCF-KIT	7 / 51	0.004	3.68e-08	1.30e-05	24 / 36	0.003
Signaling by NTRKs	9 / 118	0.008	5.76e-08	1.35e-05	22 / 127	0.01
Axon guidance	17 / 584	0.04	9.71e-08	1.71e-05	85 / 297	0.024
Developmental Biology	24 / 1,207	0.084	1.97e-07	2.78e-05	137 / 511	0.041
ERK/MAPK targets	5 / 26	0.002	6.94e-07	3.05e-05	3 / 7	5.61e-04
Nuclear Events (kinase and transcription factor activation)	5 / 29	0.002	1.18e-06	4.84e-05	4 / 11	8.81e-04
VEGFA-VEGFR2 Pathway	8 / 126	0.009	1.27e-06	4.96e-05	25 / 77	0.006
Signaling by Interleukins	16 / 639	0.044	1.75e-06	6.46e-05	50 / 490	0.039
Signaling by NTRK1 (TRKA)	7 / 93	0.006	2.00e-06	6.46e-05	12 / 65	0.005
Signaling by VEGF	8 / 135	0.009	2.11e-06	6.46e-05	25 / 83	0.007
Regulation of TP53 Activity through Phosphorylation	7 / 95	0.007	2.30e-06	6.46e-05	8 / 26	0.002
MAPK targets/ Nuclear events mediated by MAP kinases	5 / 35	0.002	2.94e-06	6.46e-05	5 / 16	0.001
MAP kinase activation	6 / 69	0.005	4.94e-06	7.90e-05	9 / 32	0.003
CD28 co-stimulation	5 / 39	0.003	4.95e-06	7.92e-05	10 / 19	0.002
Interleukin-17 signaling	6 / 77	0.005	9.17e-06	1.47e-04	9 / 35	0.003
Interleukin-3, Interleukin-5 and GM-CSF signaling	5 / 50	0.003	1.63e-05	2.44e-04	12 / 38	0.003
Regulation of signaling by CBL	4 / 24	0.002	1.67e-05	2.50e-04	4 / 7	5.61e-04
Signaling by Rho GTPases	12 / 457	0.032	2.50e-05	3.63e-04	52 / 117	0.009
MyD88 cascade initiated on plasma membrane	6 / 94	0.007	2.79e-05	3.63e-04	9 / 58	0.005
Toll Like Receptor 10 (TLR10) Cascade	6 / 94	0.007	2.79e-05	3.63e-04	9 / 59	0.005
Toll Like Receptor 5 (TLR5) Cascade	6 / 94	0.007	2.79e-05	3.63e-04	9 / 59	0.005
RHO GTPase Effectors	10 / 326	0.023	3.45e-05	4.49e-04	50 / 112	0.009
CD209 (DC-SIGN) signaling	4 / 30	0.002	3.96e-05	5.09e-04	3 / 11	8.81e-04
TRAF6 mediated induction of NFkB and MAP kinases upon TLR7/8 or 9 activation	6 / 102	0.007	4.38e-05	5.09e-04	9 / 48	0.004

* False Discovery Rate

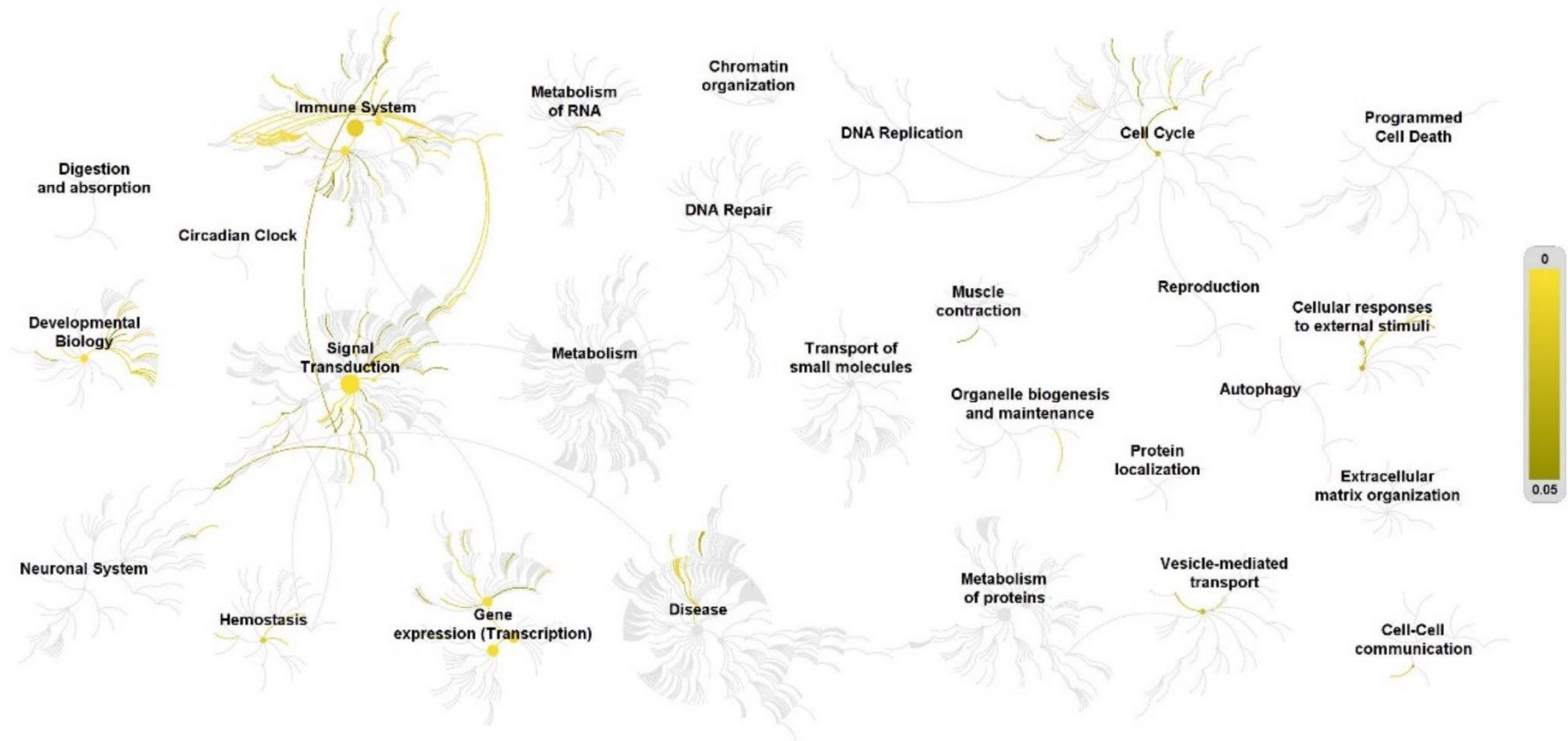


Figure 5.7: Genome-wide overview of the signalling pathway which were downregulated by treatment with HGF on A549 pEF control cells. Pathways are arranged in a hierarchy. The centre of each of the circular represents the root of the top-level pathway. Each step away from the centre represents the next level lower in the pathway hierarchy. The light-yellow colour denotes over-representation of that pathway. Light grey signifies pathways which are not significantly over-represented. Generated from: www.reactome.org.

We also compared the phosphorylation status after the treatment of HGF on A549 pEF control cells. **Table 5.7** shows the markers whose phosphorylation status were most increased after HGF treatment in the A549 pEF control cells, indicating the downstream markers of HGF/MET signalling. The website *Reacome* (www.reactome.org) was used to conduct the key pathway analysis report. The most upregulated markers after HGF treatment could be integrated to numbers of centralized signalling pathways, in which the top 25 signalling pathways are listed in **Table 5.8**. Also, the genome-wide overview schematic diagram of the signalling pathways was generated (**Figure 5.8**) to show the overall review of the main area in which the pathways upregulated by SIPA1 are located.

Table 5.7: Key markers whose phosphor-status were upregulated in A549 pEF control cells with treatment of HGF.

Target Name	P-Site	Full Target Protein Name	Average Normalized Net Signal		%CF C	Lead
			Control	Control+HGF		
NMDAR1	S896	Glutamate [NMDA] receptor subunit zeta-1	151	1918	1168	Priority
PIk1 (PLK)	Pan-specific	Polo-like protein-serine kinase 1	756	6631	777	Priority
FAK (PTK2)	Y576+Y577	Focal adhesion protein-tyrosine kinase	404	1846	357	Priority
PP1/Cb (PPP1CB)	T316	Serine/threonine-protein phosphatase PP1-beta catalytic subunit	2106	9557	354	Priority
ERK1 (MAPK3)	Y204+T207	Extracellular regulated protein-serine kinase 1 (p44 MAP kinase)	767	3355	338	Priority
RIPK2 (RICK; RIP2; CARD3)	S176	Receptor-interacting serine/threonine-protein kinase 2 (RIPK2)	3501	12641	261	Priority
ACTB	Pan-specific	Actin, cytoplasmic 1; Beta-actin	828	2912	252	Priority
Cbl	Y700	E3 ubiquitin-protein ligase CBL	458	1565	242	Priority
RIOK1	Y466	Serine/threonine-protein kinase RIO1	1206	3247	169	Priority
HePTP (PTPN7)	S44	Tyrosine-protein phosphatase non-receptor type 7	729	1870	157	Priority
CK2a1 (CSNK2A1)	T360+S362	Casein protein-serine kinase 2 alpha/ alpha prime	893	2248	152	Priority
EGFR (ErbB1)	Pan-specific	Epidermal growth factor receptor-tyrosine kinase	8596	19023	121	Priority
PKD2 (PRKD2)	S197+S198	Serine/threonine-protein kinase D2	2428	5322	119	Priority
STAT5	Y694	Signal transducer and activator of transcription 5	1745	3799	118	Priority

Akt1 (PKBa)	S473	RAC-alpha serine/threonine-protein kinase	1781	3851	116	Priority
IkBa	Pan-specific	Inhibitor of NF-kappa-B alpha (MAD3)	1324	2670	102	Priority
DLK (ZPK)	S269	Mitogen-activated protein kinase kinase kinase 12	3777	7431	97	Priority
Fgr	Pan-specific	Gardner-Rasheed feline sarcoma viral (v-fgr) oncogene	4823	8878	84	Priority
Met	T1241	Hepatocyte growth factor (HGF) receptor-tyrosine kinase	5492	9699	77	Priority
Myc	S373	Myc proto-oncogene protein	94	1092	1062	Possible
BRCA1	S1423	Breast cancer type 1 susceptibility protein	110	922	739	Possible
CDK1 (CDC2)	T161	Cyclin-dependent protein-serine kinase 1; Cell division control protein 2 homologue	445	1403	215	Possible
Jun (c-Jun)	Y170	Jun proto-oncogene-encoded AP1 transcription factor	472	1042	121	Possible
mTOR (FRAP)	S2478+S2481	Mammalian target of rapamycin (FRAP); FKBP12-rapamycin complex-associated protein	399	799	100	Possible
MLK1 (MAP3K9)	Pan-specific	Mixed-lineage protein-serine kinase 1; Mitogen-activated protein kinase kinase kinase 9	377	754	100	Possible
PKD1 (PRKCM, PKCm, PRKD1)	S910	Protein-serine kinase C mu (Protein kinase D)	619	1229	98	Possible
Met	Y1230	Hepatocyte growth factor (HGF) receptor-tyrosine kinase	6448	10846	68	Possible
IGF1R	Y1280	Insulin-like growth factor 1 receptor protein-tyrosine kinase	1722	2877	67	Possible

AR	S310	Androgen receptor	8398	14030	67	Possible
WNK1	Pan-specific	Serine/threonine-protein kinase WNK1	4291	7166	67	Possible
CTNNB1	Y489	Catenin (cadherin-associated protein) beta 1	14391	23704	65	Possible
MAT1A	T341	S-adenosylmethionine synthase isoform type-1	10216	16693	63	Possible
Caveolin 2 (CAV2)	Pan-specific	Caveolin 2	761	1228	61	Possible
Chk1 (CHEK1)	S280	Checkpoint protein-serine kinase 1	10372	16632	60	Possible
Ksr2	S490	Kinase suppressor of Ras 2	6444	10325	60	Possible
MARK1	T215	MAP/microtubule affinity-regulating protein-serine kinase 1	13737	21972	60	Possible
JNK1 (MAPK8)	Y185	Jun N-terminus protein-serine kinase (stress-activated protein kinase (SAPK)) 1	5151	8200	59	Possible
MELK	Y438	Maternal embryonic leucine zipper kinase	508	800	58	Possible
RPS6	S235+S236+S240	40S Ribosomal S6	3516	5513	57	Possible
MKK3 (MAP2K3, MEK3)	S218	MAPK/ERK protein-serine kinase 3 beta isoform (MKK3 beta); Dual specificity mitogen-activated protein kinase kinase 3	23383	36429	56	Possible
MYPT1 (MBS)	T696	Protein phosphatase 1 regulatory subunit 12A	963	1480	54	Possible
ENO2	Y25	Gamma-enolase	5672	8715	54	Possible
mTOR (FRAP)	Pan-specific	Mammalian target of rapamycin (FRAP); FKBP12-rapamycin complex-associated protein	6718	10267	53	Possible
EIF2AK3 (PERK)	T982	Eukaryotic translation initiation factor 2-alpha kinase 3	10245	15647	53	Possible
JNK1 (MAPK8)	Pan-specific	Jun N-terminus protein-serine kinase 2 (Stress-	656	998	52	Possible

		activated protein kinase-alpha)				
CK1 epsilon (CSNK1E)	Pan-specific	Casein protein-serine kinase 1 epsilon	3392	5122	51	Possible
HSP90AB1 (HSP90; HSP84; HSP90B; HSPC2; HSPCB)	Pan-specific	Heat shock 90 kDa protein beta	1056	1572	49	Possible
Jun (c-Jun)	T91	Jun proto-oncogene-encoded AP1 transcription factor	937	1386	48	Possible
Yes	Y222+Y223	Yamaguchi sarcoma proto-oncogene-encoded tyrosine kinase	10235	15101	48	Possible
MKK6 (MAP2K6, MEK6)	Pan-specific	MAPK/ERK protein-serine kinase 6 (MKK6); Dual specificity mitogen-activated protein kinase kinase 6	3719	5474	47	Possible
STAG2	Y433	Putative uncharacterized protein DKFZp781H1753	5391	7798	45	Possible

Table 5.8: Top signalling pathways which were upregulated by treatment with HGF on A549 pEF control cells. Generated from: www.reactome.org

Pathway name	Entities				Reactions	
	found	ratio	p-value	FDR*	found	ratio
ESR-mediated signaling	12 / 256	0.018	2.54e-08	1.86e-05	28 / 110	0.009
Signal Transduction	41 / 3,305	0.229	7.86e-08	1.86e-05	438 / 2,303	0.184
Cytokine Signaling in Immune system	24 / 1,261	0.087	8.13e-08	1.86e-05	94 / 699	0.056
Signaling by Interleukins	17 / 639	0.044	9.87e-08	1.86e-05	66 / 490	0.039
MAPK family signaling cascades	12 / 348	0.024	6.67e-07	7.04e-05	27 / 86	0.007
Diseases of signal transduction	14 / 496	0.034	7.77e-07	7.04e-05	101 / 322	0.026
MyD88 cascade initiated on plasma membrane	7 / 94	0.007	1.23e-06	7.04e-05	19 / 58	0.005
Toll Like Receptor 10 (TLR10) Cascade	7 / 94	0.007	1.23e-06	7.04e-05	19 / 59	0.005
Toll Like Receptor 5 (TLR5) Cascade	7 / 94	0.007	1.23e-06	7.04e-05	19 / 59	0.005
Cell Cycle	16 / 683	0.047	1.33e-06	7.04e-05	132 / 414	0.033
Signaling by Nuclear Receptors	12 / 385	0.027	1.90e-06	7.04e-05	28 / 191	0.015
TRAF6 mediated induction of NFkB and MAP kinases upon TLR7/8 or 9 activation	7 / 102	0.007	2.11e-06	7.04e-05	19 / 48	0.004
Toll Like Receptor 3 (TLR3) Cascade	7 / 102	0.007	2.11e-06	7.04e-05	19 / 61	0.005
MyD88 dependent cascade initiated on endosome	7 / 103	0.007	2.24e-06	7.04e-05	19 / 63	0.005
Toll Like Receptor 7/8 (TLR7/8) Cascade	7 / 103	0.007	2.24e-06	7.04e-05	19 / 64	0.005
Signaling by Receptor Tyrosine Kinases	14 / 554	0.038	2.82e-06	7.04e-05	202 / 657	0.053
TRIF(TICAM1)-mediated TLR4 signaling	7 / 107	0.007	2.88e-06	7.04e-05	19 / 58	0.005
MyD88-independent TLR4 cascade	7 / 107	0.007	2.88e-06	7.04e-05	19 / 60	0.005
Toll Like Receptor 9 (TLR9) Cascade	7 / 107	0.007	2.88e-06	7.04e-05	19 / 67	0.005
MAP kinase activation	6 / 69	0.005	3.06e-06	7.04e-05	16 / 32	0.003
MyD88:MAL(TIRAP) cascade initiated on plasma membrane	7 / 111	0.008	3.65e-06	7.67e-05	19 / 64	0.005
Toll Like Receptor TLR6:TLR2 Cascade	7 / 111	0.008	3.65e-06	7.67e-05	19 / 66	0.005
Cell Cycle, Mitotic	14 / 571	0.04	3.98e-06	7.96e-05	112 / 326	0.026
Toll Like Receptor TLR1:TLR2 Cascade	7 / 114	0.008	4.34e-06	8.25e-05	19 / 66	0.005
Toll Like Receptor 2 (TLR2) Cascade	7 / 114	0.008	4.34e-06	8.25e-05	19 / 68	0.005

* False Discovery Rate

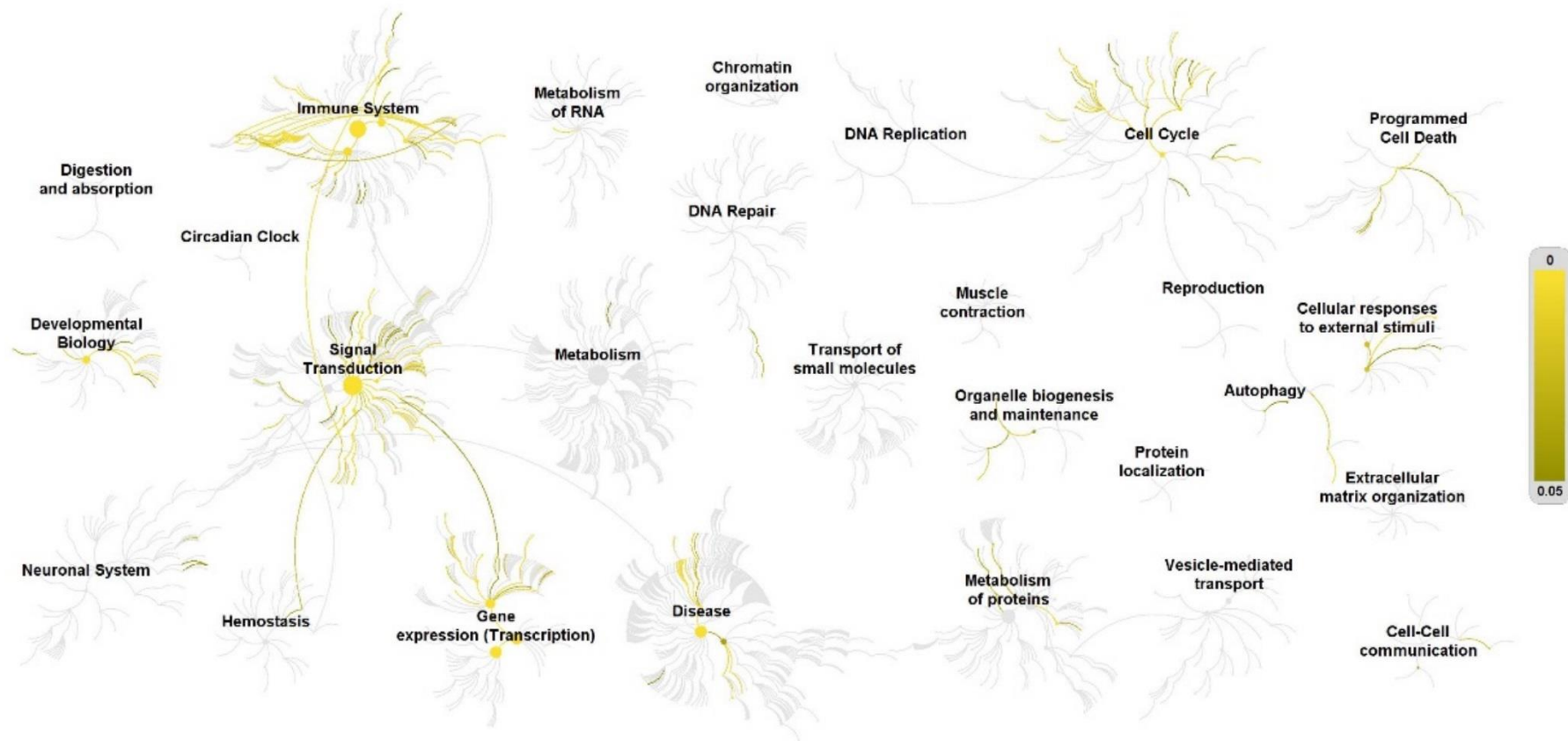


Figure 5.8: Genome-wide overview of the signalling pathway which were upregulated by treatment with HGF on A549 pEF control cells. Pathways are arranged in a hierarchy. The centre of each of the circular represents the root of the top-level pathway. Each step away from the centre represents the next level lower in the pathway hierarchy. The light-yellow colour denotes over-representation of that pathway. Light grey signifies pathways which are not significantly over-represented. Generated from: www.reactome.org.

Comparison the phosphorylation status between the A549 pEF control cells and SIPA1 knockdown cells treated with HGF was carried out. **Table 5.9** shows the markers whose phosphorylation status were most decreased after HGF treatment in the SIPA1 knockdown cells compared to pEF control cells, indicating the downstream markers which can be activated in pEF control cells but not in SIPA1 knockdown cells. The website Reacome (www.reactome.org) was used to conduct the key pathway analysis report. The most downregulated markers after HGF treatment in SIPA1 knockdown cells could be integrated to numbers of centralized signalling pathways, in which the top 25 signalling pathways are listed in **Table 5.10**. Also, the genome-wide overview schematic diagram of the signalling pathways was generated (**Figure 5.9**) to show the overall review of the main area in which the pathways downregulated by HGF treatment in SIPA1 knockdown cells are located.

Table 5.9: Key markers whose phosphor-status were down regulated in SIPA1 knock down cells compared to pEF control cells with treatment of HGF.

Target Name	P-Site	Full Target Protein Name	Average Normalized Net Signal		% CF C	Lead
			pEF+HGF	SIPA1KD +HGF		
PRKACA (PKA)	Pan-specific	cAMP-dependent protein kinase catalytic subunit alpha	771	98	-87	Possible
NFKB p65 (Rel A)	S529	NF-kappa-B p65 nuclear transcription factor	1141	384	-66	Possible
BCKD (BCKDK)	Pan-specific	[3-methyl-2-oxobutanoate dehydrogenase [lipoamide]] kinase, mitochondrial	10933	5447	-50	Possible
CK2a1 (CSNK2A1)	T360+S362	Casein protein-serine kinase 2 alpha/ alpha prime	2248	632	-72	
Jun (c-Jun)	T91	Jun proto-oncogene-encoded AP1 transcription factor	1386	619	-55	
IkBa	Pan-specific	Inhibitor of NF-kappa-B alpha (MAD3)	2670	1266	-53	
BCKD (BCKDK)	Pan-specific	[3-methyl-2-oxobutanoate dehydrogenase [lipoamide]] kinase, mitochondrial	360	178	-51	
MKK6 (MAP2K6, MEK6)	Pan-specific	MAPK/ERK protein-serine kinase 6 (MKK6); Dual specificity mitogen-activated protein kinase kinase 6	8157	4716	-42	
A6 (Twinfilin-1, TWF1)	Y309	Twinfilin, actin-binding protein, 1; Protein tyrosine kinase 9;	3958	2350	-41	
AurKC (Aurora C, AIK3)	Pan-specific	Aurora Kinase C (serine/threonine-protein kinase 13)	17085	10211	-40	
Myc	S373	Myc proto-oncogene protein	1092	692	-37	
JNK1 (MAPK8)	Y185	Jun N-terminus protein-serine kinase (stress-activated protein kinase (SAPK)) 1	8200	5353	-35	

MLK1 (MAP3K9)	Pan-specific	Mixed-lineage protein-serine kinase 1; Mitogen-activated protein kinase kinase kinase 9	754	497	-34
AurKC (Aurora C, AIK3)	Pan-specific	Aurora Kinase C (serine/threonine-protein kinase 13)	721	487	-33
IGF1R	Y1346	Insulin-like growth factor 1 receptor	4476	3083	-31
WNK1	Pan-specific	Serine/threonine-protein kinase WNK1	7166	4937	-31
ACTB	Pan-specific	Actin, cytoplasmic 1; Beta-actin	2912	2011	-31
ALK	Pan-specific	Anaplastic lymphoma receptor-tyrosine kinase	669	463	-31
GRK2 (BARK1, ADRBK1)	S670	Beta-adrenergic receptor kinase 1	957	663	-31
Plk1 (PLK)	Pan-specific	Polo-like protein-serine kinase 1	6631	4660	-30
p53 (TP53)	Pan-specific	Cellular tumor antigen p53	3201	2261	-29
DNAPK (PRKDC)	T2609	DNA-dependent protein kinase catalytic subunit	5854	4258	-27
KHS1 (MAP4K5; KHS)	S174	Kinase homologous to SPS1/STE20 (MAP kinase kinase kinase protein-serine kinase 5 (MEKKK5))	15746	11635	-26
Rb	T821	Retinoblastoma-associated protein 1	777	578	-26
Jun (c-Jun)	Y170	Jun proto-oncogene-encoded AP1 transcription factor	1042	779	-25
LTK	Y672	Leukocyte tyrosine kinase receptor	10453	7816	-25
STAG2	Y433	Putative uncharacterized protein DKFZp781H1753	7798	6190	-21
JAK2	Pan-specific	Janus protein-tyrosine kinase 2	12322	10011	-19
CaMK1d	T180	Calcium/calmodulin-dependent protein-serine kinase 1 delta	4052	3364	-17
STAT5	Y694	Signal transducer and activator of transcription 5	3799	3156	-17
AR	S310	Androgen receptor	14030	11845	-16

Bcr	Y177	Breakpoint cluster region protein	3101	2654	-14	
YAP1	T119	Yorkie homologue	17998	15464	-14	
ACLY	Y682	ATP-citrate synthase	8803	7622	-13	
MPL	Y591	Thrombopoietin receptor	2303	2017	-12	
Btk	Y551	Bruton's agammaglobulinemia tyrosine kinase	3182	2819	-11	
Yes	Y222+Y223	Yamaguchi sarcoma proto-oncogene-encoded tyrosine kinase	15101	13816	-9	
ACS1 (ACSL1)	Y567	Long-chain-fatty-acid--CoA ligase 1	3898	3731	-4	
PAK5 (PAK7)	Pan-specific	p21-activated kinase 5; Protein-serine/threonine kinase PAK 7	11348	11014	-3	
ERK2 (MAPK1)	Pan-specific	Extracellular regulated protein-serine kinase 2 (p42 MAP kinase)	25815	25143	-3	
MEK1 (MKK1, MAP2K1)	T292	MAPK/ERK protein-serine kinase 1 (MKK1); Dual specificity mitogen-activated protein kinase kinase 1	1813	1784	-2	
HIPK1	Y352	Homeodomain-interacting protein-serine kinase 1	4689	4661	-1	

Table 5.10: Top signalling pathways which were down regulated in SIPA1 knock down cells compared to pEF control cells after the treatment of HGF. Generated from: www.reactome.org.

Pathway name	Entities				Reactions	
	found	ratio	p-value	FDR*	found	ratio
Signaling by Interleukins	16 / 639	0.044	1.77e-08	5.22e-06	171 / 490	0.039
MyD88:MAL(TIRAP) cascade initiated on plasma membrane	8 / 111	0.008	4.18e-08	5.22e-06	34 / 64	0.005
Toll Like Receptor TLR6:TLR2 Cascade	8 / 111	0.008	4.18e-08	5.22e-06	34 / 66	0.005
Toll Like Receptor TLR1:TLR2 Cascade	8 / 114	0.008	5.12e-08	5.22e-06	34 / 66	0.005
Toll Like Receptor 2 (TLR2) Cascade	8 / 114	0.008	5.12e-08	5.22e-06	34 / 68	0.005
MyD88 cascade initiated on plasma membrane	7 / 94	0.007	2.49e-07	1.62e-05	19 / 58	0.005
Toll Like Receptor 10 (TLR10) Cascade	7 / 94	0.007	2.49e-07	1.62e-05	19 / 59	0.005
Toll Like Receptor 5 (TLR5) Cascade	7 / 94	0.007	2.49e-07	1.62e-05	19 / 59	0.005
Toll Like Receptor 4 (TLR4) Cascade	8 / 144	0.01	2.99e-07	1.76e-05	34 / 95	0.008
TRAF6 mediated induction of NFkB and MAP kinases upon TLR7/8 or 9 activation	7 / 102	0.007	4.28e-07	1.78e-05	19 / 48	0.004
Toll Like Receptor 3 (TLR3) Cascade	7 / 102	0.007	4.28e-07	1.78e-05	19 / 61	0.005
MyD88 dependent cascade initiated on endosome	7 / 103	0.007	4.57e-07	1.78e-05	19 / 63	0.005
Toll Like Receptor 7/8 (TLR7/8) Cascade	7 / 103	0.007	4.57e-07	1.78e-05	19 / 64	0.005
RUNX2 regulates osteoblast differentiation	5 / 34	0.002	5.33e-07	1.88e-05	13 / 24	0.002
TRIF(TICAM1)-mediated TLR4 signaling	7 / 107	0.007	5.88e-07	1.88e-05	19 / 58	0.005
MyD88-independent TLR4 cascade	7 / 107	0.007	5.88e-07	1.88e-05	19 / 60	0.005
Toll Like Receptor 9 (TLR9) Cascade	7 / 107	0.007	5.88e-07	1.88e-05	19 / 67	0.005
Cell Cycle, Mitotic	13 / 571	0.04	1.38e-06	4.27e-05	84 / 326	0.026
RUNX2 regulates bone development	5 / 43	0.003	1.67e-06	4.85e-05	13 / 32	0.003
Toll-like Receptor Cascades	8 / 184	0.013	1.84e-06	5.16e-05	34 / 182	0.015
Signaling by SCF-KIT	5 / 51	0.004	3.81e-06	1.03e-04	22 / 36	0.003
Cell Cycle	13 / 683	0.047	9.62e-06	2.50e-04	105 / 414	0.033
MAP kinase activation	5 / 69	0.005	1.62e-05	3.09e-04	16 / 32	0.003
Activation of the AP-1 family of transcription factors	3 / 12	8.31e-04	2.42e-05	3.62e-04	5 / 5	4.00e-04
Interleukin-17 signaling	5 / 77	0.005	2.74e-05	3.83e-04	16 / 35	0.003

* False Discovery Rate

Comparison the phosphorylation status between the A549 pEF control cells and SIPA1 knockdown cells treated with HGF was carried out. **Table 5.11** shows the markers whose phosphorylation status were most increased after HGF treatment in the SIPA1 knockdown cells compared to pEF control cells, indicating the downstream markers which can be activated in SIPA1 knockdown cells but not in pEF control cells. The website Reacome (www.reactome.org) was used to conduct the key pathway analysis report. The most upregulated markers after HGF treatment in SIPA1 knockdown cells could be integrated to numbers of centralized signalling pathways, in which the top 25 signalling pathways are listed in **Table 5.12**. Also, the genome-wide overview schematic diagram of the signalling pathways was generated (**Figure 5.10**) to show the overall review of the main area in which the pathways upregulated by HGF treatment in SIPA1 knockdown cells are located.

Table 5.11: Key markers whose phosphor-status were up regulated in SIPA1 knock down cells compared to pEF control cells with treatment of HGF.

Target Name	P-Site	Full Target Protein Name	Average Normalized Net Signal		%CF C	Lead
			pEF+HGF	SIPA1KD +HGF		
MEF2A	T108	Myocyte-specific enhancer factor 2A	47	2057	4304	Priority
STAT5A	Y694	Signal transducer and activator of transcription 5A	217	3135	1342	Priority
PFN1	Y129	Profilin 1	134	1728	1192	Priority
PIK3 (CNK)	Pan-specific	Polo-like protein-serine kinase 3 (cytokine- inducible kinase (CNK))	212	2324	997	Priority
CDK12 (Cdc2L7)	T893	Cell division protein kinase 12; Cell division cycle 2-related protein kinase 7	1070	11291	955	Priority
SRF	S224	Serum response factor	1214	11154	819	Priority
Syk	Y323	Spleen protein-tyrosine kinase	380	2190	477	Priority
ERK3 (MAPK6)	Pan-specific	Extracellular regulated protein-serine kinase 3	402	2110	425	Priority
TTK	T676	Dual specificity protein kinase TTK	674	3460	414	Priority
CrkL	Pan-specific	Crk-like protein	381	1835	381	Priority
PLCB3	S1105	1-phosphatidylinositol-4,5-bisphosphate phosphodiesterase beta-3	487	2170	346	Priority
PFTAIRE1 (CDK14)	Pan-specific	Serine/threonine protein kinase PFTAIRE-1	1560	6737	332	Priority
p38b MAPK (MAPK11)	T180+Y182	Mitogen-activated protein-serine kinase p38 beta; Mitogen-activated protein kinase 11	1807	7405	310	Priority
EphB1	Y594	Ephrin type-B receptor 1 protein-tyrosine kinase	1952	7854	302	Priority
PIK1 (PLK)	T210	Polo-like protein-serine kinase 1	676	2708	301	Priority

SIK3 (QSK)	T411	Salt-inducible serine/threonine-protein kinase SIK3	918	3636	296	Priority
TEC	Y519	Tyrosine-protein kinase Tec	812	3161	289	Priority
Raf1 (RafC)	S301+T303	Raf1 proto-oncogene-encoded protein-serine kinase	412	1596	287	Priority
SIT	Y95	Signaling threshold-regulating transmembrane adapter 1	7861	28073	257	Priority
STAT6	Pan-specific	Signal transducer and activator of transcription 6	513	1807	253	Priority
ITK	Pan-specific	Tyrosine-protein kinase ITK/TSK	471	1655	252	Priority
PTPN21	S637	Tyrosine-protein phosphatase non-receptor type 21	437	1506	245	Priority
SPT5	T791	Transcription elongation factor SPT5	2966	10014	238	Priority
PFTAIRE2 (ALS2CR7)	Pan-specific	Amyotrophic lateral sclerosis 2 chromosomal region candidate gene 7 protein	1642	5476	233	Priority
PFKFB3	S461	6-phosphofructo-2-kinase/fructose-2,6-biphosphatase 3	717	2363	229	Priority
RSK1 (RPS6KA1, p90RSK)	Pan-specific	Ribosomal S6 protein-serine kinase 1; Ribosomal protein S6 kinase alpha 2	540	1762	226	Priority
PAK1 (PAKa)	Pan-specific	p21-activated kinase 1 (alpha) (Protein-serine/threonine kinase PAK 1)	1299	4182	222	Priority
PYK2 (PTK2B)	Y402	Protein tyrosine kinase 2 beta	1947	6270	222	Priority
TARDBP	S409+S410	TAR DNA-binding protein 43	1470	4667	218	Priority
EZH2	T487	Histone-lysine N-methyltransferase EZH2	3983	12549	215	Priority
Raf-B (BRaf)	S446+S447	B-Raf proto-oncogene serine-threonine-protein kinase; RafB proto-oncogene-encoded protein-serine kinase	1985	6178	211	Priority
MARK2	Pan-specific	MAP/microtubule affinity-regulating protein-serine kinase 2	1205	3742	210	Priority
AAK1	S637	AP2-associated protein kinase 1	2342	7239	209	Priority
p53 (TP53)	S392	Cellular tumor antigen p53	2522	7782	209	Priority
HDAC5	S498	Histone deacetylase 5	533	1591	198	Priority

TAK1 (MAP3K7)	T184+T187	TGF-beta-activated protein-serine kinase 1; Mitogen-activated protein kinase kinase kinase 7	1169	3405	191	Priority
RSK2 (RPS6KA3)	T577	Ribosomal S6 protein-serine kinase 2; Ribosomal protein S6 kinase alpha-3	546	1549	184	Priority
PKR1 (PRKR; EIF2AK2)	T446	Double-stranded RNA-dependent protein-serine kinase; Interferon-induced, double-stranded RNA-activated protein kinase	1991	5577	180	Priority
Shc1 (Shc)	Y349+Y350	SH2 domain-containing transforming protein 1	586	1604	174	Priority
p38b MAPK (MAPK11)	Pan-specific	Mitogen-activated protein-serine kinase p38 beta; Mitogen-activated protein kinase 11	1014	2692	166	Priority
SHIP1 (INPP5D)	Y187	Phosphatidylinositol 3,4,5-trisphosphate 5-phosphatase 1	2746	7226	163	Priority
MSK2 (RPS6KA4)	T687	Ribosomal protein S6 kinase alpha-4	3539	9299	163	Priority
PKD3 (PRKCN)	Pan-specific	Protein-serine kinase C nu; Serine/threonine-protein kinase D3	598	1558	161	Priority
CDKL1	Pan-specific	Cyclin-dependent kinase-like 1; Serine/threonine protein kinase KKIALRE	1538	3994	160	Priority
RPS6	S235+S236	40S Ribosomal S6	1693	4373	158	Priority
ERK1 (MAPK3)	Y204+T207	Extracellular regulated protein-serine kinase 1 (p44 MAP kinase)	3355	8658	158	Priority
SIN3A	S832	Paired amphipathic helix protein Sin3a	9009	22656	151	Priority
Pim2	T195	Serine/threonine-protein kinase Pim-2	4044	9982	147	Priority
Raf1 (RafC)	S259	Raf1 proto-oncogene-encoded protein-serine kinase	2784	6782	144	Priority
STAT3	Y705	Signal transducer and activator of transcription 3	837	2019	141	Priority
PIK3R2	Y464	Phosphatidylinositol 3-kinase regulatory subunit beta	1486	3582	141	Priority

SIK2 (QIK)	Pan-specific	Salt-inducible serine/threonine-protein kinase SIK2; Serine-threonine-protein kinase SNF1-like kinase 2	933	2236	140	Priority
Frk	Pan-specific	Fyn-related kinase; Tyrosine-protein kinase FRK	1108	2579	133	Priority
ITK	Y512	Tyrosine-protein kinase ITK/TSK	8353	19336	131	Priority
TTK	Y833+Y836	Dual specificity protein kinase TTK	3934	9070	131	Priority
PFTAIRE2 (ALS2CR7)	Pan-specific	Amyotrophic lateral sclerosis 2 chromosomal region candidate gene 7 protein	761	1739	128	Priority
TGM2	Y369	Protein-glutamine gamma-glutamyltransferase 2	6091	13873	128	Priority
Chk1 (CHEK1)	Pan-specific	Checkpoint protein-serine kinase 1	722	1636	127	Priority
PLCG1	Y977	1-phosphatidylinositol-4,5-bisphosphate phosphodiesterase gamma-2	3511	7827	123	Priority
JAK2	Y1007+Y1008	Janus protein-tyrosine kinase 2	1930	4298	123	Priority
PRKACB (PKA)	Y69	cAMP-dependent protein-serine kinase catalytic subunit beta	1475	3250	120	Priority
CDK5	Y15	Cyclin-dependent protein-serine kinase 5	3045	6669	119	Priority
CLK1	S337	Dual specificity protein kinase CLK1	1336	2908	118	Priority
CSF1R (Fms)	Y699	Macrophage colony-stimulating factor 1 receptor	734	1595	117	Priority
NFAT5	T135	Nuclear factor of activated T-cells 5	5913	12704	115	Priority
IKKe (IKBKE)	S172	Inhibitor of nuclear factor kappa-B kinase subunit epsilon	6799	14531	114	Priority
ICK (LCK2)	Y159	Intestinal cell (MAK-like) kinase	3252	6890	112	Priority
Rb	S608	Retinoblastoma-associated protein 1	1006	2080	107	Priority
Vav	Y826	Vav 1 guanine nucleotide exchange factor	818	1654	102	Priority
LATS1	S464	Large tumour suppressor 1 protein-serine kinase (WARTS)	1273	2530	99	Priority

HSF1	S303+S307	Heat shock factor protein 1	7173	13886	94	Priority
Fes	Y713	Fes/Fps protein-tyrosine kinase	1752	3368	92	Priority
SRPK2	Pan-specific	Serine/arginine-rich protein-specific kinase 2; Serine kinase SRPK2	4222	8088	92	Priority
CDKL5 (STK9)	Y171	Cyclin-dependent kinase-like 5; Serine-threonine-protein kinase 9	5451	10391	91	Priority
p70S6K (S6Ka, RPS6KB1)	Pan-specific	Ribosomal protein S6 kinase beta-1; Ribosomal protein S6 kinase 1	1882	3519	87	Priority
VEGFR1 (Flt1)	Y1053	Vascular endothelial growth factor receptor 1	2378	4421	86	Priority
CDK7	Pan-specific	Cyclin-dependent protein-serine kinase 7	865	1598	85	Priority
Cbl	Y674	E3 ubiquitin-protein ligase CBL	2544	4654	83	Priority
Kit	Y703	Mast/stem cell growth factor receptor protein-tyrosine Kit	4461	8114	82	Priority
Kit	Y730	Mast/stem cell growth factor receptor protein-tyrosine Kit	949	1712	80	Priority
SIK (SNF1LK)	T182	Salt-inducible serine/threonine-protein kinase SIK1; Serine-threonine-protein kinase SNF1-like kinase 1	3321	5980	80	Priority
RIOK2	S332+S335+S337	Serine/threonine-protein kinase RIO2	3828	6825	78	Priority
SIT	Y90	Signaling threshold-regulating transmembrane adapter 1	4721	8410	78	Priority
ROCK2 (ROKa)	Y722	Rho-associated protein kinase 2	1511	2683	78	Priority
Raf1 (RafC)	S296	Raf1 proto-oncogene-encoded protein-serine kinase	4903	8601	75	Priority
RIPK2 (RICK; RIP2; CARD3)	S176	Receptor-interacting serine/threonine-protein kinase 2 (RIPK2)	12641	22124	75	Priority
PLCE1	S1096+T1100	1-phosphatidylinositol-4,5-bisphosphate phosphodiesterase epsilon-1	79	892	1035	Possible
CLK3	Pan-specific	Dual specificity protein kinase CLK3	146	1240	752	Possible

PLCD1	S460	1-phosphatidylinositol-4,5-bisphosphate phosphodiesterase delta-1	153	1139	646	Possible
Myc	T58	Myc proto-oncogene protein	109	789	627	Possible
CBS	S227	Cystathionine beta-synthase	171	1085	533	Possible
PLCG1	Pan-specific	1-phosphatidylinositol 4,5-bisphosphate phosphodiesterase gamma-1	255	1373	438	Possible
Plk4 (SAK; STK18)	Pan-specific	Polo-like kinase-serine 4 (SAK)	225	1041	363	Possible
NFKB p50	S337	Nuclear factor NF-kappa-B p105 subunit	272	1100	305	Possible
TAO1 (TAOK1)	S181	Serine/threonine-protein kinase TAO1	334	1351	304	Possible
InsR (IR)	Pan-specific	Insulin receptor	318	1235	288	Possible
GSK3a	Pan-specific	Glycogen synthase-serine kinase 3 alpha/beta	257	909	254	Possible
PRKACA (PKA)	Pan-specific	cAMP-dependent protein kinase catalytic subunit alpha	344	1193	247	Possible
LKB1 (STK11)	S428	Serine/threonine-protein kinase 11	287	928	223	Possible
CRYAB	S19	Crystallin aB	508	1440	184	Possible
LATS1	Pan-specific	Large tumour suppressor 1 protein-serine kinase (WARTS)	554	1490	169	Possible
Rb	S249+T252	Retinoblastoma-associated protein 1	449	1199	167	Possible
GRK2 (BARK1, ADRBK1)	Pan-specific	G protein-coupled receptor-serine kinase 2	490	1300	165	Possible
PKD1 (PRKCM, PKCm, PRKD1)	Pan-specific	Protein-serine kinase C mu (Protein kinase D)	300	792	164	Possible
JAK2	Y1007+Y1008	Janus protein-tyrosine kinase 2	360	929	158	Possible
PTEN	S380	Phosphatidylinositol-3,4,5-trisphosphate 3-phosphatase and protein phosphatase and tensin homolog deleted on	317	807	155	Possible

		chromosome 10				
PCYT1A (CTPCT; CCTA)	T342+S343	CTP: phosphocholine cytidyltransferase isoform A	298	752	152	Possible
SLK	S189	STE20-like serine/threonine-protein kinase; CTCL tumour antigen se20-9	500	1236	147	Possible
Vav	Y174	Vav 1 guanine nucleotide exchange factor	514	1237	141	Possible
GRK2 (BARK1, ADRBK1)	S670	G protein-coupled receptor-serine kinase 2	615	1422	131	Possible
Raf1 (RafC)	S621	Raf1 proto-oncogene-encoded protein-serine kinase	382	859	125	Possible
JNK1 (MAPK8)	Pan-specific	Jun N-terminus protein-serine kinase (stress-activated protein kinase (SAPK)) 1	7090	15476	118	Possible
PTPN11 (PTP1D; PTP2C; SHP2; SHPTP2; Syp)	Pan-specific	Tyrosine-protein phosphatase non-receptor type 11	517	1121	117	Possible
PKCa (PRKCA)	Y195	Protein-serine kinase C alpha	666	1422	113	Possible
PKCg (PRKCG)	Pan-specific	Protein-serine kinase C gamma	533	1134	113	Possible
Rb	T356	Retinoblastoma-associated protein 1	410	864	111	Possible
CDC2L5 (CHED, CDK13)	Pan-specific	CDC2-related protein kinase 5	542	1135	109	Possible
Fos	Pan-specific	Fos-c FBJ murine osteosarcoma oncoprotein-related transcription factor	547	1125	106	Possible
FGFR3	Y647+Y648	Fibroblast growth factor receptor 3	3749	7643	104	Possible
eIF4B	Pan-specific	Eukaryotic translation initiation factor 4B	482	980	103	Possible
NFKB1 (NFkB-p105)	S932	Nuclear factor NF-kappa-B p105 subunit	378	765	102	Possible
IGF1R	Y1161+T11	Insulin-like growth factor 1 receptor protein-tyrosine	1058	2056	94	Possible

	63	kinase				
Pim3	Pan-specific	Serine/threonine-protein kinase Pim-3	418	786	88	Possible
TAO1 (TAOK1)	Y309	Serine/threonine-protein kinase TAO1	1814	3348	85	Possible
ZC2 (TNIK)	Pan-specific	TRAF2 and NCK-interacting kinase	419	767	83	Possible
Lyn	Pan-specific	Yes-related protein-tyrosine kinase; Tyrosine-protein kinase Lyn	467	849	82	Possible
MELK	Y438	Maternal embryonic leucine zipper kinase	800	1416	77	Possible
LEDGF	S273+S275	PC4 and SFRS1-interacting protein	680	1194	76	Possible
Tyro3	Y685+Y686	Tyrosine-protein kinase receptor TYRO3	1798	3121	74	Possible
SOCS7	Y561	Suppressor of cytokine signaling 7	6744	11599	72	Possible
PTPN1 (PTP1B)	Y66	Tyrosine-protein phosphatase non-receptor type 1	1498	2545	70	Possible
MARK4	Pan-specific	MAP/microtubule affinity-regulating protein-serine kinase 4	492	827	68	Possible
PU.1 (SPI1)	S146	Transcription factor PU.1	758	1264	67	Possible
ILK1 (ILK)	S343	Integrin-linked protein-serine kinase-1	698	1158	66	Possible
Rb	T826	Retinoblastoma-associated protein 1	1524	2522	65	Possible
PIK3R1	Y467	Phosphatidylinositol 3-kinase regulatory subunit alpha	7791	12760	64	Possible
SIK3 (QSK)	T163	Salt-inducible serine/threonine-protein kinase SIK3	8840	14444	63	Possible
JNK2 (MAPK9)	Pan-specific	Jun N-terminus protein-serine kinase (stress-activated protein kinase (SAPK)) 2	5195	8391	62	Possible
LATS2 (KPM)	Pan-specific	Large tumour suppressor 2 protein-serine kinase	4051	6453	59	Possible
Ron (RONa)	Y1238	Macrophage-stimulating protein receptor alpha chain	10756	16801	56	Possible
Raf-B (BRaf)	S729	B-Raf proto-oncogene serine-threonine-protein kinase; RafB proto-oncogene-encoded protein-serine kinase	2486	3827	54	Possible
CDK6	Y24	Cyclin-dependent protein-serine kinase 6	4531	6941	53	Possible

NDR1 (NDR, STK38)	S281+T282	Serine/threonine-protein kinase 38	10051	15336	53	Possible
ErbB2 (HER2, Neu)	Y735	ErbB2 (Neu) receptor-tyrosine kinase	5339	8084	51	Possible
Met	Y1234	Hepatocyte growth factor (HGF) receptor-tyrosine kinase	5777	8705	51	Possible
VIM	Y117	Vimentin	3333	4965	49	Possible
mTOR (FRAP)	Pan-specific	Mammalian target of rapamycin (FRAP); FKBP12-rapamycin complex-associated protein	12239	18124	48	Possible
TBK1	S172	TANK binding kinase TBK1; Serine/threonine-protein kinase TBK1	3455	5111	48	Possible
MSK1 (RPS6KA5)	S212	Mitogen & stress-activated protein-serine kinase 1; Ribosomal protein S6 kinase alpha 5	8139	12015	48	Possible
CSF1R (Fms)	Y809	Macrophage colony-stimulating factor 1 receptor	2365	3447	46	Possible
PKD2 (PRKD2)	S197+S198	Serine/threonine-protein kinase D2	5322	7741	45	Possible
CDKL2	Pan-specific	Cyclin-dependent kinase-like 2; Serine/threonine protein kinase KKIAMRE	3657	5312	45	Possible

Table 5.12: Top signalling pathways which were upregulated in SIPA1 knock down cells compared to pEF control cells after the treatment of HGF. Generated from: www.reactome.org.

Pathway name	Entities				Reactions	
	found	ratio	p-value	FDR*	found	ratio
Signaling by Receptor Tyrosine Kinases	48 / 554	0.038	1.11e-16	1.22e-13	428 / 657	0.053
Signaling by Interleukins	41 / 639	0.044	7.11e-15	3.90e-12	260 / 490	0.039
Intracellular signaling by second messengers	30 / 362	0.025	8.08e-14	2.36e-11	59 / 113	0.009
Interleukin-3, Interleukin-5 and GM-CSF signaling	14 / 50	0.003	8.62e-14	2.36e-11	34 / 38	0.003
Signaling by SCF-KIT	14 / 51	0.004	1.12e-13	2.46e-11	34 / 36	0.003
Signaling by NTRKs	18 / 118	0.008	6.19e-13	1.13e-10	60 / 127	0.01
Cytokine Signaling in Immune system	54 / 1,261	0.087	2.69e-12	4.22e-10	343 / 699	0.056
TRIF(TICAM1)-mediated TLR4 signaling	16 / 107	0.007	1.65e-11	2.01e-09	38 / 58	0.005
MyD88-independent TLR4 cascade	16 / 107	0.007	1.65e-11	2.01e-09	38 / 60	0.005
Diseases of signal transduction	31 / 496	0.034	3.87e-11	4.22e-09	173 / 322	0.026
MAP kinase activation	13 / 69	0.005	8.60e-11	4.65e-09	28 / 32	0.003
Toll Like Receptor 3 (TLR3) Cascade	15 / 102	0.007	9.04e-11	4.70e-09	38 / 61	0.005
Signal Transduction	93 / 3,305	0.229	1.43e-10	7.01e-09	804 / 2,303	0.184
MAPK targets/ Nuclear events mediated by MAP kinases	10 / 35	0.002	2.63e-10	8.95e-09	14 / 16	0.001
Signaling by NTRK1 (TRKA)	14 / 93	0.006	2.88e-10	9.51e-09	37 / 65	0.005
Interleukin-17 signaling	13 / 77	0.005	3.22e-10	1.03e-08	28 / 35	0.003
Signaling by FGFR3	11 / 53	0.004	9.20e-10	2.78e-08	36 / 43	0.003
PIP3 activates AKT signaling	23 / 316	0.022	9.26e-10	2.78e-08	52 / 86	0.007
Toll Like Receptor 4 (TLR4) Cascade	16 / 144	0.01	1.17e-09	3.38e-08	40 / 95	0.008
Generic Transcription Pathway	55 / 1,553	0.108	2.00e-09	5.59e-08	256 / 824	0.066
MyD88 cascade initiated on plasma membrane	13 / 94	0.007	3.43e-09	8.84e-08	34 / 58	0.005
Toll Like Receptor 10 (TLR10) Cascade	13 / 94	0.007	3.43e-09	8.84e-08	34 / 59	0.005
Toll Like Receptor 5 (TLR5) Cascade	13 / 94	0.007	3.43e-09	8.84e-08	34 / 59	0.005
PI3K/AKT Signaling in Cancer	15 / 134	0.009	3.54e-09	8.84e-08	5 / 21	0.002
TRAF6 mediated induction of NFkB and MAP kinases upon TLR7/8 or 9 activation	13 / 102	0.007	8.93e-09	2.14e-07	34 / 48	0.004

* False Discovery Rate

Different comparison methods can obtain many signalling pathways that regulate SIPA1 and/or HGF/MET. Among those we selected some high-frequency, representative signalling pathways for further discussion (**Figure 5.11-5.12**), and more figures of the selected signalling pathways can be found in the appendix.

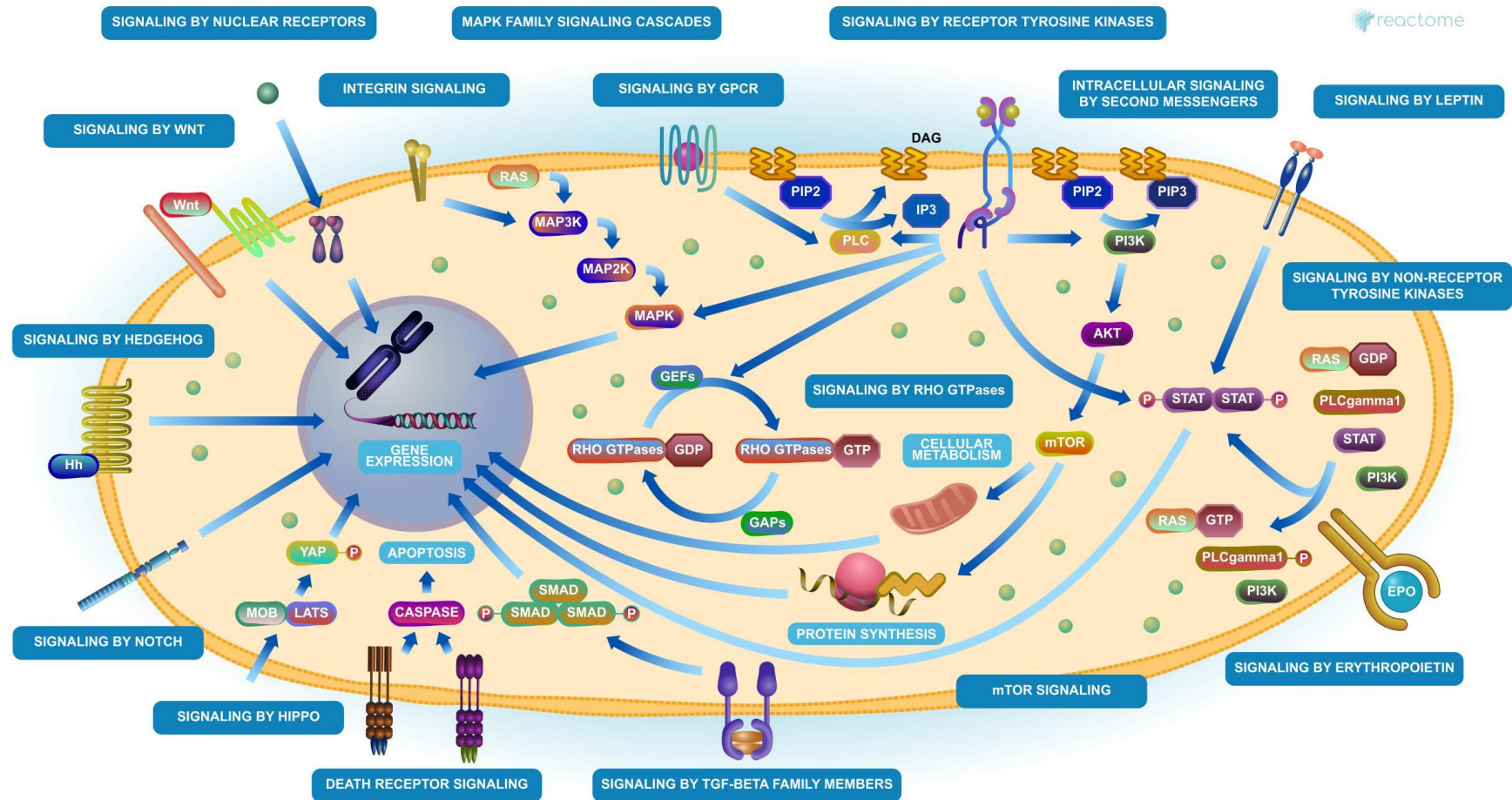


Figure 5.11: Schematic diagram of signalling transduction process. Generated from: www.reactome.org.

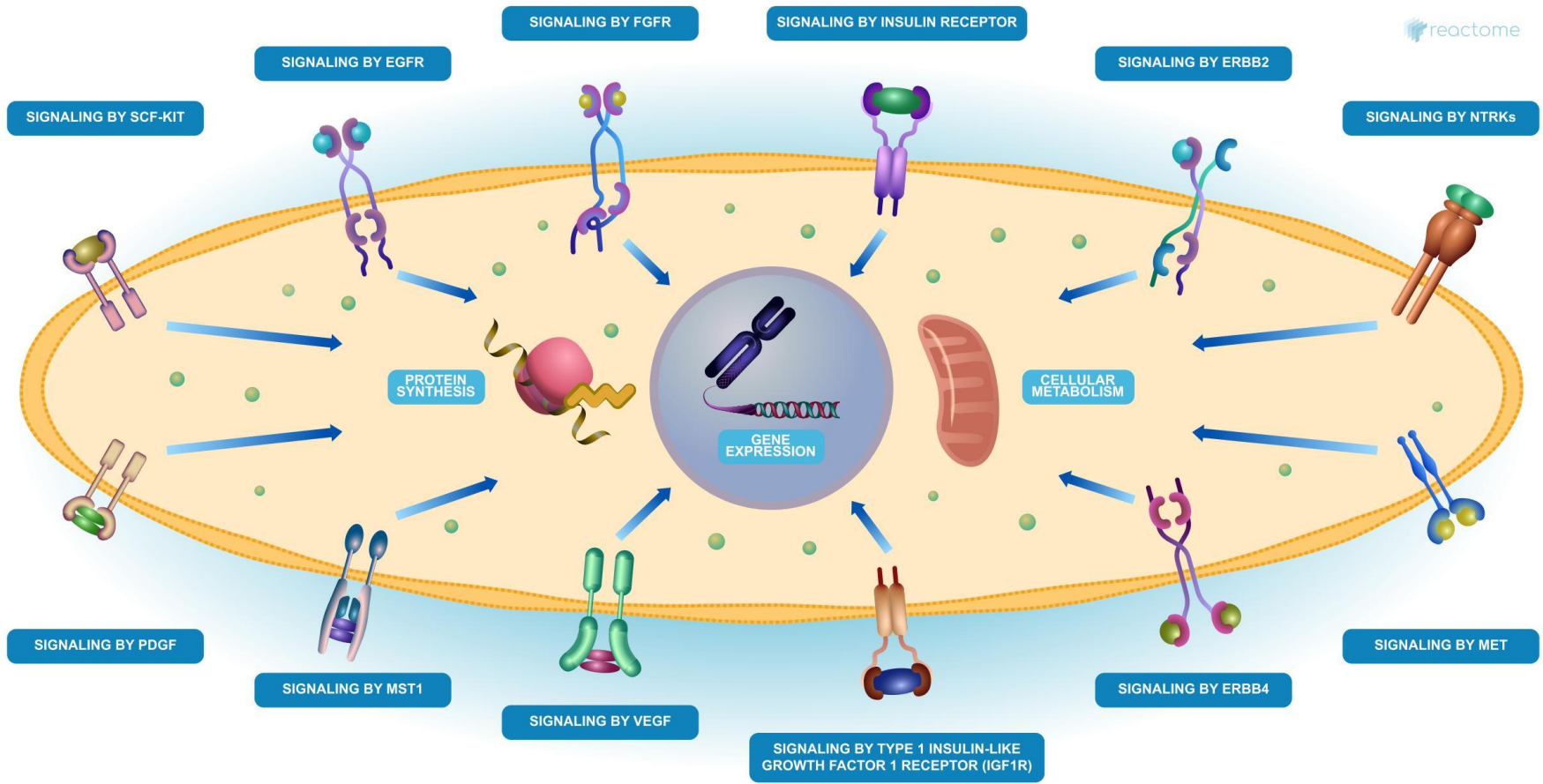


Figure 5.12: Schematic diagram of signalling by receptor tyrosine kinases. Generated from: www.reactome.org.

5.4 Discussion

The results of the gene expression correlation analysis with SIPA1 both in our lung cancer cohorts and the TCGA database demonstrate that SIPA1 is highly correlated with the key markers within the HGF/MET signalling pathway and TJs. Focus on the HGF/MET signalling pathway related markers, HGF, MET, HGFAC are found high correlated with SIPA1 in our lung cancer cohort, and in TCGA cohort besides MET, downstream markers of HGF/MET signalling pathway such as MST1, MST1R, PTK2, PXN, PRKCA, PTEN, and SRC are all highly correlated with SIPA1. Moreover, another major RTK family member EGFR have highly expression correlation with SIPA1 as well. The correlated expressions of these molecules have been tested and confirmed by two cohorts and all these results indicate that SIPA1 is more likely to synergize with these molecules in lung cancer cells.

The gene expression correlation analysis also shows us the potential regulation role of SIPA1 on TJs. In our Peking lung cancer cohort, transcript level of some TJs markers such as JAM2, OCLD, MARVEL D2, and NECTIN2 are highly correlated with SIPA1, and JAM1 protein encoding gene F11R, ZO family encoding genes, Claudin proteins encoding genes such as CLDN4, CLDN7, CLDN12, CLDN15, and PDZ domain containing protein encoding gene Marvel D3 were found highly expressed with SIPA1. Correlation analysis of gene expression can confirm our previous hypothesis to a certain extent. The results reveal that SIPA1 not only interacts with the HGF/MET pathway, but their interaction can regulate tight junctions. However, the correlation at the transcript level cannot fully explain the specific mechanism of SIPA1 interacting with HGF/MET in tumours. We performed the protein array analysis, aiming to find out the difference on the protein level, investigating the effect of SIPA1 on the phosphorylation status of intercellular protein.

Firstly, all the genome-wide figures of the signalling pathway (**Figure 5.5-5.10**) indicate that regulation of the interaction between SIPA1 and HGF/MET focus on the area of signal transduction, immune system, disease, cell cycle, developmental

biology, and cellular responses to external stimuli (the yellow colour is more pronounced in these areas). These are very consistent with our previous assumptions. As described in the introduction, HGF/MET signalling pathway belongs to the RTK family, and the RTKs are major cell surface proteins involved in Signal Transduction. The interaction of SIPA1 with HG/MET regulates cell signal transduction, further confirming our previous experimental hypothesis. Meanwhile, in chapter 4, we confirmed knockdown SIPA1 could decrease the lung cancer cells' proliferation and invasion potential, which was also further proved by the protein array results, since the cell cycle pathway is deeply adjusted.

It was very interesting indeed to find that signal transduction pathway and receptor tyrosine kinases (RTK) pathway were both upregulated and downregulated with the collective effect of SIPA1 and HGF/MET. This demonstrated that the combined effect of SIPA1 and HGF/MET is not a simple one-way regulation, there are extremely complicated regulation mechanisms involved. Inhibition of one key molecule or one critical pathway may lead to feedback activation of other pathways. For instance, Knockdown SIPA1 inhibits the signalling by the signal transduction and RTK significantly (**Table 5.2**), while in **Table 5.4**, signal transduction and RTK related pathways were activated by SIPA1 knockdown, which looks rather contradictory and confusing. However as discussed in Chapter 1, the signal transduction and RTKs are extremely complex, knockdown SIPA1 inhibits some members of RTKs such as SCF-KIT signalling pathway, ESR-mediated signalling pathway, and regulation of KIT signalling (**Table 5.2, Figure 5.13-5.15**), but the Interleukin-17 (IL-17) signalling pathway was increased (**Table 5.4, Figure 5.16**) which could also stimulate the signal transduction. Knockdown of SIPA1 decreased the RTKs downstream Akt signalling pathway (**Table 5.2, Figure 5.13-5.15**), and increased MAP kinase activation signalling pathway (**Table 5.4, Figure 5.17**) at the same time. In terms of HGF treatment and the synergy of SIPA1 and HGF, the MET downstream pathways MAP kinases activation signalling and MAPK family signalling cascades signalling were both activated by treatment of HGF, which was consistent with general understanding.

ESR signalling was activated with MET synergistically (**Table 5.8**), further enhanced RTK signalling and signal transduction. Treatment with HGF inhibits SCF-KIT signalling, VEGFA-VEGFR2 signalling, and VEGF signalling, indicating that they may be competitive with MET. Downstream of RTKs such as MAPK target, ERK/MAPK targets, and MAP kinase activation signalling pathway were all downregulated by HGF (**Table 5.6**). Compared to its role in control cells, knocking down SIPA1 can reduce the active effect of HGF on cell cycle signalling, indicating that the regulation of SIPA1 on proliferation of lung cancer A549 cells was mediated by interacting with HGF/MET (**Table 5.10**). Interaction between SIPA1 and HGF/MET enhanced RTKs signalling by activating the SCF-KIT, FGFR3 signalling pathway, further strengthening intracellular downstream PI3K/Akt and PIP3 activates Akt signalling (**Table 5.12**).

Extremely complex interaction between SIPA1 and HGF/MET is consistent with the clinical status of lung cancer. As stated previously, 5-22% lung cancer patients with acquired resistance to EGFR-TKI have MET amplification and oncogenic mutation. The amplification and oncogenic mutation at Exon 14 of MET are the second most common cause for acquired resistance to EGFR-TKI after EGFR T790M resistance mutation (Wu et al., 2017). This all proves the complexity of the positive/negative regulation within the RTKs family from distinct perspectives. Certain treatment may inhibit one or more RTKs, but at the same time it will cause other RTKs members to rise in a feedback manner. Therefore, the specific interaction mechanism between SIPA1 and HGF/MET signalling pathway requires further investigation. The regulation of interaction between SIPA1 and HGF/MET in lung cancer cells and lung cancer metastasis is worthy of more detail explanation in order to have a better understanding for clinical application.

**Chapter-6 SIPA1 is a modulator of
the regulation of HGF on cellular
function behaviour of human lung
cancer cells**

6.1 Introduction

As discussed in Chapter 1 and Chapter 5, intracellular signalling pathways regulated by the interaction of SIPA1 and HGF/MET in human lung cancer cells are complicated, with various positive and/or negative feedback adjustments which are still unclear. SIPA1 can interact with many Intracellular molecules to play an essential role in the regulation of cancer cell aggressive behaviours. In the nucleus, SIPA1 can bind to the promoter region of ITGB1 gene and enhance ITGB transcription, increase the expression of Integrin β 1, which accordingly activates the integrin-mediated FAK/Akt signalling pathway (Takahara et al., 2017, Zhang et al., 2015). SIPA1 directly binds to AQP2 and participates in the regulation of AQP2 transportation (Noda et al., 2004). It was found that Brd4 could bind to the SIPA1 GRD domain, and SIPA1 reduces the expression of BRD4 in the nucleus. This interaction further enhances the expression of MMP7, leading to tumour invasion and metastasis, and tumour growth (Takahara et al., 2017, Alsarraj et al., 2013). The regulatory mechanism of the MET pathway is multi-dimensional. The regulation may be directly on the MET receptor or the key molecules of the downstream signalling (Zhang and Babic, 2016). Moreover, the regulation of the MET receptor is also multifaceted, which includes MET oncogene mutations, methylation of the MET oncogene, regulation by transcription factors, alternative splicing of mRNA, mRNA regulated by microRNAs, regulation of translation of the MET receptor, proteolysis of MET, modifications of the MET receptor such as glycosylation and phosphorylation, MET internalization and degradation, nuclear localization of MET, and MET autoregulation. Furthermore, other membrane molecules such as RTKs EGFR, and other oncogenes such as p53 are all involved in the regulation of MET (Zhang and Babic, 2016).

Since the regulation of MET is extremely complicated, which regulatory process involving SIPA1 and the specific mechanisms involved require clarification. At the same time, we see that the effect of HGF on cells requires the presence of SIPA1. How the interaction of SIPA1 and HGF/MET affects cell aggressive behaviour and barrier function requires further investigation.

One of the limited numbers of molecules known to be the target of SIPA1 signalling is Rap1/MEK/ERK. It is a target of SIPA1 and is also located downstream of the HGF signalling pathway, responding to the action of HGF (Kurachi et al., 1997, Birchmeier et al., 2003b). Meanwhile, SIPA1 and AF6 have been shown to be able to interact with each other (Su et al., 2003). AF6 is one member of the membrane integral protein at the TJ in the cell. It directly or indirectly interacts with other TJ proteins including ZO1, Occludin and JAMs (Singh et al., 2003, Martin, 2014, Tracey A. Martin, 2013, Martin et al., 2013). Collectively, these studies suggest that SIPA1 may have the potential to regulate TJs under the induction of HGF, which in turn may play a role in the development and metastasis of the tumour. In this chapter, we aim to find out the mechanism of the interaction of SIPA1 and HGF/MET. We performed a series of experiment to examine the effect of SIPA1 knockdown on MET and tight junction components.

In this chapter, we aim to find out the mechanism of the interaction of SIPA1 and HGF/MET. We performed a series of experiment to examine the effect of SIPA1 knockdown on MET and tight junction components.

6.2 Materials and methods

6.2.1 RNA extraction, RT-PCR, and QPCR

The RNA was extracted by using Tri Reagent as described in section 2.8.1. After the isolation of RNA was completed, the quantification of RNA was carried out as described in section 2.8.2, followed by RT-PCR to obtain the cDNA. The cDNA could then be used for PCR and QPCR as describes in section 2.4.3 to 2.4.6.

6.2.2 Primers and antibody

All the primers used were synthesised and provided by Invitrogen (Paisley, UK). Primer sequences are shown in **Table 2.3, 2.4**. The name, molecular weight, supplier,

and the product code of the primary and secondary antibodies used in this chapter is shown in **Table 2.5**.

6.2.3 Protein extraction, SDS-PAGE, and western blot analysis

The extraction of protein was carried out as the description in section 2.5.1. Proteins were extracted using lysis buffer and then quantified using the Bio-Rad DC Protein Assay kit (Bio-Rad Laboratories, Hemel-Hempstead, UK). After separation in the SDS-PAGE gel, proteins were transferred onto PVDF membranes as described in section 2.5.2. The membranes with protein were subsequently blocked and probed with various primary antibody and a corresponding peroxidase-conjugated secondary antibody. The antibodies' information in this study is shewed in **Table 2.5**. Finally, the protein bands on the membrane were visualised using the chemiluminescence detection kit (Luminata, Millipore).

6.2.4 *In vitro* cell growth assay

Due to the difference growth speed between different cell lines, 3,000 - 5,000 cells were seeded into 200µl medium in three 96-well plates appropriately. After incubation for 1, 3, and 5 days respectively, the cells were fixed and stained by crystal violet. The absorbance was measured after dissolving the crystal violet with acetic acid (10% v/v) and the absorbance was determined at a wave length of 560nm using a spectrophotometer (BIO-TEK, Elx800, UK).

6.2.5 *In vitro* cell invasion assay

20,000-40,000 cells were seeded into transwell inserts (pore size, 8µm, Millicell, Merck KGaA, Darmstadt, Germany) coated with 50µg Matrigel. After the incubation of three days, cells that had invaded through the Matrigel and migrated on to the other side of the insert were fixed and stained with crystal violet and then counted. The

absorbance was measured after dissolving the crystal violet with acetic acid (10% v/v) and the absorbance was determined at a wave length of 560nm using a spectrophotometer (BIO-TEK, Elx800, UK).

6.2.6 Electric Cell-Substrate Impedance Sensing (ECIS)

ECIS assay to detect the resistance of cells was performed as described in section 2.7.8. 50,000 cells were seeded in the 96W1E+ electrode array plate after stabilization, following with measurement over different frequencies were to study different functional and structural cell properties. In this study, resistance measured under 1,000-4000Hz frequencies were chosen to analyse cell resistance referring to the function of tight junction.

6.2.7 Immunofluorescence staining

Immunofluorescence staining to detect the cell location and the target molecules' location of cells was performed as described in section 2.4.9. Cells were seeded into 8 or 16 well glass chamber slides to reach about 90% confluency. Cells were fixed and washed, then treated with a permeabilisation buffer before additional washing. Block the cells and add primary antibody and secondary antibodies. Secondary antibodies tagged with either FITC or TRITC, and DAPI for nuclear staining. laid over the slides, examined under a fluorescent microscope.

6.2.8 Statistical Analysis

In this chapter, *t*-tests, Mann-Whitney test, and one-way ANOVA test were performed using the Graphpad Prism 6 software. Image J software was used to analyse the PCR and western blotting bands. The results of the ECIS assay was analysed using the ECIS software. Differences were considered to be statistically significant when $p < 0.05$.

6.3 Results

6.3.1 The impact of HGF on the cellular behaviour of lung cancer cells

We carried out a series of *in vitro* function assay to determine the effect of HGF in the A549 and SKMES1 cells and whether the effect was regulated after knockdown of SIPA1 on the A549 and SKMES1 cells.

In vitro trans-well invasion assay was performed to investigate the effect of HGF on the invasion function of pEF-CT and SIPA1-knockdown A549 and SKMES1 lung cancer cell lines. Results showed that invasion potential was markedly increased after the treatment with HGF on the pEF-CT A549 and SKMES1 cells. After knockdown of SIPA1 in A549 and SKMES1 cells, the reaction of the invasion potential to HGF was reduced (**Figure 6.1**).

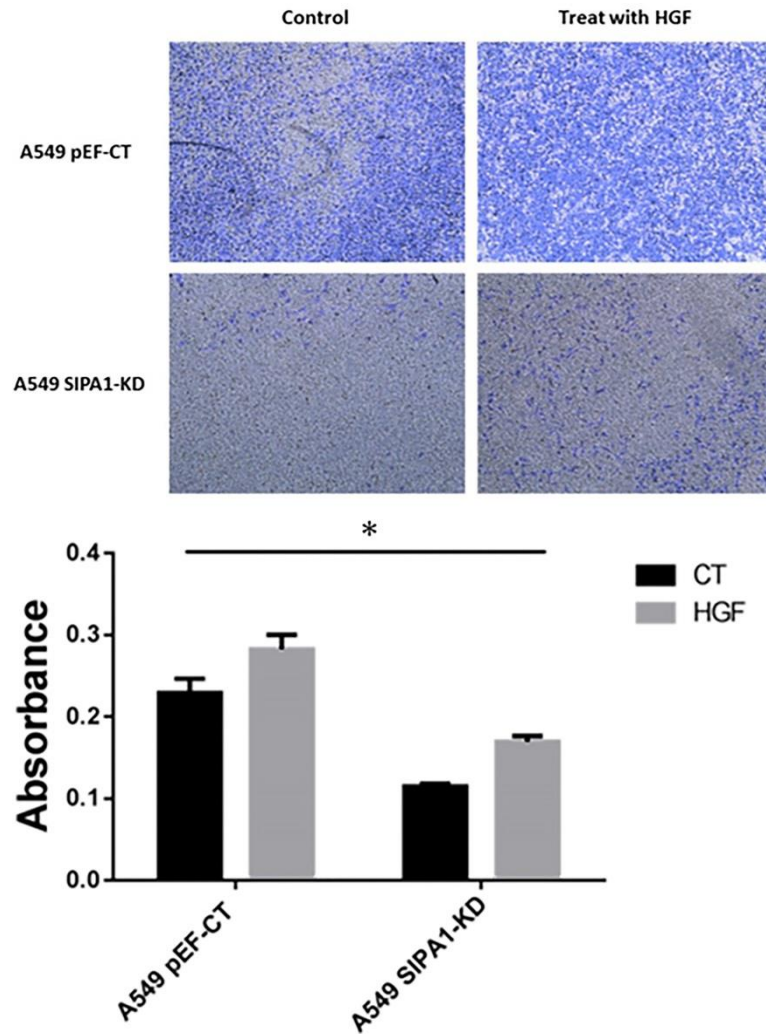


Figure 6.1: HGF increased the invasion potential of pEF-CT A549 cells, and knockdown of SIPA1 decreased invasion both in A549 pEF control and SIPA1 knockdown cells. Representative images of A549 invaded cells after staining (upper) and the absorbance measured by dissolving the crystal violet from stained invaded cells, bar graph shows the absorbance measured by dissolving the crystal violet from stained invaded cells. Error bars show Sd.

6.3.2 The impact of HGF on the barrier function of lung cancer cells

Electric cell-substrate impedance sensing (ECIS) assay was performed to measure the change of TJ function on lung cancer cells after treatment of HGF. The data from the ECIS assay showed HGF reduced the barrier function of the pEF-CT A549 cells, and the inhibitor of MET could counteract the effect of HGF on pEF-CT cells, and HGF did not reduce tight junction barrier function after knockdown of SIPA1 on A549 cells **(Figure 6.2)**.

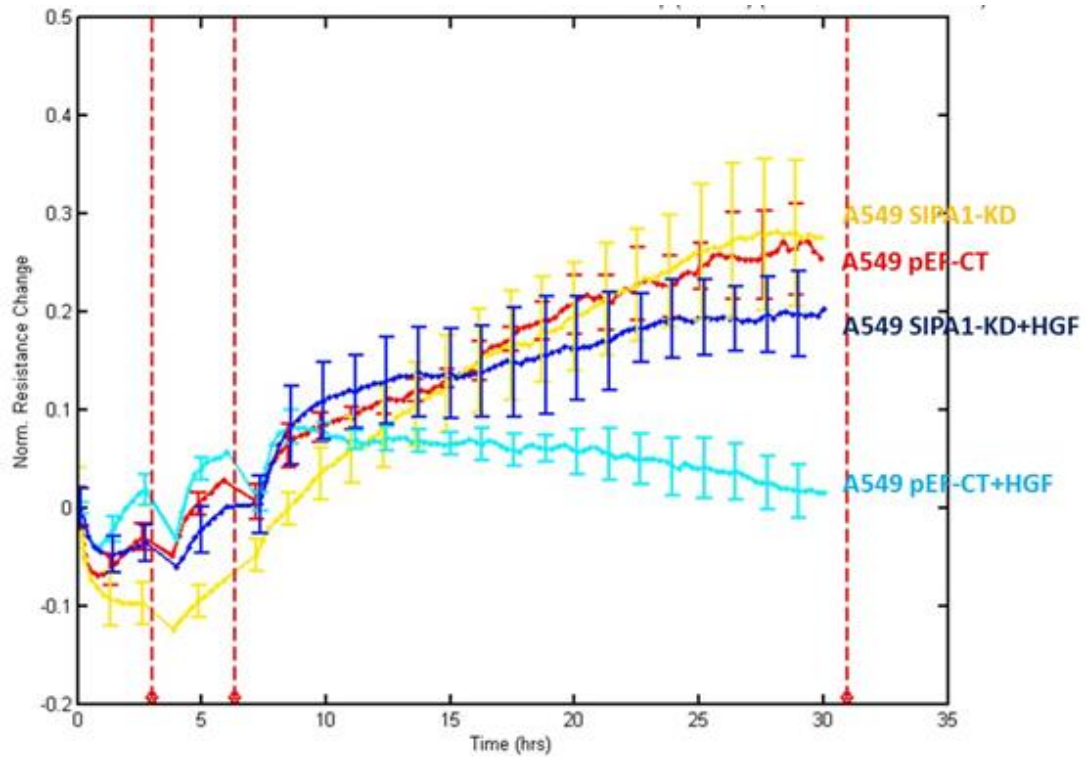


Figure 6.2 A: HGF decreases cell-cell tight junction function of A549 pEF-CT cells significantly, but did not decrease tight junction function of A549 SIPA1 knockdown cells. Graph indicates measurement of the change of resistance at the 1000Hz frequency to analyse cell resistance which can be used to assess to the function of tight junctions. First time point = wounding, second time point = treatment with HGF.

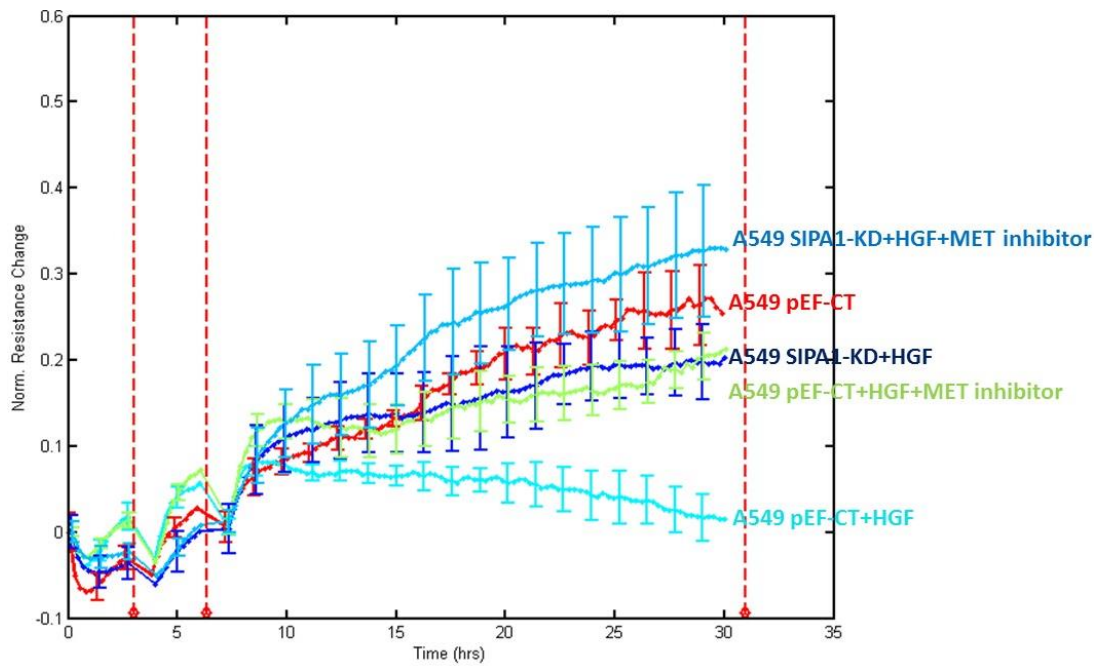


Figure 6.2 B: HGF decreases cell-cell tight junction function of A549 pEF-CT cells significantly, but did not decrease tight junction function of A549 SIPA1 knockdown cells and this effect produced a similar result as that achieved when using the MET inhibitor. The combination of SIPA1 knockdown and MET inhibitor could further prevent regulation of HGF on A549 cells. Graph indicates measurement the change of the resistance using 1000Hz frequency to analyse cell resistance resistance which can be used to assess to the function of tight junctions. First time point = wounding, second time point = treatment with HGF.

6.3.3 The interaction of SIPA1 and MET

To determine the role of SIPA1 in the HGF/MET signalling pathway, we first detected the expression level of MET in the control and SIPA1 knockdown A549 and SKMES1 cells. Both the results from the normal PCR and QPCR showed the transcript level of MET was not influenced by the knockdown of SIPA1 in A549 lung cancer cell lines, and in SK-MES1 lung cancer cell lines, QPCR showed the transcript level of MET was even higher in SIPA1-KD cells compared to pEF-CT cells (**Figure 6.3, 6.4**). Western blotting result showed that the protein level of MET was reduced in SIPA1 knockdown A549 and SKMES1 cells (**Figure 6.5, 6.6**). And the phosphorylation of MET was also reduced in SIPA1 knockdown cells (**Figure 6.7**).

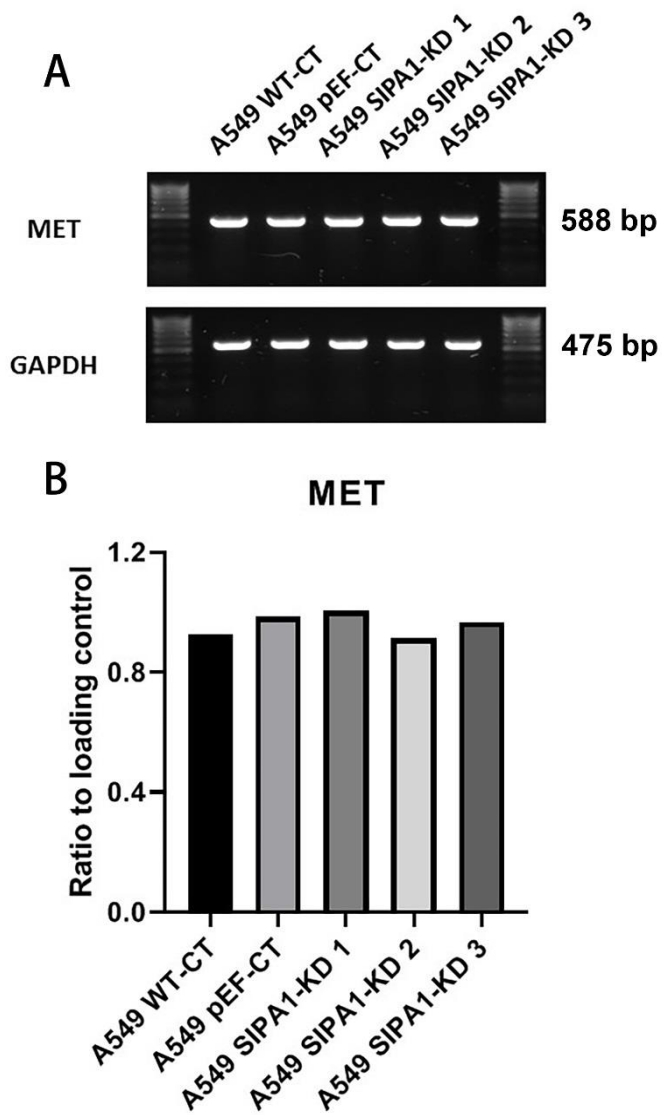


Figure 6.3: The mRNA level of MET was not regulated by the knockdown of SIPA1 in A549 lung cancer cell lines examined using conventional PCR. A. PCR bands of MET and GAPDH in the wide type control, pEF-control and SIPA1 knockdown cells. **B.** Quantitative analysis of the PCR bands.

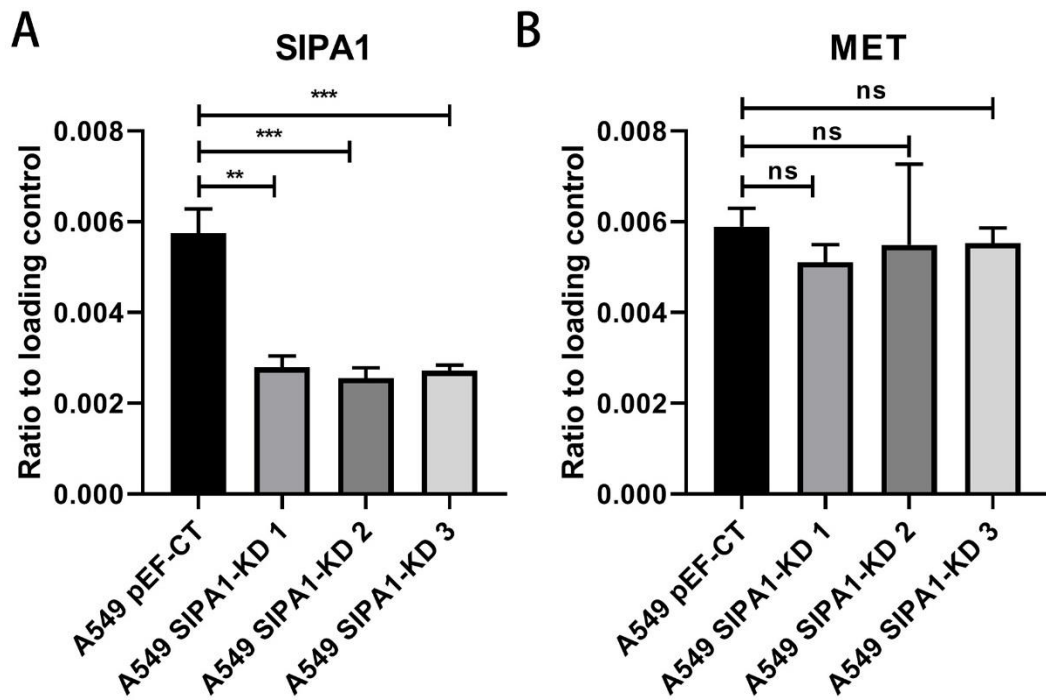


Figure 6.4 A: The mRNA level of MET was not regulated by the knockdown of SIPA1 in A549 lung cancer cell lines examined using QPCR. **A.** SIPA1 transcript level was reduced in SIPA1 knockdown cells significantly. **B.** MET transcript level was not changed in SIPA1 knockdown cells.

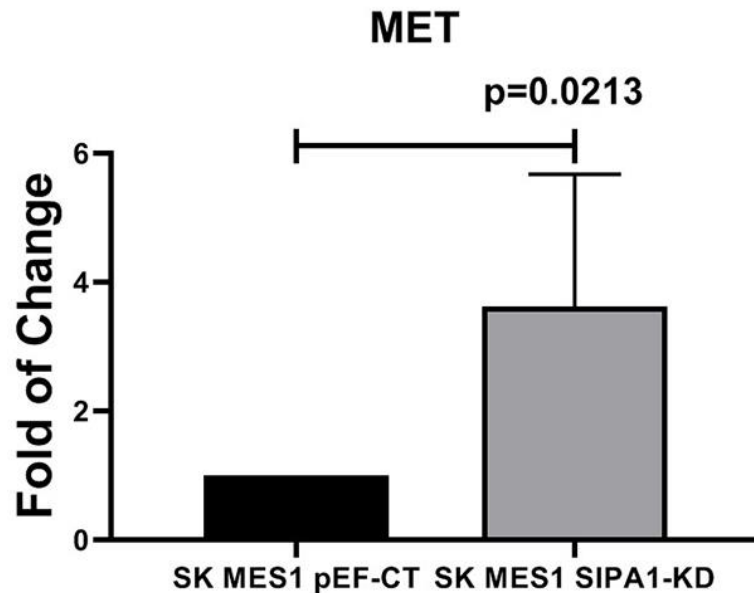


Figure 6.4 B: The mRNA level of MET was not regulated by the knockdown of SIPA1 in SK MES1 lung cancer cell lines examined using QPCR. MET transcript level was even improved in SIPA1 knockdown cells.

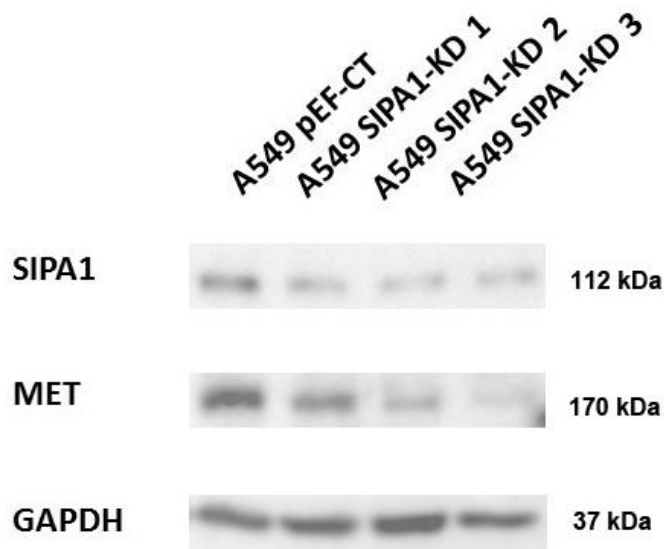


Figure 6.5: The protein level of MET was down regulated by the knockdown of SIPA1 in A549 lung cancer cell lines examined using western blotting. Figure showed the bands of SIPA1, MET and GAPDH in three repeated protein samples from SIPA1 knockdown A549 cells and one A549 pEF-CT sample.

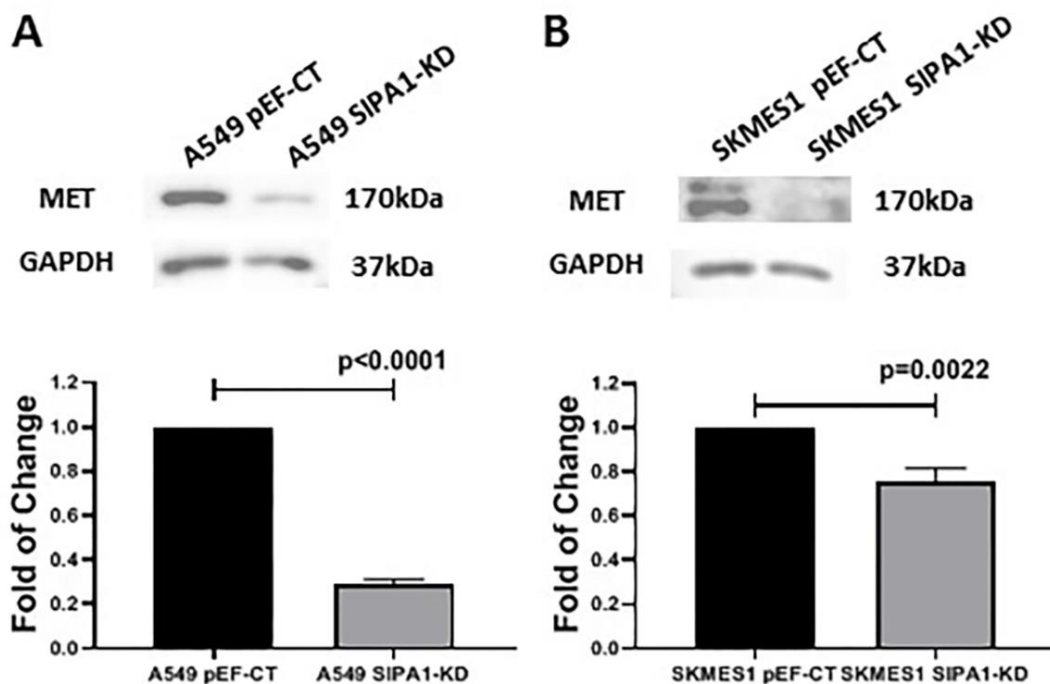


Figure 6.6: The protein level of MET was down regulated by the knockdown of SIPA1 in A549 and SKMES1 lung cancer cell lines examined using western blotting. The column shows ratio of MET to GAPDH as loading control in SIPA1-KD cells compared to pEF-CT cells in (A) A549 cell line and (B) SKMES1 cell line. Image J software was used to analyse the bands quantitatively. Error bars show SD.

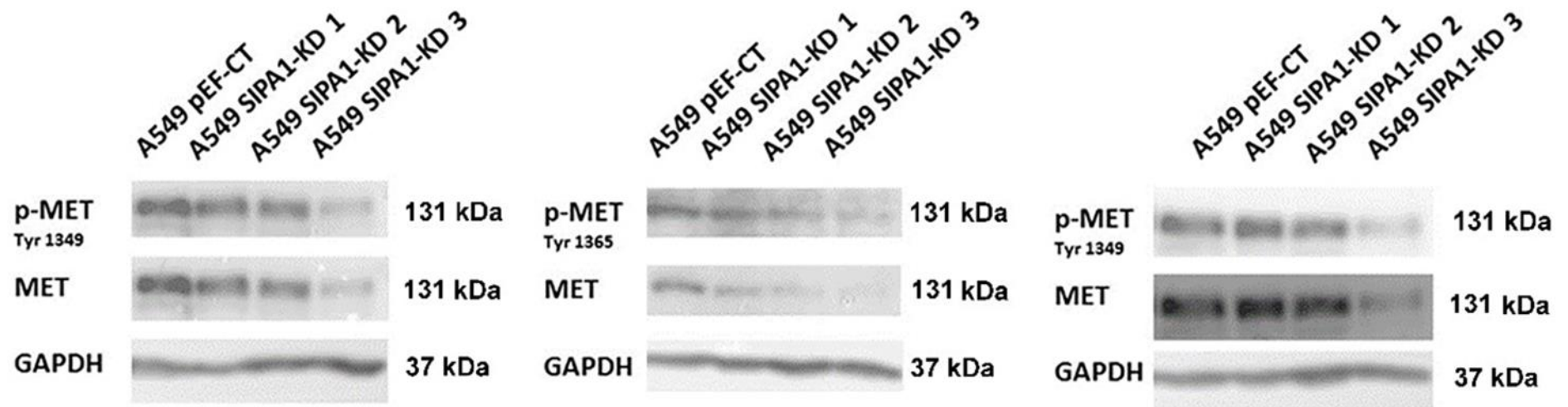
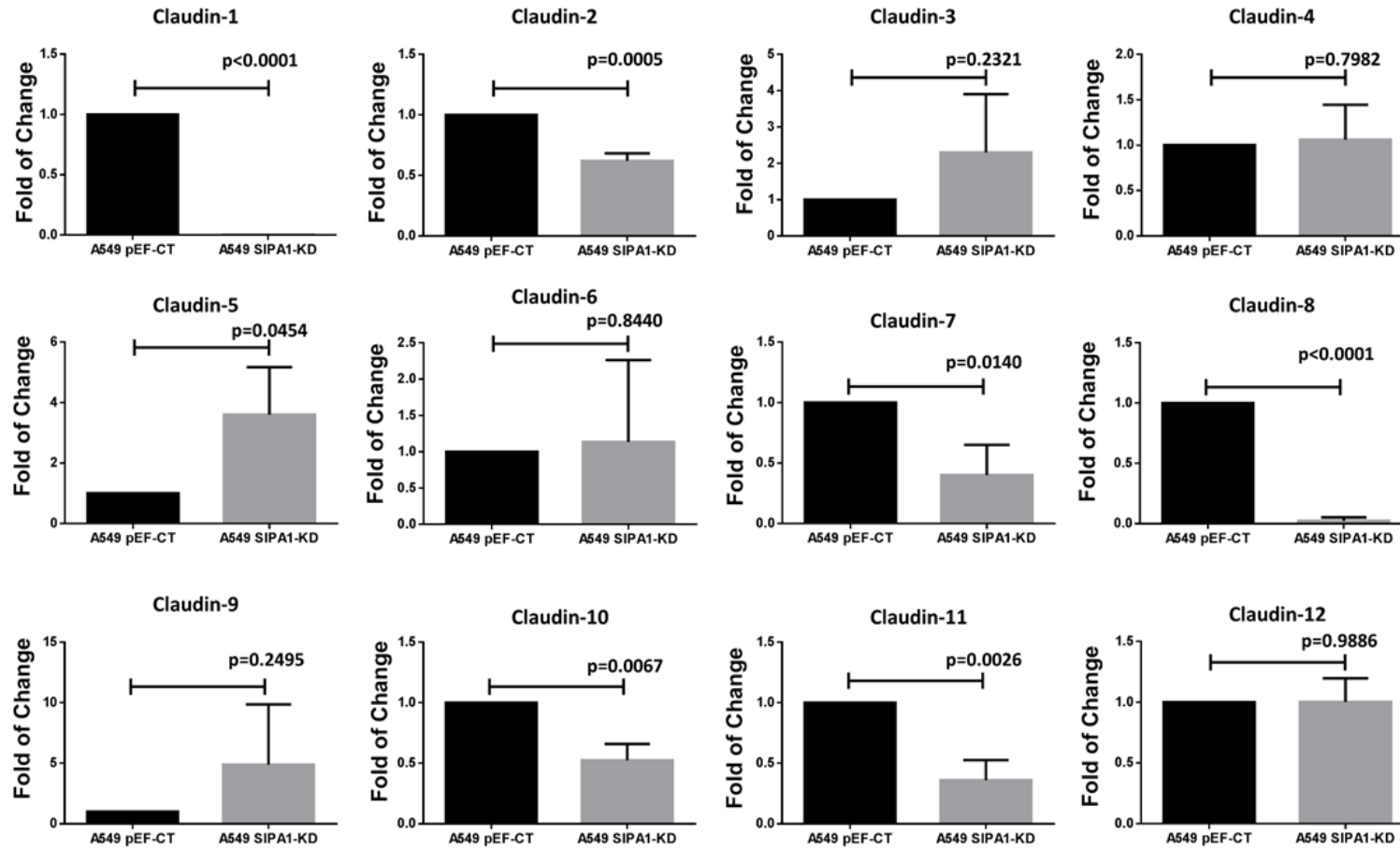


Figure 6.7: The phosphorylation level of MET was down regulated by the knockdown of SIPA1 in A549 lung cancer cell lines examined using western blotting. Figure showed the bands of MET, phosphor-MET and GAPDH in three repeated protein samples from SIPA1 knockdown A549 cells and one A549 pEF-CT sample. Three phosphorylation sites of MET were detected using different antibodies.

6.3.4 Impact of SIPA1 on the expression of TJ components

To begin exploring the potential relationship between SIPA1 and TJ components in A549 cells, QPCR aiming to investigate gene expression of the major TJ proteins was performed (**Figure 6.8**). Claudin1, Claudin2, Claudin7, Claudin8, Claudin10, Claudin11, Claudin14, Claudin17 from the Claudin family, constituting an important transmembrane TJ protein family, were statistically downregulated and Claudin5 was statistically upregulated in SIPA1 knockdown A549 cells. The effects of knockdown of SIPA1 on the JAM family or ZO family were not significantly significant. Whilst AF6 was upregulated, MUPP1 was downregulated significantly; both of these two proteins contain a PDZ domain. Marvel D3, binding protein belonging to TAMP family was statistically downregulated by knockdown of SIPA1, while the Occludin, another TAMP protein was upregulated by knockdown of SIPA1 in terms of transcript level.



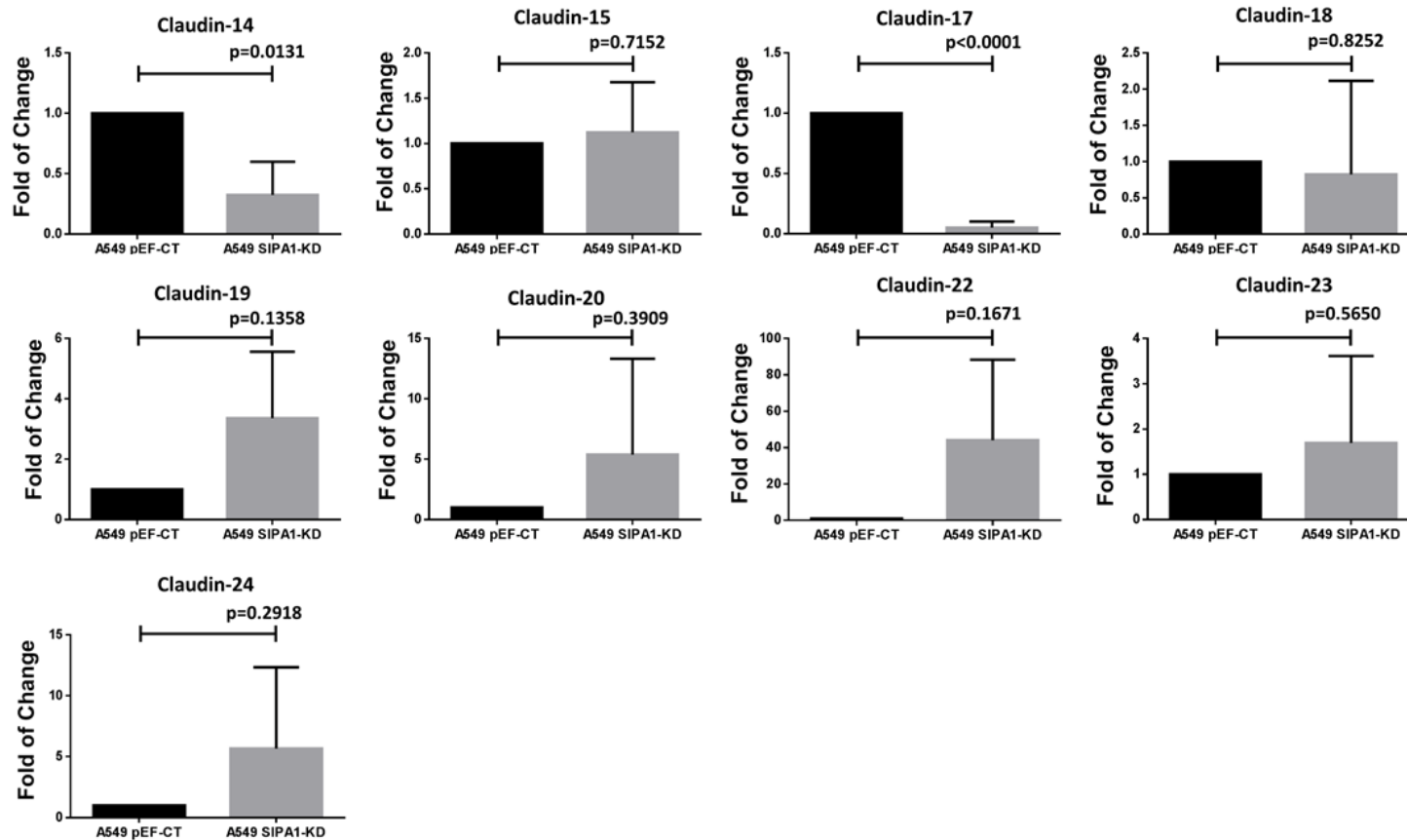


Figure 6.8 A: The effect of SIPA1 knockdown on gene expression of Claudin family in A549 cells. Gene expression was assessed using QPCR, expression was normalised to GAPDH and is shown as fold change relative to pEF control. Error bars show SD.

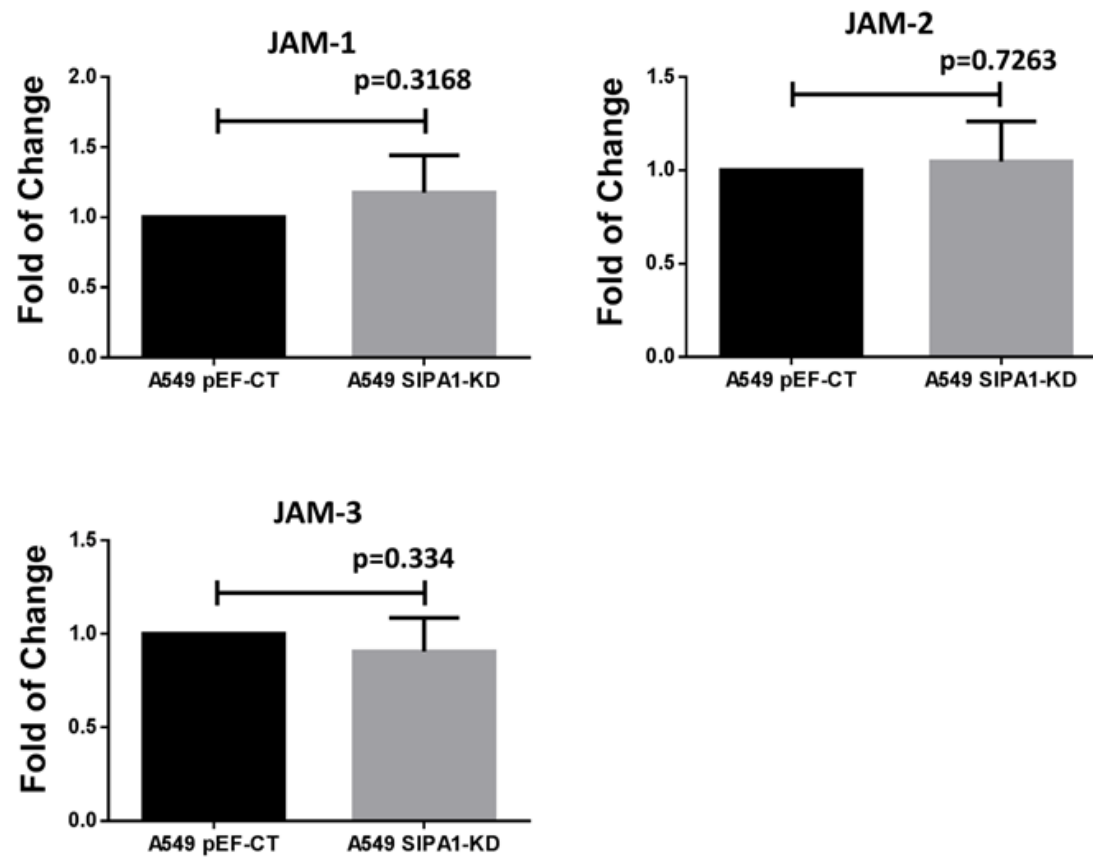


Figure 6.8 B: The effect of SIPA1 knockdown on gene expression of JAM family in A549 cells. Gene expression was assessed using QPCR, expression was normalised to GAPDH and is shown as fold change relative to pEF control. Error bars show SD.

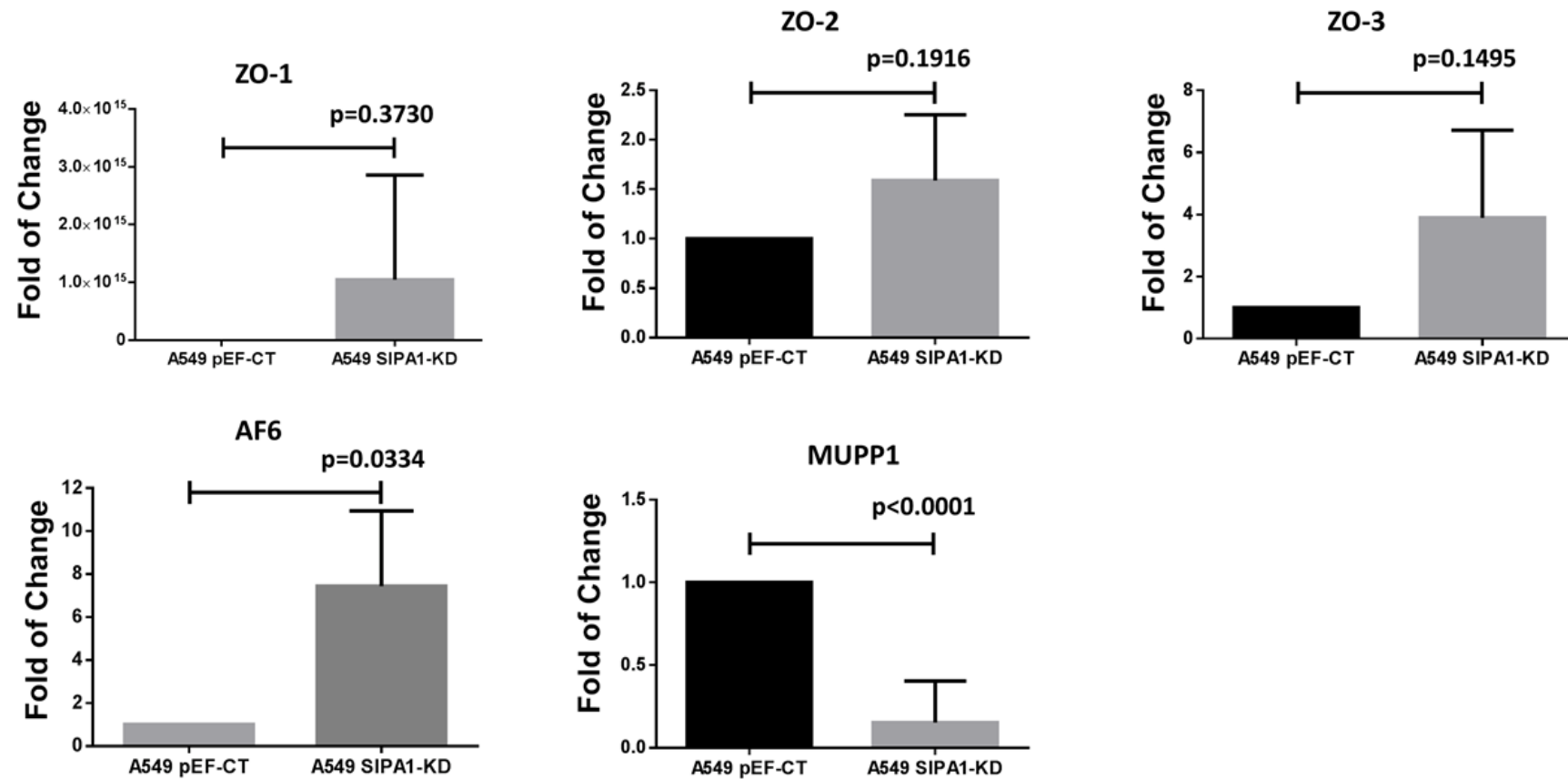


Figure 6.8 C: The effect of SIPA1 knockdown on gene expression of TJ proteins containing a PDZ domain in A549 cells. Gene expression was assessed using QPCR, expression was normalised to GAPDH and is shown as fold change relative to pEF control. Error bars show SD.

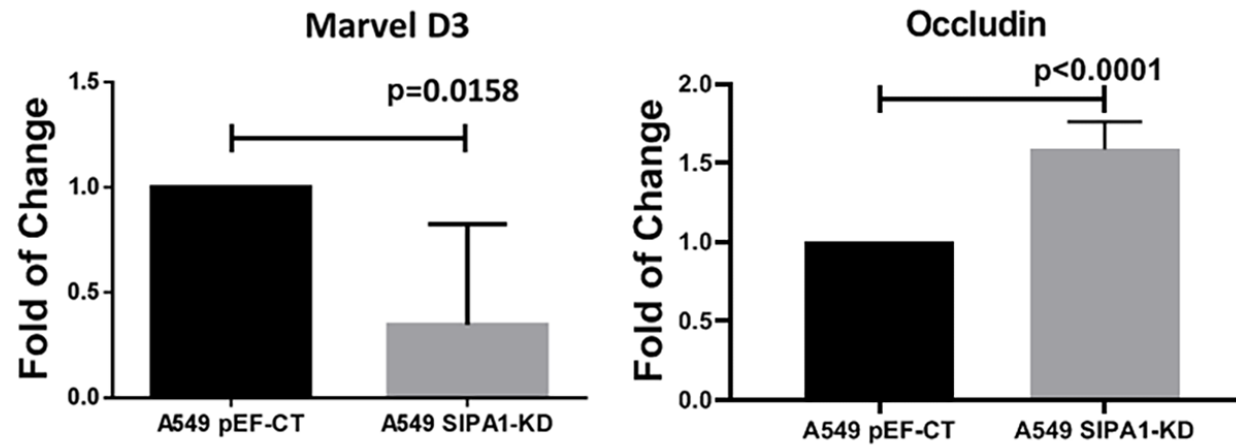


Figure 6.8 D: The effect of SIPA1 knockdown on gene expression of TAMP proteins in A549 cells. Gene expression was assessed using QPCR, expression was normalised to GAPDH and is shown as fold change relative to pEF6 control. Error bars show SD.

in SK MES1 cells, potential relationship between SIPA1 and TJ components was investigated using QPCR in transcript level (**Figure 6.9**). The knockdown of SIPA1 upregulated the transcript level of ZO family significantly with the same trend we found in A549 cells (**Figure 6.8 C**) (while the trend in A549 cells were not significantly). Whilst AF6 was downregulated with significantly significant, MUPP1 was upregulated; the trend of these two were not same with A549 cells. Both Marvel D3 and Occludin, binding protein belonging to TAMP family, were statistically upregulated by knockdown of SIPA1 in transcript level.

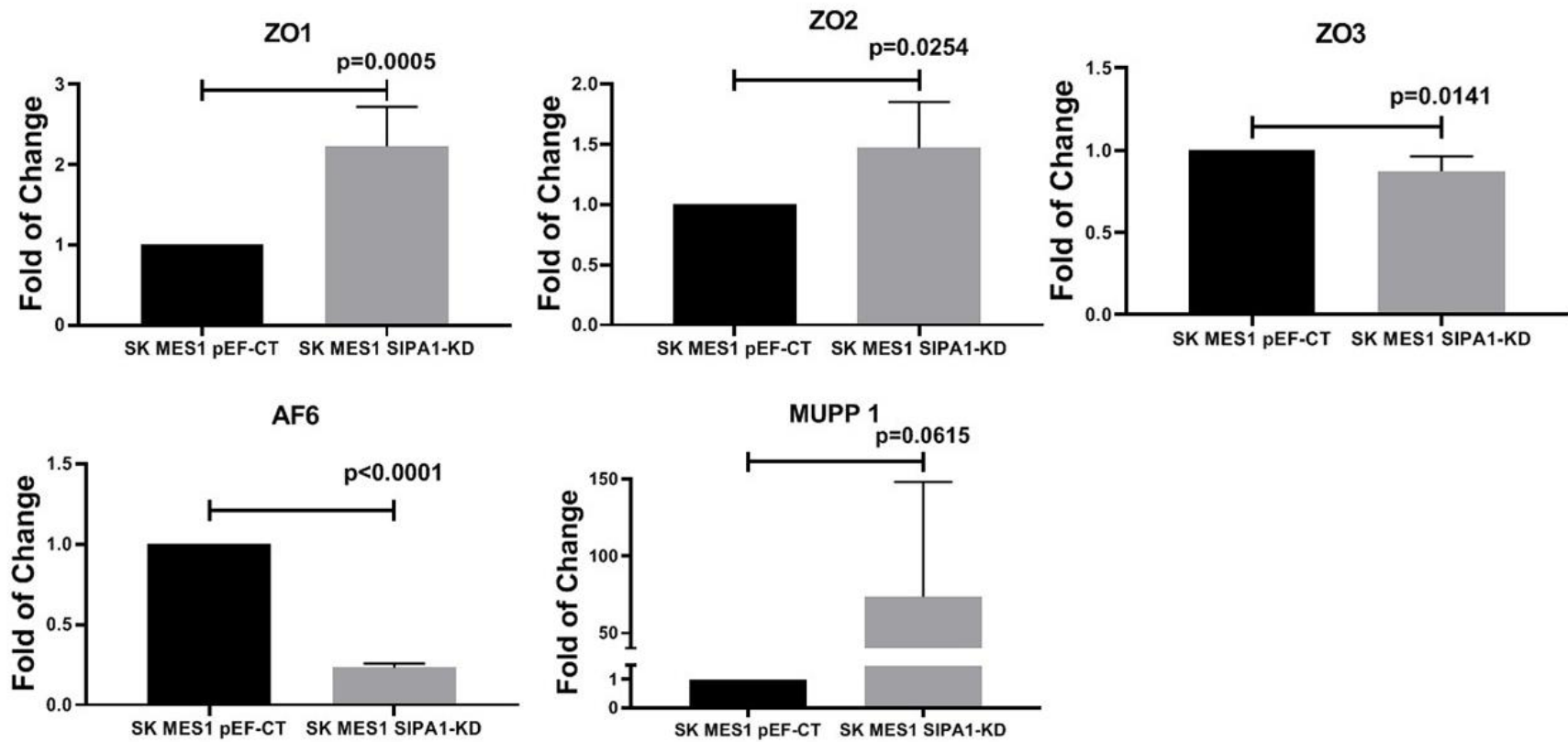


Figure 6.9 A: The effect of SIPA1 knockdown on gene expression of TJ proteins containing a PDZ domain in SK MES1 cells. Gene expression was assessed using QPCR, expression was normalised to GAPDH and is shown as fold change relative to pEF control. Error bars show SD.

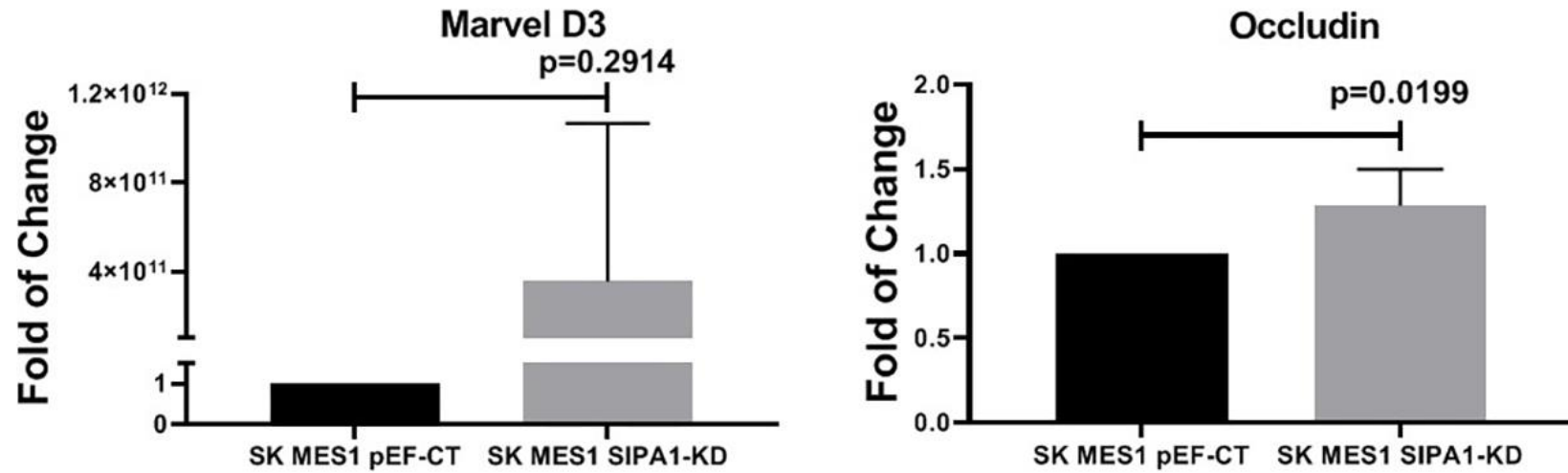


Figure 6.9 B: The effect of SIPA1 knockdown on gene expression of TAMP proteins in SK MES1 cells. Gene expression was assessed using QPCR, expression was normalised to GAPDH and is shown as fold change relative to pEF control. Error bars show SD.

Western blotting was performed to further investigate the potential relationship between SIPA1 and TJ components in A549 cells (**Figure 6.10, 6.11**). Claudin7, Claudin10 and Claudin15 protein levels were decreased by knockdown of SIPA1 in A549 cells, with the trend supporting the results of assessment at the mRNA level. The effect of knockdown of SIPA1 on the JAM family, Occludin and PDZ domain containing proteins was not significant. In CORL23 cells the effect of knockdown of SIPA1 on AF6 or ZO1 was not significant.

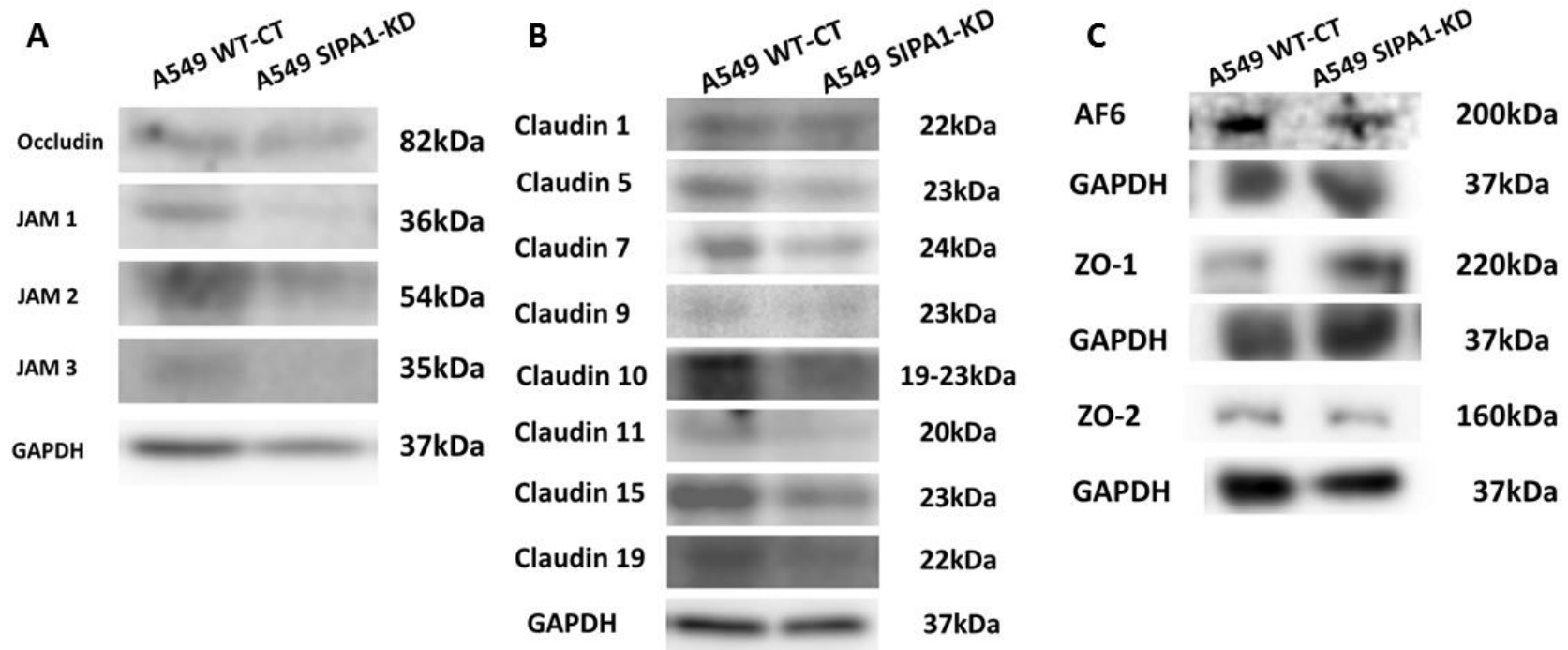


Figure 6.10: The effect of SIPA1 knockdown on expression TJ proteins in protein level in A549 cell line. Protein level of TJ proteins was assessed using western blotting, protein expression in SIPA1-KD cells was compared to pEF-CT cells. **(A)** The effect of SIPA1 knockdown on JAM family components. **(B)** The effect of SIPA1 knockdown on Claudin family components. **(C)** The effect of SIPA1 knockdown on AF6 and ZO family components.

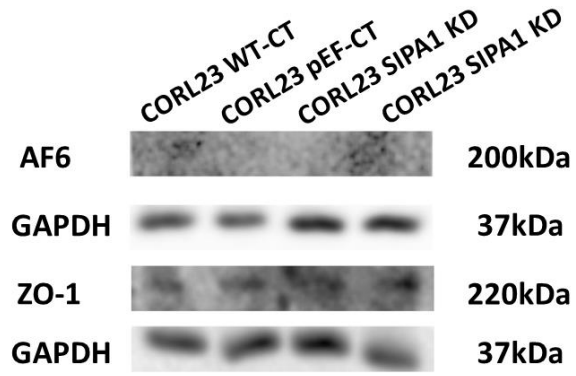


Figure 6.11: The effect of SIPA1 knockdown on expression of AF6 and ZO1 in protein level in CORL23 cell line. Protein level of TJ proteins was assessed using western blotting, protein expression in SIPA1-KD cells was compared to pEF-CT and WT-CT cells.

6.3.5 The impact of SIPA1 on the morphology of the cells and TJs

As we described, knockdown SIPA1 downregulated the tight junction based cell to cell barrier function, and numerous tight junction molecules were affected by knockdown of SIPA1 at the transcript level and/or protein level. Following this, we carried out immunofluorescence staining to further investigate the visible impact of SIPA1 on the cell morphology and tight junctions. ZO1 was chosen to stain in the A549 pEF-CT cells and SIPA1-KD cells. The immunofluorescence staining demonstrated that the intensity of ZO1 was strong in the pEF control cells but weak in the SIPA1 knockdown cells, and the tight junctions between cells were rather loose and spotty. In the control group, the cells were spread on the surface of the slides with strong and tight binding, but the SIPA1 knockdown cells were separated from each other with rather more isolated cells due to cell to cell association after tight junction disassembly (**Figure 6.12, 6.13**).

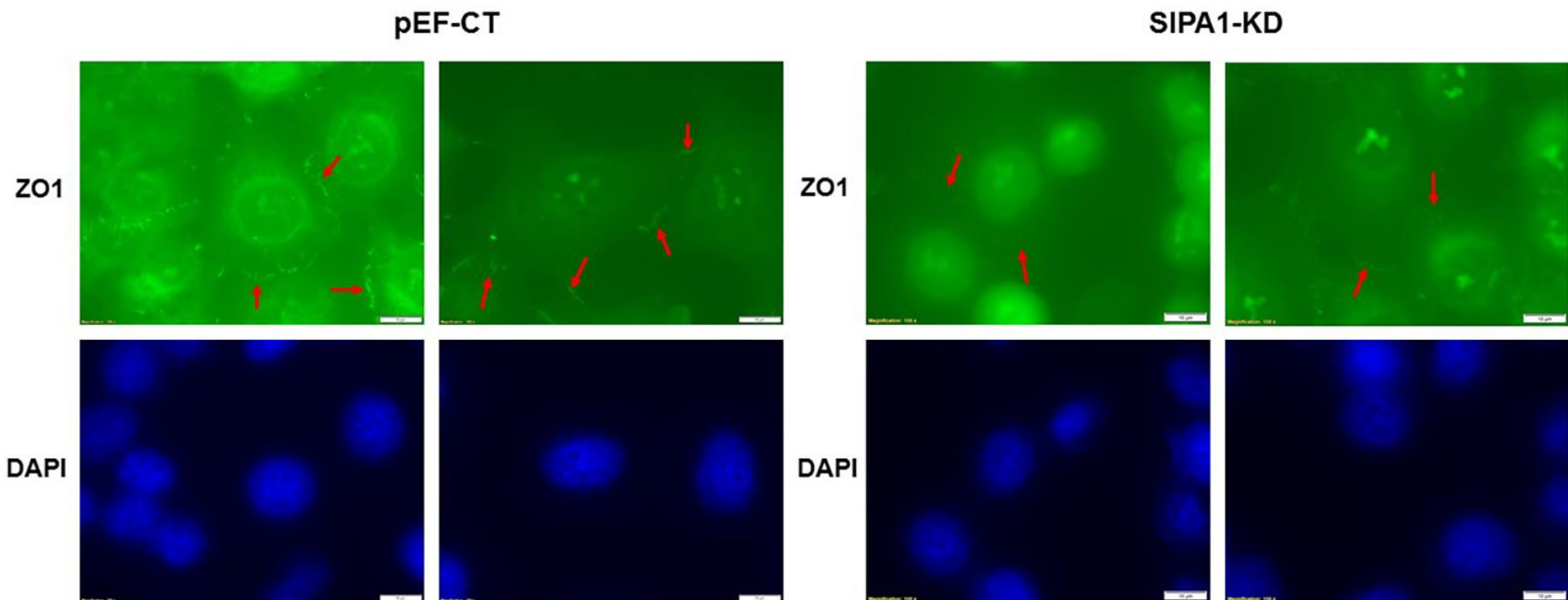


Figure 6.12: Immunofluorescence staining for ZO1 in A549 pEF-CT cells and SIPA1-KD cells. The pEF-CT cells have good ZO1 staining and tight junction integrity compared to the SIPA1-KD cells. The staining for ZO-1 in knockdown cells much reduced. Red arrows indicate the ZO1 staining indicating intact to tight junctions between cells. DAPI was used to show the nuclear staining. The bars correspond to 10 μ m.

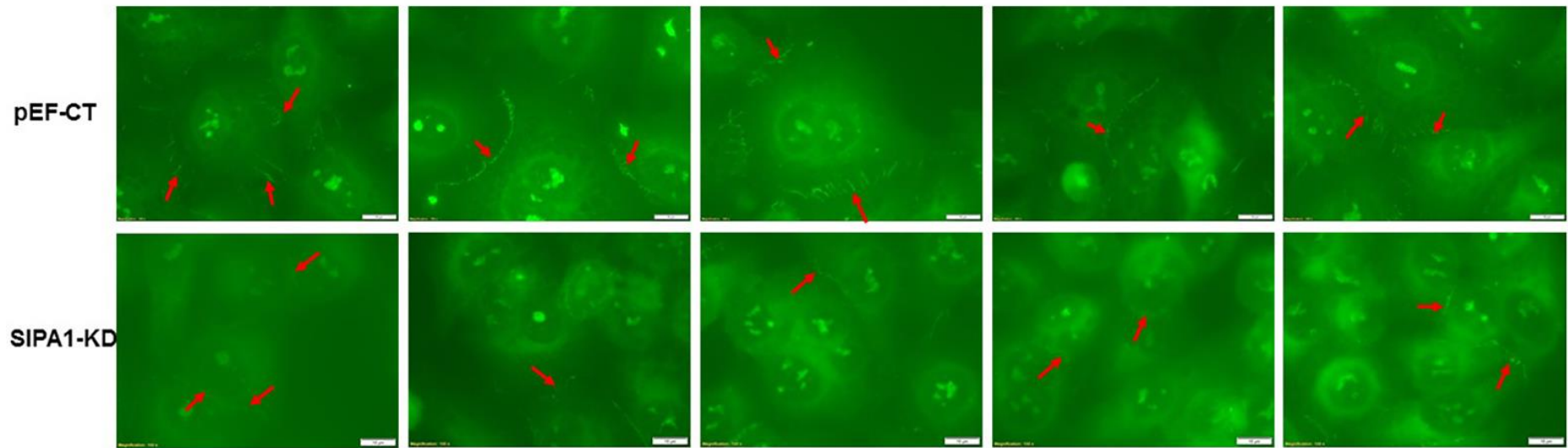


Figure 6.13: Typical images displaying the immunofluorescence staining of ZO1 in the A549 pEF-CT cells and SIPA1-KD cells. The pEF-CT cells have stronger ZO1 staining and tight junctions compared to the SIPA1-KD cells where the staining is much reduced of spotty. Red arrows indicate ZO1 staining indicating intact tight junctions between cells. The bars correspond to 10 μ m.

6.4 Discussion

In the previous chapters, an unanticipated finding from the present study was the highly significant correlation between SIPA1, HGF and MET in lung cancer tissues. This provides evidence at a tissue level of this important link, and to some degree is indicated in previous studies (Kurachi et al., 1997, Birchmeier et al., 2003b). It was also interesting to note that SIPA1 did not correlate with HGFL and its receptor, RON, which to a good degree argue the close link between HGF/MET. Similarly, to the results found in breast cancer, the promotion of invasion and the reduction of tight junctions by HGF in lung cancer cells also require the participation of SIPA1 (**Figure 6.1-6.2**). We also found that knockdown of SIPA1 decreased the reaction of lung cancer cells to HGF, which was similar to the MET targeted inhibitor Crizotinib. These results indicate that targeting SIPA1 could be a potential treatment for lung cancer patients with abnormal MET activity, amplification or mutation. However, as described earlier, the mechanism by which SIPA1 participates in the complex regulation of HGF/MET pathways is indefinite, and at which level SIPA1 is involved in the regulation of HGF/MET undefined explicitly. There exist dozens of approaches to the regulation of MET, such as transcriptional regulation, translational regulation, and phosphorylation, etc(Zhang and Babic, 2016). Previous research revealed SIPA1 could either bind to the promoter region and regulate the transcription in the nucleus, or directly act on the protein molecule to regulate its biological function (Zhang et al., 2015, Alsarraj et al., 2013). Here we found in lung cancer cells, transcription of MET was not regulated by SIPA1, the regulation of SIPA1 on MET was actually at the protein level, and both expression and phosphorylation level of MET are reduced after SIPA1 knockdown (**Figure 6.3-6.7**). This shows that in the regulation of MET, SIPA1 is not working as a transcription factor, but a regulator of MET at the protein levels, which includes two aspects. Firstly, the decreasing MET receptor reduces the number of targeted sites on the cell surface for HGF, which inhibits the HGF/MET signalling in the ligand/receptor binding level. Secondly, the downregulated phosphorylation of Tyr1349 and Tyr1356 makes MET lose its ability to provide a binding site for

downstream molecules, which silences the HGF/MET signalling by blocking downstream activation. These data largely explain how SIPA1 regulates the HGF/MET signalling pathway.

Simultaneously, SIPA1 decreased TJ function in lung cancer, so QPCR and western blotting were performed to detect the effect of SIPA1 on gene transcription and protein expression of TJ components. At the mRNA level, Claudin1, Claudin2, Claudin7, Claudin8, Claudin10, Claudin11, Claudin14 and Claudin17 from the Claudin family were downregulated after knockdown of SIPA1, as well as MUPP1 which contains a PDZ domain. Claudin5 and another PDZ domain containing protein, AF6 were upregulated. Previous studies showed that SIPA1 also contains a PDZ domain (Hattori, 2011) and several TJ markers such as ZO1, ZO2, AF6, MAGI1, MAGI2, MAGI3, PAR3, PAR6 and MUPP1 all contain a PDZ domain (Martin and Jiang, 2009). These proteins all constitute the plaque or anchoring function for TJs and link the transmembrane components with the signalling mechanism of the cell. The IF staining result showed that ZO1 was strong in the pEF control cells but weak in the SIPA1 knockdown cells, and knockdown of SIPA1 loose the tight junctions between cells. These all suggest that SIPA1 could be a potential regulator of TJs. Previous studies also showed that SIPA1 co-localised with AF6 in Hela cells (Su et al., 2003) and that AF6 could bind to ZO1 in MDCK2, Rat1 and PC12 cells (Yamamoto et al., 1997). Thus, we may have a conclusion indicating that the mechanism of SIPA1 regulating TJs in lung cancer may be via the interaction between SIPA1 and AF6 or ZO1.

Therefore, we can conclude that in lung cancer cells, HGF binds to the MET receptors on the cell surface, reducing the cell to cell tight junctions via acting on the regulating components of TJs such as AF6 and ZO family. This process requires the presence of SIPA1 to maintain the MET expression at a rather high level, which make sure that there exist sufficient MET receptors on the surface of lung cancer cell membrane to acquire adequate respond to the stimulation of HGF.

**Chapter-7 The key molecules
regulated by the interaction of
SIPA1 with HGF/MET signalling
pathway in human lung cancer
cells**

7.1 Introduction

In the previous chapter 5 and 6, we summarized the interaction mechanism of SIPA1 and HGF/MET signalling pathway: the high expression of SIPA1 in lung cancer cells maintains a high level of MET. As a result, the cells obtain a higher response to HGF stimulation, which enhances the ability to invade and proliferate, and reduces the tight junction-dependent barrier function through the regulation on AF6 and ZO families. Focusing on the regulation of SIPA1 on the protein level of MET, we further investigated the changes of other key molecules brought by the interaction of SIPA1 with HGF/MET signalling pathway.

Growth factor receptor bound protein 2 (Grb2) is a 25 kDa adaptor protein, which is a 217 amino acid sequence with a Src homology 2 (SH2) domain and two Src homology 3 (SH3) domains. Grb2 works as an intermediate linker between the activated receptors on the cell membrane surface and downstream targets through the SH2 and SH3 domains. Downstream of the MET signalling, activated MET has phosphorylated tyrosine residues Tyr1234 and Tyr1235 in the catalytic region, which could phosphorylate the Tyr1349 and Tyr1356 tyrosine residues in the C-terminal docking site, providing the docking site for the SH2 domain of Grb2. Meanwhile the SH3 domain of SH3 could recruit other key molecules such as SOS, leading the activation of Ras mediated PI3K/PDK/Akt signalling pathway and RAF/MEK/ERK signalling pathway (Ijaz et al., 2018).

Suppressor of cytokine signalling (SOCS) protein family includes SOCS1-7 and CIS (cytokine-inducible SH2-containing protein), which are the essential components that regulate RTK signalling. All the SOCS proteins contain a SH2 domain which could also be recruited by the phosphorylated Tyr1349 and Tyr 1356 tyrosine residues in the docking site of MET. Expression of the SOCS family is enhanced by RTKs signalling. Nevertheless once SOCS proteins bind to the RTKs, the RTKs are silenced by the interaction (Yoshimura et al., 2007, Kile and Alexander, 2001). The RTKs downstream JAK/STAT signalling was confirmed to be suppressed by SOCS family (Kazi et al., 2014).

The protein kinase C (PKC) family consists of a series of serine/threonine kinases with conserved structures. PKC family are involved in a group of metabolic processes and implicated in multiple signal transduction networks (Isakov, 2018).

Although knockdown SIPA1 decreased MET at the protein level, the mechanism by which SIPA1 is involved during the procedure of the generation and degradation of MET receptor protein needs to be explained. As stated previously, Grb2, SOCS family proteins and PKC are involved in the internalization and recycling of MET (Viticchiè and Muller, 2015). In the initial stages of internalization and recycling, docking tyrosine Tyr1349 and Tyr 1356 are activated to recruit related molecules, in which Grb2 is involved to enhance the recruitment effect. A crucial molecule in internalization is Cbl (Castias B-lineage lymphoma), which is an E3 ubiquitin ligase responsible for MET ubiquitination, and Grb2 is confirmed to be required for Cbl-dependent MET internalization and endocytosis (Hausser et al., 2002, Zhang and Babic, 2016). The SH2 domain of SOCS binds to the Met protein while its SOCS box recruits the E3 ubiquitin, leading to MET ubiquitination and internalization (Gui et al., 2011). PKC is a major molecule in the progress from MET internalization to the formation of endosomes (Viticchiè and Muller, 2015). Therefore, in this chapter we further examined the expression of Grb2, SOCS family, and PKC proteins after SIPA1 knockdown in lung cancer cells, and further investigated whether MET internalization and recycling were regulated by SIPA1.

7.2 Materials and methods

7.2.1 Primary and secondary antibody

The name, molecular weight, supplier, and the product code of the primary and secondary antibodies used in this chapter is shown in **Table 2.5**.

7.2.2 Protein extraction, SDS-PAGE, and western blot analysis

The extraction of protein was carried out as the description in section 2.5.1. Proteins were extracted using lysis buffer and then quantified using the Bio-Rad DC Protein Assay kit (Bio-Rad Laboratories, Hemel-Hempstead, UK). After separation in the SDS-PAGE gel, proteins were transferred onto PVDF membranes as described in section 2.5.2. The membranes with protein were subsequently blocked and probed with various primary antibody and a corresponding peroxidase-conjugated secondary antibody. The antibodies' information in this study is shewed in **Table 2.5**. Finally, the protein bands on the membrane were visualised using the chemiluminescence detection kit (Luminata, Millipore).

7.2.3 Statistical Analysis

In this chapter, *t*-tests, Mann-Whitney test, and one-way ANOVA test were performed using the Graphpad Prism 6 software. Image J software was used to analyse the PCR and western blotting bands. Differences were considered to be statistically significant when $p < 0.05$.

7.3 Results

In order to investigate whether the internalization and recycling of MET is regulated by SIPA1, we have selected a series of molecules that have been shown by previous studies to regulate the internalization and recycling of MET. Grb2, suppressor of cytokine signalling (SOCS) protein family, and protein kinase C Mu (PKC μ) were examined in A549 and SKMES1 SIPA1-KD cells using western blotting compared to pEF-CT cells. **Figure 7.1** shows the expression of Grb2 was downregulated by SIPA1 knockdown in A549 and SKMES1 cells. **Figure 7.2** shows the expression of most SOCS family was inhibited by SIPA1 knockdown in A549 and SKMES1 cells. **Figure 7.3** shows PKC μ was down regulated by SIPA1 knockdown in A549 and SKMES1 cells.

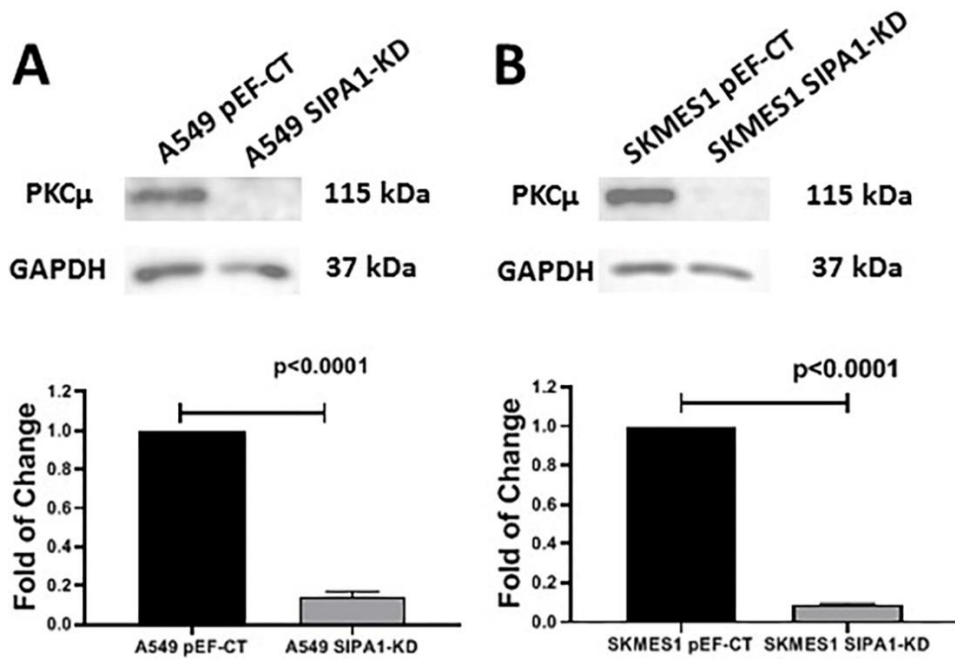


Figure 7.1: The protein level of PKC μ is down regulated by the knockdown of SIPA1 in A549 and SKMES1 lung cancer cell lines examined using western blotting. The column shows ratio of PKC μ to GAPDH as loading control in SIPA1-KD cells compared to pEF-CT cells in **(A)** A549 cell line and **(B)** SKMES1 cell line. Image J software was used to analyse the bands quantitatively. Error bars show SD.

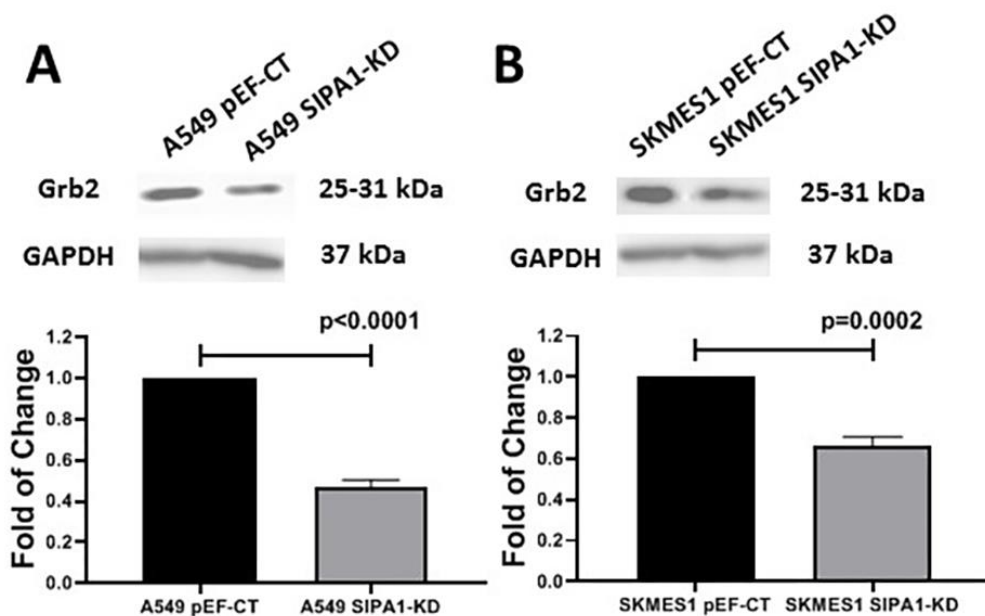


Figure 7.2: The protein level of Grb2 is down regulated by the knockdown of SIPA1 in A549 and SKMES1 lung cancer cell lines examined using western blotting. The column shows ratio of Grb2 to GAPDH as loading control in SIPA1-KD cells compared to pEF-CT cells in **(A)** A549 cell line and **(B)** SKMES1 cell line. Image J software was used to analyse the bands quantitatively. Error bars show SD.

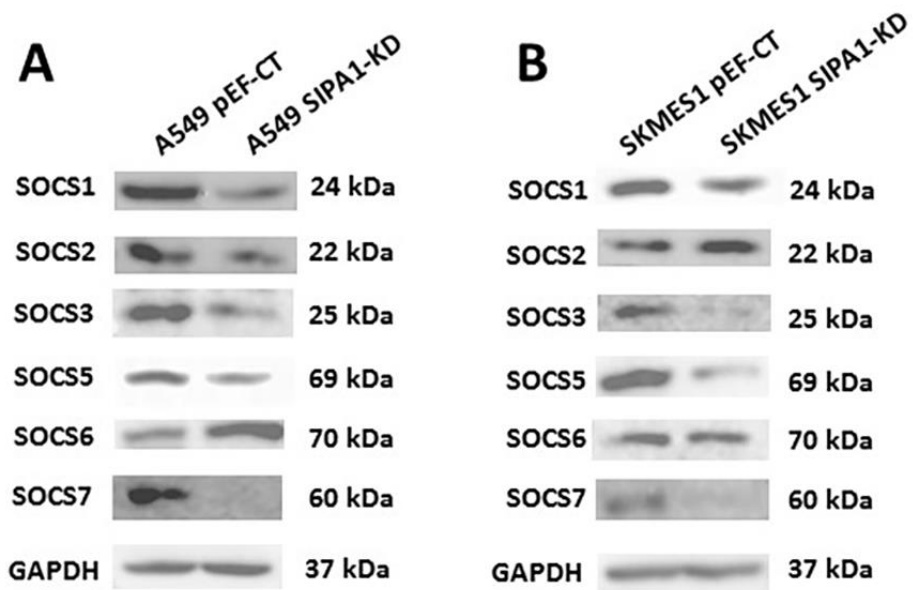


Figure 7.3: The protein level of SOCS family in A549 and SKMES1 lung cancer cell lines examined using western blotting. The overall level of SOCS family is down regulated by the knockdown of SIPA1 in **(A)** A549 and **(B)** SKMES1 lung cancer cell lines.

7.4 Discussion

As stated in the introduction, Grb2, PKC μ , and the SOCS 1-7 have all been shown to play key roles in MET internalization and recycling. Grb2, as the most direct recruitment factor of MET, can recruit Cbl to bind with MET and promote ubiquitination of MET, which could be regarded as one of the initial factors of MET internalization. The SOCS family together with MET form the SOCS box, with the ability to recruit E3 ubiquitin to promote MET internalization. PKC ensures that internalized METs form internal endosomes, which can then be recycled to the surface of the cell membrane instead of being degraded. In this chapter, we found Grb2, PKC μ , and some of the SOCS family members (SOCS1, 3, 4, 7) are all down regulated in SIPA1 knockdown lung cancer A549 and SKMES1 cells compared to pEF control cells. These results indicate that in lung cancer cells, SIPA1 works as a promoting factor for MET internalization and recycling. Without the participation of SIPA1, the recycling of MET will be suppressed. This could be the potential approach by which SIPA1 regulates the MET receptor at the protein level.

Chapter-8 General discussion

8.1 The aims of the thesis

Independently of region, lung cancer is the leading cause of malignant tumour death. Although in the past decades, basic research and clinical trial on lung cancer have developed rapidly, the prognosis of lung cancer is still not ideal and metastatic lung cancer which has a poor prognosis and limited treatment options. This is largely due to the inadequate understanding of the mechanisms of development and metastasis of lung cancer. Extensive evidence has suggested that the HGF/MET signalling pathway is essential in lung cancer tumorigenesis and progression via the alteration of cell apoptosis, growth, migration, morphology and motivation. MET can be regarded as one of the driving oncogenes in lung cancer and the cause of drug resistance to EGFR TKIs (Trusolino et al., 2010). Based on previous research results in the host lab, we selected SIPA1 as a potential modulator of the HGF/MET signalling pathway. Therefore, this thesis aimed to evaluate the interaction mechanism of SIPA1 and HGF/MET, as well as their influence on lung cancer in terms of molecular activation, cellular behaviour and clinical relevance.

8.2 Influence of SIPA1 on the function of lung cancer cells

Gradually, more and more studies indicate the importance of the TJ in cancer metastasis. The function of the TJ is not only maintaining the formation of basic structure of local tissue, but also to extracellular signal transduction, maintenance of cell morphology, and participation in intracellular signalling pathways (Martin, 2014). SIPA1 has been shown to work as a driving factor in a variety of tumours, such as breast, gastric, cervical, OSCC, colorectal, and prostate cancer (Takahara et al., 2017, Li et al., 2017, Yi and Li, 2014, Pei et al., 2013, Ji et al., 2012, Shimizu et al., 2011). The potential of SIPA1 in regulating TJs was also confirmed in breast cancer and prostate cancer in the host lab (Jiang, 2013, Jiang, 2006). Aiming to find out the regulation of SIPA1 on the function of lung cancer cells, we performed a series of functional assay in this project. In this current study, the TJ function of the cells was

assessed using ECIS analysis, and TER analysis, all of which demonstrated that TJs of lung cancer cells were enhanced by SIPA1 knockdown. TJ is seen as the first obstacle to overcome in the process of cancer metastasis. More than this, after overcoming the barrier function, SIPA1 also enhanced the ability of lung cancer cells to invade and proliferate, providing necessary conditions for further spread and metastasis of lung tumour cells after breaking through the barrier into adjacent stromal tissues. Therefore, we can consider that SIPA1 is a crucial driving force for the development and metastasis of lung cancer with the potential to promote proliferation and invasion, as well as reduce the TJs of lung cancer cells.

8.3 Influence of SIPA1 interaction with HGF/MET on the function of lung cancer cells

The effect of the HGF/MET signalling pathway on breast cancer cells requires the presence of SIPA1 (Jiang, 2013, Jiang, 2006). Likewise, in our current study, we found that knockdown of SIPA1 reduced the response of lung cancer cells to HGF in terms of invasion and barrier function. HGF enhanced the invasion of pEF control cells, while the enhancement could be blocked by SIPA1 knockdown. HGF decreased the barrier function of lung cancer cells, which was counteracted by SIPA1 knockdown was similar to the small molecule MET targeted inhibitor. Since knockdown of SIPA1 has a similar outcome to pharmacological MET inhibition on blocking the regulation of HGF signalling on tight junctions, we assume that SIPA1 could have some potential interaction with MET.

8.4 Intracellular interaction between SIPA1 and MET signalling pathway

The mechanism of interaction between SIPA1 and MET is an important issue to be determined in this thesis. We analysed SIPA1 gene expression correlation in the Peking lung cancer cohort and the TCGA database, and the results showed that SIPA1 is highly correlated with key markers in HGF/MET signalling pathways and TJ

components. At the same time, protein phosphorylation array revealed that SIPA1 is involved in the regulation of complex signal transduction and RTK activation. This confirms what we have described previously - that SIPA1 and MET interact to affect changes in cell barrier function. It is known that the regulation of RTKs is an extremely complicated process involving multiple signalling pathways. Although protein array analysis has shown us that there exists a co-relationship between SIPA1 and RTKs family to which MET belongs, the specific mechanism of interaction requires to be further demonstrated. However, the protein expression level of MET was suppressed by SIPA1 knockdown detected by western blotting, which made the cell surface lack sufficient MET receptors to transmit extracellular HGF signals. At the same time, the level of MET phosphorylation is also affected by the knockdown of SIPA1. The phosphorylation status of key sites of the MET receptor's domain used to anchor downstream molecules is inhibited, limiting the function of MET to down-stream transmission signals.

8.5 Influence of SIPA1 on the regulation of MET receptor

As mentioned in Chapter 1 and Chapter 5, MET regulation involves more than a dozen different processes from transcription to degradation, which include MET oncogene mutations, MET gene methylation, transcription factors regulation, alternative splicing, microRNAs regulation, MET translational regulation, proteolysis of MET, glycosylation and phosphorylation on MET, internalization, degradation and recycling of MET, nuclear localization of MET, and autoregulation of MET. We have proved that SIPA1 can regulate the expression of MET, but the specific process (or processes) by which SIPA1 acts is still one an area for future study. We selected some key regulatory molecules during the MET recycling process such as Grb2, SCOS, and PKC μ for further analysis. WB results for these molecules showed that the protein expression of these molecules decreased after SIPA1 knockdown. In previous publications, Grb2, SCOS, and PKC μ all promoted internalization of MET, leading the process towards recycling to the membrane rather than degradation

(Viticchiè and Muller, 2015). Knockdown of SIPA1 decreased the expression of these molecules which could be the potential approach to regulate MET receptors. Therefore, we can conclude that in lung cancer cells, the presence of SIPA1 promotes the recycling of MET via Grb2, SCOS, and PKC μ , maintaining the MET receptor at a rather high level, thereby further transmitting the HGF signal into the cells.

8.6 Influence of SIPA1 interaction with HGF/MET on tight junction components

Therefore, the findings in Chapter 4 and Chapter 7 strongly suggest that the expression of SIPA1 in lung cancer cells is closely related to the expression of TJ molecules and the cell's barrier function. Gene expression correlation analysis showed us the potential regulatory effect of SIPA1 on TJs. We analysed data from our Peking cohort and the TGCA database. The components of tight junction proteins that are highly correlated with expression SIPA1 include JAM1, JAM2, ZO family, OCLD, Marvel D2, Marvel D3, NECTIN2, and CLDN4, CLDN7, CLDN12, and CLDN15, which are proven in at least one database. QPCR and/or western blotting demonstrated that Claudin1, Claudin2, Claudin7, Claudin8, Claudin10, Claudin11, Claudin14 and Claudin17 from the Claudin family, and MUPP1 which contains a PDZ domain were downregulated after knockdown of SIPA1. Claudin5, and PDZ domain containing protein AF6 and ZO family proteins were upregulated in SIPA1 knockdown cells compared to pEF control cells. Previous studies showed that SIPA1 contains a PDZ domain (Hattori, 2011), and other TJ markers such as the ZO family, AF6, MAGI1, MAGI2, MAGI3, PAR3, PAR6 and MUPP1 all contain a PDZ domain (Martin, 2014, Martin and Jiang, 2009). PDZ domain is the binding site for those molecules. SIPA1, AF6, and ZO family all contain the PDZ domain, which could be the potential regulation site at the molecular level. And AF6 and ZO family should be the regulation point for SIPA1 to regulate the tight junction

8.7 Clinical relevance of SIPA1

Firstly, the transcriptional expression level of SIPA1 is higher in cancer than adjacent normal tissue or normal tissue. In this thesis we examined SIPA1 expression transcriptional level in the Peking clinical cohort, which consists of 148 lung tumour tissue samples with 148 adjacent normal tissue samples, and 139 tumour tissues which were paired to the cancer tissue. SIPA1 transcript levels were high in 148 tumour tissues compared with both normal tissue ($p=0.0141$) and paired normal tissue ($p=0.0358$). The IHC staining score of the lung tumour TMA lacks statistical significance. The protein level of SIPA1 in tumour tissue samples was higher than that in normal lung tissue and adjacent normal lung tissue, but the difference was not statistically significant. There may be inconsistencies between SIPA1 gene transcripts and SIPA1 protein analysis. As previously discussed, there is a possibility that difference exists between the transcription level of SIPA1 gene and the protein level of translation, but our Peking clinical cohort is larger than the TMA cohort, and most importantly, it has much more normal tissue. The clinical cohort samples are fresh frozen from surgery and capable of quantifying the expression of SIPA1 whilst the TMA samples are blocked collection only used for qualitative or semi-quantitative analysis. In terms of tumorigenesis, the Peking clinical cohort data showed that the transcription level of SIPA1 was significantly higher in the advanced T stage and TNM stage tumours. From the prognostic analysis of lung cancer database, the median survival time of patients with high SIPA1 expression was significantly shorter than that of patients with low SIPA1 expression, and the difference is particularly pronounced in patients with adenocarcinoma with statistical significance. Transcription of SIPA1 was high in lung cancer tumour and more advanced TNM stages of lung cancer, and the high level of SIPA1 correlated with the worst prognosis of lung cancer patients, which all indicate that SIPA1 can be used as a potential independent clinical biomarker to detect the occurrence of lung cancer, measure the staging of lung cancer progression, and evaluate the prognosis.

Secondly, MET is the driving factor and therapeutic target for NSCLC. Crizotinib (Xalkori) is approved by the FDA as a MET targeted inhibitor used in NSCLC patients

with MET amplification and/or exon 14 skipping mutation. Since SIPA1 can interact with MET, and SIPA1 can regulate the MET receptor protein, and the inhibition of SIPA1 has similar effects on the TJs of lung cancer cells as MET inhibitors- Crizotinib, we believe that SIPA1 may be a potential therapeutic target in NSCLC and a potential substitute target for MET targeted therapy resistance in NSCLC.

The clinical relevance of SIPA1 in NSCLC is reflected in several aspects. SIPA1 could be a biomarker of diagnosis, staging and assessment of lung cancer development, and prediction of NSCLC patients' prognosis. In terms of the treatment, SIPA1 could be utilised to evaluate the curative effect of MET targeted therapy, and targeted inhibition of SIPA1 may be synergistic with MET inhibitors for NSCLC.

8.8 Final conclusion and perspectives

In concluding this work, SIPA1 plays an essential role in NSCLC tumorigenesis and metastasis, by enhancing invasion and proliferation and suppressing the barrier function of lung cancer cells. This is achieved via promoting Grb2, SOCS and PKC μ , ensuring the recycling of MET, and further ensuring normal transmission of the HGF/MET signalling pathway (**Figure 8.1**). This summarises the findings of this thesis: SIPA1 and HGF form an axis that is able to regulate the function of TJ's in human lung cancer cells. This novel discovery offers a pathway that may be explored both biologically and clinically. Biologically, this is of interest as there has previously been little information regarding the exact pathway involved in HGF effected changes of TJ function. Clinically, this pathway may provide possible routes of therapeutic intervention. How this can be achieved is beyond the scope of the current work and remains an important area of future research.

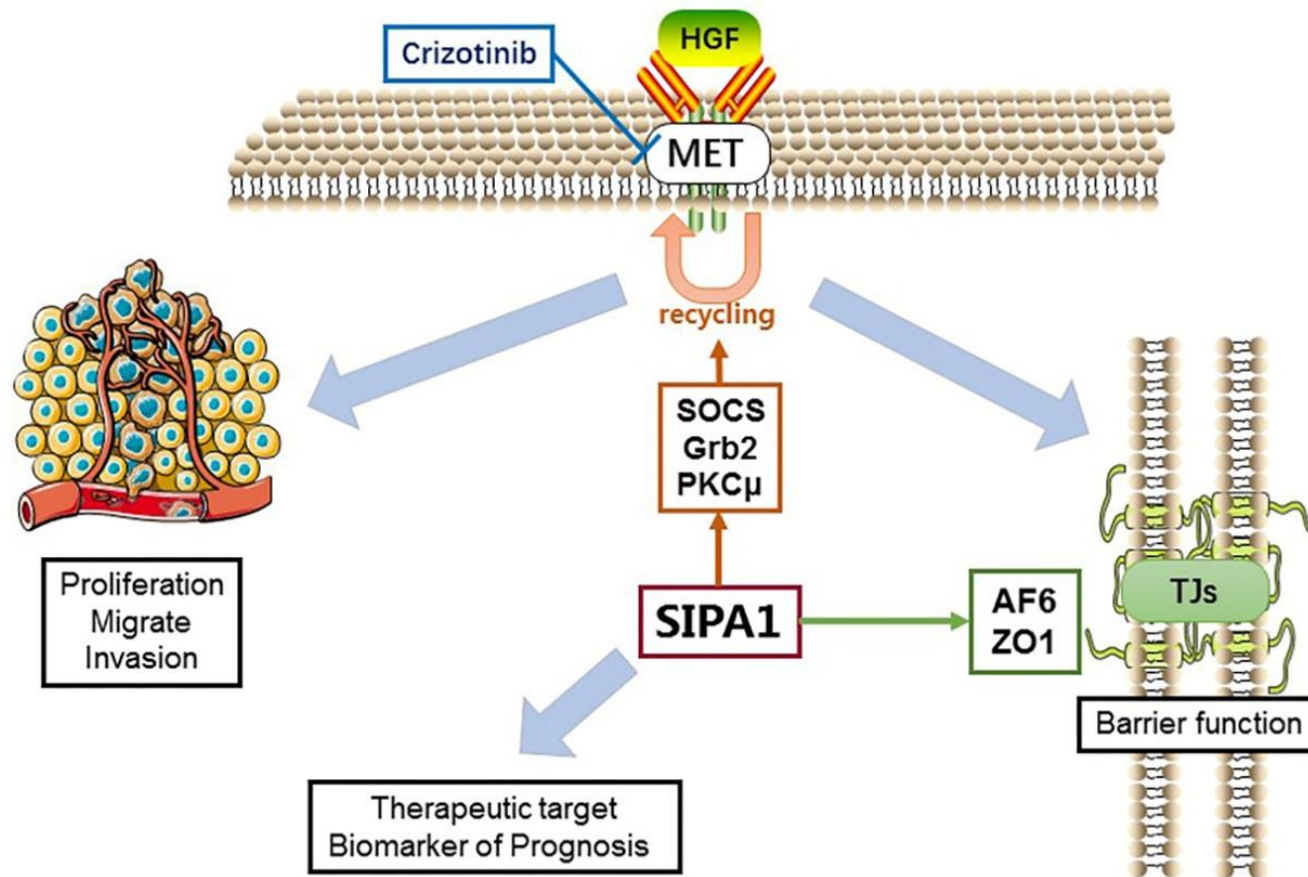


Figure 8.1: Diagram of the overview of the thesis outline. Schematic indicating the possible regulatory pathway for of SIPA1 in lung cancer cells and the control of tight junction function and assembly by HGF.

8.9 Future directions:

- In addition to affecting the recirculation of MET, in what other ways can SIPA1 regulate the expression of the MET receptor?
- Since SIPA1 can interact with MET, can it also interact with other RKTs family members, especially the crucial EGF/EGFR signalling pathway in non-small cell lung cancer?
- Besides HGF/MET, does SIPA1 interact with other key intercellular signalling pathways to regulate lung cancer metastasis?
- What are the other mechanisms by which SIPA1 regulates the tight junctions of lung cancer cells?
- A targeted inhibitor of SIPA1 protein needs to be developed, and examining its effect at different levels of molecules, cells, and further study the possibility for clinical use.
- The role and mechanism of SIPA1 in other types of tumours require further exploration and investigation.

Chapter-9 Reference

-
- ALBER, T. 1992. Structure of the leucine zipper. *Curr Opin Genet Dev*, 2, 205-10.
- ALSARRAJ, J., FARAJI, F., GEIGER, T. R., MATTAINI, K. R., WILLIAMS, M., WU, J., HA, N. H., MERLINO, T., WALKER, R. C., BOSLEY, A. D., XIAO, Z., ANDRESSON, T., ESPOSITO, D., SMITHERS, N., LUGO, D., PRINJHA, R., DAY, A., CRAWFORD, N. P., OZATO, K., GARDNER, K. & HUNTER, K. W. 2013. BRD4 short isoform interacts with RRP1B, SIPA1 and components of the LINC complex at the inner face of the nuclear membrane. *PLoS One*, 8, e80746.
- ALTORKI, N. K., MARKOWITZ, G. J., GAO, D., PORT, J. L., SAXENA, A., STILES, B., MCGRAW, T. & MITTAL, V. 2019. The lung microenvironment: an important regulator of tumour growth and metastasis. *Nat Rev Cancer*, 19, 9-31.
- ASAMURA, H., CHANSKY, K., CROWLEY, J., GOLDSTRAW, P., RUSCH, V. W., VANSTEENKISTE, J. F., WATANABE, H., WU, Y. L., ZIELINSKI, M., BALL, D. & RAMI-PORTA, R. 2015. The International Association for the Study of Lung Cancer Lung Cancer Staging Project: Proposals for the Revision of the N Descriptors in the Forthcoming 8th Edition of the TNM Classification for Lung Cancer. *J Thorac Oncol*, 10, 1675-84.
- BARKAN, D., KLEINMAN, H., SIMMONS, J. L., ASMUSSEN, H., KAMARAJU, A. K., HOENORHOFF, M. J., LIU, Z. Y., COSTES, S. V., CHO, E. H., LOCKETT, S., KHANNA, C., CHAMBERS, A. F. & GREEN, J. E. 2008. Inhibition of metastatic outgrowth from single dormant tumor cells by targeting the cytoskeleton. *Cancer Res*, 68, 6241-50.
- BIRCHMEIER, C., BIRCHMEIER, W., GHERARDI, E. & VANDE WOUDE, G. F. 2003a. Met, metastasis, motility and more. *Nat Rev Mol Cell Biol*, 4, 915-25.
- BIRCHMEIER, C., BIRCHMEIER, W., GHERARDI, E. & WOUDE, G. F. V. 2003b. Met, metastasis, motility and more. *Nature reviews Molecular cell biology*, 4, 915.
- BIRCHMEIER, W., BRINKMANN, V., NIEMANN, C., MEINERS, S., DICESARE, S., NAUNDORF, H. & SACHS, M. 1997. Role of HGF/SF and c-Met in morphogenesis and metastasis of epithelial cells. *Ciba Found Symp*, 212, 230-40; discussion 240-6.
- BISSELL, M. J. & HINES, W. C. 2011. Why don't we get more cancer? A proposed role of the microenvironment in restraining cancer progression. *Nat Med*, 17, 320-9.
- BOS, J. L., REHMANN, H. & WITTINGHOFER, A. 2007. GEFs and GAPs: Critical Elements in the Control of Small G Proteins. *Cell*, 129, 865-877.
- BOTTARO, D. P., RUBIN, J. S., FALETTO, D. L., CHAN, A. M., KMIECIK, T. E., VANDE WOUDE, G. F. & AARONSON, S. A. 1991. Identification of the hepatocyte growth factor receptor as the c-met proto-oncogene product. *Science*, 251, 802-4.
- BRAY, F., FERLAY, J., SOERJOMATARAM, I., SIEGEL, R. L., TORRE, L. A. & JEMAL, A. 2018. Global cancer statistics 2018: GLOBOCAN estimates of incidence and mortality worldwide for 36 cancers in 185 countries. *CA Cancer J Clin*, 68, 394-424.
- BROOKS, R., KIZER, N., NGUYEN, L., JAISHUEN, A., WANAT, K., NUGENT, E., GRIGSBY, P., ALLSWORTH, J. E. & RADER, J. S. 2010. Polymorphisms in MMP9 and SIPA1 are associated with increased risk of nodal metastases in early-stage cervical cancer. *Gynecol Oncol*, 116, 539-43.
- BROWN, K. F., RUMGAY, H., DUNLOP, C., RYAN, M., QUARTLY, F., COX, A., DEAS, A., ELLISS-BROOKES, L., GAVIN, A., HOUNSOME, L., HUWS, D., ORMISTON-SMITH, N., SHELTON, J., WHITE, C. & PARKIN, D. M. 2018. The fraction of cancer attributable to modifiable risk factors in England, Wales, Scotland, Northern Ireland, and the United Kingdom in 2015. *Br J Cancer*, 118, 1130-1141.
- CARMELIET, P. & JAIN, R. K. 2011. Principles and mechanisms of vessel normalization for cancer and other angiogenic diseases. *Nat Rev Drug Discov*, 10, 417-27.
- CAVALLARO, U. & CHRISTOFORI, G. 2004. Cell adhesion and signalling by cadherins and Ig-CAMs in cancer. *Nat Rev Cancer*, 4, 118-32.
- CHEN, Z., FILLMORE, C. M., HAMMERMAN, P. S., KIM, C. F. & WONG, K. K. 2014. Non-small-cell

-
- lung cancers: a heterogeneous set of diseases. *Nat Rev Cancer*, 14, 535-46.
- CHEUNG, K. J. & EWALD, A. J. 2016. A collective route to metastasis: Seeding by tumor cell clusters. *Science*, 352, 167-9.
- CHIBA, H., OSANAI, M., MURATA, M., KOJIMA, T. & SAWADA, N. 2008. Transmembrane proteins of tight junctions. *Biochim Biophys Acta*, 1778, 588-600.
- COLLISSON, E. A., CAMPBELL, J. D., BROOKS, A. N., BERGER, A. H., LEE, W., CHMIELECKI, J., BEER, D. G., COPE, L., CREIGHTON, C. J., DANILOVA, L., DING, L., GETZ, G., HAMMERMAN, P. S., NEIL HAYES, D., HERNANDEZ, B., HERMAN, J. G., HEYMACH, J. V., JURISICA, I., KUCHERLAPATI, R., KWIATKOWSKI, D., LADANYI, M., ROBERTSON, G., SCHULTZ, N., SHEN, R., SINHA, R., SOUGNEZ, C., TSAO, M.-S., TRAVIS, W. D., WEINSTEIN, J. N., WIGLE, D. A., WILKERSON, M. D., CHU, A., CHERNIACK, A. D., HADJIPANAYIS, A., ROSENBERG, M., WEISENBERGER, D. J., LAIRD, P. W., RADENBAUGH, A., MA, S., STUART, J. M., AVERETT BYERS, L., BAYLIN, S. B., GOVINDAN, R., MEYERSON, M., ROSENBERG, M., GABRIEL, S. B., CIBULSKIS, K., SOUGNEZ, C., KIM, J., STEWART, C., LICHTENSTEIN, L., LANDER, E. S., LAWRENCE, M. S., GETZ, G., KANDOTH, C., FULTON, R., FULTON, L. L., MCLELLAN, M. D., WILSON, R. K., YE, K., FRONICK, C. C., MAHER, C. A., MILLER, C. A., WENDL, M. C., CABANSKI, C., DING, L., MARDIS, E., GOVINDAN, R., CREIGHTON, C. J., WHEELER, D., BALASUNDARAM, M., BUTTERFIELD, Y. S. N., CARLSEN, R., CHU, A., CHUAH, E., DHALLA, N., GUIN, R., HIRST, C., LEE, D., LI, H. I., MAYO, M., MOORE, R. A., MUNGALL, A. J., SCHEIN, J. E., SIPAHIMALANI, P., TAM, A., VARHOL, R., GORDON ROBERTSON, A., WYE, N., THIESSEN, N., HOLT, R. A., JONES, S. J. M., MARRA, M. A., CAMPBELL, J. D., BROOKS, A. N., CHMIELECKI, J., IMIELINSKI, M., ONOFRIO, R. C., HODIS, E., ZACK, T., et al. 2014. Comprehensive molecular profiling of lung adenocarcinoma. *Nature*, 511, 543-550.
- COOPER, C. S., PARK, M., BLAIR, D. G., TAINSKY, M. A., HUEBNER, K., CROCE, C. M. & VANDE WOUDE, G. F. 1984. Molecular cloning of a new transforming gene from a chemically transformed human cell line. *Nature*, 311, 29-33.
- COTE, M. L., LIU, M., BONASSI, S., NERI, M., SCHWARTZ, A. G., CHRISTIANI, D. C., SPITZ, M. R., MUSCAT, J. E., RENNERT, G., ABEN, K. K., ANDREW, A. S., BENCKO, V., BICKEBOLLER, H., BOFFETTA, P., BRENNAN, P., BRENNER, H., DUELL, E. J., FABIANOVA, E., FIELD, J. K., FORETOVA, L., FRIIS, S., HARRIS, C. C., HOLCATOVA, I., HONG, Y. C., ISLA, D., JANOUT, V., KIEMENEY, L. A., KIYOHARA, C., LAN, Q., LAZARUS, P., LISSOWSKA, J., LE MARCHAND, L., MATES, D., MATSUO, K., MAYORDOMO, J. I., MCLAUGHLIN, J. R., MORGENSTERN, H., MUELLER, H., ORLOW, I., PARK, B. J., PINCHEV, M., RAJI, O. Y., RENNERT, H. S., RUDNAI, P., SEOW, A., STUCKER, I., SZESZENIA-DABROWSKA, N., DAWN TEARE, M., TJONNELAN, A., UGOLINI, D., VAN DER HEIJDEN, H. F., WICHMANN, E., WIENCKE, J. K., WOLL, P. J., YANG, P., ZARIDZE, D., ZHANG, Z. F., ETZEL, C. J. & HUNG, R. J. 2012. Increased risk of lung cancer in individuals with a family history of the disease: a pooled analysis from the International Lung Cancer Consortium. *Eur J Cancer*, 48, 1957-68.
- CRAWFORD, N. P., ZIOGAS, A., PEEL, D. J., HESS, J., ANTON-CULVER, H. & HUNTER, K. W. 2006. Germline polymorphisms in SIPA1 are associated with metastasis and other indicators of poor prognosis in breast cancer. *Breast Cancer Res*, 8, R16.
- DARBY, S., HILL, D., AUVINEN, A., BARROS-DIOS, J. M., BAYSSON, H., BOCHICCHIO, F., DEO, H., FALK, R., FORASTIERE, F., HAKAMA, M., HEID, I., KREIENBROCK, L., KREUZER, M., LAGARDE, F., MAKELAINEN, I., MUIRHEAD, C., OBERAIGNER, W., PERSHAGEN, G., RUANO-RAVINA, A., RUOSTEENOJA, E., ROSARIO, A. S., TIRMARCHE, M., TOMASEK, L., WHITLEY, E., WICHMANN, H. E. & DOLL, R. 2005. Radon in homes and risk of lung cancer: collaborative analysis of individual data from 13 European case-control studies. *Bmj*, 330, 223.

-
- DENARDO, D. G., BARRETO, J. B., ANDREU, P., VASQUEZ, L., TAWFIK, D., KOLHATKAR, N. & COUSSENS, L. M. 2009. CD4(+) T cells regulate pulmonary metastasis of mammary carcinomas by enhancing protumor properties of macrophages. *Cancer Cell*, 16, 91-102.
- DHILLON, A. S., HAGAN, S., RATH, O. & KOLCH, W. 2007. MAP kinase signalling pathways in cancer. *Oncogene*, 26, 3279-90.
- DIRAT, B., BOCHET, L., DABEK, M., DAVIAUD, D., DAUVILLIER, S., MAJED, B., WANG, Y. Y., MEULLE, A., SALLES, B., LE GONIDEC, S., GARRIDO, I., ESCOURROU, G., VALET, P. & MULLER, C. 2011. Cancer-associated adipocytes exhibit an activated phenotype and contribute to breast cancer invasion. *Cancer Res*, 71, 2455-65.
- DOLL, R., PETO, R., BOREHAM, J. & SUTHERLAND, I. 2005. Mortality from cancer in relation to smoking: 50 years observations on British doctors. *Br J Cancer*, 92, 426-9.
- DUPLAQUET, L., KHERROUCHE, Z., BALDACCI, S., JAMME, P., CORTOT, A. B., COPIN, M.-C. & TULASNE, D. 2018. The multiple paths towards MET receptor addiction in cancer. *Oncogene*, 37, 3200-3215.
- EBERHARDT, W. E., MITCHELL, A., CROWLEY, J., KONDO, H., KIM, Y. T., TURRISI, A., 3RD, GOLDSTRAW, P. & RAMI-PORTA, R. 2015. The IASLC Lung Cancer Staging Project: Proposals for the Revision of the M Descriptors in the Forthcoming Eighth Edition of the TNM Classification of Lung Cancer. *J Thorac Oncol*, 10, 1515-22.
- ERLER, J. T., BENNEWITH, K. L., COX, T. R., LANG, G., BIRD, D., KOONG, A., LE, Q. T. & GIACCIA, A. J. 2009. Hypoxia-induced lysyl oxidase is a critical mediator of bone marrow cell recruitment to form the premetastatic niche. *Cancer Cell*, 15, 35-44.
- FARINA, A., HATTORI, M., QIN, J., NAKATANI, Y., MINATO, N. & OZATO, K. 2004. Bromodomain protein Brd4 binds to GTPase-activating SPA-1, modulating its activity and subcellular localization. *Mol Cell Biol*, 24, 9059-69.
- FERRACINI, R., LONGATI, P., NALDINI, L., VIGNA, E. & COMOGLIO, P. M. 1991. Identification of the major autophosphorylation site of the Met/hepatocyte growth factor receptor tyrosine kinase. *J Biol Chem*, 266, 19558-64.
- FIDLER, I. J. 2003. The pathogenesis of cancer metastasis: the 'seed and soil' hypothesis revisited. *Nat Rev Cancer*, 3, 453-8.
- FRAMPTON, G. M., ALI, S. M., ROSENZWEIG, M., CHMIELECKI, J., LU, X., BAUER, T. M., AKIMOV, M., BUFILL, J. A., LEE, C., JENTZ, D., HOOVER, R., OU, S.-H. I., SALGIA, R., BRENNAN, T., CHALMERS, Z. R., JAEGER, S., HUANG, A., ELVIN, J. A., ERLICH, R., FICHTENHOLTZ, A., GOWEN, K. A., GREENBOWE, J., JOHNSON, A., KHAIRA, D., MCMAHON, C., SANFORD, E. M., ROELS, S., WHITE, J., GRESHOCK, J., SCHLEGEL, R., LIPSON, D., YELENSKY, R., MOROSINI, D., ROSS, J. S., COLLISSON, E., PETERS, M., STEPHENS, P. J. & MILLER, V. A. 2015. Activation of MET via Diverse Exon 14 Splicing Alterations Occurs in Multiple Tumor Types and Confers Clinical Sensitivity to MET Inhibitors. 5, 850-859.
- FRANK H. NETTER 2018. *Atlas of Human Anatomy, Seventh Edition*.
- FUSTER, L. M. & SANDLER, A. B. 2004. Select clinical trials of erlotinib (OSI-774) in non-small-cell lung cancer with emphasis on phase III outcomes. *Clin Lung Cancer*, 6 Suppl 1, S24-9.
- GAO, C. F. & VANDE WOUDE, G. F. 2005. HGF/SF-Met signaling in tumor progression. *Cell Res*, 15, 49-51.
- GAUDET, M. M., HUNTER, K., PHAROAH, P., DUNNING, A. M., DRIVER, K., LISSOWSKA, J., SHERMAN, M., PEPLONSKA, B., BRINTON, L. A., CHANOCK, S. & GARCIA-CLOSAS, M. 2009. Genetic variation in SIPA1 in relation to breast cancer risk and survival after breast cancer diagnosis. *Int J Cancer*, 124, 1716-20.
- GADOWICZ-KLOSOK, A., GIGLOK, M., DROSIK, A., SUWINSKI, R. & BUTKIEWICZ, D. 2015. The SIPA1 -313A>G polymorphism is associated with prognosis in inoperable non-small cell

-
- lung cancer. *Tumour Biol*, 36, 1273-8.
- GHERARDI, E., BIRCHMEIER, W., BIRCHMEIER, C. & VANDE WOUDE, G. 2012. Targeting MET in cancer: rationale and progress. *Nat Rev Cancer*, 12, 89-103.
- GHERARDI, E. & STOKER, M. 1990. Hepatocytes and scatter factor. *Nature*, 346, 228-228.
- GHOSE, R., SHEKHTMAN, A., GOGER, M. J., JI, H. & COWBURN, D. 2001. A novel, specific interaction involving the Csk SH3 domain and its natural ligand. *Nature Structural Biology*, 8, 998-1004.
- GIAMPIERI, S., MANNING, C., HOOPER, S., JONES, L., HILL, C. S. & SAHAI, E. 2009. Localized and reversible TGFbeta signalling switches breast cancer cells from cohesive to single cell motility. *Nat Cell Biol*, 11, 1287-96.
- GOLDSTRAW, P., CHANSKY, K., CROWLEY, J., RAMI-PORTA, R., ASAMURA, H., EBERHARDT, W. E., NICHOLSON, A. G., GROOME, P., MITCHELL, A. & BOLEJACK, V. 2016. The IASLC Lung Cancer Staging Project: Proposals for Revision of the TNM Stage Groupings in the Forthcoming (Eighth) Edition of the TNM Classification for Lung Cancer. *J Thorac Oncol*, 11, 39-51.
- GONCALVES, M. D., HOPKINS, B. D. & CANTLEY, L. C. 2018. Phosphatidylinositol 3-Kinase, Growth Disorders, and Cancer. *New England Journal of Medicine*, 379, 2052-2062.
- GOTTS, J. E., JORDT, S.-E., MCCONNELL, R. & TARRAN, R. 2019. What are the respiratory effects of e-cigarettes? *BMJ*, 366, l5275.
- GRAVEEL, C. R., TOLBERT, D. & VANDE WOUDE, G. F. 2013. MET: a critical player in tumorigenesis and therapeutic target. *Cold Spring Harbor perspectives in biology*, 5, a009209.
- GUI, Y., YEGANEH, M., RAMANATHAN, S., LEBLANC, C., POMERLEAU, V., FERBEYRE, G., SAUCIER, C. & ILANGUMARAN, S. 2011. SOCS1 controls liver regeneration by regulating HGF signaling in hepatocytes. *Journal of hepatology*, 55, 1300-1308.
- GUPTA, G. P. & MASSAGUE, J. 2006. Cancer metastasis: building a framework. *Cell*, 127, 679-95.
- GUPTA, G. P., NGUYEN, D. X., CHIANG, A. C., BOS, P. D., KIM, J. Y., NADAL, C., GOMIS, R. R., MANOVA-TODOROVA, K. & MASSAGUE, J. 2007. Mediators of vascular remodelling co-opted for sequential steps in lung metastasis. *Nature*, 446, 765-70.
- HAMMERMAN, P. S., LAWRENCE, M. S., VOET, D., JING, R., CIBULSKIS, K., SIVACHENKO, A., STOJANOV, P., MCKENNA, A., LANDER, E. S., GABRIEL, S., GETZ, G., SOUGNEZ, C., IMIELINSKI, M., HELMAN, E., HERNANDEZ, B., PHO, N. H., MEYERSON, M., CHU, A., CHUN, H.-J. E., MUNGALL, A. J., PLEASANCE, E., GORDON ROBERTSON, A., SIPAHIMALANI, P., STOLL, D., BALASUNDARAM, M., BIROL, I., BUTTERFIELD, Y. S. N., CHUAH, E., COOPE, R. J. N., CORBETT, R., DHALLA, N., GUIN, R., HE, A., HIRST, C., HIRST, M., HOLT, R. A., LEE, D., LI, H. I., MAYO, M., MOORE, R. A., MUNGALL, K., MING NIP, K., OLSHEN, A., SCHEIN, J. E., SLOBODAN, J. R., TAM, A., THIESSEN, N., VARHOL, R., ZENG, T., ZHAO, Y., JONES, S. J. M., MARRA, M. A., SAKSENA, G., CHERNIACK, A. D., SCHUMACHER, S. E., TABAK, B., CARTER, S. L., PHO, N. H., NGUYEN, H., ONOFRIO, R. C., CRENSHAW, A., ARDLIE, K., BEROUKHIM, R., WINCKLER, W., HAMMERMAN, P. S., GETZ, G., MEYERSON, M., PROTOPOPOV, A., ZHANG, J., HADJIPANAYIS, A., LEE, S., XI, R., YANG, L., REN, X., ZHANG, H., SHUKLA, S., CHEN, P.-C., HASELEY, P., LEE, E., CHIN, L., PARK, P. J., KUCHERLAPATI, R., SOCCI, N. D., LIANG, Y., SCHULTZ, N., BORSU, L., LASH, A. E., VIALE, A., SANDER, C., LADANYI, M., TODD AUMAN, J., HOADLEY, K. A., WILKERSON, M. D., SHI, Y., LIQUORI, C., MENG, S., LI, L., TURMAN, Y. J., TOPAL, M. D., TAN, D., et al. 2012. Comprehensive genomic characterization of squamous cell lung cancers. *Nature*, 489, 519-525.
- HAMRA, G. B., GUHA, N., COHEN, A., LADEN, F., RAASCHOU-NIELSEN, O., SAMET, J. M., VINEIS, P., FORASTIERE, F., SALDIVA, P., YORIFUJI, T. & LOOMIS, D. 2014. Outdoor particulate matter exposure and lung cancer: a systematic review and meta-analysis. *Environ Health*

- HANAHAH, D. & WEINBERG, R. A. 2011. Hallmarks of cancer: the next generation. *Cell*, 144, 646-74.
- HATTORI, M. 2011. SIPA1 (signal-induced proliferation-associated 1). *Atlas of Genetics and Cytogenetics in Oncology and Haematology*.
- HATTORI, M., TSUKAMOTO, N., NUR-E-KAMAL, M. S., RUBINFELD, B., IWAI, K., KUBOTA, H., MARUTA, H. & MINATO, N. 1995. Molecular cloning of a novel mitogen-inducible nuclear protein with a Ran GTPase-activating domain that affects cell cycle progression. *Mol Cell Biol*, 15, 552-60.
- HAUSSER, A., LINK, G., BAMBERG, L., BURZLAFF, A., LUTZ, S., PFIZENMAIER, K. & JOHANNES, F.-J. 2002. Structural requirements for localization and activation of protein kinase C mu (PKC mu) at the Golgi compartment. *The Journal of cell biology*, 156, 65-74.
- HENRY GRAY, T. P. P., ROBERT HOWDEN, H.V. CARTER 2010. *Gray's Anatomy*.
- HERBST, R. S., HEYMACH, J. V. & LIPPMAN, S. M. 2008. Lung cancer. *N Engl J Med*, 359, 1367-80.
- HERBST, R. S., MORGENSZTERN, D. & BOSHOFF, C. 2018. The biology and management of non-small cell lung cancer. *Nature*, 553, 446-454.
- HIRSCH, F. R., VARELLA-GARCIA, M., BUNN, P. A., JR., DI MARIA, M. V., VEVE, R., BREMMES, R. M., BARON, A. E., ZENG, C. & FRANKLIN, W. A. 2003. Epidermal growth factor receptor in non-small-cell lung carcinomas: correlation between gene copy number and protein expression and impact on prognosis. *J Clin Oncol*, 21, 3798-807.
- HOEVEL, T., MACEK, R., MUNDIGL, O., SWISSHELM, K. & KUBBIES, M. 2002. Expression and targeting of the tight junction protein CLDN1 in CLDN1-negative human breast tumor cells. *J Cell Physiol*, 191, 60-8.
- HOOD, J. D. & CHERESH, D. A. 2002. Role of integrins in cell invasion and migration. *Nature Reviews Cancer*, 2, 91.
- HOSGOOD, H. D., 3RD, WEI, H., SAPKOTA, A., CHOUDHURY, I., BRUCE, N., SMITH, K. R., ROTHMAN, N. & LAN, Q. 2011. Household coal use and lung cancer: systematic review and meta-analysis of case-control studies, with an emphasis on geographic variation. *Int J Epidemiol*, 40, 719-28.
- HSIEH, S. M., LOOK, M. P., SIEUWERTS, A. M., FOEKENS, J. A. & HUNTER, K. W. 2009a. Distinct inherited metastasis susceptibility exists for different breast cancer subtypes: a prognosis study. *Breast Cancer Res*, 11, R75.
- HSIEH, S. M., SMITH, R. A., LINTELL, N. A., HUNTER, K. W. & GRIFFITHS, L. R. 2009b. Polymorphisms of the SIPA1 gene and sporadic breast cancer susceptibility. *BMC Cancer*, 9, 331.
- HYNES, N. E. & LANE, H. A. 2005. ERBB receptors and cancer: the complexity of targeted inhibitors. *Nat Rev Cancer*, 5, 341-54.
- IJAZ, M., WANG, F., SHAHBAZ, M., JIANG, W., FATHY, A. H. & NESA, E. U. 2018. The Role of Grb2 in Cancer and Peptides as Grb2 Antagonists. *Protein and peptide letters*, 24, 1084-1095.
- ISAKOV, N. 2018. Protein kinase C (PKC) isoforms in cancer, tumor promotion and tumor suppression. *Seminars in cancer biology*, 48, 36-52.
- JAMAL-HANJANI, M., WILSON, G. A., MCGRANAHAN, N., BIRKBAK, N. J., WATKINS, T. B. K., VEERIAH, S., SHAFI, S., JOHNSON, D. H., MITTER, R., ROSENTHAL, R., SALM, M., HORSWELL, S., ESCUDERO, M., MATTHEWS, N., ROWAN, A., CHAMBERS, T., MOORE, D. A., TURAJLIC, S., XU, H., LEE, S. M., FORSTER, M. D., AHMAD, T., HILEY, C. T., ABBOSH, C., FALZON, M., BORG, E., MARAFIOTI, T., LAWRENCE, D., HAYWARD, M., KOLVEKAR, S., PANAGIOTOPOULOS, N., JANES, S. M., THAKRAR, R., AHMED, A., BLACKHALL, F., SUMMERS, Y., SHAH, R., JOSEPH, L., QUINN, A. M., CROSBIE, P. A., NAIDU, B.,

-
- MIDDLETON, G., LANGMAN, G., TROTTER, S., NICOLSON, M., REMMEN, H., KERR, K., CHETTY, M., GOMERSALL, L., FENNELL, D. A., NAKAS, A., RATHINAM, S., ANAND, G., KHAN, S., RUSSELL, P., EZHIL, V., ISMAIL, B., IRVIN-SELLERS, M., PRAKASH, V., LESTER, J. F., KORNASZEWSKA, M., ATTANOOS, R., ADAMS, H., DAVIES, H., DENTRO, S., TANIÈRE, P., O'SULLIVAN, B., LOWE, H. L., HARTLEY, J. A., ILES, N., BELL, H., NGAI, Y., SHAW, J. A., HERRERO, J., SZALLASI, Z., SCHWARZ, R. F., STEWART, A., QUEZADA, S. A., LE QUESNE, J., VAN LOO, P., DIVE, C., HACKSHAW, A. & SWANTON, C. 2017. Tracking the Evolution of Non-Small-Cell Lung Cancer. *N Engl J Med*, 376, 2109-2121.
- JI, K., YE, L., TOMS, A. M., HARGEST, R., MARTIN, T. A., RUGE, F., JI, J. & JIANG, W. G. 2012. Expression of signal-induced proliferation-associated gene 1 (SIPA1), a RapGTPase-activating protein, is increased in colorectal cancer and has diverse effects on functions of colorectal cancer cells. *Cancer Genomics Proteomics*, 9, 321-7.
- JIANG, T. M. A. W. 2006. Human breast cancer cell tight junction function is regulated by SIPA1. *29th Annual San Antonio Breast Cancer Symposium: December 14-17, 2006*. Springer.
- JIANG, T. M. A. W. 2013. Regulation of barrier function in human breast cancer can be controlled by the ROCK signalling pathway via interaction with SIPA-1. *EUROPEAN JOURNAL OF CANCER*. ELSEVIER SCI LTD THE BOULEVARD, LANGFORD LANE, KIDLINGTON, OXFORD OX5 1GB ...
- JIANG, W. G., MARTIN, T. A., MATSUMOTO, K., NAKAMURA, T. & MANSEL, R. E. 1999. Hepatocyte growth factor/scatter factor decreases the expression of occludin and transendothelial resistance (TER) and increases paracellular permeability in human vascular endothelial cells. *J Cell Physiol*, 181, 319-29.
- KAZI, J. U., KABIR, N. N., FLORES-MORALES, A. & RÖNNSTRAND, L. 2014. SOCS proteins in regulation of receptor tyrosine kinase signaling. *Cellular and molecular life sciences : CMLS*, 71, 3297-3310.
- KESSENBROCK, K., PŁAKS, V. & WERB, Z. 2010. Matrix metalloproteinases: regulators of the tumor microenvironment. *Cell*, 141, 52-67.
- KHUDER, S. A. 2001. Effect of cigarette smoking on major histological types of lung cancer: a meta-analysis. *Lung Cancer*, 31, 139-48.
- KILE, B. T. & ALEXANDER, W. S. 2001. The suppressors of cytokine signalling (SOCS). *Cellular and molecular life sciences : CMLS*, 58, 1627-1635.
- KIM, C. H., LEE, Y. C., HUNG, R. J., MCNALLAN, S. R., COTE, M. L., LIM, W. Y., CHANG, S. C., KIM, J. H., UGOLINI, D., CHEN, Y., LILOGLOU, T., ANDREW, A. S., ONEGA, T., DUELL, E. J., FIELD, J. K., LAZARUS, P., LE MARCHAND, L., NERI, M., VINEIS, P., KIYOHARA, C., HONG, Y. C., MORGENSTERN, H., MATSUO, K., TAJIMA, K., CHRISTIANI, D. C., MCLAUGHLIN, J. R., BENCKO, V., HOLCATOVA, I., BOFFETTA, P., BRENNAN, P., FABIANOVA, E., FORETOVA, L., JANOUT, V., LISSOWSKA, J., MATES, D., RUDNAI, P., SZESZENIA-DABROWSKA, N., MUKERIA, A., ZARIDZE, D., SEOW, A., SCHWARTZ, A. G., YANG, P. & ZHANG, Z. F. 2014. Exposure to secondhand tobacco smoke and lung cancer by histological type: a pooled analysis of the International Lung Cancer Consortium (ILCCO). *Int J Cancer*, 135, 1918-30.
- KRAUSE, D. S. & VAN ETTEN, R. A. 2005. Tyrosine kinases as targets for cancer therapy. *N Engl J Med*, 353, 172-87.
- KURACHI, H., WADA, Y., TSUKAMOTO, N., MAEDA, M., KUBOTA, H., HATTORI, M., IWAI, K. & MINATO, N. 1997. Human SPA-1 gene product selectively expressed in lymphoid tissues is a specific GTPase-activating protein for Rap1 and Rap2. Segregate expression profiles from a rap1GAP gene product. *J Biol Chem*, 272, 28081-8.
- KURMI, O. P., ARYA, P. H., LAM, K. B., SORAHAN, T. & AYRES, J. G. 2012. Lung cancer risk and solid fuel smoke exposure: a systematic review and meta-analysis. *Eur Respir J*, 40, 1228-

- LABELLE, M., BEGUM, S. & HYNES, R. O. 2011. Direct signaling between platelets and cancer cells induces an epithelial-mesenchymal-like transition and promotes metastasis. *Cancer Cell*, 20, 576-90.
- LEE, E. Y. & MULLER, W. J. 2010. Oncogenes and tumor suppressor genes. *Cold Spring Harb Perspect Biol*, 2, a003236.
- LEE, J. H., HAN, S. U., CHO, H., JENNINGS, B., GERRARD, B., DEAN, M., SCHMIDT, L., ZBAR, B. & VANDE WOUDE, G. F. 2000. A novel germ line juxtamembrane Met mutation in human gastric cancer. *Oncogene*, 19, 4947-53.
- LEMMON, M. A. & SCHLESSINGER, J. 2010a. Cell signaling by receptor tyrosine kinases. *Cell*, 141, 1117-1134.
- LEMMON, M. A. & SCHLESSINGER, J. 2010b. Cell signaling by receptor tyrosine kinases. *Cell*, 141, 1117-34.
- LEMMON, M. A., SCHLESSINGER, J. & FERGUSON, K. M. 2014. The EGFR family: not so prototypical receptor tyrosine kinases. *Cold Spring Harb Perspect Biol*, 6, a020768.
- LI, J. Y., WANG, J. B., LIU, C. B., MA, D. L. & MA, J. H. 2017. Dynamic relationship between SIPA1 gene and protein expression and the development of gastric cancer. *Genet Mol Res*, 16.
- LIU, Y., SUN, W., ZHANG, K., ZHENG, H., MA, Y., LIN, D., ZHANG, X., FENG, L., LEI, W., ZHANG, Z., GUO, S., HAN, N., TONG, W., FENG, X., GAO, Y. & CHENG, S. 2007. Identification of genes differentially expressed in human primary lung squamous cell carcinoma. *Lung Cancer*, 56, 307-17.
- LOGAN, C. Y. & NUSSE, R. 2004. The Wnt signaling pathway in development and disease. *Annu Rev Cell Dev Biol*, 20, 781-810.
- MA, P. C., JAGADEESWARAN, R., JAGADEESH, S., TRETIAKOVA, M. S., NALLASURA, V., FOX, E. A., HANSEN, M., SCHAEFFER, E., NAOKI, K., LADER, A., RICHARDS, W., SUGARBAKER, D., HUSAIN, A. N., CHRISTENSEN, J. G. & SALGIA, R. 2005. Functional Expression and Mutations of c-Met and Its Therapeutic Inhibition with SU11274 and Small Interfering RNA in Non-Small Cell Lung Cancer. 65, 1479-1488.
- MA, P. C., KIJIMA, T., MAULIK, G., FOX, E. A., SATTLER, M., GRIFFIN, J. D., JOHNSON, B. E. & SALGIA, R. 2003. c-MET mutational analysis in small cell lung cancer: novel juxtamembrane domain mutations regulating cytoskeletal functions. *Cancer Res*, 63, 6272-81.
- MANJUNATH, G. P., RAMANUJAM, P. L. & GALANDE, S. 2018. Structure function relations in PDZ-domain-containing proteins: Implications for protein networks in cellular signalling. *J Biosci*, 43, 155-171.
- MARTIN, T. A. 2014. The role of tight junctions in cancer metastasis. *Semin Cell Dev Biol*, 36, 224-31.
- MARTIN, T. A. & JIANG, W. G. 2009. Loss of tight junction barrier function and its role in cancer metastasis. *Biochim Biophys Acta*, 1788, 872-91.
- MARTIN, T. A., MANSEL, R. & JIANG, W. G. 2001. Hepatocyte growth factor modulates vascular endothelial-cadherin expression in human endothelial cells. *Clin Cancer Res*, 7, 734-7.
- MARTIN, T. A., MANSEL, R. E. & JIANG, W. G. 2002. Antagonistic effect of NK4 on HGF/SF induced changes in the transendothelial resistance (TER) and paracellular permeability of human vascular endothelial cells. *J Cell Physiol*, 192, 268-75.
- MARTIN, T. A., WATKINS, G., MANSEL, R. E. & JIANG, W. G. 2004. Hepatocyte growth factor disrupts tight junctions in human breast cancer cells. *Cell Biol Int*, 28, 361-71.
- MARTIN, T. A., YE, L., SANDERS, A. J., LANE, J. & JIANG, W. G. 2013. Cancer invasion and metastasis: molecular and cellular perspective. *Madame Curie Bioscience Database [Internet]*. Landes Bioscience.

-
- MASSAGUE, J. & OBENAU, A. C. 2016. Metastatic colonization by circulating tumour cells. *Nature*, 529, 298-306.
- MATHIEU, V., PIRKER, C., SCHMIDT, W. M., SPIEGL-KREINECKER, S., LOTSCH, D., HEFFETER, P., HEGEDUS, B., GRUSCH, M., KISS, R. & BERGER, W. 2012. Aggressiveness of human melanoma xenograft models is promoted by aneuploidy-driven gene expression deregulation. *Oncotarget*, 3, 399-413.
- MEURETTE, O. & MEHLEN, P. 2018. Notch Signaling in the Tumor Microenvironment. *Cancer Cell*, 34, 536-548.
- MINN, A. J., GUPTA, G. P., SIEGEL, P. M., BOS, P. D., SHU, W., GIRI, D. D., VIALE, A., OLSHEN, A. B., GERALD, W. L. & MASSAGUE, J. 2005. Genes that mediate breast cancer metastasis to lung. *Nature*, 436, 518-24.
- MITSUDOMI, T. & YATABE, Y. 2007. Mutations of the epidermal growth factor receptor gene and related genes as determinants of epidermal growth factor receptor tyrosine kinase inhibitors sensitivity in lung cancer. *Cancer Sci*, 98, 1817-24.
- MOORE, K. L. P., T. V. N.; TORCHIA, MARK G. 2011. The Developing Human
- MORIKAWA, M., DERYNCK, R. & MIYAZONO, K. 2016. TGF-beta and the TGF-beta Family: Context-Dependent Roles in Cell and Tissue Physiology. *Cold Spring Harb Perspect Biol*, 8.
- NAGRATH, S., SEQUIST, L. V., MAHESWARAN, S., BELL, D. W., IRIMIA, D., ULKUS, L., SMITH, M. R., KWAK, E. L., DIGUMARTHY, S., MUZIKANSKY, A., RYAN, P., BALIS, U. J., TOMPKINS, R. G., HABER, D. A. & TONER, M. 2007. Isolation of rare circulating tumour cells in cancer patients by microchip technology. *Nature*, 450, 1235-9.
- NCCN.ORG 2020a. NCCN Clinical Practice Guidelines in Oncology (NCCN Guidelines®): None small cell lung cancer. Version 2. 2020. www.nccn.org.
- NCCN.ORG 2020b. NCCN Clinical Practice Guidelines in Oncology (NCCN Guidelines®): Small cell lung cancer. Version 2. 2020. www.nccn.org
- NETTER, F. H. 2014. *Atlas of Human Anatomy, Sixth Edition*.
- NICHOLSON, R. I., GEE, J. M. & HARPER, M. E. 2001. EGFR and cancer prognosis. *Eur J Cancer*, 37 Suppl 4, S9-15.
- NODA, Y., HORIKAWA, S., FURUKAWA, T., HIRAI, K., KATAYAMA, Y., ASAI, T., KUWAHARA, M., KATAGIRI, K., KINASHI, T., HATTORI, M., MINATO, N. & SASAKI, S. 2004. Aquaporin-2 trafficking is regulated by PDZ-domain containing protein SPA-1. *FEBS Lett*, 568, 139-45.
- OHSAKI, Y., TANNO, S., FUJITA, Y., TOYOSHIMA, E., FUJIUCHI, S., NISHIGAKI, Y., ISHIDA, S., NAGASE, A., MIYOKAWA, N., HIRATA, S. & KIKUCHI, K. 2000. Epidermal growth factor receptor expression correlates with poor prognosis in non-small cell lung cancer patients with p53 overexpression. *Oncol Rep*, 7, 603-7.
- OVALLE WILLIAM K., N., PATRICK C., NETTER, FRANK H. ET AL 2007. Netter's Essential Histology
- PAGET, S. 1889. The distribution of secondary growths in cancer of the breast. *The Lancet*, 133, 571-573 %@ 0140-6736.
- PASCHOUD, S., BONGIOVANNI, M., PACHE, J. C. & CITI, S. 2007. Claudin-1 and claudin-5 expression patterns differentiate lung squamous cell carcinomas from adenocarcinomas. *Mod Pathol*, 20, 947-54.
- PEI, R., XU, Y., WEI, Y., OUYANG, T., LI, J., WANG, T., FAN, Z., FAN, T., LIN, B. & XIE, Y. 2013. Association of SIPA1 545 C > T polymorphism with survival in Chinese women with metastatic breast cancer. *Front Med*, 7, 138-42.
- PESCH, B., KENDZIA, B., GUSTAVSSON, P., JOCKEL, K. H., JOHNEN, G., POHLABELN, H., OLSSON, A., AHRENS, W., GROSS, I. M., BRUSKE, I., WICHMANN, H. E., MERLETTI, F., RICHIARDI,

-
- L., SIMONATO, L., FORTES, C., SIEMIATYCKI, J., PARENT, M. E., CONSONNI, D., LANDI, M. T., CAPORASO, N., ZARIDZE, D., CASSIDY, A., SZESZENIA-DABROWSKA, N., RUDNAI, P., LISSOWSKA, J., STUCKER, I., FABIANOVA, E., DUMITRU, R. S., BENCKO, V., FORETOVA, L., JANOUT, V., RUDIN, C. M., BRENNAN, P., BOFFETTA, P., STRAIF, K. & BRUNING, T. 2012. Cigarette smoking and lung cancer--relative risk estimates for the major histological types from a pooled analysis of case-control studies. *Int J Cancer*, 131, 1210-9.
- PESCHARD, P., FOURNIER, T. M., LAMORTE, L., NAUJOKAS, M. A., BAND, H., LANGDON, W. Y. & PARK, M. 2001. Mutation of the c-Cbl TKB domain binding site on the Met receptor tyrosine kinase converts it into a transforming protein. *Mol Cell*, 8, 995-1004.
- PYLAYEVA-GUPTA, Y., GRABOCKA, E. & BAR-SAGI, D. 2011. RAS oncogenes: weaving a tumorigenic web. *Nat Rev Cancer*, 11, 761-74.
- QUAIL, D. F. & JOYCE, J. A. 2013. Microenvironmental regulation of tumor progression and metastasis. *Nat Med*, 19, 1423-37.
- RAGHAV, K. P. S., GONZALEZ-ANGULO, A. M. & BLUMENSCHNEIN, G. R., JR. 2012. Role of HGF/MET axis in resistance of lung cancer to contemporary management. *Translational lung cancer research*, 1, 179-193.
- RAMI-PORTA, R., BOLEJACK, V., CROWLEY, J., BALL, D., KIM, J., LYONS, G., RICE, T., SUZUKI, K., THOMAS, C. F., JR., TRAVIS, W. D. & WU, Y. L. 2015. The IASLC Lung Cancer Staging Project: Proposals for the Revisions of the T Descriptors in the Forthcoming Eighth Edition of the TNM Classification for Lung Cancer. *J Thorac Oncol*, 10, 990-1003.
- RAMI-PORTA, R., BOLEJACK, V., GIROUX, D. J., CHANSKY, K., CROWLEY, J., ASAMURA, H. & GOLDSTRAW, P. 2014. The IASLC lung cancer staging project: the new database to inform the eighth edition of the TNM classification of lung cancer. *J Thorac Oncol*, 9, 1618-24.
- RAMI-PORTA, R., WITTEKIND, C. & GOLDSTRAW, P. 2005. Complete resection in lung cancer surgery: proposed definition. *Lung Cancer*, 49, 25-33.
- RANGANATHAN, P., WEAVER, K. L. & CAPOBIANCO, A. J. 2011. Notch signalling in solid tumours: a little bit of everything but not all the time. *Nat Rev Cancer*, 11, 338-51.
- REN, J., HAMADA, J., TAKEICHI, N., FUJIKAWA, S. & KOBAYASHI, H. 1990. Ultrastructural differences in junctional intercellular communication between highly and weakly metastatic clones derived from rat mammary carcinoma. *Cancer Res*, 50, 358-62.
- ROBERTS, M. R., HONG, C. C., EDGE, S. B., YAO, S., BSHARA, W., HIGGINS, M. J., FREUDENHEIM, J. L. & AMBROSONE, C. B. 2013. Case-only analyses of the associations between polymorphisms in the metastasis-modifying genes BRMS1 and SIPA1 and breast tumor characteristics, lymph node metastasis, and survival. *Breast Cancer Res Treat*, 139, 873-85.
- SACHER, A. G. & GANDHI, L. 2016. Biomarkers for the Clinical Use of PD-1/PD-L1 Inhibitors in Non-Small-Cell Lung Cancer: A Review. *JAMA Oncology*, 2, 1217-1222.
- SATOH, H., ZHONG, Y., ISOMURA, H., SAITOH, M., ENOMOTO, K., SAWADA, N. & MORI, M. 1996. Localization of 7H6 tight junction-associated antigen along the cell border of vascular endothelial cells correlates with paracellular barrier function against ions, large molecules, and cancer cells. *Exp Cell Res*, 222, 269-74.
- SCHILLER, J. H., HARRINGTON, D., BELANI, C. P., LANGER, C., SANDLER, A., KROOK, J., ZHU, J. & JOHNSON, D. H. 2002. Comparison of four chemotherapy regimens for advanced non-small-cell lung cancer. *N Engl J Med*, 346, 92-8.
- SCHMIDT, L., DUH, F. M., CHEN, F., KISHIDA, T., GLENN, G., CHOYKE, P., SCHERER, S. W., ZHUANG, Z., LUBENSKY, I., DEAN, M., ALLIKMETS, R., CHIDAMBARAM, A., BERGERHEIM, U. R., FELTIS, J. T., CASADEVALL, C., ZAMARRON, A., BERNUES, M., RICHARD, S., LIPS, C. J.,

-
- WALTHER, M. M., TSUI, L. C., GEIL, L., ORCUTT, M. L., STACKHOUSE, T., LIPAN, J., SLIFE, L., BRAUCH, H., DECKER, J., NIEHANS, G., HUGHSON, M. D., MOCH, H., STORKEL, S., LERMAN, M. I., LINEHAN, W. M. & ZBAR, B. 1997. Germline and somatic mutations in the tyrosine kinase domain of the MET proto-oncogene in papillary renal carcinomas. *Nat Genet*, 16, 68-73.
- SEOANE, J. & GOMIS, R. R. 2017. TGF-beta Family Signaling in Tumor Suppression and Cancer Progression. *Cold Spring Harb Perspect Biol*, 9.
- SHARMA, S. V., BELL, D. W., SETTLEMAN, J. & HABER, D. A. 2007. Epidermal growth factor receptor mutations in lung cancer. *Nat Rev Cancer*, 7, 169-81.
- SHI, Y., AU, J. S., THONGPRASERT, S., SRINIVASAN, S., TSAI, C. M., KHOA, M. T., HEEROMA, K., ITOH, Y., CORNELIO, G. & YANG, P. C. 2014. A prospective, molecular epidemiology study of EGFR mutations in Asian patients with advanced non-small-cell lung cancer of adenocarcinoma histology (PIONEER). *J Thorac Oncol*, 9, 154-62.
- SHIGEMATSU, H., LIN, L., TAKAHASHI, T., NOMURA, M., SUZUKI, M., WISTUBA, II, FONG, K. M., LEE, H., TOYOOKA, S., SHIMIZU, N., FUJISAWA, T., FENG, Z., ROTH, J. A., HERZ, J., MINNA, J. D. & GAZDAR, A. F. 2005. Clinical and biological features associated with epidermal growth factor receptor gene mutations in lung cancers. *J Natl Cancer Inst*, 97, 339-46.
- SHIMIZU, Y., HAMAZAKI, Y., HATTORI, M., DOI, K., TERADA, N., KOBAYASHI, T., TODA, Y., YAMASAKI, T., INOUE, T., KAJITA, Y., MAENO, A., KAMBA, T., MIKAMI, Y., KAMOTO, T., YAMADA, T., KANNO, T., YOSHIKAWA, K., OGAWA, O., MINATO, N. & NAKAMURA, E. 2011. SPA-1 controls the invasion and metastasis of human prostate cancer. *Cancer Sci*, 102, 828-36.
- SHINOMIYA, N., GAO, C. F., XIE, Q., GUSTAFSON, M., WATERS, D. J., ZHANG, Y. W. & VANDE WOUDE, G. F. 2004. RNA interference reveals that ligand-independent met activity is required for tumor cell signaling and survival. *Cancer Res*, 64, 7962-70.
- SINGH, L., GAO, Q., KUMAR, A., GOTOH, T., WAZER, D. E., BAND, H., FEIG, L. A. & BAND, V. 2003. The high-risk human papillomavirus type 16 E6 counters the GAP function of E6TP1 toward small Rap G proteins. *J Virol*, 77, 1614-20.
- SMITTENAAR, C. R., PETERSEN, K. A., STEWART, K. & MOITT, N. 2016. Cancer incidence and mortality projections in the UK until 2035. *Br J Cancer*, 115, 1147-1155.
- SONOSHITA, M., AOKI, M., FUWA, H., AOKI, K., HOSOGI, H., SAKAI, Y., HASHIDA, H., TAKABAYASHI, A., SASAKI, M., ROBINE, S., ITOH, K., YOSHIOKA, K., KAKIZAKI, F., KITAMURA, T., OSHIMA, M. & TAKETO, M. M. 2011. Suppression of colon cancer metastasis by Aes through inhibition of Notch signaling. *Cancer Cell*, 19, 125-37.
- STAYNER, L., BENA, J., SASCO, A. J., SMITH, R., STEENLAND, K., KREUZER, M. & STRAIF, K. 2007. Lung cancer risk and workplace exposure to environmental tobacco smoke. *Am J Public Health*, 97, 545-51.
- SU, L., HATTORI, M., MORIYAMA, M., MURATA, N., HARAZAKI, M., KAIBUCHI, K. & MINATO, N. 2003. AF-6 controls integrin-mediated cell adhesion by regulating Rap1 activation through the specific recruitment of Rap1GTP and SPA-1. *J Biol Chem*, 278, 15232-8.
- SULZMAIER, F. J., JEAN, C. & SCHLAEPFER, D. D. 2014. FAK in cancer: mechanistic findings and clinical applications. *Nat Rev Cancer*, 14, 598-610.
- TAKAHARA, T., KASAMATSU, A., YAMATOJI, M., IYODA, M., KASAMA, H., SAITO, T., TAKEUCHI, S., ENDO-SAKAMOTO, Y., SHIIBA, M., TANZAWA, H. & UZAWA, K. 2017. SIPA1 promotes invasion and migration in human oral squamous cell carcinoma by ITGB1 and MMP7. *Exp Cell Res*, 352, 357-363.
- TALMADGE, J. E. & FIDLER, I. J. 2010. AACR centennial series: the biology of cancer metastasis: historical perspective. *Cancer Res*, 70, 5649-69.
- THIERY, J. P., ACLOQUE, H., HUANG, R. Y. & NIETO, M. A. 2009. Epithelial-mesenchymal

-
- transitions in development and disease. *Cell*, 139, 871-90.
- TOBIOKA, H., TOKUNAGA, Y., ISOMURA, H., KOKAI, Y., YAMAGUCHI, J. & SAWADA, N. 2004. Expression of occludin, a tight-junction-associated protein, in human lung carcinomas. *Virchows Arch*, 445, 472-6.
- TRACEY A. MARTIN, W. G. J. 2013. *Tight Junctions in Cancer Metastasis*.
- TRAVIS, W. D., BRAMBILLA, E., NICHOLSON, A. G., YATABE, Y., AUSTIN, J. H. M., BEASLEY, M. B., CHIRIEAC, L. R., DACIC, S., DUHIG, E., FLIEDER, D. B., GEISINGER, K., HIRSCH, F. R., ISHIKAWA, Y., KERR, K. M., NOGUCHI, M., PELOSI, G., POWELL, C. A., TSAO, M. S. & WISTUBA, I. 2015a. The 2015 World Health Organization Classification of Lung Tumors: Impact of Genetic, Clinical and Radiologic Advances Since the 2004 Classification. *Journal of thoracic oncology : official publication of the International Association for the Study of Lung Cancer*, 10, 1243-1260.
- TRAVIS, W. D., BRAMBILLA, E., BURKE, A.P., MARX, A., NICHOLSON, A. G. 2015. WHO Classification of Tumours of the Lung, Pleura, Thymus and Heart. Fourth edition.
- TRAVIS, W. D., CANCER, I. A. F. R. O. & NICHOLSON, A. G. 2015b. *WHO Classification of Tumours of the Lung, Pleura, Thymus and Heart*, International Agency for Research on Cancer.
- TRUSOLINO, L., BERTOTTI, A. & COMOGLIO, P. M. 2010. MET signalling: principles and functions in development, organ regeneration and cancer. *Nat Rev Mol Cell Biol*, 11, 834-48.
- TSUKITA, S., FURUSE, M. & ITOH, M. 2001. Multifunctional strands in tight junctions. *Nat Rev Mol Cell Biol*, 2, 285-93.
- UGENSKIENE, R., MYRZALIYEVA, D., JANKAUSKAITE, R., GEDMINAITE, J., JANCIAUSKIENE, R., SEPETAUSKIENE, E. & JUOZAITYTE, E. 2016. The contribution of SIPA1 and RRP1B germline polymorphisms to breast cancer phenotype, lymph node status and survival in a group of Lithuanian young breast cancer patients. *Biomarkers*, 21, 363-70.
- VALASTYAN, S. & WEINBERG, R. A. 2011. Tumor metastasis: molecular insights and evolving paradigms. *Cell*, 147, 275-92.
- VANHAESEBROECK, B., GUILLERMET-GUIBERT, J., GRAUPERA, M. & BILANGES, B. 2010. The emerging mechanisms of isoform-specific PI3K signalling. *Nat Rev Mol Cell Biol*, 11, 329-41.
- VITICCHIÈ, G. & MULLER, P. A. J. 2015. c-Met and Other Cell Surface Molecules: Interaction, Activation and Functional Consequences. *Biomedicines*, 3, 46-70.
- WEIDNER, K. M., ARAKAKI, N., HARTMANN, G., VANDEKERCKHOVE, J., WEINGART, S., RIEDER, H., FONATSCH, C., TSUBOUCHI, H., HISHIDA, T., DAIKUHARA, Y. & ET AL. 1991. Evidence for the identity of human scatter factor and human hepatocyte growth factor. *Proc Natl Acad Sci U S A*, 88, 7001-5.
- WEIS, S., CUI, J., BARNES, L. & CHERESH, D. 2004. Endothelial barrier disruption by VEGF-mediated Src activity potentiates tumor cell extravasation and metastasis. *J Cell Biol*, 167, 223-9.
- WEN-SHENG WU, C.-T. H. 2010. *Signal Transduction in Cancer Metastasis*
- WHEELER, D. L., DUNN, E. F. & HARARI, P. M. 2010. Understanding resistance to EGFR inhibitors-impact on future treatment strategies. *Nat Rev Clin Oncol*, 7, 493-507.
- WU, Y. L., SOO, R. A., LOCATELLI, G., STAMMBERGER, U., SCAGLIOTTI, G. & PARK, K. 2017. Does c-Met remain a rational target for therapy in patients with EGFR TKI-resistant non-small cell lung cancer? *Cancer Treat Rev*, 61, 70-81.
- WYCKOFF, J. B., WANG, Y., LIN, E. Y., LI, J. F., GOSWAMI, S., STANLEY, E. R., SEGALL, J. E., POLLARD, J. W. & CONDEELIS, J. 2007. Direct visualization of macrophage-assisted tumor cell intravasation in mammary tumors. *Cancer Res*, 67, 2649-56.
- XIE, C., YANG, L., YANG, X., YANG, R., LI, Y., QIU, F., CHEN, M., FANG, W., BIN, X., DENG, J., HUANG, D., LIU, B., ZHOU, Y. & LU, J. 2013. Sip1 promoter polymorphism predicts risk and

-
- metastasis of lung cancer in Chinese. *Mol Carcinog*, 52 Suppl 1, E110-7.
- YAMAMOTO, T., HARADA, N., KANO, K., TAYA, S., CANAANI, E., MATSUURA, Y., MIZOGUCHI, A., IDE, C. & KAIBUCHI, K. 1997. The Ras target AF-6 interacts with ZO-1 and serves as a peripheral component of tight junctions in epithelial cells. *J Cell Biol*, 139, 785-95.
- YE, X. & WEINBERG, R. A. 2015. Epithelial-Mesenchymal Plasticity: A Central Regulator of Cancer Progression. *Trends Cell Biol*, 25, 675-686.
- YI, S. M. & LI, G. Y. 2014. The association of SIPA1 gene polymorphisms with breast cancer risk: evidence from published studies. *Tumour Biol*, 35, 441-5.
- YOSHIMURA, A., NAKA, T. & KUBO, M. 2007. SOCS proteins, cytokine signalling and immune regulation. *Nature reviews. Immunology*, 7, 454-465.
- ZHANG, J. & BABIC, A. 2016. Regulation of the MET oncogene: molecular mechanisms. *Carcinogenesis*, 37, 345-355.
- ZHANG, X. H., WANG, Q., GERALD, W., HUDIS, C. A., NORTON, L., SMID, M., FOEKENS, J. A. & MASSAGUE, J. 2009. Latent bone metastasis in breast cancer tied to Src-dependent survival signals. *Cancer Cell*, 16, 67-78.
- ZHANG, Y., GONG, Y., HU, D., ZHU, P., WANG, N., ZHANG, Q., WANG, M., ALDEEWAN, A., XIA, H., QU, X., RING, B. Z., MINATO, N. & SU, L. 2015. Nuclear SIPA1 activates integrin beta1 promoter and promotes invasion of breast cancer cells. *Oncogene*, 34, 1451-62.

Chapter-10 Appendix

Appendix 1: Peking University Cancer Hospital Patients in Consent Information

 <p>北京大学肿瘤医院 PEKING UNIVERSITY CANCER HOSPITAL</p>	<p>北京大学肿瘤医院 北京肿瘤医院</p> <p>患者样本开展科学研究的知情同意书</p>	 <p>ID 号: T001242514 病案号: 759604</p>
姓名: 李洪祥	第1页	
患者姓名: 李洪祥	性别: 男 年龄: 70岁	出生日期: 1945年04月27日 科室: 肝胆外二病房

尊敬的患者及家属:

为了对肿瘤或其他疾病做更深入的了解, 保障开展科学研究和提高生物医学水平, 我们将对使用患者样本开展科学研究的情况向您进行详细介绍, 具体内容如下:

一、患者样本在科学研究中的重要作用

1. 为了对您所患疾病的诊断和治疗, 临床上可能通过活检、外科手术等技术方法获取您的一部分组织、体液(主要是血液、尿液), 并进行必要的临床检测。您的医生会告知您这些检测结果, 对于准确诊断和指导治疗十分重要。

2. 检测完成后可能会剩余部分组织和/或体液, 如果您同意, 医务人员可以将其保存起来并进一步用于与疾病有关的科学研究, 这些研究将会对肿瘤或其他疾病做更深入的了解并为有效治疗提供科学依据, 促进医学的发展、解决人类面临的健康问题。

3. 我们郑重向您承诺, 用于研究的组织和体液是您的临床检测完成后剩余的组织和体液, 研究不会影响检测的顺利进行, 不会影响您目前的治疗, 更不会造成您正常检查以外的伤害。

4. 研究结果将严格保密, 由于属于科学研究, 所以研究报告可能不会告知您本人或您的医生, 也不会存入您的健康档案。

二、需要考虑的问题:

1. 我们将尊重您的选择, 不论您是否同意保存剩余的组织样本和体液, 都不会影响对您的治疗。

2. 您可以现在就做出决定, 同意保留您的组织样本和体液并用于科学研究, 但也可以随时改变您的决定, 请与我们联系并及时告知您的想法。

3. 在有些情况下, 您的部分组织样本和体液可能会用于家族性或遗传性疾病的研究, 即使您的体液和组织样本用于这一类研究, 其结果也不会存入您的健康档案。

4. 您提供的组织样本和体液只用于科学研究, 获得的部分研究结果有可能会发展成为具有临床应用价值的检测方法, 但是您目前不能直接获益。

三、利益与风险

1. 科学研究工作主要是推动科学和技术的进步, 没有直接的经济效益或福利。您不会因此得到任何物质补偿, 但相关研究成果可能对包括您在内的广大患者有益。

2. 组织样本和体液地开展科学研究的重要资源, 对人类认识相关疾病的发病规律、探索有效的预防和治疗方法具有不可替代的作用。

	
---	---



北京大学肿瘤医院 北京肿瘤医院

患者样本开展科学研究的知情同意书

10 号: T001242514

病案号: 759604

姓名: 李洪祥

第2页

3. 您的样本及相关资料信息将保存于北京肿瘤医院标本库, 由专业人员进行科学规范的管理, 在标本收集、保管和使用过程中, 您提供的组织样本、体液和您的临床资料将会用一个编号表示, 与您的姓名和编号联系的基本信息将以电子档案的形式保存到计算机中, 只有参与研究人员、伦理委员、政府主管部门才可以看到您的相关信息, 研究人员和其他采样及收集临床资料的工作人员都不会知道您的身份。

4. 您参加本研究最大的风险在于, 随着研究的进展, 您与研究有关的健康信息可能被研究者、伦理委员、政府主管部门以外的其他人了解, 但这种可能性非常小, 研究者将尽最大努力避免。

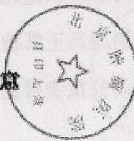
四、请您考虑并做出选择

请您仔细阅读下面项目并做出选择, 在同意和不同意处标注。如果有什么疑问请与您的医生和护士咨询或与我们的伦理委员会联系, 我们将尊重您的选择, 不论您是否同意保存剩余的体液和组织样本, 都不会影响对您的治疗。

我的组织样本和体液可以用于肿瘤预防和诊治、其他危害健康等方面的科学研究, 我的临床资料信息可以与我提供的组织样本和体液相联系。

A 同意

B 不同意

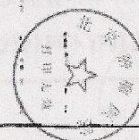


回答上述问题后请您签名。

患者/法定监护人(签名): _____ 日期: _____

授权委托人(签名, 须注明与患者关系): 李欣好 日期: 2015.7.1

医生签名: [Signature] 日期: 2015-7-1





北京大学肿瘤医院
北京肿瘤医院

患者样本开展科学研究的知情同意书



姓名: 陈萌

第1页

ID 号:T00L195749

病案号:755859

患者姓名:陈萌 性别:男 年龄:38岁 出生日期:1976年10月21日 科室:肝胆外二病房

尊敬的患者及家属:

为了对肿瘤或其他疾病做更深入的了解,保障开展科学研究和提高生物医学水平,我们将对使用患者样本开展科学研究的情况向您进行详细介绍,具体内容如下:

一、患者样本在科学研究中的重要作用

1. 为了对您所患疾病的诊断和治疗,临床上可能通过活检、外科手术等技术方法获取您的一部分组织、体液(主要是血液、尿液),并进行必要的临床检测。您的医生会告知您这些检测结果,对于准确诊断和指导治疗十分重要。

2. 检测完成后可能会剩余部分组织和/或体液,如果您同意,医务人员可以将其保存起来并进一步用于与疾病有关的科学研究,这些研究将会对肿瘤或其他疾病做更深入的了解并为有效治疗提供科学依据,促进医学的发展、解决人类面临的健康问题。

3. 我们郑重向您承诺,用于研究的组织和体液是您的临床检测完成后剩余的组织 and 体液,研究不会影响检测的顺利进行,不会影响您目前的治疗,更不会造成您正常检查以外的伤害。

4. 研究结果将严格保密。由于属于科学研究,所以研究报告可能不会告知您本人或您的医生,也不会存入您的健康档案。

二、需要考虑的问题:

1. 我们将尊重您的选择,不论您是否同意保存剩余的组织样本和体液,都不会影响对您的治疗。

2. 您可以现在就做出决定,同意保留您的组织样本和体液并用于科学研究,但也可以随时改变您的决定,请与我们联系并及时告知您的想法。

3. 在有些情况下,您的部分组织样本和体液可能会用于家族性或遗传性疾病的研究,即使您的体液和组织样本用于这一类研究,其结果也不会存入您的健康档案。

4. 您提供的组织样本和体液只用于科学研究,获得的部分研究结果有可能会发展成为具有临床应用价值的检测方法,但是您目前不能直接获益。

三、利益与风险

1. 科学研究工作主要是推动科学和技术的进步,没有直接的经济效益或福利,您不会因此得到任何物质补偿,但相关研究成果可能对包括您在内的广大患者有益。

2. 组织样本和体液是开展科学研究的重要资源,对人类认识相关疾病的发病规律、探索有效的预防和治疗方法具有不可替代的作用。



北京大学肿瘤医院
北京肿瘤医院

患者样本开展科学研究的知情同意书



ID 号: T061195749
病案号: 755859

姓名: 陈萌

第2页

3. 您的样本及相关资料信息将保存于北京肿瘤医院标本库, 由专业人员进行科学规范的管理, 在标本收集、保管和使用过程中, 您提供的组织样本、体液和您的临床资料将会用一个编号表示, 与您的姓名和编号联系的基本信息将以电子档案的形式保存到计算机中, 只有参与研究人员、伦理委员、政府主管部门才可以看到您的相关信息, 研究人员和其他采样及收集临床资料的工作人员都不会知道您的身份。

4. 您参加本研究最大的风险在于, 随着研究的进展, 您与研究有关的健康信息可能被研究者、伦理委员、政府主管部门以外的其他人了解, 但这种可能性非常小, 研究者将尽最大努力避免。

四、请您考虑并做出选择

请您仔细阅读下面项目并做出选择, 在同意和不同意处标注。如果有什么疑问请与您的医生和护士咨询或与我们的伦理委员会联系。我们将尊重您的选择, 不论您是否同意保存剩余的体液和组织样本, 都不会影响对您的治疗。

我的组织样本和体液可以用于肿瘤预防和诊治、其他危害健康等方面的科学研究, 我的临床资料信息可以与我提供的组织样本和体液相联系。

A 同意

B 不同意



回答上述问题后请您签名。

患者/法定监护人(签名): _____ 日期: _____

授权委托人(签名, 须注明与患者关系): 夫妻 张华 日期: 2015.1.19

医生签名: [Signature] 日期: 2015.1.19



Peking University Cancer Hospital
Patients in Consent Information

Name: Gender: Date of Birth: Department:

Dear patients,

In order to make your disease further understood, guarantee scientific research quality and improve the level of medical research, we would like to introduce how we use the Patient Sample to do medical research.

1. The importance of your specimens in medical research

1.1 For the benefit of your diagnosis and treatment, we would like to collect your specimens and blood in order to do necessary clinical examine through bioscopy or surgery.

1.2 If you permit, we would like to reserve the rest of your specimens and blood to do further medical research in order to make a full understanding of cancer and other diseases, and provide more evidence to medicine and treatment.

1.3 We hereby guarantee that we use the rest of your specimens and blood for medical research. This will not affect your examine, treatment and health.

1.4 The medical research is fully confidential. The research reports will not inform you and your doctor, and at the same time, it will not be saved in your personal healthy file.

2. Problems to be considered

2.1 We respect your decision, whether you agree or disagree to preserve your specimens, which will not affect your treatment.

2.2 You can make a decision now, and change your mind at any time. Please keep in touch with us and let us know your decision.

2.3 Your specimens will be used in the study of hereditary diseases; however, results will not be saved in your personal healthy file.

2.4 Your specimens may greatly contribute to research. However, you may not get benefit from them.

3. Benefits and Risks

3.1 The purpose of medical research is to make a contribution to all patients, and you will not get any financial benefit and welfare from them.

3.2 Your specimens and blood are important resources for the understanding of the development of diseases and exploration of effective methods of treatment.

[Date]

1

- 3.3 Your specimens and information will be preserved in the tissue bank of Peking University Cancer Hospital. All of your information will be coded with uniform numbers, and the basic information will be stored in electronic files in the computer. Only involvement of researchers, ethics committees and government officer of departments in charge can get access to your information, researchers and other staff collecting the clinical data will not know your information.
- 3.4 The risk of your participation in this study is that, within the progress of research, you and your health-related information may be accessible by other people besides researchers, ethics committees and government departments, but researchers will try to avoid it.
4. Please read the above information carefully and make your own choice. If you have any questions, please feel free to contact our doctors and nurses or ethics committees.

My specimens are used for cancer prevention, diagnostics and scientific research, and at the same time, my clinical data can be associated with my specimens.

A. Agree

B. Disagree

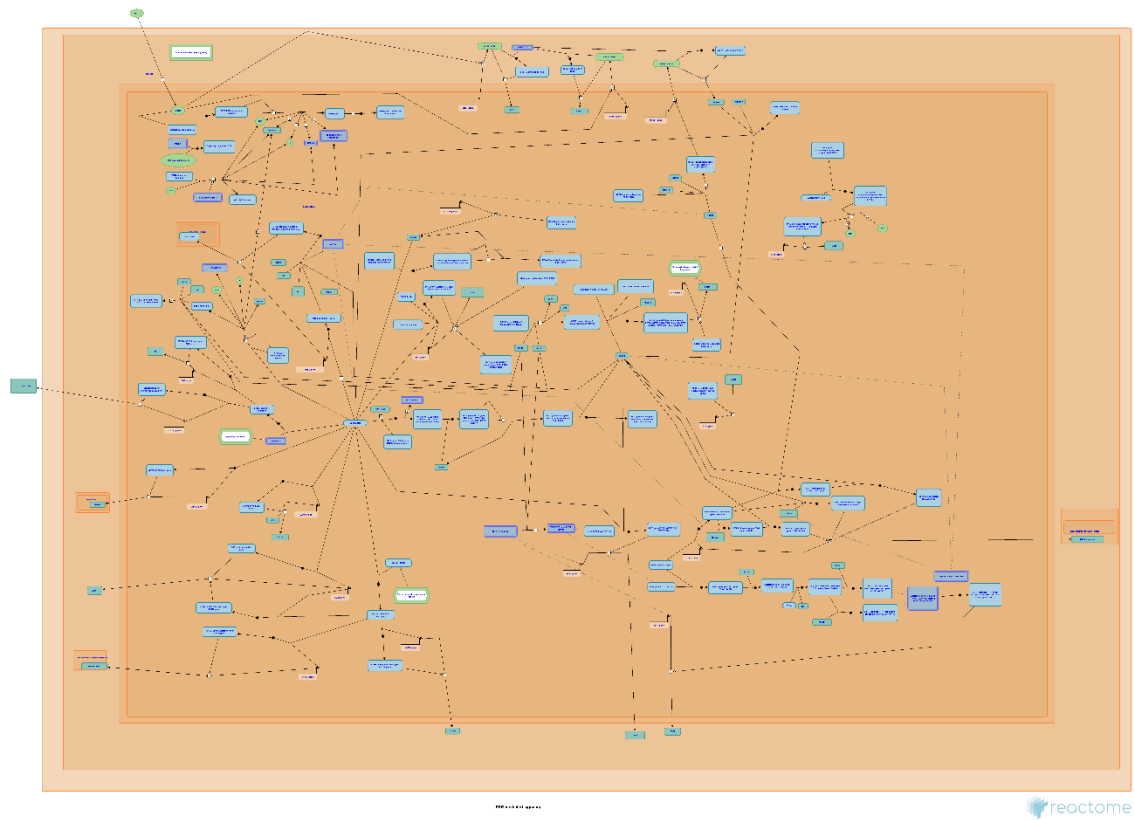
Patient's name:

Date:

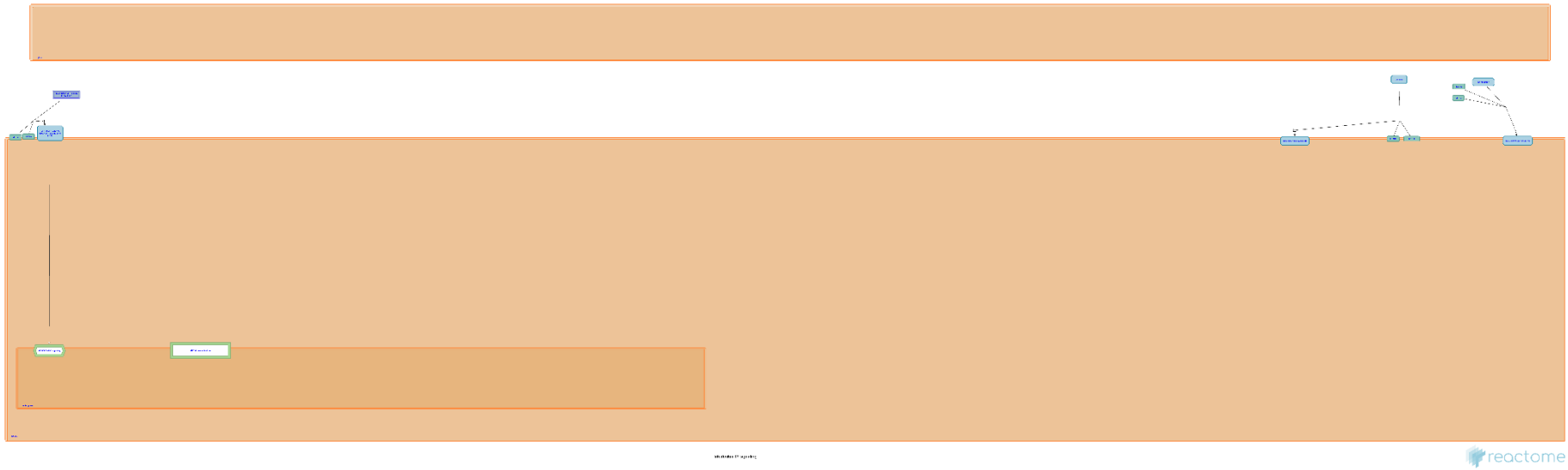
Doctor's name:

Date:

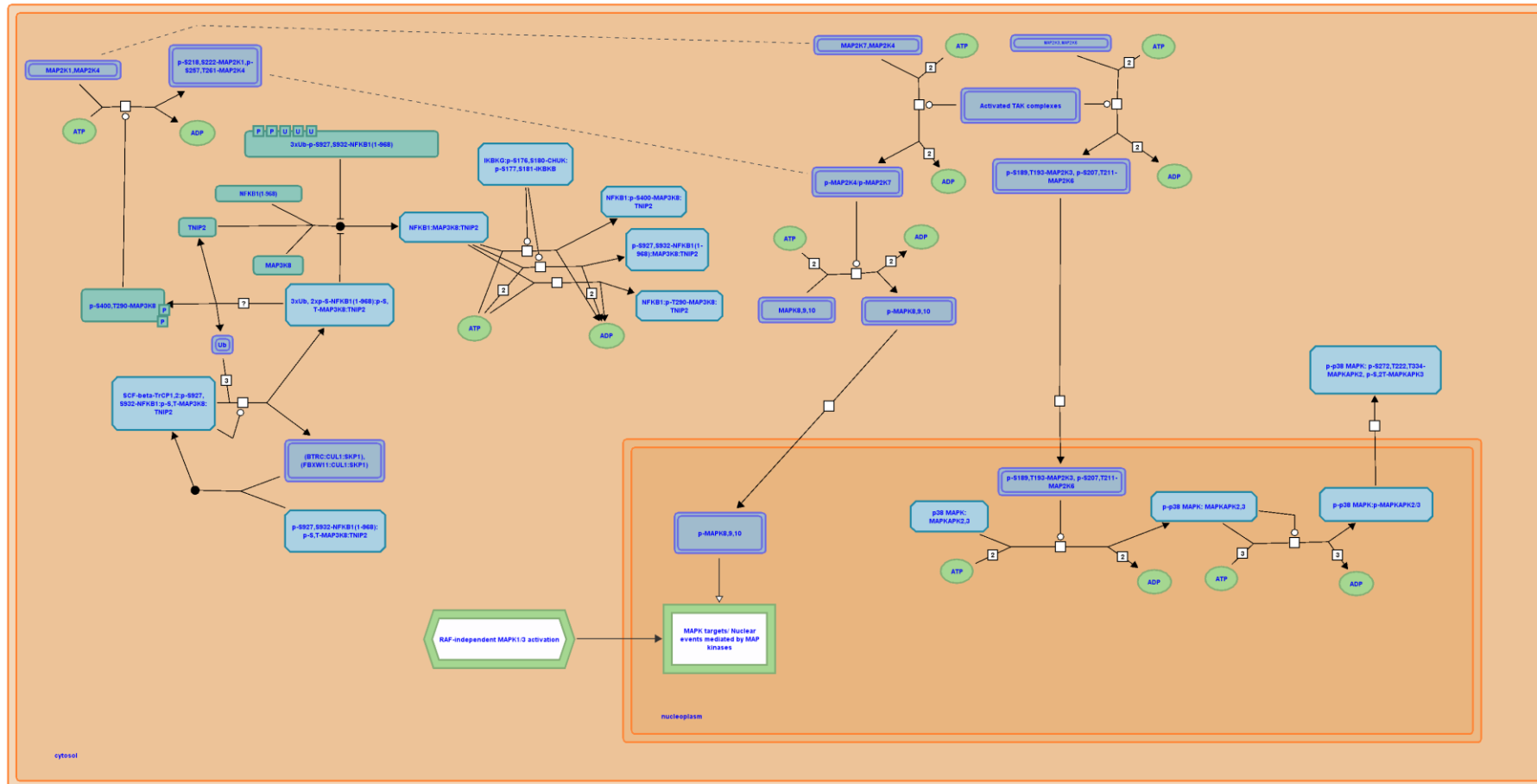
Appendix 2: figures of the selected representative signalling pathways.



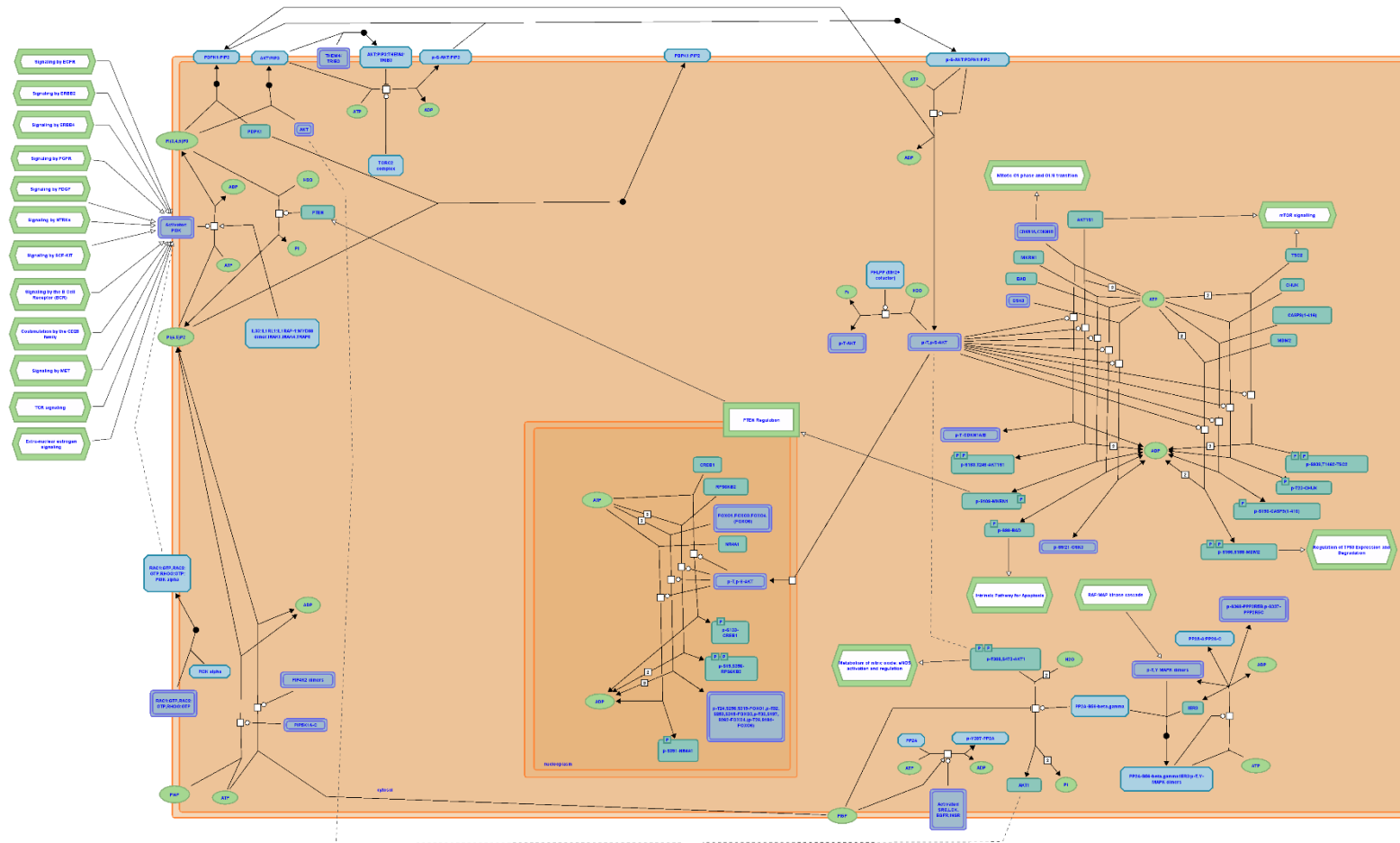
Schematic diagram of ESR-mediated signalling. Generated from: <https://reactome.org/content/detail/R-HSA-8939211>.



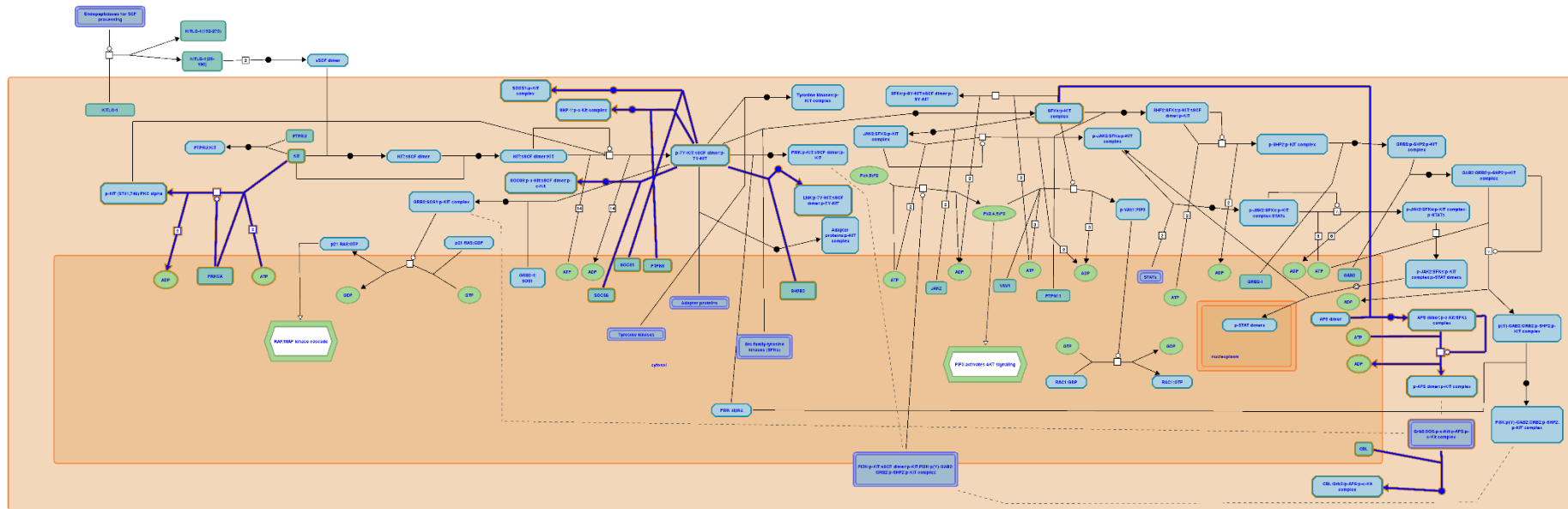
Schematic diagram of Interleukin-17 signalling. Generated from: <https://reactome.org/content/detail/R-HSA-448424>.



Schematic diagram of MAP kinase activation. Generated from: <https://reactome.org/content/detail/R-HSA-450294>.



Schematic diagram of PIP3 activates Akt signalling. Generated from: <https://reactome.org/content/detail/R-HSA-1257604>.



Schematic diagram of regulation of KIT signalling. Generated from: <https://reactome.org/content/detail/R-HSA-1433559>.

